Evaluation of the Performance of Activated Carbon and Titanium Dioxide Composites for Pharmaceutical Adsorption and Photocatalysis in Water

Ph.D.

David Keane B.Sc.

Supervisors

Dr. Anne Morrissey

Dr. Kieran Nolan

Dr. John Tobin

School of Biotechnology

Dublin City University

Dublin 9

Ireland

Declaration

I hereby certify that this material, which I now submit for assessment on the programme of study leading to the award of Ph.D. is entirely my own work, that I have exercised reasonable care to ensure that the work is original, and does not to the best of my knowledge breach any law of copyright, and has not been taken from the work of others save and to the extent that such work has been cited and acknowledged within the text of my work.

Signed: _____

ID No.: 58120441

Date: _____

TABLE OF CONTENTS

ACKNOWLEDGEMENTS

I would like to thank the EPA under the Science, Technology, Research and Innovation for the Environment (STRIVE) Programme 2007–2013 (project number 2008-S-ET) and DCU for funding.

I would like to thank my lab colleagues Mark, Ann Marie, Sharon, Nora, Ross, Basha, Cecilia and Zahra for their help, support and kindness.

I would like to thank all the technical staff in the School of Biotechnology, Chemical Sciences, Mechanical Engineering and the NCSR. A special thanks to David Cunningham for all his help.

Thanks to Astellas Ireland Ltd, ENVA Environmental Ltd, Activated Carbon Technologies PTY Ltd and Degussa for the free samples and technical support.

I would like to acknowledge the hard work and dedication of my supervisors, Anne, John, Kieran and from Australia, Michael. Thank you for your guidance and support.

Thanks to my family and friends for their encouragement.

ABSTRACT

In this project the adsorptive properties of activated carbons (AC) are coupled with the photocatalytic properties of titanium dioxide (TiO_2) to create a synergistic composite - an integrated photocatalytic adsorbent (IPCA) - that can adsorb and photodegrade pollutants better than the two materials separately. Two active pharmaceutical ingredients, famotidine and solifenacin succinate, were chosen as model pollutants in this study. Active pharmaceutical ingredients are an important group of organic environmental contaminants that have the potential to cause health risks for humans as well as biota. An ultrasonication preparation method was used to combine the AC and TiO_2 to prepare the IPCA.

Characterisation of the IPCA using SEM, EDX and FESEM analysis revealed that TiO_2 particles approximately 25 nm in diameter were dispersed across the AC surface. XRD analysis provided information on the molecular structure of the IPCAs and TiO_2. Adsorption studies indicated that TiO_2 has limited adsorption capacity. The AC and IPCA have higher adsorption capacity but require long equilibrium times due to rate limiting intraparticle diffusion.

IPCA photodegradation studies at an initial concentration of 100 mg/L can remove more solifenacin from solution than either TiO_2 or AC separately; however for famotidine removal the IPCAs showed no improvement compared to AC or TiO_2 controls. The contrast is postulated to be the high adsorption strength of famotidine compared to solifenacin, which retards migration from the adsorption sites on the AC to the TiO_2 on the IPCA surface. This lowers the photodegradation rate for famotidine but not solifenacin. These results suggest that substrate desorption is required to prepare effective IPCAs. Future work would involve IPCA photodegradation studies of compounds similar to famotidine to confirm this hypothesis.

LIST OF FIGURES

LIST OF TABLES

ABBREVIATIONS

α	Bangham equation constant
β	Redlich and Peterson isotherm constant
AC	Activated carbon
ACC	Activated carbon cloth
ACE inhibitor	Angiotensin-converting enzyme inhibitor
ACF	Activated carbon fibres
AOT/AOP	Advanced oxidation technology/process
API	Active pharmaceutical ingredient
Aqua 2k	AquaSorb 2000
A_{r-p}	Redlich and Peterson isotherm constant
ASTM	American Society for Testing and Materials
B	Temkin energy constant
b	Variation of adsorption energy (Temkin isotherm)
BOD	Biochemical oxygen demand
C	Concentration (at specific t (time))
C_i	Concentration initial
C_{22h}:	Concentration of sorbate in solution after 22 h, mg/L
C_f	Concentration final (after a given length of time)
C_0	Concentration at t = 0
COD	Chemical oxygen demand
CVD	Chemical vapour deposition
DEET	N,N-Diethyl-meta-toluamide
DI	Deionised (water)
DO	Dissolved oxygen
DOC	Dissolved organic carbon
EAC	Extruded activated carbon
EDC	Endocrine disrupting chemical
EDX	Energy dispersive X-ray
E2	17β-estradiol
EE2	17 β-ethinylestradiol
FESEM	Field emission scanning electron microscopy
FTIR	Fourier transform infrared spectrometer
GAC	Granular activated carbon
HOP	Hazardous organic pollutant
HPLC	High performance liquid chromatography
IPCA	Integrated photocatalytic adsorbents
IUPAC	International Union of Pure and Applied Chemistry
k_{app}	Apparent pseudo first-order rate constant

k_b	Bangham equation constant
k_{int}	Intraparticle diffusion rate constant
K_F:	Freundlich isotherm constant, l/g
K_f	External mass transfer coefficient
K_L:	Langmuir isotherm equilibrium binding constant, l/mg
K_{r-p}	Redlich and Peterson isotherm constant
LCA	Life cycle assessment
LOD	Limit of detection (HPLC)
LOQ	Limit of quantification (HPLC)
LC-MS	Liquid chromatography tandem mass spectrometry
Log D_{ow}	Log distribution coefficient (Log P at pH 7)
Log P_{ow}	Log partition coefficient octanol water
LPCVD	Low pressure chemical vapour deposition
m:	Number of experimental data points
MB	Methylene blue
MBR	Membrane bioreactor
MCPA	2-methyl-4-chlorophenoxyacetic acid
Min	Minute
MOCVD	Metal organic chemical vapour deposition
n:	Exponent in Freundlich isotherm
NSAID	Non-steroidal anti-inflammatory drug
NOM	Natural organic material
p:	Number of parameters in the sorption isotherm
pKa	Logarithmic acid dissociation constant
P25	AEROXIDE® P25
PAC	Powdered activated carbon
PAH	Polycyclic aromatic hydrocarbon
PCBs	Polychlorobiphenyls
PE	Population equivalent (60g BOD/day)
pH_f	Final pH
pH_i	Initial pH
PMR	Photocatalytic membrane reactors
PPCP	Pharmaceutical and personal care products
PZC	Point of zero charge
q	Adsorption loading (final)
qf	Adsorption final
qt	Adsorption at a given time
q_{22h}:	Amount of sorbate adsorbed after 22 h, mg/g
q_m:	Maximum sorption capacity, mg/g
R:	Universal gas constant, 8.314 J/mol/K

RSSCT	Rapid small-scale column test
R^2:	Correlation coefficient
ROS	Reactive oxygen species
SD	Standard deviation
SE:	Standard error
SEM	Scanning electron microscopy
SOF	Surface oxygen functionalities
SRT	Solid retention times
SSE:	Sum of squares error
t	Time
TOC	Total organic carbon
UV	Ultra violet (Light)
UV-vis	Ultra violet and visible (Light)
VUV	Vacuum UV
WTP	Water treatment plant
WWTP	Waste water treatment plant
XRD	X-ray diffraction

PUBLICATIONS, POSTERS AND ORAL PRESENTATIONS

Print publications

1) Keane, D., Basha, S., Nolan, K., Morrissey, A., Oelgemöller, M., Tobin, J. (2012) "Overview of the development of Integrated PhotoCatalytic Adsorbents (IPCAs) for water treatment using titanium dioxide (TiO_2) and activated carbon" IN Griesbeck, A., Oelgemoeller, M., Ghetti, F (eds.) CRC Handbook of Organic Photochemistry and Photobiology, Third Edition. ed. Boca Raton, Florida, USA. CRC Press Llc 935-962.

Journal publications

1) Basha, S., Colin, B., Keane, D., Nolan, K., Morrissey, A., Oelgemöller, M., and Tobin, J. M. (2011) On the adsorption/photodegradation of amoxicillin in aqueous solutions by an integrated photocatalytic adsorbent (IPCA): experimental studies and kinetics analysis. Photochemical and Photobiological sciences. 10, 1014-1022.
2) Keane, D., Basha, S., Nolan, K., Morrissey, A., Oelgemöller, M., Tobin, J. (2010) Photodegradation of famotidine by integrated photocatalytic adsorbent (IPCA) and kinetic study. Catalysis Letters. 144, 300 - 308.
3) Basha, S., Keane, D., Nolan, K., Morrissey, A., Oelgemöller, M., Tobin, J. (2010) Studies on the Adsorption and Kinetics of Photodegradation of Pharmaceutical Compound, Indomethacin Using Novel Photocatalytic Adsorbents (IPCAs). Industrial & Engineering Chemical Research. 49, 11302 - 11309.

Oral presentations

1) Development of novel integrated photocatalytic adsorbents (IPCAs) for hazardous organics removal from water & wastewater. Photochemistry and Photochemical Techniques in University College Dublin and Trinity College Dublin. 16-18th May 2011.
2) Removal of famotidine from aqueous solutions by novel integrated photocatalytic adsorbents (IPCAs). 3rd School of Biotechnology research day in DCU. 28th January 2011.
3) Removal of famotidine from aqueous solutions by novel integrated photocatalytic adsorbents. Environ 2010 colloquium in Limerick I.T. 18th February 2010.

Posters

1) IWA World Congress on Water, Climate and Energy 2012 in the Convention Centre Dublin 13-18th May 2012.
2) Environ 2012 colloquium in University College Dublin 7-9th March 2012.
3) Environ 2011 colloquium in University College Cork 6-8th April 2011.
4) EPA Post-graduate Seminar 2010 in Convention Centre, Dublin. 11th November 2010.
5) EPA National Research Conference 2010 in Croke Park Conference centre, Dublin. 23rd June 2010.
6) Environ 2009 colloquium in Waterford I.T. 19-21st February 2009.
7) School of Biotechnology research day in DCU. 30th January 2009.
8) EPA Fellowships & Scholarships Seminar 2008. 13th November 2008.

Chapter 1 Literature Review

1.1 Pharmaceuticals in natural waters, drinking water and wastewater - approaches for their removal

Pharmaceuticals in surface waters, wastewaters and drinking waters are an issue of growing concern (Gültekin and Ince, 2007, Khetan and Collins, 2007, Oulton *et al.*, 2010, Parson, Jefferson and Christopher, 2007, von Gunten and Hoigne, 1994). This concern was triggered after the occurrence of pharmaceuticals in river water was linked to feminisation of fish living downstream of wastewater treatment plant (WWTP) outfalls (Ternes *et al.*, 1999). The overall impact of such discharges on fish populations is uncertain and the risks to other biota are still being accessed (Mills and Chichester, 2005).

Sources of pharmaceuticals in the environment include municipal WWTPs, WWTPs of pharmaceutical production facilities, hospital effluent, agricultural run-off, land spreading of sewage sludge, aquaculture, landfills and even graveyards (Khetan and Collins, 2007, Mompelat *et al.*, 2009) (Figure 1-1). The metabolism of active pharmaceutical ingredients varies greatly from 98 % for carbamazepine, diazepam and propranolol to less than 25 % for valsartan, sotalol and amoxicillin (Mompelat *et al.*, 2009). The unmetabolised active pharmaceutical ingredients (APIs) is excreted in feces or urine which is disposed via the sewer system. Hence the most investigated route of entry of pharmaceuticals into the environment is through municipal wastewater treatment plants where the APIs are the most concentrated. Human excretion of unchanged or slightly transformed APIs, conjugated to polar molecules such as glucuronides enters WWTPs and may be cleaved, releasing the original API into the environment (Heberer, 2002). Consequently numerous studies have investigated the removal efficiencies of pharmaceuticals at municipal WWTPs in particular activated sludge plants as it is the dominant technology (Castiglioni *et al.*, 2006, Kasprzyk-Hordern *et al.*, 2009, Phillips *et al.*, 2010, Radjenović *et al.*, 2009, Watkinson *et al.*, 2007). Routine monitoring of the levels of APIs released from WWTPs is largely neglected by regulatory authorities (Verlicchi *et al.*, 2012) as the importance of such releases for humans and biota has not been fully established (Deegan, 2011, Enick and Moore, 2007).

Figure 1-1 Flow chart of pharmaceutical entry into the environment.

One of the most cited examples of the dangers of pharmaceuticals in the environment is the effect of diclofenac, a non-steroidal anti-inflammatory drug (NSAID) on the populations of long-billed vulture (*Gyps indicus*), oriental white-backed vulture, (*Gyps bengalensis*) and slender-billed vulture (*Gyps tenuirostris*) on the Indian subcontinent. In the period 1992–2007 the populations of the former two declined by 96.8 % and 99.9 % respectively (Markandya *et al.*, 2008) and similar declines occurred in the slender-billed vulture (*Gyps tenuirostris*). Post-mortem examinations on 259 adult and sub-adult oriental white-backed vultures found that 85 % showed evidence of renal failure (Oaks *et al.*, 2004). Tests for diclofenac residue found concentrations of diclofenac (0.051 µg/g – 0.643 µg/g) in the 100 % of the vultures that died of renal failure, while no diclofenac was found in vultures that died from other causes. These concentrations were high enough to trigger renal failure in vultures that were orally administered diclofenac in a control study. Diclofenac was prescribed for veterinary use on livestock due to its analgesic, anti-inflammatory and antipyretic properties.

The decline of the vulture populations is not just a loss for ecosystems. The human health and economic losses resulting for the vulture population decline have been

investigated (Markandya *et al.*, 2008). In India vultures are typically used to dispose of animal carcasses. The vulture's absence means that the animal remains become a breeding ground for disease and are eaten (incompletely) by other scavengers such as dogs. Markandya *et al.*, uses a series of crude estimates to determine how many extra feral dogs the uneaten carcasses could support. Based on the number of rabies cases from dog bites per dog multiplied by the increase in the hypothetical dog population the author is able to calculate the human health impact and resulting economic cost. The cost spread over the 14 years of vulture decline (1993–2006) would amount to about $34 billion, using the average exchange rates during that time. The total number of human rabies cases remained constant (or declining slightly) in this time period therefore this assessment is counterfactual to the decline of vulture populations. This makes the projected economic cost speculative.

While the previous example is well characterised, accurately determining all the hazards (hence risks) associated with APIs in the environment is difficult as it is impossible to provide unequivocal safety data for every chemical, every chemical composition, every specific situation and exposed species (Enick and Moore, 2007). With this in mind the precautionary principal should be exercised and the exposure of humans and biota to APIs limited. However, this approach lacks of scientific rigor as it can be evoked with a small or nonexistent burden of proof. The advantages and limitations of the application of this principle is discussed elsewhere (Enick and Moore, 2007).

1.1.1 Removal of pharmaceuticals from drinking water

Pharmaceuticals have been detected in drinking water but are not as well documented as APIs in wastewater or natural waters (Mompelat *et al.*, 2009). This is due to lower quantities of APIs in the raw water used for drinking water abstraction (compared to wastewater), more efficient removal by water treatment processes and the breakdown of APIs caused by residual chlorine in the water distribution system (Gibs *et al.*, 2007). However some APIs are present in drinking water at detectable levels and the approaches used to remove them are not without limitations. One solution to the removal of APIs from drinking water and natural waters is the use of advanced oxidation technologies. Advanced oxidation technologies are defined as the "*in situ generation of highly reactive species*" (Gültekin and Ince, 2007) or "*near ambient temperature treatment processes based on*

highly reactive radicals, especially the hydroxyl radical (˙OH), as the primary oxidant" (Zhou and Smith, 2002). The promise of advanced oxidation technologies is that they will deliver superior performance to conventional technologies and thus be able to clean water to a higher standard. A brief list of the advanced oxidative technologies (also called advanced oxidative processes) is contained in Table 1-1. It is not possible to review every type of advanced oxidation technology for removal of APIs and/or other micro pollutants as they are very diverse and can be combined with conventional and/or novel water treatment techniques to yield optimum results. The advanced oxidation technologies listed in Table 1-1 can be used in isolation or they can be combined together e.g. UV/H_2O_2 and photocatalysis.

Table 1-1 Most common Advanced oxidation technologies evaluated for water and wastewater treatment.

Photochemical processes	Non-photochemical processes
UV oxidative process	O_3, O_3/H_2O_2
UV/H_2O_2	Fenton reagent
UV/O_3	Ultrasound
UV/H_2O_2/O_3	US/H_2O_2, US/O_3, US/Fenton
UV/Ultrasound	Electrochemical oxidation
Photo-Fenton	Supercritical water oxidation
Photocatalysis	Ionizing radiation
Sonophotocatalysis	Electron-beam irradiation
Vacuum UV (VUV)	Wet-air oxidation
Microwave	Pulsed plasma

Source: (Gültekin and Ince, 2007). Combinations of the above processes are possible.

A study of raw water into a municipal water treatment plant (WTP) found 35 out of 55 pharmaceuticals investigated, at detectable concentrations (Huerta-Fontela *et al.*, 2011). The raw water was pre-chlorinated which was effective at removing >99 % of some compounds (e.g. amlodipine and tamoxifen) particularly those with primary and secondary amines. Other compounds such as atenolol were barely (<5 %) removed by this step. This was followed by flocculation (poly-DADMAC), sand filtration and sedimentation. Of the 18 APIs remaining in the water at this stage the overall removal was <30 % and in other

cases (e.g. carbamazepine) it was negligible. Ozonation (5 mg/L) had effectiveness between 5 % and >99 % and the author notes that non-biodegradable carbamazepine was removed by >99 %. The water was then passed through granular activated carbon (GAC) filtration. Removal efficiencies of 55 % -75 % were influenced by the hydrophobicity of the molecule with greater removal seen in more hydrophobic compounds. Post-chlorination removed between 14 % and 72 % of the APIs in solution and the removal of individual compounds corresponded to what occurred in pre-chlorination. Of the 35 APIs in the raw water only five were found in the finished water at much lower concentrations. This indicates that conventional water treatment can remove APIs from drinking water but the process is not 100 % effective and is complex, as ozonation, GAC filtration and two cycles of chlorination were required. The paper does not discuss if the treatment processes could be improved or if the current treatment configuration could be optimized. The GAC might need frequent regeneration or require a longer hydraulic retention time to remove such low concentrations of APIs.

In another study a river receiving effluent from agricultural sources as well as 12 WWTPs was passed through a pilot-scale WTP and the removal of APIs investigated (Vieno *et al.*, 2007). The WTP consisted of coagulation (ferric sulfate), flocculation, vertical sedimentation, rapid sand filtration, ozonation and filtration through two GAC beds and UV disinfection. Coagulation, flocculation, and sand filtration were found to reduce the API concentration by 5 % to 35 % depending on the molecule. Ozonation (1 mg/L - 1.3 mg/L) was found to be very effective removing 75 % - 92 % of some APIs (naproxen and ibuprofen) in solution, although due to its selective oxidation, ozone creates degradation byproducts which may pose a problem. GAC filtration was found to be effective at API removal both after ozonation and when the ozonation step was bypassed. Efficient GAC performance required regular regeneration of the carbon. UV disinfection was used as a final step; however, since most of the APIs were removed by the preceding steps it did not give much insight into the overall performance of this method. Only ciprofloxacin was found to pass almost unaffected through the WTP. The concentration of ciprofloxacin (20 ng/L) in drinking water over lifetime ingestion (2 L water/day for 70 years) would lead to lifetime consumption of approximately one milligram of ciprofloxacin. This is 1000 times lower than the 1000 mg oral daily therapeutic dose of ciprofloxacin. This calculation ignores the effects caused by chronic exposure to low concentrations of pharmaceuticals over a long period of time.

The previously reviewed studies used GAC for the removal of APIs; however powdered activated carbon (PAC) is also an option for removing APIs. The use of PAC for removing APIs and other micro-pollutants from spiked surface water has been investigated using jar and column tests (Snyder *et al.*, 2007). The pollutant removal was measured by 5 h jar tests of spiked surface water and a pilot plant using a 5 h contact time. In both cases it was 4 h of contact time and 1 h of settling. Jar tests removed between 15 % (ibuprofen) to >90 % (pyrene, a PAH) of the pollutants in solution indicating that PAC can remove APIs but with the disadvantage of high contact time. At pilot scale, two PAC doses were selected with 4 h contact time followed by coagulation. Five milligrams per litre of PAC removed 3 % (iopromide) to 80 % (oxybenzone) of the pollutants while a PAC dose of 35 mg/L substantially increased the removal of some APIs e.g. iopromide removal increased from 3 % to 68 %. The enhanced removal at a 35 mg/L PAC dose was not as pronounced for other APIs e.g. oxybenzone removal went from 80 % to 100 %. This highlights that the cost effectiveness of this method depends on what pollutant was to be removed as this requirement influences the PAC dosing rates. It is possible that the selection of a different PAC might remove the pollutants more efficiently. An increased contact time might increase effectiveness but the 5 h period is standard for this type of treatment. Cost can be an issue as PAC is typically single use and consequently it is not recovered and regenerated. The long contact times and possible need for a batch system / coagulation also adds to system complexity which must be considered when using PAC compared to a fixed bed GAC system. In addition to PAC several GACs were investigated using the rapid small-scale column test (Snyder *et al.*, 2007). This test used spiked influent which passed through a column filled with GAC and then calculated how many bed volumes are filtered effectively before there is 5 %, 10 % and 20 % break through (see Figure 1-2). For example 5 % breakthrough occurs when 5 % of the concentration in the influent is found in the effluent. The influent treated before 5 % breakthrough occurred varied from 3090 bed volumes (sulfamethoxazole) to >55,000 bed volumes (oxybenzone). This is important as a particular AC may preferentially remove one API over another but the requirement for API free drinking water and hence regeneration will be decided by the first compound to breakthrough a GAC bed.

In combination with the above bench scale laboratory studies the API removal performance of two WTPs employing GAC filtration was investigated (Snyder *et al.*, 2007). WTP1 was a surface water treatment facility while WTP2 was a water reuse

treatment facility. No information was given on the treatment steps preceding the GAC beds; presumably it would have consisted of screening, flocculation and sand filtration. The GAC in WTP1 was regularly regenerated while the GAC in WTP2 was not. The removal rates for different pollutants and the results for each WTP are shown in Table 1-2. The removal of pollutants was minimal for WTP2 even when influent concentrations were low, although it is difficult to make a direct comparison as different pollutant and pollutant concentrations occurred at each plant. In the case of atrazine (a pesticide) for WPT1 the concentration was reduced from 182.5 ng/L to 72 ng/L while for WPT2 it was reduced from 33 ng/L to 32 ng/L. This highlights the importance of regular regeneration of the AC for efficient API removal.

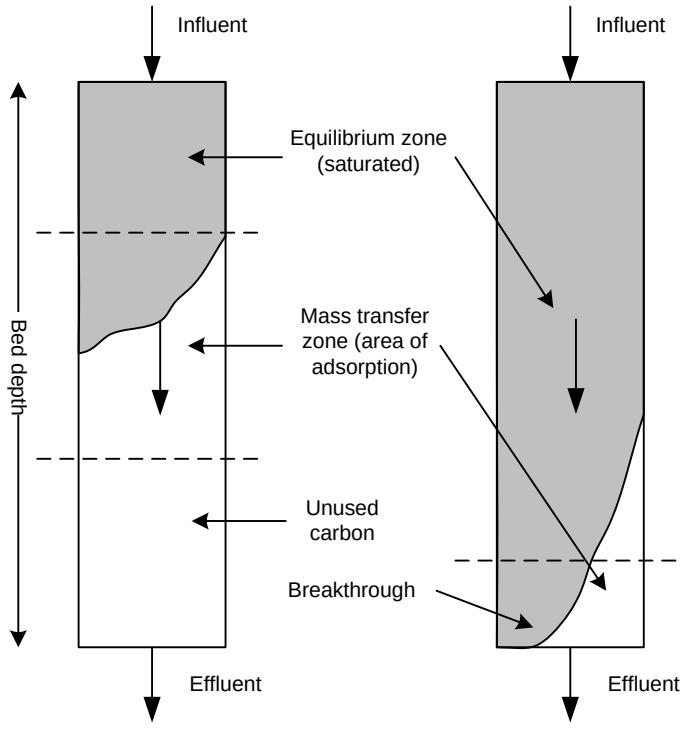

Figure 1-2 Diagram of a GAC bed gradually becoming saturated leading to break through (Moreno-Castilla, 2004).

Table 1-2 Removal of selected compounds by GAC filtration in two water treatment plants (Snyder *et al.*, 2007).

Group	API	GAC influent (ng/L)	GAC effluent (ng/L)
Analgesic, antipyretic	Acetaminophen	WPT1 10,650	47
Analgesic, antitussive	Hydrocodone	WTP1 57	<25
NSAID	Ibuprofen	WTP1 1.1	<1
		WTP2 8760	7325
Antibiotic	Erythromycin-H_2O	WPT1 1.8	<1
		WPT2 139	128
Analgesic, NSAID	Diclofenac	WPT2 3.2	<1
NSAID	Naproxen	WTP1 3545	3320
Antibiotic	Sulfamethoxazole	WTP1 6	<1
		WTP2 426	69
		WPT2 33	32
Antibiotic, antifungal	Triclosan	WTP2 3.8	4.2
Antibiotic	Trimethoprim	WTP2 135	48
Anticonvulsant	Carbamazepine	WPT1 2.2	<1
		WPT2 199	168
		WPT2 42,650	35,700
Antiepileptic	Dilantin (Phenytoin)	WPT1 1.8	<1
		WPT2 110	85
Anxiolytic	Meprobamate	WTP 1 1.2	<1
		WTP 2 226	196
Contrast medium (x-ray)	Iopromide	WTP1 3.3	<1
Fibrates (anti lipid)	Gemfibrozil	WPT1 1.2	<1
Herbicide	Atrazine	WPT1 650	6.1
		WTP2 5	1.4
Herbicide	Metolachlor	WTP 1122	<10
Hormone	Androstenedione	WPT1 182.5	72
		WTP2 3710	3405
Hormone	Testosterone	WTP2 150.5	39
Insect repellents	DEET	WTP1 1.8	<1
Phosphodiesterase inhibitor	Pentoxifylline (improves blood flow)	WTP2 34	<25
Stimulant	Caffeine	WPT1 17	<10

DEET: N,N-Diethyl-meta-toluamide

In a similar study to Snyder *et al.*, (2007), APIs removal by laboratory studies and in two full-scale WTP was investigated (Ternes *et al.*, 2002). The APIs (bezafibrate, clofibric acid, diclofenac, carbamazepine and primidone) were investigated for biodegradation and sorption in bench scale studies. Only a small reduction in the concentration of APIs occurred due to biodegradation and sorption in bench tests, although in typical water treatment conditions higher removal might occur. Pilot and bench scale tests for API removal sometimes worked better than full scale facilities due to lower complexity of the bench scale systems.

Two full scale WTPs treating surface water were studied (Ternes *et al.*, 2002). WTP1 used pre-ozonation, flocculation, ozonation and GAC filtration while WPT2 used flocculation and GAC filtration and separately performs artificial groundwater recharge using bank filtration and slow sand filtration. In contrast to Snyder *et al.*, (2007) the API removal at each stage of the process was measured. Initial visits to WTP1 and WTP2 investigated the removal of clofibric acid (herbicide and metabolite clofibrate), diclofenac and carbamazepine. Flocculation was ineffective for both WTPs as no observable removal occurred. In WTP1 pre-ozonation removed >90 % carbamazepine, reduced diclofenac below the limit of quantification (LOQ) but had no effect on clofibric acid. Main ozonation reduced carbamazepine below the LOQ and halved the clofibric acid concentration. The final GAC filtration removed any clofibric acid below the LOQ. In WTP2 the influent from flocculation was filtered using GAC which reduced the carbamazepine and diclofenac below the LOQ while the clofibric acid concentration was halved. This is significant as it demonstrates that a GAC can achieve equivalent performance to ozonation (the DOC values for WTP1 and WTP2 were similar). A subsequent test of WPT2 later in the year showed API concentrations in the effluent twice that of the earlier study. The GAC removed all of the diclofenac and >90 % removal of carbamazepine at this higher concentration.

Perozonation (O_3/H_2O_2) is an AOP for API removal. The H_2O_2 addition is intended to increase the $^{\bullet}OH$ production from O_3 and thus act as an unselective oxidant to complement the specific oxidation properties of O_3 which target unsaturated hydrocarbons and electron transfer reactions (e.g. reactions with phenolate ions). A comparison of O_3 and O_3/H_2O_2 for API degradation (clofibric acid, ibuprofen and diclofenac) removal in surface water has been studied (Zwiener and Frimmel, 2000). Both river and deionised water were used to investigate the pollutant removal and different ratios and gradually rising

concentrations of O_3: H_2O_2 were investigated. Degradation of diclofenac was effective at low O_3 concentrations but there was very little degradation of clofibric acid and Ibuprofen. The addition of H_2O_2 to the O_3 increased API removal significantly. At the highest concentration of O_3 and H_2O_2 (5 mg/L and 1.8 mg/L) >98 % of all the pollutants were degraded, indicating that the O_3/H_2O_2 combination can be very effective for degradation in a natural water matrix typically used for preparing drinking water. A feature of note was that the effective O_3 dose was the same as the dissolved organic carbon concentration in the water indicating that dissolved organic carbon was being oxidized by the O_3. The paper did not discuss the cost associated with the use of H_2O_2 which would increase treatment cost and might not be cost effective if it did not promote more efficient use of the O_3.

1.1.2 Removal of pharmaceuticals from wastewater

Literature on the release of APIs into the environment is focused on APIs in effluent from municipal wastewater. APIs in this effluent are the main source of APIs in surface water. A schematic of a typical wastewater treatment process is shown in Figure 1-3. This consists of a primary treatment or screening stage where large debris and grit are removed. This step may also include fat oils and grease removal, pH adjustment, hydraulic flow equalization, temperature adjustment and an initial sedimentation stage depending on local plant conditions/requirements. Secondary treatment is designed to lower the biological content of the wastewater: biological oxygen demand (BOD). The most common type of secondary wastewater treatment is activated sludge type processes. The wastewater flows to an aeration tank containing microorganisms that oxidise the wastewater. This suspension is then pumped to a settling tank where the microorganisms settle and are removed as sludge or re-circulated back into the aeration tank. The super latent from the settling tank is discharged or flows to a tertiary treatment step where nutrients and/or micro-pollutants are removed. At this stage AOPs could be used to remove APIs.

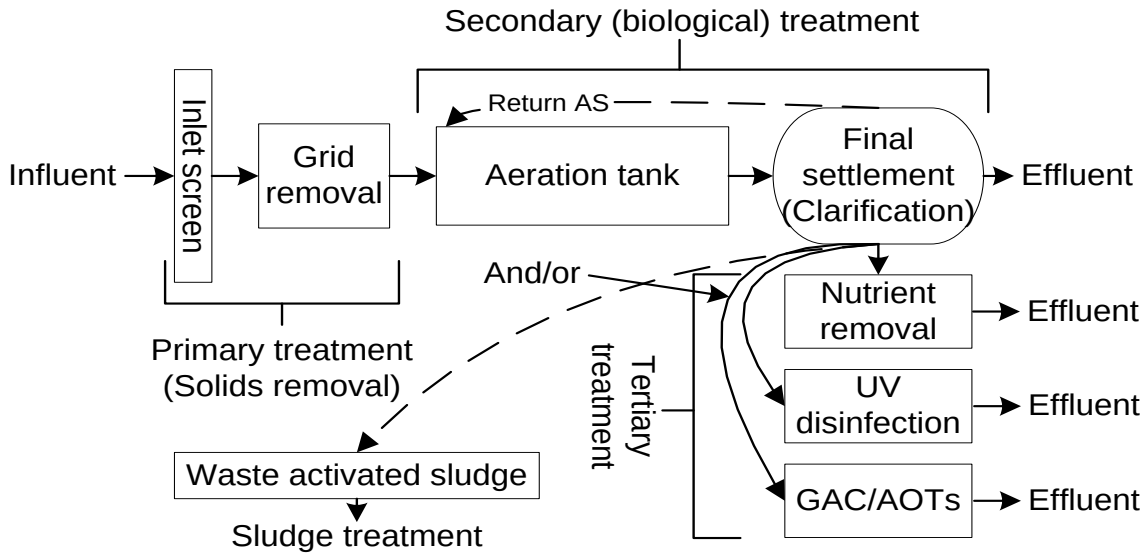

Figure 1-3 Diagram of typical activated sludge WWTP process with treatment stages indicated (Grover *et al.*, 2011).

A critical review of API removal by different water treatment technologies analysed over 40 published studies on 100 pilot- and full-scale WWTPs or treatment configurations Oulton *et al.*, (2010). The review included 140 compounds with 1500 data points related to site specific pharmaceutical and personal care products (PPCP) concentrations in the influents and effluents of specific treatment processes. The analysis included plants that used conventional activated sludge and other unconventional designs; membrane bioreactors (MBRs), sand filtration, ultra-, micro-, and nano-filtration, reverse osmosis, activated carbon, and chemical oxidation via ozonation for water treatment. Treatment efficiencies varied for APIs, for example, in conventional treatment ibuprofen was removed by greater than 1-$\log_{10}$ (90 %); in contrast antiepileptic carbamazepine is barely removed as influent and effluent concentrations are almost identical. Removal efficiency also varies between technologies. Conventional activated sludge demonstrated an average removal rate of 61 % for all APIs. Proponents of MBR technology claim it offers significant improvement compared to activated sludge with an average API removal rate of 86 %. However these results vary significantly between studies and range of values of these systems is the same as activated sludge (Verlicchi *et al.*, 2012). Even if MBR does not remove more APIs, they possess other advantages such as higher solids removal and high solid retention times (SRT) within compact reactor volumes which improves pollutant removal (Clara *et al.*, 2005).

Technologies intended as a tertiary "*polishing*" step after primary and secondary treatments were also reviewed by Oulton *et al.*, (2010). Ozonation is effective for API removal in a wastewater matrix and can degrade species such as carbamazepine which are recalcitrant to conventional biological degradation. Activated carbon (AC) has not been used for treating raw wastewater as it would become saturated very quickly with the organic matter in the wastewater. The results surveyed were from a test facility treating high total organic carbon (TOC) wastewater. AC was successful at removing APIs in this matrix but performance hinged on the use of fresh AC with frequent regeneration. Removal by membrane technologies varied depending on membrane type. Microfiltration membranes outperformed ultrafiltration membranes, while nanofiltration and reverse osmosis performed the best with average removal rates >98 %. The issue of membrane fouling and the treatment of concentrates (the rejected water containing a higher concentration of pollutants and minerals) were not investigated. In contrast, ultrafiltration was found to have low effectiveness as studies using it removed on average >15 % of the APIs in the influent as the pores of these membranes are too large to exclude APIs. The results showing that microfiltration is better than ultrafiltration appear contradictory; however, this is like due to the low number of studies for these technologies.

While Oulton *et al.*, (2010) provides a broad overview it is necessary to look more closely at specific studies to get an idea of the different levels of pharmaceutical removal in a variety of settings and WWTPs. Table 1-3 details a selection of studies investigating removal rates of APIs in WWTPs. In some cases the concentration of API in the effluent is higher than the influent which can be caused by several effects, some of which are described below. API loads into a WTTP will vary depending on the time of day, day to day and season to season. Given that a WWTP may have a hydraulic retention time (HRT) of many hours, an increase in APIs in the influent would not appear in the effluent for some time and possibly not during the sampling period and vice versa. A composite sample might reduce this risk but only if the flow of the API into the WWTP is constant over the sampling period. Matrix effects can also influence the relative concentrations of compounds in the influent and effluent. Most mass spectrometry studies use electrospray ionisation to transfer the compound of interest into the gas phase and to charge the analyte if it is not already in a charged state. Matrix effects "*are the alteration of ionization efficiency by the presence of coeluting substances*" and cause signal suppression making the concentration of analyte appear lower than it is (Taylor, 2005). The results will be affected by the

different matrix in the effluent compared to the influent. Sample treatment is also an issue. The influent will contain a larger amount of solids than the effluent and filtering the samples may remove API that is adsorbed onto the solids. A compound may not appear in the influent because it has been conjugated during metabolism and can then be cleaved to release the parent compound during the wastewater treatment process (Lacey *et al.*, 2008).

The removal efficiencies of WWTPs vary between study and analyte. It is necessary to consider the details of several studies to appreciate these differences (Table 1-3). Several typical studies are discussed below. Six Italian activated sludge WWTPs were studied for the removal of APIs using 24h composite samples (Castiglioni *et al.*, 2006). An API load was determined by analyzing for 26 APIs, normalisied and expressed as g/day/1000 inhabitants. Removal efficiencies varied from <0 i.e. the API load in the effluent was higher than the influent - to 64 % removal, but were generally <40 %.

The treatment of influent by a pilot scale MBR and a municipal activated sludge WWTP (WWTP1) with nitrification and denitrification capability was investigated (Clara *et al.*, 2005). Two other plants were included for comparison: a highly loaded plant used for reducing carbonaceous (BOD) loading only (WWTP2) and a low-loaded plant designed for nutrient removal (WWTP3). Comparable effluent API concentrations and removal rates were observed in the conventional WWTPs and the MBR. The total removal rates varied between APIs (Table 1-3). The carbamazepine concentration was not reduced while ibuprofen and bezafibrate were reduced by greater than 90 % but this removal rate varied between WWTPs.

In an Irish context APIs have been sampled in three municipal WWTPs in the greater Dublin area with population equivalents (PE) of 60,000, 90,000 and 1.7 million (Lacey *et al.*, 2008). The range of APIs found in both the influent and effluent is reported in Table 1-3. Of the 20 APIs investigated, 10 could be detected above the limit of quantification (LOQ) in the influent and 9 in the effluent. Nimesulide, indomethacin, gemfibrozil, trimethoprim and clotrimazole are detected in both the influent and effluent while the other APIs appear either in the influent or the effluent but not both. This study demonstrates that APIs are emerging pollutants in an Irish context and that biological processes in the WWTP can alter APIs metabolites during wastewater treatment releasing the parent (unmodified) APIs in WWTP effluent.

Table 1-3 Removal of selected pharmaceuticals using activated sludge type processes.

Pharmaceutical class	Pharmaceutical	Median influent (ng/L)	Mean influent (ng/L)	Median effluent (ng/L)	Mean effluent (ng/L)	Reference
Antibiotics	Amoxicillin	190		n.d.		(Watkinson *et al.*, 2007)
		13 mg/d/1000 pop		n.d.		(Castiglioni *et al.*, 2006)
	Cefaclor	500		n.d.		(Watkinson *et al.*, 2007)
	Cephalexin	4600		n.d.		(Watkinson *et al.*, 2007)
	Ciprofloxacin	3800		640		(Watkinson *et al.*, 2007)
		259 mg/d/1000 pop		97 mg/d/1000 pop		(Castiglioni *et al.*, 2006)
	Clarithromycin	21 mg/d/1000 pop		55 mg/d/1000 pop[a]		(Castiglioni *et al.*, 2006)
	Clindomycin	2		5		(Watkinson *et al.*, 2007)
	Enrofloxacin	10		10		(Watkinson *et al.*, 2007)
	Lincomycin	3.4 mg/d/1000 pop		5.4 mg/d/1000 pop[a]		(Castiglioni *et al.*, 2006)
		60		50		(Watkinson *et al.*, 2007)
	Monensin	10		25 [a]		(Watkinson *et al.*, 2007)
	Nalidixic acid	n.d.		55 [a]		(Watkinson *et al.*, 2007)
	Norfloxacin	170		25		(Watkinson *et al.*, 2007)
	Ofloxacin	360 mg/d/1000 pop		233 mg/d/1000 pop		(Castiglioni *et al.*, 2006)
	Penicillin V	50		30		(Watkinson *et al.*, 2007)
	Roxithromycin		WWTP1: 69		31	(Clara *et al.*, 2005)
			WWTP2: 78		57	(Clara *et al.*, 2005)
			WWTP3: 25		45	(Clara *et al.*, 2005)
	Spiramysin	4.8 mg/d/1000 pop		35 mg/d/1000 pop		(Castiglioni *et al.*, 2006)
	Sulfamethoxazole	n.d.		<166-<553 [a]		*(Lacey *et al.*, 2008)
		65 mg/d/1000 pop		10 mg/d/1000 pop		(Castiglioni *et al.*, 2006)
		360		270		(Watkinson *et al.*, 2007)
		145		50		(Clara *et al.*, 2005)
	Sulphathiazole	2		n.d.		(Watkinson *et al.*, 2007)
	Trimethoprim	<171-< 57		<67-<360		*(Lacey *et al.*, 2008)

Pharmaceutical class	Pharmaceutical	Median influent (ng/L)	Mean influent (ng/L)	Median effluent (ng/L)	Mean effluent (ng/L)	Reference
Antibiotics	Trimethoprim	340		50		(Watkinson *et al.*, 2007)
Lipid regulators	Gemfibrozil	<26-<86		<32-<330		*(Lacey *et al.*, 2008)
	Bezafibrate		WWTP1: 1960		n.d.	(Clara *et al.*, 2005)
			WWTP2: 7600		4800	
			WWTP3: 1550		715	
		50 mg/d/1000 pop		29mg/d/1000 pop		Castiglioni et al., 2006
	Clofibric acid		<222-<740		n.d.	*(Lacey *et al.*, 2008)
Antiepileptics	Carbamazepine		n.d.		<163–<881[a]	*(Lacey *et al.*, 2008)
		12 mg/d/1000 pop		28mg/d/1000 pop		(Castiglioni *et al.*, 2006)
			WWTP1: 1850		1594	(Clara *et al.*, 2005)
			WWTP2: 670		690	
			WWTP3: 325		465	
			Pre-GAC 70ng/L		50ng/L	(Grover *et al.*, 2011)
Antiphlogistics (NSAID)	Diclofenac		n.d.		<743-<2478	*(Lacey *et al.*, 2008)
			WWTP1: 3250		1536	(Clara *et al.*, 2005)
			WWTP2: 1400		1300	
			WWTP3: 905		780	
			Pre-GAC 12 ng/L		<LOD	(Grover *et al.*, 2011)
	Ibuprofen		WWTP1: 1480		nd	(Clara *et al.*, 2005)
			WWTP2: 2300		2400	
			WWTP3: 1200		24	
			< 760-3204		n.d.	*(Lacey *et al.*, 2008)
		122 mg/d/1000 pop		28 mg/d/1000 pop		(Castiglioni *et al.*, 2006)
Antispasmodic	Mebeverine		Pre-GAC 38 ng/L		5 ng/L	(Grover *et al.*, 2011)
β-Blockers	Atenolol	494 mg/d/1000 pop		281 mg/d/1000 pop		(Castiglioni *et al.*, 2006)
	Propranolol		Pre-GAC 50 ng/L		40 ng/L	(Grover *et al.*, 2011)
Keratolytic†	Salicylic acid		351–9172		<115	*(Lacey *et al.*, 2008)

Pharmaceutical class	Pharmaceutical	Median influent (ng/L)	Mean influent (ng/L)	Median effluent (ng/L)	Mean effluent (ng/L)	Reference
Diuretic	Furosemide		<313–490		n.d. [a]	*(Lacey *et al.*, 2008)
		277 mg/d/1000 pop		195 mg/d/1000 pop		(Castiglioni *et al.*, 2006)
	Hydrochlorothiazide	354 mg/d/1000 pop		415 mg/d/1000 pop		(Castiglioni *et al.*, 2006)
Statins	Pravastatin		<72–<239		n.d. [a]	*(Lacey *et al.*, 2008)
NSAID	Nimesulide		<2–441		<3–450	*(Lacey *et al.*, 2008)
	Indomethcin		<263–<877		<238–<792	*(Lacey *et al.*, 2008)
			Pre-GAC 8 ng/L		<LOD	(Grover *et al.*, 2011)
	Mefenamic		n.d.		540–1050 [a]	*(Lacey *et al.*, 2008)
Antifungal	Clotrimazole		<34–232		34–475	*(Lacey *et al.*, 2008)
ACE inhibitor	Enalapril	31 mg/d/1000 pop		1.2 mg/d/1000 pop		(Castiglioni *et al.*, 2006)
Hormone	Estrone	5.4 mg/d/1000 pop		6.4 mg/d/1000 pop		(Castiglioni *et al.*, 2006)
	Estrone		Pre-GAC 2 ng/L		1 ng/L	(Grover *et al.*, 2011)
	17β-estradiol		Pre-GAC 2 ng/L		<LOD	
	17 β – ethinylestradiol		Pre-GAC 1 ng/L		<LOD	
H_2 receptor antagonists	Ranitidine	188 mg/d/1000 pop		96 mg/d/1000 pop		(Castiglioni *et al.*, 2006)
β2-adrenergic receptor agonist	Salbutamol	4.3 mg/d/1000 pop		4 mg/d/1000 pop		(Castiglioni *et al.*, 2006)
Contrast medium	Iopromide		WWTP2: 3840		5060	(Clara *et al.*, 2005)
			WWTP3: 26		250	

Concentrations of APIs in effluent greater than influent due to matrix and other effects.
n.d.: not detected, Pop: population.
*The values from Lacey et al. (2008) are maximum and minimum values. An "<" bracket indicates that the value is below the LOD, while a second "<" bracket indicates that the concentration is below the LOQ.
† skin peeling agent

Pharmaceutical production facilities are a poorly investigated source of APIs in the environment either from outlets at WWTPs attached to the production facility or via discharges from the production facility into sewers which flow into municipal WWTPs (Deegan, 2011, Enick and Moore, 2007, Phillips *et al.*, 2010). This wastewater presents a challenging composition as it can contain solvents, catalysts, reactants, some intermediates, raw materials and APIs (Sreekanth *et al.*, 2009). It might also have high COD, high BOD and high COD: BOD ratio, extremes of pH and the presence of toxic compounds e.g. cyanide (Suman Raj and Anjaneyulu, 2005). Regulation of the production facility varies between countries and centred around the quality of the wastewater before it is permitted to be released. In the US and Europe the majority of discharge licences focus on BOD, COD, suspended solids and pH without any control on the release of specific APIs, intermediates, raw materials or other recalcitrant substances (Joakim Larsson and Fick, 2009). Ireland appears to be the only jurisdiction where specific regulatory limits have been established for APIs (estrogentic compounds) (Helmig *et al.*, 2005). These regulatory licence limits focused on endocrine disrupting chemicals (EDCs) such as estrone, ethinyl estradiol and 17-β-estradiol. The presence of other APIs remains largely unmonitored.

An AS WWTP using GAC filtration as a polishing step has been investigated (Grover *et al.*, 2011). The presence of steroidal estrogens (17β-estradiol and 17 β-ethinylestradiol) and five APIs was examined before and after treatment by a GAC filter system. The concentrations of APIs in pre- and post-GAC treatment are shown in Table 1-3. The removal of the estrogens was very effective; however the removal of the APIs varied. Diclofenac and indomethacin were reduced by 98 % while propranolol and carbamazepine were reduced by 17 % and 23 % respectively. However, the study did have the opportunity to sample the river downstream of the WWTP before and after the addition of the GAC plant. The concentration of estrogens and APIs in the water downstream (after accounting for dilution) dropped in the same proportions as they were removed by the GAC although there was a lag (approximately three months) for some molecules e.g. estrone as they took a longer time to degrade or be washed away.

The influent and effluent of a pharmaceuticals wastewater treatment plant were sampled and analysed for the APIs manufactured in the pharmaceutical production facility that it served: famotidine, solifenacin succinate and tamsulosin hydrochloride (Deegan, 2011). Twice weekly samples were taken over a twenty six

week period and analysed for the three APIs. Famotidine, solifenacin succinate and tamsulosin hydrochloride were detected in the 85 %, 65 % and 88 % of the influent samples respectively. The average concentration of famotidine, solifenacin and tamsulosin in the influent was 1.6 mg/L, 0.039 mg/L and 0.005 mg/L and effluent concentrations were 2.6 mg/L, 0.004 mg/L and 0.028 mg/L respectively. The effluents are discharged into the municipal sewer for further treatment at a municipal WWTP. The treatment options for pharmaceutical industry wastewater are reviewed elsewhere (Deegan *et al.*, 2011).

The Fenton reaction has been studied extensively for wastewater treatment (Comninellis *et al.*, 2008, Sirtori *et al.*, 2009). The Fenton process (Neyens and Baeyens, 2003) consists of the generation of hydroxyl radicals ($^{\bullet}OH$) by the reaction between ferrous ions and H_2O_2 (Fenton's reagent), according to eq (1).

$$Fe^{2+} + H_2O_2 \rightarrow Fe^{3+} + OH^- + {}^{\bullet}OH \quad (1)$$

Light also reacts with H_2O_2 to create hydroxyl radicals:

$$H_2O_2 \xrightarrow{h\nu} 2OH^- \quad (2)$$

In a photo-Fenton reaction light adsorption aids the conversion of Fe^{3+} back to Fe^{2+} which also creates additional $^{\bullet}OH$.

$$Fe^{3+} + H_2O \xrightarrow{h\nu} Fe^{2+} + H^+ + {}^{\bullet}OH \quad (3)$$

The additional $^{\bullet}OH$ can degrade organic contaminants but it also allows the Fe^{2+} to undergo additional reactions with H_2O_2. Fe^{2+} at low pH (2 - 4) absorbs light > 400nm and therefore allows a great proportion of the solar spectrum (Figure 1-4) to be used removing the need for UV lamps (Malato *et al.*, 2002). Fenton reactions operate at or near room temperature and normal pressure. Intricate apparatus are not required for its use, therefore it is claimed there will be a smooth transition from laboratory to full scale wastewater treatment (Kavitha and Palanivelu, 2004). Disadvantages of Fentons reagent include the need to remove the iron salts following treatment, requirement for pH neutralisation, sludge disposal and reagent costs.

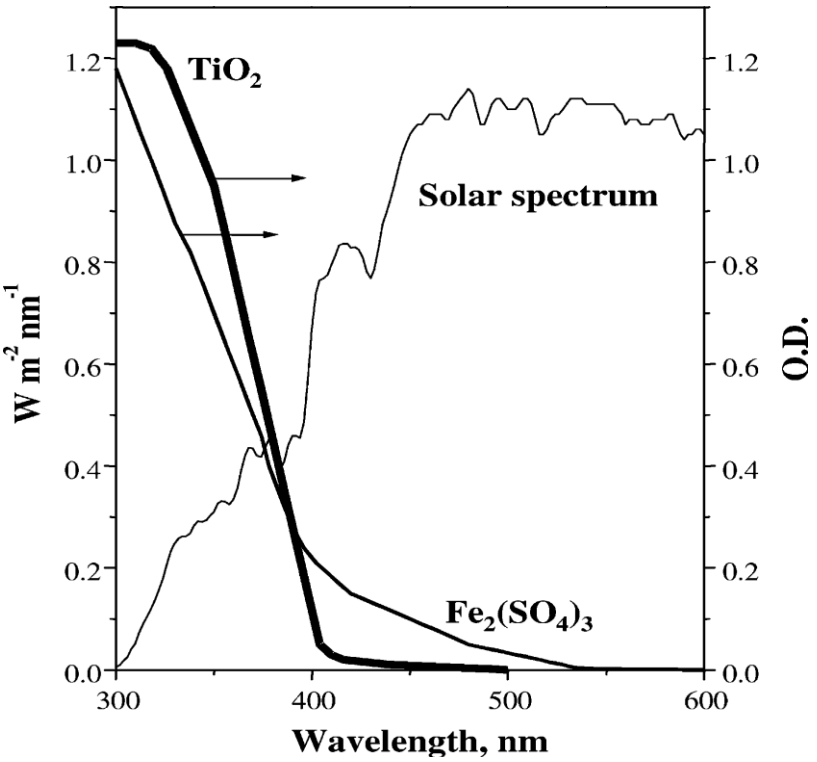

Figure 1-4 Typical solar spectrum at Plataforma Solar de Almería in Spain and the optical density (O.D., optical path length 1cm) of a $Fe_2(SO_4)_3$ solution (0.25mM as Fe) and TiO_2 powder (Malato *et al.*, 2002).

Important factors in the optimisation of Fenton conditions include pH, temperature, and concentration of hydrogen peroxide, iron salts and pollutant(s). The ratio of iron to hydrogen peroxide is important. If the concentration of Fe^{2+} exceeds the H_2O_2 concentration chemical coagulation will occur, resulting in the settling out of iron salts and pollutants rather than chemical oxidation (Deegan, 2011).

Following detection of all three APIs in industrial wastewater at a pharmaceutical production facility (Deegan, 2011) photo-Fenton oxidation was investigated as a possible removal method. Fe^{2+} and H_2O_2 concentrations were optimised and kinetic results evaluated. The reactant controls: photolysis, Fe^{2+} and Fe^{2+}/light on the removal of the three APIs showed negligible removal. A H_2O_2 concentration of twenty micro molar degraded approximately 18 % of the famotidine (0.1 mM) in solution, while tamsulosin and solifenacin showed no degradation at 5 mM H_2O_2 in the light or dark. Famotidine reduction using Fenton reagent (Fe^{2+} and H_2O_2) was 32 % while photo-Fenton reduction was 38 %. Fenton reagent reduced the tamsulosin concentration by 96 %, while photo-Fenton reduced the concentration by 99 % after 10min of contact time. Fenton reagent reduced the solifenacin

concentration by 100 % after 10 min of contact time. These studies used deionised water rather than wastewater so studies in a wastewater matrix would be required to develop the Fenton process for the treatment of pharmaceutical production facility wastewater.

Olive mill wastewater has been treated by solar photocatalysis and solar photo-Fenton (Gernjak *et al.*, 2004). This wastewater is problematic because it has high TOC, BOD, suspended solids and contains polyphenols which can be toxic to bacteria in WWTPs. High suspended solids was reduced with a flocculation agent as a pre-treatment step and this improved light transmission. Two photoreactor types were used; a compound parabolic collector and a falling film reactor. The former was used for TiO_2 studies (see Section 1.2). It was found that 1 g/L TiO_2 reduced the COD from 89 mg/L to 78 mg/L with no change in the phenol index compared to photo-Fenton which reduced the COD from 81 mg/L to 21 mg/L and reduced the phenol index from 3.8 to 0.5. The concentration of Fe^{2+} was low at 5mM but the concentration of H_2O_2 was very high at 20 g/L which would make the system expensive to operate as H_2O_2 costs typically contribute 50 % of the cost of photo-Fenton. The falling film reactor operated at a lower temperature which prevented the decomposition of the H_2O_2 but the falling film did not remain homogeneous during strong wind. Wastewater from the same facility was not used in both reactors simultaneously so a direct comparison cannot be made.

Herbicides and APIs degradation using a mild (low Fe and TiO_2 content) photo-Fenton and TiO_2 photodegradation in two compound parabolic collector solar plants each with 11 L volume has been undertaken (Klamerth *et al.*, 2009). Nine compounds (100 μg/L) were dissolved using methanol which added a TOC of 12 mg/L. After Fenton the TiO_2 was added and homogenized for 15 min before illumination. In terms of initial reaction rates photo-Fenton performed significantly better than TiO_2 e.g. the initial caffeine reaction rate was 3.4 and >11.3 for TiO_2 and photo Fenton respectively. It may not be a suitable comparison as kinetic analysis of this kind will favor Fenton. This study demonstrated that photo-Fenton can perform well at normal pH in hard water.

Fenton and photo-Fenton has been used to regenerate AC that is saturated with substrate in order to recover its adsorption capacity (Muranaka *et al.*, 2010). The process was intended to improve the removal efficiency of the Fenton process by concentrating the pollutant (phenol) on the AC and then regenerating the AC to its

original adsorption capacity. Two different ACs designated "L27" and "S23" were investigated for regeneration. After four consecutive regeneration cycles 50 % and >20 % of the original adsorption capacity was recovered for L27 and S23 respectively. Two regeneration cycles achieved 30 – 40 % and 10 % adsorption capacity recover for L27 and S23. A photo-Fenton regeneration of L27 using a UVC lamp shows almost complete mineralization (contrary to "*dark*" Fenton) and improved the recovery of AC adsorption capacity to 56 % after two cycles. The optimum Fe^{2+} and H_2O_2 concentrations for regenerating the AC were double the stoichiometry concentrations for mineralising phenol in solution suggesting that the regeneration process is less efficient than Fenton and photo-Fenton in solutions of the same substrate. Combined with the inability to recover more than 50 % of the adsorption capacity suggests that the process has poor economics.

1.2 TiO_2 photocatalysis

In recent times considerable attention has focused on the safety and efficiency of water treatment technology (Choi *et al.*, 2007, Hrudey, 2009). Conventional water treatment processes such as ozonolysis and chlorination create disinfection by-products (DBP) such as bromate and trihalomethanes respectively, which have health risks (Boorman *et al.*, 1999, Hamidin *et al.*, 2008, Hrudey, 2009, Nieuwenhuijsen *et al.*, 2000, von Gunten and Hoigne, 1994). In order to avoid such problems attention is now being focused on AOPs including photocatalysis using TiO_2. Photodegradation is defined by the International Union of Pure and Applied Chemistry (IUPAC) as "*the photochemical transformation of a molecule into lower molecular weight fragments, usually in an oxidation process*" (Verhoeven, 1996). This process is usually too slow and inefficient to be useful in water treatment and requires the addition of a photocatalyst. These catalysts are activated by light and the resulting photocatalytic reactions are defined by IUPAC as "*catalytic reaction involving light absorption by a catalyst or by a substrate*" (Verhoeven, 1996). Several types of photocatalysts are available but most scientific effort is concentrated on titanium dioxide due to its high photocatalytic activity, chemical stability, non-toxic nature and relatively low price (Fujishima *et al.*, 2000).

When titanium dioxide is irradiated with light that exceeds its bandgap energy (3.2 eV for anatase) i.e. UV light (wavelength <385 nm for anatase), electron-hole

pairs are created. The electron-hole pairs degrade organic pollutants on the catalyst surface either directly or indirectly in a water solution by creating hydroxyl and superoxide radicals (Hoffmann *et al.*, 1995). An energy diagram of the creation of electron hole pairs is shown in Figure 1-5. This diagram demonstrates the various steps in the photocatalysis process. The first step is the formation of charge carriers (electron hole pairs) by a photon (1). The most likely next step is electron hole pair recombination to liberate heat given that the quantum yield for the reaction is only about 0.04–0.05. This means that the electron hole pair recombine 96 % of the time (Zhou and Smith, 2002) (2); If recombination does not occur, an oxidative pathway by a valence-band hole will occur (3); A reduction pathway by a conduction-band electron to complement step (3) at (4); Further ROS and photocatalytic reactions yield intermediates and potentially mineralisation products (5). It is also possible for the trapping of a conduction-band electron in a surficial molecule to yield Ti(III) (6) and trapping of a valence-band hole at a surficial titanol group (7).

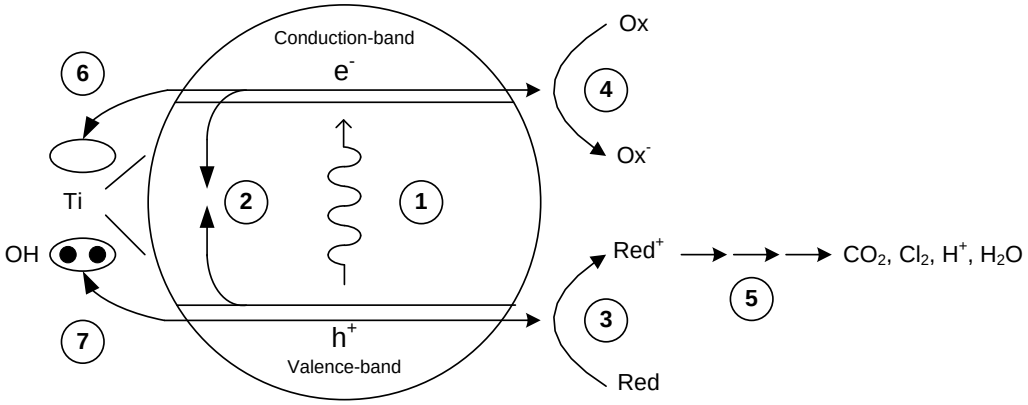

Figure 1-5 Primary steps in the photoelectrochemical mechanism (Hoffmann *et al.*, 1995, Peralta-Hernández *et al.*, 2007).

The chemical reactions occurring at the catalyst surface (steps 3 and 4 in Figure 1-5) have been summarised (Benabbou *et al.*, 2007, Kim *et al.*, 2005). An electron is extracted from the valence band (VB) to the conduction band (CB). This process results in a positive region in the VB Hole (h^+) and a free electron (e^-) in the CB. (Eq. 4):

$$TiO_2 \xrightarrow{h\nu} TiO_2 + e^-(CB) + h^+(VB) \quad (4)$$

The hole at the catalyst surface reacts with hydroxyl ions (OH^-) and adsorbs water to form hydroxyl free radicals ($^{\bullet}OH$) (Eqs. 5 and 6):

$$TiO_2(h^+) + OH^- \longrightarrow TiO_2 + {}^{\bullet}OH \quad (5)$$

$$TiO_2(h^+) + H_2O_{ads} \longrightarrow TiO_2 + {}^{\bullet}OH + H^+ \quad (6)$$

The CB electron reduces oxygen to the superoxide ion: $O_2^{\bullet-}$ (Eq 7). This reaction prevents the e^-/h^+ recombination, in the absence of other electron acceptors (pollutants).

$$O_2 + e^- \longrightarrow O_2^{\bullet-} \quad (7)$$

The further reduction of $O_2^{\bullet-}$ produces H_2O_2, as described in Eq. (8)

$$O_2^{\bullet-} + e^- + 2H^+ \longrightarrow H_2O_2 \quad (8)$$

The superoxide ion and its protonated form subsequently dismute to yield hydrogen peroxide or a peroxide anion (Eq's. 9–11):

$$O_2^{\bullet-} + H^+ \longrightarrow HO_2^{\bullet} \quad (9)$$

$$O_2^{\bullet-} + 4HO_2^{\bullet} \longrightarrow 2{}^{\bullet}OH + 3O_2 + H_2O_2 \quad (10)$$

$$2HO_2^{\bullet} \longrightarrow O_2 + H_2O_2 \quad (11)$$

The addition of H_2O_2 can increase the photodegradation rate under certain conditions, probably by the formation of $^{\bullet}OH$ radicals via the Harber–Weiss reaction (Eq. 12) or through the reduction of H_2O_2 by the CB e^- (Eq. 15)

$$O_2^{\bullet-} + H_2O_2 \longrightarrow {}^{\bullet}OH + OH^- + O_2 \quad (12)$$

$$H_2O_2 + e^- \longrightarrow {}^{\bullet}OH + OH^- \quad (13)$$

Recombination of $^{\bullet}OH$ radicals can also lead to the production of hydrogen peroxide (Eq. 14):

$$2{}^{\bullet}OH \longrightarrow H_2O_2 \quad (14)$$

It is suggested that H_2O_2 production ceases in the absence of O_2. Of all the ROS generated the $^{\bullet}OH$ radical is the most important oxidant species since it has the most positive redox potential (see Table 1-4).

Table 1-4 Redox potential for oxidizing agents in water.

Oxidative species	Redox potential (V) vs. NHE	Redox potential relative to chlorine
Fluorine (F^-)	3.06	2.25
Hydroxyl radical ($^{\bullet}OH$)	2.80	2.05
Oxygen (atomic)	2.42	1.78
Ozone (O_3)	2.08	1.52
Hydrogen peroxide (H_2O_2)	1.78	1.30
Permanganate (MnO_4^-)	1.69	1.24
Hypochlorite (ClO^-)	1.49	1.1
Chlorine (Cl^-)	1.36	1.00
Oxygen (molecular)	1.23	0.9

Source: (Al-Kdasi *et al.*, 2004, Zhou and Smith, 2002).

The original research on the photocatalytic properties of TiO_2 focused on solar energy conversion using an electrochemical photocell with TiO_2 and platinum electrodes (Fujishima *et al.*, 2000). Under illumination with near UV light photoelectrolysis occurred resulting in the splitting of water into hydrogen and oxygen. The hydrogen yield from this experiment was too low to be of practical use although there are continuing developments in this field (Ni *et al.*, 2007). In the late 1970s the ability of TiO_2 to oxidise organic matter was applied to cyanide degradation and this led to a substantial increase in research interest in the environmental applications of photocatalysts (Fujishima and Zhang, 2006). This research focused on air purification especially the photodegradation of volatile organic carbons (VOCs) and nitrogen oxides (NO_x), water pollutants and microorganisms (Hoffmann *et al.*, 1995). Photocatalysts were commercialised in several consumer and industrial products, especially self-cleaning surfaces and air cleaning equipment/surfaces more than a decade ago (Anpo, 2000).

Titanium dioxide offers a series of advantages over other semiconductor photocatalysts: high catalyst stability, low toxicity and low cost. TiO_2 has poor adsorption of pollutants which can be considered a limitation if the concentration of pollutant is very low (Hu *et al.*, 2007, Molinari *et al.*, 2008, Zhang *et al.*, 2007).

TiO_2 occurs in several phases or polymorphs which are different arrangements of the TiO_2 crystal structure. The three polymorphic forms (Figure 1-6) of note are anatase, rutile, and brookite (Mo and Ching, 1995, Ovenstone and Yanagisawa, 1999, Wang *et al.*, 2001). Rutile is the most thermodynamically stable phase, whereas anatase and brookite are metastable and are readily transformed to rutile when heated. The phase change from anatase to rutile occurs in different temperature ranges from 600°C to 1100°C, depending on the preparation conditions, particle size, and the presence of impurities (Djaoued *et al.*, 2004, Ovenstone and Yanagisawa, 1999). The most photoactive form of TiO_2 is the anatase phase and it is widely studied due to its technological importance in various applications. The rutile phase has lower photoactivity although it has a high refractive index that is useful for optical devices (Yamabi and Imai, 2002). The basic difference between anatase and rutile is the symmetry about oxygen atoms as well as differences in the polarization of the oxygen ions (Kumar *et al.*, 2000, Smith *et al.*, 2009, Xu *et al.*, 2008).

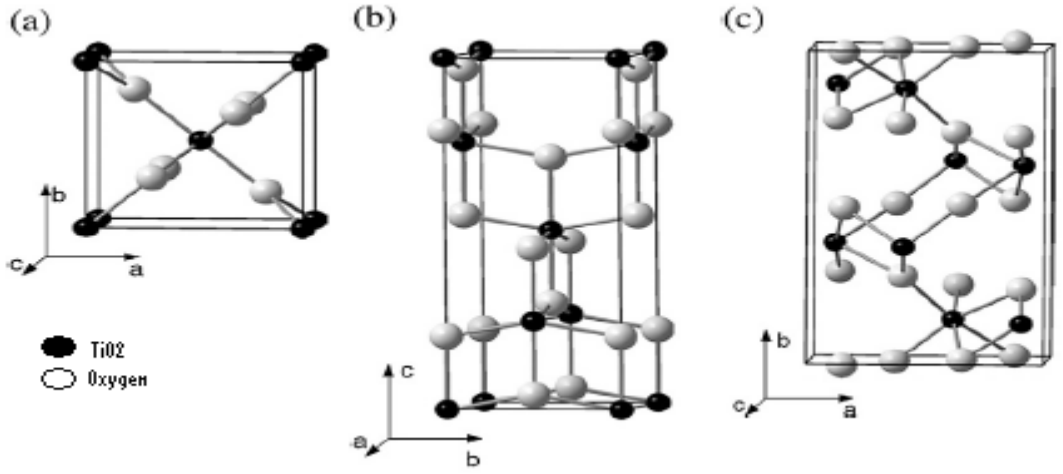

Figure 1-6 TiO_2 polymorphs (a) rutile, (b) anatase, (c) brookite (Foo and Hameed, 2010a).

One way of improving the photocatalytic performance of TiO_2 is doping. The purpose of doping is to apply a transition metal (V, Cr, Mo, Fe), lanthanide metal (La, Eu, Nd, Ce) or non-metal atom (C, N) to the TiO_2, either to alter its band gap (Begum and Farveez Ahmed, 2008) or to lower the electron-hole recombination rate (Li *et al.*, 2010, Xu *et al.*, 2008) lowering recombination of the electron hole pairs. The doped TiO_2 is an extrinsic semiconductor i.e. it has different electrical properties than an undoped or intrinsic semiconductor. Schematics of the mechanisms by which doping

decreases the band-gap of anatase TiO_2 (Serpone, 2006) is shown below (Figure 1-7). It is claimed (Zaleska, 2008) that decreasing the band gap allows $^{\bullet}OH$ to be created with lower energy photons i.e. created by light with a longer wavelength (>400 nm).

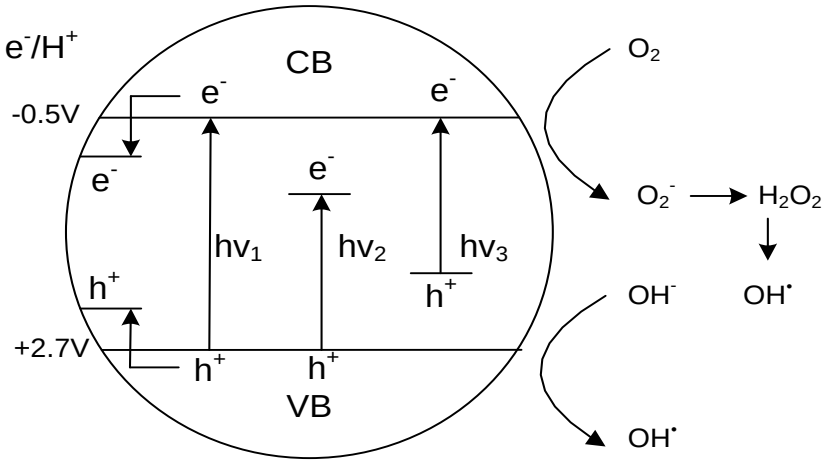

Figure 1-7 Schematic mechanism of doped TiO_2 photocatalysis. $h\nu_1$: pure TiO_2; $h\nu_2$: metal-doped TiO_2 and $h\nu_3$: nonmetal-doped TiO_2 (Zaleska, 2008).

1.3 Origin and structure of activated carbon

Activated carbon in the broadest sense is a wide range of heat treated, porous carbon-based materials. Activated carbon (AC) is defined by IUPAC as:

> "*a porous carbon material, a char which has been subjected to reaction with gases, sometimes with the addition of chemicals, e.g. $ZnCl_2$, before, during or after carbonization in order to increase its adsorptive properties*" (Fitzer *et al.*, 1995).

Another definition is that "*activated carbon is porosity (space) enclosed by carbon atoms*" (Marsh and Rodríguez-Reinoso, 2006b). AC is not an amorphous material, it is partial amorphous as it has a poorly ordered microcrystalline structure shown in Figure 1-8.

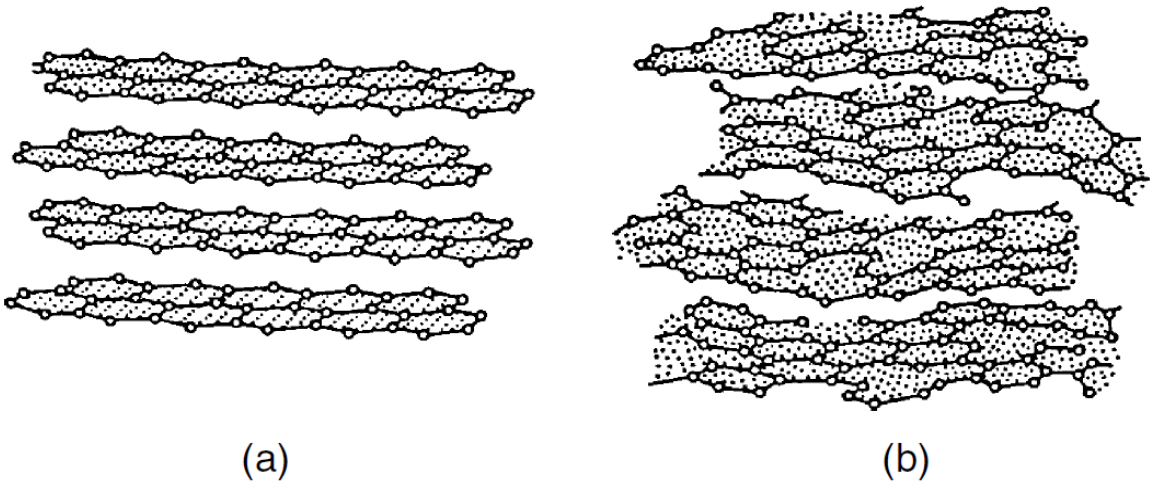

Figure 1-8 Comparison of three-dimensional crystal lattice of graphite (a) and the less ordered structure typical of AC (b) (Bansal and Goyal, 2005).

This microcrystalline structure has been described as defective graphene assemblies or alternatively stacks of aromatic sheets that differs from graphite with respect to interlayer spacing, which is 0.335 nm in the case of graphite and ranges between 0.34 nm and 0.35 nm in activated carbons. The orientation of the stacks of carbon is also less ordered in activated carbons (Bansal and Goyal, 2005).

Activated carbons have a highly developed porosity which gives them an enormous surface area (Bansal and Goyal, 2005); typically 1g of activated carbon will have a surface area between 500-3000m^2/g *et al.*, 2005, Rodríguez-Reinoso and Molina-Sabio, 1998). This value is determined by N_2 gas adsorption (Rouquerol *et al.*, 1994). It is this surface area that allows AC to adsorb large amounts of pollutants.

AC preparation follows two broad steps: the carbonisation of the carbonaceous raw material (in this work coal) at high temperatures (700 - 850°C) (Mazyck and Cannon, 2000) in an inert atmosphere and the activation of the carbonised product. During the carbonization process, most of the non-C elements such as O, H, and N are eliminated as gaseous species (CO_x, NO_x) by the pyrolysis of the parent material. The carbon atoms group themselves into stacks of flat, aromatic sheets cross-linked in a random manner in a nanocrystalline structure that chemists refer to as disordered and physicists refer to as defective layers. These aromatic sheets are irregularly arranged, which leaves free spaces. These spaces give rise to pores, which give the AC its high surface area. During carbonization these pores are filled with the tarry matter or the products of decomposition or at least blocked partially by disorganized carbon. This

pore structure in carbonized char is further developed and enhanced during the activation process, which converts the carbonized raw material into a form that contains the greatest possible number of randomly distributed pores of various sizes and shapes, giving rise to an extended and extremely high surface area of the product. The activation of the char (steam activation) uses an atmosphere of air, CO_2, or steam in the temperature range of 750°C to 900°C (Bansal and Goyal, 2005, Mazyck and Cannon, 2000).

The "activation" results in the oxidation of some of the regions within the char in preference to others, so that as combustion proceeds, a preferential etching takes place. There is considerable diversity in how the pores and pore structure of an AC are described. The pores are generally classified into micropores (widths smaller than 2 nm), mesopores (widths between 2 nm and 50 nm) and macropores (widths larger than 50 nm) (Rouquerol *et al.*, 1994). Mesopores are often expressed as a methylene blue (MB) number as it is assumed that a large molecule such as MB cannot penetrate the micropores. Micropores capacity can be expressed as an iodine number. It is assumed that iodine can penetrate into the micropores while larger molecules such as MB cannot. By comparing the iodine and methylene blue numbers of an AC it is possible to determine the relative microporosity to mesoporosity ratio. No comprehensive model of the microporious nature of carbons has been devised that can tie together all the properties of an AC (Marsh and Rodríguez-Reinoso, 2006c). The majority of papers assume the "*branched tree*" model is the structure of the AC (Figure 1-9). This model assumes that the macropores lead to mesopores which in turn lead to the micropores. It assumes that the micropores (or at least the bulk of them) do not connect to the surface and must be accessed through the other pore sizes. Critics of this model note that there is no reason to assume that the AC's pores contract from larger to smaller and it implies that parts of the carbon have no porosity (Marsh and Rodríguez-Reinoso, 2006c).

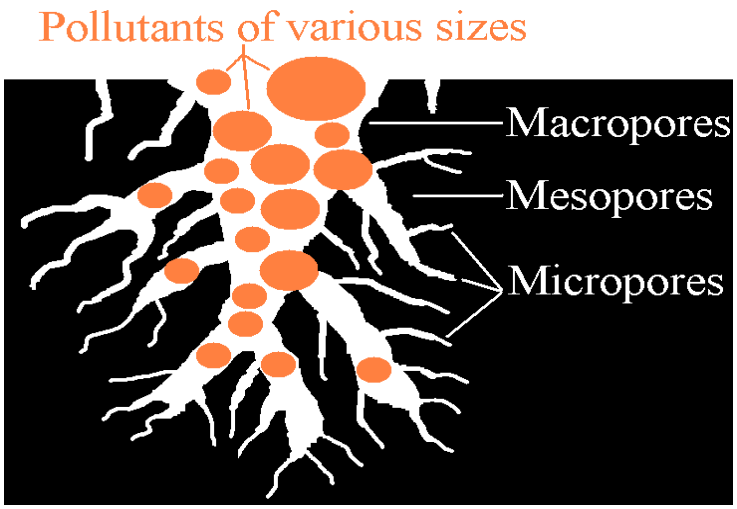

Figure 1-9 Unmodified activated carbon (Baup *et al.*, 2000, Marsh and Rodríguez-Reinoso, 2006d).

Electron spin resonance studies have shown that the aromatic sheets in activated carbons contain free radical structure or structure with unpaired electrons. These unpaired electrons are remnants of the carbonization process; due to the breaking of bonds at the edges of the aromatic sheets create edge carbon atoms. These edge carbon atoms have unsaturated valences and can interact with elements such as O, H, N, and S (present in the parent material or added by the activating agent) creating surface oxygen functionalities (SOF) (Figure 1-10).

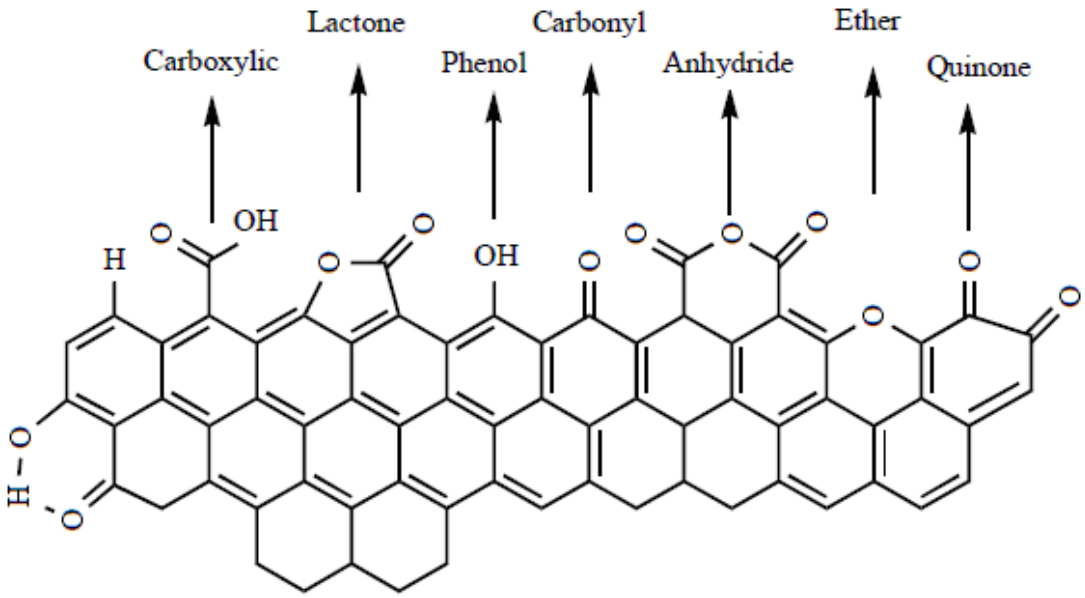

Figure 1-10 Diagram of Surface Oxygen Functionalities (SOF) on the edges of the aromatic sheets of an AC surface (Shen *et al.*, 2008).

The surface of activated carbon can be characterized into three zones: the carbon basal planes (including basal edges and crystal defects), heterogeneous surface groups (mainly SOF, but includes sulphur groups) and inorganic ash (Franz *et al.*, 2000). The majority of the adsorption sites are on the basal planes, which form more than 90 % of the carbon surface. However, the much higher activity of the heterogeneous groups can affect the overall adsorption capacity. Heteroatoms (non carbon atoms) may be combined both with peripheral carbon atoms at the corner and edges of crystallites, in intercrystalline spaces and even in defect zones of particular planes constituting the AC's crystalline structure. Most heteroatoms are grouped at the surface of the AC and they differ in terms of their reactivity. Surface bound heteroatoms are believed to adopt the character of the functional groups typical for aromatic compounds and to react in a similar way to reagents. If they are bound in the core of the crystalline structure they are often inert due to their low accessibility and interaction with local atoms (Jankowska *et al.*, 1991).

Other factors can influence the adsorption of the AC. The point of zero charge of an AC is the pH at which the AC has no net charge (Hameed *et al.*, 2009). At a pH below this, the carbon is net positively charged and above this it is negatively charged. This property significantly influences the adsorption on the carbon surface and is an important consideration for creating ACs as changes in pH will greatly influence adsorption (Khan, 2002).

The elemental composition of a typical AC has been found to be 88 % C, 0.5 % H, 0.5 % N, 1 % S, and 6 to 7 % O, with the balance representing inorganic ash constituents (Bansal and Goyal, 2005). ACs used in applications where high purity is required are typically treated - usually acid washed - to reduce the ash content as it could leach into solution. The oxygen content of an AC can vary depending on the type of raw material and the conditions of the activation process, ACs with more SOF will consequently have higher oxygen content. In theory, all carbonaceous materials can be made into AC, although the properties of the resulting AC will vary, depending on the raw material, the activating agent, and the conditions of the carbonization and activation processes.

It is worth considering how the sorbate adsorbs onto the AC. The entire process can be broken down into four steps (Kumar *et al.*, 2003) shown in Figure 1-11. The diffusion through the bulk solution is usually assumed and is not considered a step by some literature (Choy *et al.*, 2004, Nevskaia *et al.*, 1999). For this work the

four steps will be considered. The four steps can be divided into two broad processes: the crossing of the boundary layer surrounding the particle onto its surface or *external mass transfer* (steps 1 - 2) and the diffusion within the particle, *the intraparticle mass transfer* (steps 3 - 4). The first step is the diffusion of the adsorbate through the bulk liquid solution followed by mass transfer through a laminar boundary layer around the particle that is referred to as the *diffusional boundary layer* or the *film diffusion* stage of adsorption. This phenomenon occurs in adsorption but also relevant to catalysis. It is influenced by the hydraulic behaviour in the vessel (column), the surrounding area of the particle, physical properties of the solvent(s) and the molecular diffusion of the solute, particle size of the AC, but is not affected by the nature or the porosity of the GAC (as this is accounted for in the next step). The intraparticle mass transfer involves two different phenomena: *porous diffusion* (the adsorbate first diffuses in the liquid filling the pores and then is adsorbed) and *surface diffusion* (the adsorbate is first adsorbed then diffuses from one site to another).

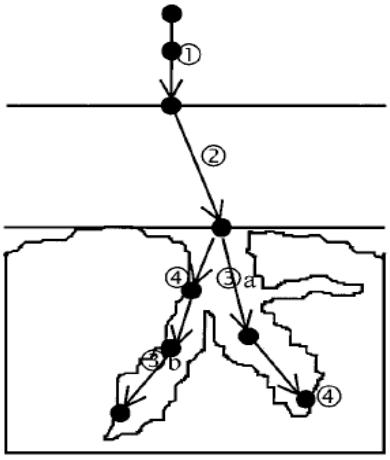

Position	Phenomenon	Coefficient
Bulk of solution	① Diffusion/Convection	Fast
Outer layer	② External Mass Transfer	k_f
GAC particle	③a Porous Diffusion	D_p
	③b Surface Diffusion	D_s
	④ Adsorption	Instantaneous

Figure 1-11 Four step model of AC adsorption in this case a GAC (Baup *et al.*, 2000).

The diffusion of the solute in the bulk fluid (Hossain and McLaughlan, 2011) (Step 1) is very fast compared to the diffusion through the outer layer and within the particle which can take a considerable time. The concentrations of the liquid bulk will be governed by the overall mass balance (the amount of adsorbed substrate vs. the equilibrium concentration) and the hydraulic mixing behaviour of the vessel. An instantaneous reversible reaction is assumed for the real adsorption step (step 4). The

liquid phase concentration of adsorbate and the adsorbate load at the carbon's surface are locally related by an equilibrium law.

Thus adsorption kinetics is governed by external mass transfer and internal diffusion and can be represented by homogeneous surface diffusion model (Abuzaid and Nakhla, 1997). Where the coefficients K_f (external mass transfer coefficient), D_p (pore diffusion coefficient) and D_s (the surface diffusion coefficient) represent the contribution of each of their phases to the adsorption kinetics. It has been noted that the contribution of D_s is 20 times as important as the D_p contribution (migration of the substrate though the pore volume) and consequently most homogeneous surface diffusion models consider only K_f and D_s.

The best AC for a particular application is usually determined empirically as there are many parameters that influence adsorption. Prediction of adsorption capacity in advance is limited to models that deal with idealized cases (Franz *et al.*, 2000). There are greater than 400 parameters of an AC that can be measured which makes it impractical to determine every property of an AC (Lever, 2010). BET isotherms using N_2 is a very popular method for comparing ACs (Rolando M.A., 2007, Rouquerol *et al.*, 1999). There is no fundamental reason for the use of N_2, other substances: H_2, He, CO_2, Ar, Kr**,** Xe, C_4H_{10} (butane), C_5H_{12} (pentane), Li and Hg can also be used, each of which gives different results. It is impossible to accurately determine surface area, as distinct from determining reproducibility (Marsh and Rodríguez-Reinoso, 2006d). The surface area provided is the maximum adsorption capacity under the arbitrary conditions of the adsorption experiment. N_2 is used due to its relative convenience and it should be noted that it is not in the ASTM International manual for material testing while phenol adsorption and iodine adsorption are included (Jankowska *et al.*, 1991, Marsh and Rodríguez-Reinoso, 2006d).

1.4 Integrated photocatalytic adsorbents

The first study of integrated photocatalytic adsorbents (IPCAs) to degrade water pollutants was conducted in 1996 (Torimoto *et al.*, 1996) and the number of published studies using IPCAs has grown steadily since then (Figure 1-12). The term IPCA was coined much later in 2005 (Haque *et al.*, 2005). Photocatalysts are

commercially deployed in one large scale water treatment plant and research and development is on-going worldwide (Blanco *et al.*, 2009).

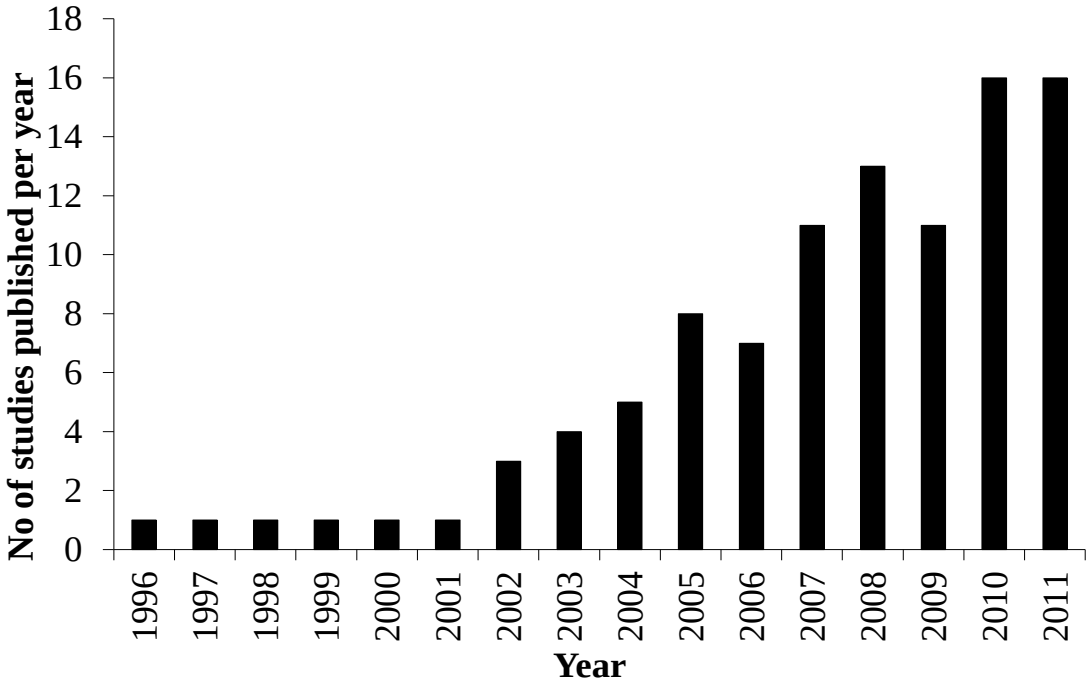

Figure 1-12 Number of surveyed AC/TiO_2 IPCA (degrading water pollutants) studies published per year 1996- December 2011.

By combining the adsorption potential of activated carbons with the photocatalytic properties of titanium dioxide it is possible to create an integrated photocatalytic adsorbent (Figure 1-13) with improved photocatalytic potential. IPCAs may consist of either activated carbon coated with TiO_2 or TiO_2 coated with a carbonaceous material that was heat treated to form an activated carbon. Numerous studies have reported synergistic effects between mixtures of TiO_2 and AC (a mass of each is separately added to solution) in contrast to composites (where both substances are combined together) of TiO_2 and AC (Areerachakul *et al.*, 2008, Cordero *et al.*, 2007a, Cordero *et al.*, 2007b, Matos *et al.*, 2007, Matos *et al.*, 1998, Qourzal *et al.*, 2004, Zhang *et al.*, 2004). Other adsorbent types have been used to create IPCAs including zeolites (Haque *et al.*, 2005, Huang *et al.*, 2008, Kabir *et al.*, 2006, Shankar *et al.*, 2006, Vaisman *et al.*, 2005, Wang *et al.*, 2008, Yoneyama and Torimoto, 2000), alumina silicates (Ding *et al.*, 2001a, Kun *et al.*, 2006, Maekawa *et al.*, 2006, Ménesi *et al.*, 2008, Yamashita *et al.*, 2004, Yamashita *et al.*, 2007), TiO_2 coated carbonaerogel (Jin *et al.*, 2011), carbon nanofibres (Kim *et al.*, 2011) and carbon

nanotubes (Gao *et al.*, 2011, Lee, 2004, Wang *et al.*, 2009a, Wu *et al.*, 2008, Xia *et al.*, 2007, Yao *et al.*, 2008, Yu *et al.*, 2005, Zhu *et al.*, 2007).

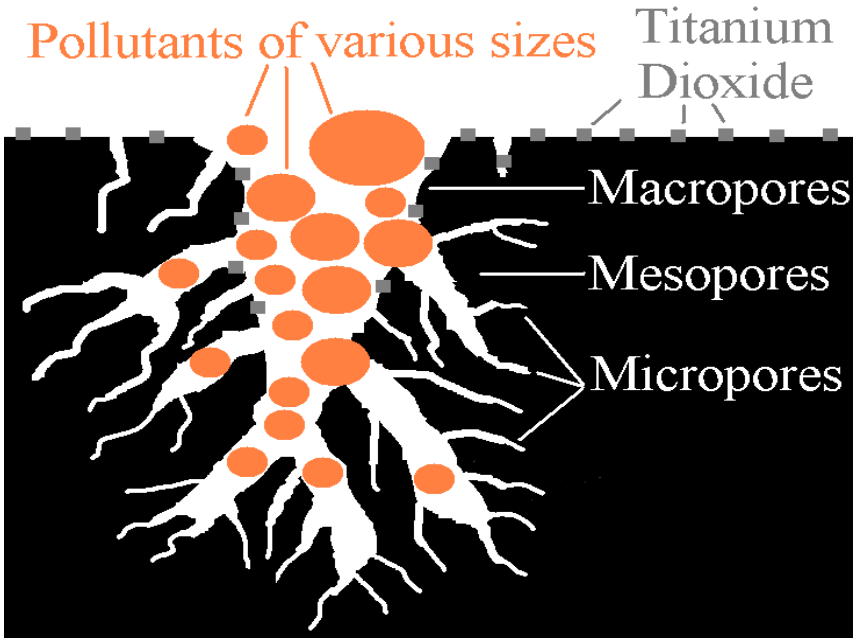

Figure 1-13 Activated carbon modified with TiO_2: an IPCA.

Source: (Gao *et al.*, 2011, Lim *et al.*, 2011, Liu *et al.*, 2007a, Wang *et al.*, 2009b, Zhang *et al.*, 2011a)

It is claimed that AC provides a synergistic effect (Cordero *et al.*, 2007b, Foo and Hameed, 2010a, Li Puma *et al.*, 2008, Lim *et al.*, 2011, Liu *et al.*, 2007a, Wang *et al.*, 2007) due to enhanced adsorption of the target pollutant onto the activated carbon phase followed closely by a transfer through an interphase to the TiO_2 phase, giving a complete photodegradation process. The literature cited in this chapter does not offer conclusive evidence of this effect which can be confused with extra adsorption due to the presence of the adsorbent (see Chapter 6).

The proposed mechanism(s) for IPCA action and synergy as described in the literature is summarised here. The AC in the IPCA is said to concentrate the pollutant near the photocatalyst surface allowing more efficient usage of the electron hole pairs created by illumination of the TiO_2. A diagram of the process is shown in Figure 1-14. This process has not been fully explained in the literature. It may work by the transfer of the substrate from the solution to adsorption sites in close proximity to the TiO_2 only or it might work by the diffusion of the substrate from the pores of the AC to the TiO_2 surface. It is also possible that a combination of the two processes occurs. If the

substrate does not diffuse out of the ACs pores then the adsorption capacity of the IPCA cannot be fully regenerated and after the initial adsorption capacity is exhausted the IPCA would only be effective at substrate removal during illumination. The lack of diffusion out of the pores could have several causes:

1. Covalent bonding with the ash or functional groups on the AC surface.
2. Clogging of the pores with substrate, preventing desorption.
3. Due to the higher activation energy of desorption the rate of desorption is always lower than adsorption of the sorbate when the adsorbent is placed in clean water to desorb therefore a slow adsorption rate will lead to a slow desorption rate.

Several factors could influence this process depending on which model is correct. Faster desorption kinetics would allow more efficient transfer of the substrate from the pores of the AC to the TiO_2 while increased TiO_2 loading on the surface of the AC may reduce the number of available adsorption sites thus lowering the adsorption capacity.

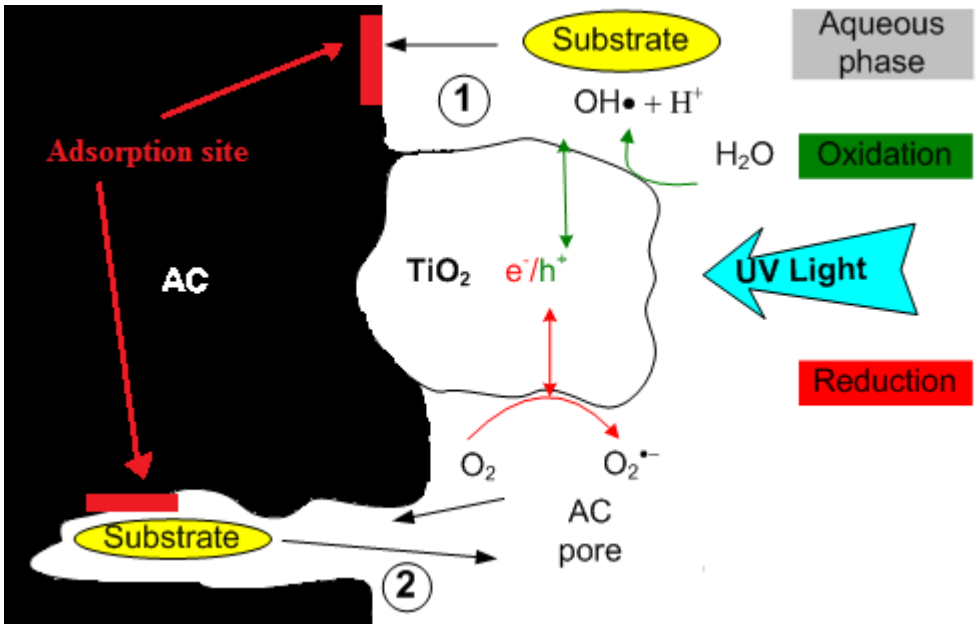

Figure 1-14 Diagram of IPCA photodegradation mechanisms. (1) Transfer of the substrate to the adsorption sites close to the TiO_2. (2) Diffusion of the substrate from the ACs pores to the TiO_2 surface. (Devipriya and Yesodharan, 2005).

The relative importance of each mechanism must be considered. If the substrate can diffuse out of the AC pores in a reasonable timeframe then a thin surface layer of TiO_2 on the AC will be effective for photodegradation as the substrate can

diffuse out of the pores onto this layer and be photo-degraded. If surface adsorption is more important, a system with a large surface area is required to adsorb and then photodegrade pollutants as the adsorption capacity of the TiO_2 surface layer is very low compared to the pores of an AC.

1.4.1 Photocatalyst choice for IPCAs

Of the photocatalysts surveyed for preparing IPCAs, pure anatase TiO_2 is the most popular (Figure 1-15, Appendix A and B). Anatase TiO_2 can be prepared in the laboratory by either wet or dry methods without calcination (heat treatment) although its phase can be maintained when using low calcination temperatures. Alternatively it can be bought commercially in powdered form. The majority of studies used anatase that was prepared in the laboratory.

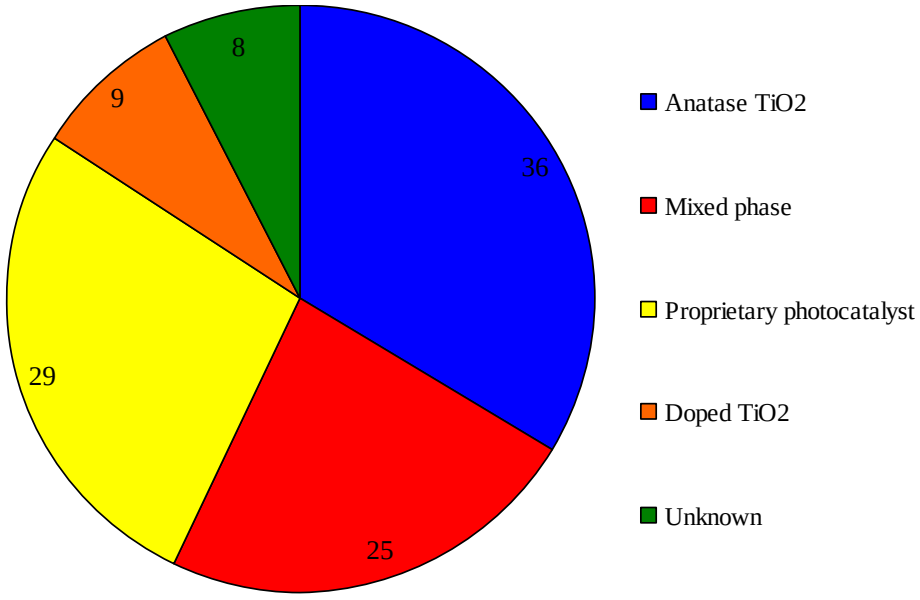

Figure 1-15 Photocatalyst used for preparing IPCAs.

Proprietary photocatalysts are the next most popular TiO_2 type. These include P25 (Evonik Industries formerly the Degussa Corporation), ST-01 (Ishihara Corporation) and Tytanpol A11 (Police Company) and other miscellaneous types. The vast majority of studies that use commercial TiO_2 use P25. P25 is a photocatalyst manufactured commercially and sold under the trade mark AEROXIDE® P25. P25 is a mixture of anatase and rutile in the region of 70 % – 90 % anatase and is manufactured by flame synthesis. P25 has an average particle diameter of 35–40 nm

(anatase), 85–95 nm (rutile) - as determined by X-ray diffraction (XRD) and transmission electron microscopy (TEM) analysis - and a specific surface area of 44–50 m^2g^{-1} (Balázs *et al.*, 2008). There is disagreement in the literature about the precise composition of P25, for example it is cited as anatase 92 %, rutile 8 % (Yamashita *et al.*, 2007), 75 % anatase, 25 % rutile (Xia *et al.*, 2007) and 80 % anatase, 20 % rutile (Yu *et al.*, 2005). The anatase and rutile phases exist separately in powdered form (Ohno *et al.*, 2001) and while the anatase phase is more photoactive (although this depends on the reaction conditions and catalyst morphologies (Shi and Weng, 2008, Sun and Xu, 2010), the mixture of the two phases is synergetic and allows P25 to have better activity than anatase and rutile separately (Hurum *et al.*, 2003, Ohno *et al.*, 2001). The synergy of P25 is claimed (Hurum *et al.*, 2003, Shi and Weng, 2008) to be due to:

1. The smaller band gap of rutile (3.0 eV) extending the range of photoactivity into the visible spectrum.
2. Stabilization of charge separation due to electron transfer from rutile to anatase phase slows recombination (known as the antennae effect).
3. The small size of the rutile crystallites facilitates this transfer, creating catalytic hot spots at the rutile/anatase interface.

The wide availability of P25 means that it is used both as photocatalyst in IPCAs but also as a reference photocatalyst to compare IPCA performance (Mills and Le Hunte, 1997).

Laboratory prepared IPCAs composed of a mixture of anatase and rutile TiO_2 are the next largest group of IPCA studied. Studies that use high calcination temperature for preparing IPCAs create mixed phase photocatalysts comprising of a mixture of rutile and anatase, for instance 30:70 % rutile: anatase (Fu *et al.*, 2004a, Xu *et al.*, 2008). These mixtures are an inevitable consequence of using a calcination step to prepare IPCAs as the anatase phase is converted to the rutile phase by high temperatures. These studies usually investigate a range of temperatures (e.g. 700-900°C) to create different IPCAs in order to determine which temperature produces the most photoactive IPCA (Xu *et al.*, 2008). Higher calcination temperatures cause more anatase to be converted to the rutile phase. However, increasing calcination temperature will cause the TiO_2 particles to become larger and it is suggested that the larger TiO_2 particles will not block the pores of the AC thus increasing the adsorption

capacity of the IPCA (Xu *et al.*, 2008). It was noted that activated carbon fibres (ACFs) can protect the anatase phase thus allowing the use of high calcination temperatures without causing a phase change (Fu *et al.*, 2004a). AC has been used as a support to prepare TiO_2 for use in photocatalytic studies (Slimen *et al.*, 2011). The AC reduces the particle size and agglomeration of the TiO_2 which gives it significantly higher photocatalytic activity compared to the TiO_2 prepared without a support and higher activity than a P25 control. The AC is burned at 700°C in air so that only the TiO_2 powder (the ash of the AC is washed off) remains for use in photocatalytic studies.

Several authors cited (Lee *et al.*, 2004a, Liu *et al.*, 2010, Torimoto *et al.*, 1996, Torimoto *et al.*, 1997, Zhang *et al.*, 2010) did not state the TiO_2 phase that they were using.

There is considerable literature (Al-Kdasi *et al.*, 2004, Anpo, 2000, Choi *et al.*, 2007, Comninellis *et al.*, 2008, Fujishima *et al.*, 2000, Fujishima and Zhang, 2006, Gogate and Pandit, 2004, Hoffmann *et al.*, 1995, Mills and Le Hunte, 1997, Wahi *et al.*, 2005, Yurdakal *et al.*, 2007, Zhou and Smith, 2002, Zwiener and Frimmel, 2000) describing the degradation of APIs and other organics by TiO_2 (on its own). TiO_2 photocatalysis has advantages over other AOPs:

1. pH adjustment is not required compared to photo-Fenton (Rizzo *et al.*, 2009).
2. As a catalytic process reagents such as H_2O_2 are not required as is the case with UV/ H_2O_2, perozonation and photo-Fenton.
3. The $^{\bullet}OH$ radical is a nonspecific oxidant which improves mineralisation (Zwiener and Frimmel, 2000).

There is considerable literature on the doping of pure TiO_2 (Hoffmann *et al.*, 1995, Wu *et al.*, 2010, Zaleska, 2008) and several studies have created doped TiO_2 that were subsequently converted into IPCAs. Chemical vapour deposition was used to add Ag to the surface of TiO_2 on an IPCA in order to overcome its lower photocatalytic performance compared to TiO_2 slurry (Zhang *et al.*, 2005a). Six IPCAs using different Ti:Ag ratios and deposition times were prepared and compared to an IPCA using P25 as the photocatalyst. The performance of the doped IPCAs increased with the Ti:Ag ratio and, deposition time and with the exception of the IPCA with the highest deposition time and Ti:Ag ratio, all of the doped IPCAs had higher photodegradation ability for methyl orange than the P25 IPCA.

P25 modified with CdS was prepared using separate sol gel and precipitation methods (Zhao *et al.*, 2010). The modified P25 was applied to an ACF and used to degrade methylene blue with sunlight as the irradiation source. The apparent reaction rate constant of the doped IPCA prepared using the precipitation methods and sol gel methods were 70 % and 21 % higher respectively than the unmodified P25 IPCA. Another approach used co-doping of anatase TiO_2 with Fe(III) and Ho(III) followed by application to a activated carbon fibres (ACF) (Shi, 2009). It was noted that the doping could prevent the formation of cracks in TiO_2 films on the surface of the ACF although the mechanism remains unknown. The study lacked a TiO_2 control therefore it is unclear if the doping had a positive effect on the photodegradation ability. Fe(0) was applied to TiO_2 and then impregnated onto an ACF (Liu *et al.*, 2009). The doped IPCA degraded approximately 20 % more 2,4-dichlorophenol than the unmodified P25 IPCA. The improved photocatalytic performance was attributed to the superior dechlorination ability of Fe(0) combined with the synergistic properties of the TiO_2 ACF IPCA.

A Fe doped TiO_2 was used to prepare an ACF IPCA for degrading dye wastewater (Li *et al.*, 2010). COD removal was approximately 50 % higher than the unmodified TiO_2 while colour removal (determined by an undefined colorimetry method) was comparable. Li *et al.* attributed this improvement in performance to trapping of photo-generated electrons in the conduction band of Fe^{3+} which decreased electron/hole pair recombination in the TiO_2 although no direct evidence of this was provided. Vanadium (V) doped TiO_2 was used to degrade X-3B (Reactive Brilliant Red dye) (Xu *et al.*, 2010) under visible light. The doped IPCA, V doped TiO_2 and P25 degraded 89 %, 60 % and 7 % of the X-3B respectively. The diffuse reflection spectra of the V doped TiO_2 showed enhanced absorption of visible light (380nm - 800 nm) compared to the unmodified TiO_2. The enhanced performance was attributed to this higher visible light absorption. The V doped TiO_2 also displayed enhanced hydrophilicity which was attributed to photo-generated holes diffusing to the surface and reacting with the surface oxygen lattice leading to the dissociative adsorption of water at those defective sites.

TiO_2 was doped with C and then surrounded by AC (Lee *et al.*, 2010). Anatase TiO_2 grains were prepared in a co-polymer that was then heat treated to form an AC. The anatase grains become doped with C during the carbonisation process and are claimed to develop enhanced visible light absorption. Under visible light illumination

methylene blue was effectively degraded in under one hour compared to no removal seen in the anatase TiO_2 control.

The choice of substrate for degradation is an important consideration in measuring doping performance. At visible wavelengths photo-adsorption of visible light by methylene blue (MB) induces electron injection into TiO_2 (photosensitization) leading to reduction of molecular oxygen and oxidative decomposition of the electron-deficient MB (Yan *et al.*, 2006). This is a separate effect to conventional doping allowing the TiO_2 to photodegrade under visible light and has led to the recommendation that "*transparent substrates*" be used for determining photocatalytic activity of visible light photocatalysis in the 540 nm – 680 nm range (Ryu and Choi, 2008, Yan *et al.*, 2006).

1.4.2 Adsorbent types

In this work the AC used to prepare IPCAs is categorised based on physical form as the diverse physical and chemical properties of AC such as iodine number, N_2 adsorption, density, mesopore and micropore volume are not detailed in the majority of articles cited. The most popular forms of AC in the reviewed literature (Figure 1-16) are powdered activated carbon (PAC) and granular activated carbon (GAC). Other forms such as extruded activated carbon (EAC) and activated carbon cloths/activated carbon filters (ACC/ACF) are also available but are not widely used in water treatment. Granular activated carbon is most commonly used in water treatment due to its relatively large grain size which makes it easy to handle and form filter beds, unlike PAC which due to its small grain size becomes easily suspended in solution and thus must be filtered or coagulated out of the solution.

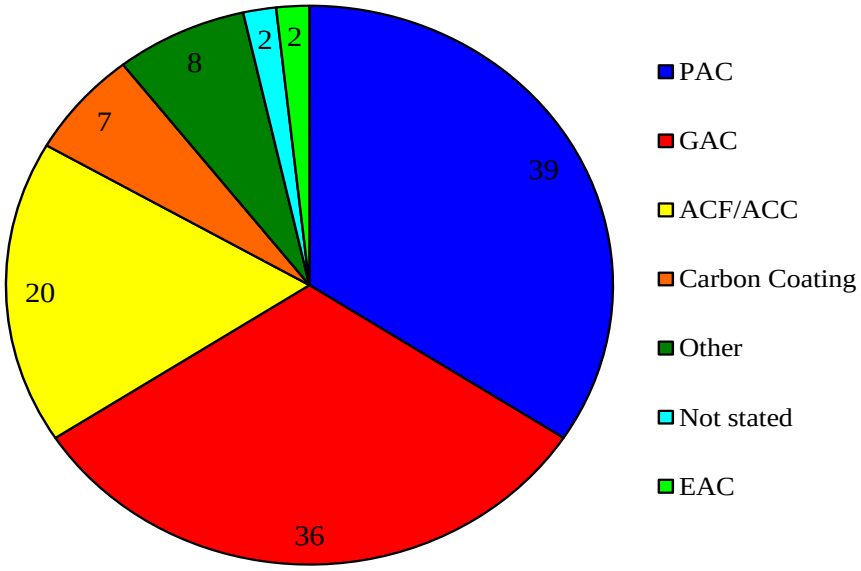

Figure 1-16 AC type and number used in IPCA studies.

The abundance of literature describing the use of PAC is most likely due to its ease of use in photocatalytic reactors and preparation compared to GAC and EAC especially given that the GAC and EAC are prepared by compressing PAC and a binder. IPCAs have also been prepared using AC created in the laboratory from a diverse set of precursors including wood (Cordero *et al.*, 2007a, Cordero *et al.*, 2007b), coconut shell (Lee *et al.*, 2004a, Lee *et al.*, 2004b), Jordanian olive stone (El-Sheikh *et al.*, 2004), pyrolysed sewage sludge (Zhang *et al.*, 2004), waste Canola hulls (Mahmoodi *et al.*, 2011) and coal tar pitch (Velasco *et al.*, 2010a). In theory, any natural organic material can be converted to activated carbon although economic considerations limit the number of viable feedstocks for commercial production (Marsh and Rodríguez-Reinoso, 2006b). The flexibility of source materials for activated carbon production enables IPCAs to be prepared from a multitude of raw - materials and industrial wastes.

A more costly approach to IPCAs production involves composites of TiO_2 and carbon nanotubes (CNTs). The CNT acts as an adsorbent providing all the associated benefits (adsorption capacity, substrate concentration) as activated carbon (Gao *et al.*, 2007). The conductive properties of CNTs allow electrons that have been promoted to the conduction band by the photocatalysis process to be transferred away from the TiO_2 surface. This reduces electron/hole pair recombination and by prolonging the electron holes on the TiO_2 surface, increases the likelihood of a photodegradation reaction and therefore a corresponding increase in the photodegradation rate (Gao *et*

al., 2007, Yao *et al.*, 2008). CNTs are also claimed to increase the adsorption spectrum of TiO_2 in the visible region allowing photodegradation using visible light (Wang *et al.*, 2009a). The progress and challenges of CNT IPCAs have been reviewed elsewhere (Woan *et al.*, 2009).

Doping of the adsorbent used in the IPCA has been attempted but with limited success (Oh *et al.*, 2009). A laboratory prepared ACF doped with Fe by immersion in ferric nitrate solutions was then added to a tetrabutyl orthotitanate solution in order to apply TiO_2 to the IPCA. The resulting IPCAs possessed similar photodegradation ability as the non-doped TiO_2 ACF which suggests that doping the AC is not as effective a strategy as doping the TiO_2 on its own.

1.4.3 Wet methods for preparation of IPCAs

IPCA preparation methods are broadly divided into "dry" and "wet" methods. Dry methods use a physical and/or gaseous/vapour process whereas wet processes use an aqueous phase in applying the TiO_2 to the adsorbent. Wet processes including sol gel, boiling impregnation, liquid phase deposition and electrophoretic deposition constitute the majority of methods used to prepare IPCAs (Appendix A and B).

Proponents of dry methods cite as advantages the absence of waste streams and avoidance of several of the preparation steps needed for sol gel methods such as saturation, ageing and drying (Wu *et al.*, 2003, Zhang *et al.*, 2005a). In spite of these claimed advantages, wet methods are much more common in the literature. Wet methods are generally more accessible because complex, specialist and proprietary equipment is not a prerequisite for their use (Wang *et al.*, 2009b).

1.4.3.1 Sol-gel

Sol-gel methods are used to prepare either the virgin TiO_2 or the complete IPCA. Although many methods are generally categorised as sol-gel there is considerable variation relating to precursor and adsorbent choice and the method of impregnation.

While the majority of IPCAs are prepared by applying TiO_2 to activated carbon, a smaller subset of IPCA preparation methods apply either the TiO_2 to a

carbonaceous material (or vice versa) that is then converted to activated carbon. For instance hydroxypropyl cellulose was applied to commercial TiO_2 powder (ST-01) and then activated at 700°C in N_2 and the resulting IPCA was used to decolourise methylene blue (Tsumura *et al.*, 2002). The most important parameter affecting the degradation efficiency was the use of pre-saturation (the IPCA was loaded with the substrate). For example the IPCA with the highest carbon content was the least effective at decolourising methylene blue when the IPCA was not pre-saturated before illumination. However, when the IPCAs were pre-saturated the reverse was true. This was attributed to the need for migration of the substrate from the AC to the TiO_2 surface which was higher when the IPCA was pre-saturated. Cellulose microspheres have been used as a supporting material for P25 which was carbonised to create an IPCA (Yamashita *et al.*, 2007). The IPCA was twice as effective at degrading acetaldehyde as unmodified TiO_2 of the same particle size. Poly vinyl butyral and poly vinyl alcohol have been used as supports for TiO_2 and are carbonised to create IPCAs (Tryba *et al.*, 2003a).

The second category of the sol gel studies (and the most numerous types) uses a sol gel process to prepare the TiO_2 used in the impregnation process. Typically the TiO_2 is prepared using a Ti precursor such as tetrabutyl orthotitanate dissolved in absolute ethanol (Liu *et al.*, 2007b). An acid can be added to control the pH (Zhu and Zou, 2009) and a hygroscopic compound such as diethanolamine can be added to optimise the solution (Li *et al.*, 2006). The AC is added to the TiO_2 by:

1. Dip coating into the sol gel solution (Liu *et al.*, 2009, Liu *et al.*, 2007b),
2. Drop coating of the solution onto the AC (He *et al.*, 2009, Wang *et al.*, 2009b)
3. Stirring/immersion of the AC in the solution (Wang *et al.*, 2007, Yao *et al.*, 2010, Zhang *et al.*, 2010)
4. Ultrasonication of the TiO_2 solution with the AC (Li *et al.*, 2007, Li *et al.*, 2010, Xu *et al.*, 2008).

Regardless of the impregnation method used, the resulting IPCAs are usually heat treated at low temperatures (200-250°C) (Hou *et al.*, 2009, Inagaki *et al.*, 2006) in air and then calcined at 300-800°C in an inert atmosphere e.g. N_2.

Low temperature methods can be used to prepare IPCAs and these methods are reported to be superior to high temperature preparation methods as the surface area of the TiO_2 particles is not decreased as a result of heat treatment (Ao *et al.*, 2008a, Ao *et al.*, 2008c, Basha *et al.*, 2010). Preparation involved a sol-gel method to

prepare TiO_2 and ultrasonication to mix the TiO_2 and PAC (or GAC) solution followed by drying with a rotary evaporator. Another low temperature preparation method stirred different proportions of commercial TiO_2 powder (P25) and AC in an aqueous solution for an hour followed by filtration and drying (Araña *et al.*, 2003a). The resulting IPCA had improved photodegradation ability in terms of apparent first-order rate constants that were 619 % higher for natural sunlight and 67 % higher for UV light compared to virgin TiO_2.

1.4.3.2 Other wet methods

The majority of papers in the reviewed literature that used wet methods to prepare TiO_2 used sol-gel type processes, other studies used alternative wet methods to prepare the TiO_2 including boiling impregnation, liquid phase deposition and electrophoretic deposition. Wet chemical impregnation techniques are of interest due to their straightforward protocols, low temperature and energy costs.

Boiling impregnation was used to apply TiO_2 to GAC (Khan, 2002). The method involves mixing TiO_2 and AC and repeatedly boiling dry the solution to create an IPCA. The resulting IPCA degraded 80 % and 90 % of methylene blue at concentrations of 10 mg/L and 20 mg/L, respectively, and it was regenerated twice. This method was also used to apply a solution of P25 (ultrasonicated beforehand) to a series of inert and adsorbent supports including GAC and zeolite (Lu *et al.*, 1999). The coated supports were then calcined and used to degrade propoxur (a carbamate insecticide). The GAC based IPCA removed almost four times more propoxur than P25 alone. When the adsorption capacity of the IPCA was taken into account (it had a lower concentration at t = 0 due to adsorption) its mineralisation rate was roughly equivalent to P25.

The liquid phase deposition (LPD) method is a simple and easily-controlled process for fabricating thin films of coating on ACF and does not require special equipment (Hou *et al.*, 2009). It consists of submerging a pre-treated ACF into a solution of TiO_2 precursor for several hours followed by drying and annealing for 180 min at 350°C in an N_2 atmosphere. The resulting IPCA demonstrated much higher photodegradation (49 %) of Acid Orange II (dye) compared to virgin TiO_2 (11 %). In the same study electro-photocatalysis was used parallel to conventional UV photocatalysis. The IPCA was used as an anode and an electric current was passed

through it to decrease electron-hole recombination and this achieved a degradation rate approximately 10 % greater than conventional UV photocatalysis (Hou *et al.*, 2009).

Electrophoretic deposition was used to apply a suspension of commercial P25 (in a 5 % (v/v) 2-propanol) and PAC to conductive glass plates coated with SnO_2 films doped with indium (Peralta-Hernández *et al.*, 2007). The indium glass plates function as the cathode in the process. The resulting nano-composite electrodes prepared using a range of different synthesis suspensions were sintered (heat treated) in air. The IPCA present on the surface of the electrodes was three times more effective at decolourising Orange-II dye (30 % reduction of Orange-II compared to a 10 % reduction in the TiO_2 control after 200min of UV irradiation). The study did not use a photolysis control or total organic carbon (TOC) to monitor degradation but measured the production of H_2O_2 (a key reactive oxygen species) and determined that it was 50 % higher in the IPCA compared to virgin TiO_2.

1.4.4 Dry methods of preparation

Dry methods constitute less than a one sixth of the methods used in the literature, with Chemical Vapour Deposition (CVD) and its variants comprising the majority of these methods.

1.4.4.1 Chemical Vapour Deposition

Chemical vapour deposition (CVD) creates a vapour using an inert carrier gas (typically N_2) and a chemical precursor(s) that is to be applied to a substrate. CVD can be categorised according to the pressure or the physical characteristics of the vapour used for deposition. Atmospheric pressure (AP) CVD (Ding *et al.*, 2001b, El-Sheikh *et al.*, 2007, Zhang *et al.*, 2005a) and MOCVD (metal organic chemical vapour deposition) (Zhang *et al.*, 2005b, Zhang *et al.*, 2006) have been used to prepare IPCAs. Although not explicitly mentioned in every study, the majority of CVD methods appear to have been used at atmospheric pressure. Low pressure MOCVD was used to prepare supported anatase TiO_2 on the surface of silica gel (Ding *et al.*, 2000). The photocatalytic activity of the supported TiO_2 was nearly half

of that of the powder photocatalyst (P25). CVD was used to create an EAC-based IPCA as well as IPCAs using silica gel and γ- Al_2O_3 (a polymorph of alumina) (Ding *et al.*, 2001b). The silica gel had the highest photodegradation ability of the IPCAs for degrading phenol and this is attributed to its greater surface area. An initial increase in phenol concentration was attributed to the release of phenol from the EAC-based IPCA and no TiO_2 slurry was included as a control. These factors limit the usefulness of this study in comparing AC to other adsorbents.

Molecular adsorption-deposition was used to apply a TiO_2 precursor ($TiCl_4$) to ACFs (Fu *et al.*, 2004a). The method consists of heating the ACF under vacuum followed by adsorption of $TiCl_4$ vapour and saturated water vapour at room temperature. The system was then heated to 90°C and evacuated, followed by calcination. As this method creates a vapour that is deposited on a substrate it could also be considered lower pressure chemical vapour deposition (LPCVD). IPCAs prepared by exclusively by CVD have been reviewed in detail elsewhere (Li Puma *et al.*, 2008).

1.4.4.2 Mechanofusion: Theta composer

Mechanofusion processes grind materials together and can be used to apply TiO_2 to an AC to create an IPCA. One example is the Theta Composer®; it is a proprietary elliptical rotor type powder mixer that uses a rotating vessel and rotor to create high shear forces that bind the particles together. Resulting IPCAs exhibited methylene blue decolourising potential comparable to IPCAs prepared by boiling impregnation (Khan, 2002). The most important consideration for IPCAs prepared using this method was the process used to activate the activated carbon as the ACs prepared by acid washing were ineffective compared to AC activated by steam. The increasing number of dry methods and equipment available to prepare composite powders has been reviewed elsewhere (Yang *et al.*, 2005). Proponents of mechanofusion have reviewed other mechanofusion methods such as magnetic assisted impaction coating, hybridiser and rotating fluidized bed coater that could be used to prepare IPCA (Pfeffer *et al.*, 2001). None of these methods have been used to prepare IPCA in the ten years since the first mechanofusion IPCA.

1.4.5 Substrate for photodegradation

IPCAs have been used principally to photodegrade a variety of organic contaminates, typically hazardous substances such as phenol, chlorophenol, azo dyes, pesticides and other chlorinated compounds (Figure 1-17). However, only five studies in the literature surveyed involved an actual characterised wastewater sample and two other studies looked at the degradation of commercially purchased humic acid, a constituent of the natural organic materials found in water.

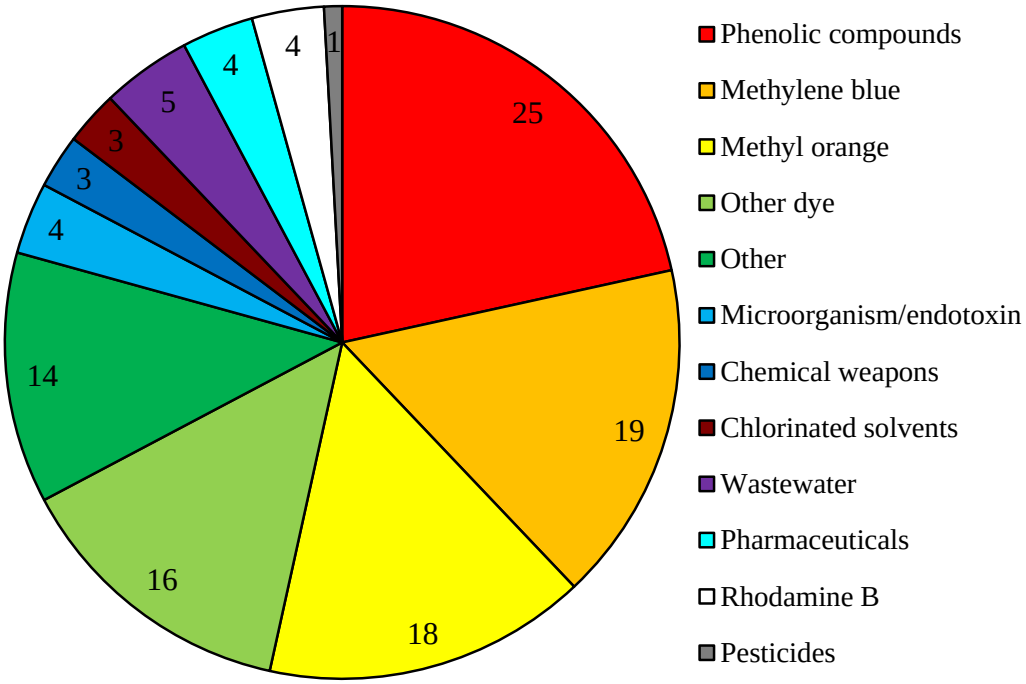

Figure 1-17 Number of substrates (numbers on the inside of the graph) used for photodegradation in the 104 surveyed studies (some studies use more than one substrate).

For paper mill wastewater, the best performing ACF- based IPCAs removed 15 mg/L more COD and colour removal was 50 % faster when compared to P25 (Yuan *et al.*, 2007). The IPCA showed minimal loss of photocatalysis ability after three adsorption cycles. A similar study used a Fe doped, ACF based IPCA (Li *et al.*, 2010). The Fe-doped IPCA could reduce COD by a third more than the IPCA containing non doped TiO_2 and was twice as effective as unmodified TiO_2. The same pattern was repeated for colour removal although the differences in the colour

removal rate were much smaller with the Fe-doped IPCA removing almost 100 % of the colour compared to 80 % for unmodified TiO_2. Regeneration using UV light allowed it to maintain a 50 % removal rate for COD under pilot plant conditions. The IPCA was also used to reduce the COD of effluent from a municipal sewage plant demonstrating the longevity of the IPCA in typical operating conditions. This study is one of only two in the surveyed IPCA literature to use an IPCA on municipal wastewater. No other information was provided on the characteristics of the wastewater other than the COD the IPCA removed. This means assessing the overall effectiveness of this IPCA - as a polishing treatment for municipal wastewater - is not possible with the information detailed in this study. An IPCA based on a GAC designed for wastewater treatment was used to remove colour compounds (absorbance at 254 nm, with molecular weights of 400–10,000 Dalton) for a municipal sewage treatment plant (Zhu and Zou, 2009). The initial colour removal declined from 90 % to 50 % after 10 adsorption cycles and using separate regeneration steps the colour removal could be returned to approximately original levels. The comparison for the regeneration step was undertaken only once and there was no comparison with an unmodified IPCA. Therefore there is no indication of the lifespan of the IPCA compared to an unmodified AC.

A PAC IPCA was prepared using sol-gel TiO_2 doped with N. This TiO_2 was then applied to the PAC using either stirring or a self-assembly method using AC treated with poly(sodium styrene sulfonate) to attract the TiO_2 particles to the AC surface (Zhang *et al.*, 2011a). The 11.2 mg/L concentration of humic acid is found in the environment and the IPCA prepared using the self-assembly method degraded approximately half of the humic acid after 250 min of illumination. This rate of degradation was no higher than the TiO_2 control and the effect of photolysis was not investigated in this study.

A similar study used a slightly higher concentration of humic acid (15 mg/L); a sol gel prepared IPCA and measured the degradation rate using UV adsorption and total organic carbon (TOC). The best performing IPCA achieved a TOC removal rate greater than 95 % in 180 min and a corresponding reduction in UV absorbance. The IPCA performed better than photolysis and photocatalysis using TiO_2, however the catalyst concentration of TiO_2 was lower than the IPCA and this may have been detrimental to its performance. The difference in TOC between the TiO_2 control and IPCA was around 20 % which corresponds to approximately 1 mg/L in a solution that

had a 5 mg/L initial concentration. This may not be a significant difference in terms of overall performance. GAC IPCAs prepared using a sol gel method with a TiO_2:AC ratio from 0.03:1 to 0.63:1 have been used to inactivate (kill or prevent from reproducing) microorganisms (Li *et al.*, 2008a). The best performing IPCA (47 % TiO_2) sterilised the sample in 175 min compared to a 70 % reduction in viable *E.coli* numbers in 250 min for 100 % TiO_2 slurry. Another IPCA prepared by a sol gel method was used to degrade 50 mg/L and 200 mg/L of microcystin-LR (cyanobacteria endo toxin) (Lee *et al.*, 2004a, Lee *et al.*, 2004b). The removal of microcystin-LR was accomplished in 15 min under UV illumination compared to a 60 % reduction in 60 min without illumination. No TiO_2 slurry control was included so it is unclear if this IPCA has enhanced photodegradation properties compared to unmodified TiO_2.

A mixture of P25 and activated carbon - prepared by pyrolysis (activation) of sewage sludge - was used to reduce ionic mercury Hg(II) to metallic mercury Hg(0) (Zhang *et al.*, 2004). Hg(0) is insoluble in water in contrast to Hg(II) and thus has higher affinity for activated carbon. Under UV illumination this system was able to remove a third more mercury than the activated carbon on its own. Recovery from the AC of 40 % to 65 % of the adsorbed Hg(0) was possible using separate chemical processing.

Generally studies of dyes as target compounds use decolouration to measure degradation (Fu *et al.*, 2004a, Khan, 2002, Li *et al.*, 2006, Liu *et al.*, 2007b) while studies using HOPs (hazardous organic pollutant) measure the degradation of the target compound (Torimoto *et al.*, 1997, Yoneyama and Torimoto, 2000). Total organic carbon (TOC) and/or dissolved organic carbon (DOC) or CO_2 released during photodegradation can also be used to measure the mineralisation of the compound (Eggins *et al.*, 1997, Torimoto *et al.*, 1996, Torimoto *et al.*, 1997). If the substrate is a simple compound or is well characterised then investigation of intermediate formation yields additional information on IPCA efficiency. For instance methyl orange photodegradation creates phenol as an intermediate product. In a comparison of a sol gel and CVD IPCAs both are equally efficient in degrading methyl orange, however the CVD IPCA was more effective at degrading the intermediate product (phenol) and consequently the mineralisation rate measured by TOC was 100 % higher (Zhang and Lei, 2008).

Artificial aeration is incorporated into some experimental designs (Ding *et al.*, 2001b, Fu *et al.*, 2004b, Li *et al.*, 2005, Li *et al.*, 2008b, Sun *et al.*, 2009, Wang *et al.*, 2009a, Zhang *et al.*, 2005c, Zhang and Lei, 2008). Aeration may improve photodegradation by ensuring that there is sufficient O_2 that can be reduced to the superoxide radical $O_2^{\bullet-}$ which speeds up degradation (Zhang *et al.*, 2008). However, it remains unclear if O_2 addition improved performance in all cases. IPCAs have also been used to degrade gaseous or volatile pollutants such as formaldehyde (Mo and Ye, 2009), methanol (Tao *et al.*, 2006), ethylene (Ye *et al.*, 2009), BTEX compounds (benzene, toluene, ethylbenzene, and xylenes) (Jo and Yang, 2009) and dimethyl sulphide (Jo *et al.*, 2011). This application of IPCAs was commercialised for air cleaners (Fujishima and Zhang, 2006) and remains the only current practical demonstration of the technology.

1.4.6 Regeneration/reuse of IPCAs

The ability of IPCAs to be regenerated and/or reused is a primary consideration if practical applications of IPCAs are to be demonstrated. Repeated adsorption/degradation tests have been conducted on a limited number of IPCAs using either three (Gao *et al.*, 2011, Khan, 2002, Mozia *et al.*, 2007b, Yuan *et al.*, 2007), four (Shi, 2009, Yao *et al.*, 2010), five (Ao *et al.*, 2008d, Basha *et al.*, 2010), six (Ao *et al.*, 2008a, Ao *et al.*, 2008c, Ao *et al.*, 2009, Cao *et al.*, 2010, Liu *et al.*, 2010), seven (Liu *et al.*, 2009), fifteen (Li *et al.*, 2010) or 20 (Li *et al.*, 2005) regeneration/degradation cycles. Regeneration degrades the substrate on the surface and in the pores of the AC in order to restore its original adsorption capacity. This step necessitates desorption of the substrate from the pores in the AC into solution – either the bulk solution or the fluid in the pore volume - and then migration to the illuminated TiO_2 particles otherwise the adsorption sites on the AC cannot become available for the adsorption of more substrate i.e. they cannot be regenerated (Foo and Hameed, 2010a, Leary and Westwood, 2011, Lim *et al.*, 2011, Wang *et al.*, 2009b). The effectiveness of IPCA regeneration varies based on their properties which influence the migration from the pores of the AC to the illuminated surface. For example fifteen adsorption/degradation cycles using methylene blue led to a reduction of its removal rate from 100 % to 92 % with a 7 % loss of the TiO_2 on the IPCA (Fu

et al., 2006). The photodegradation ability decreased with each cycle to varying degrees. This was attributed to the blocking of micropores and the inability of the UV light to enter these pores to trigger photodegradation. Other studies reported approximately 20 % lower substrate removal after six cycles (Ao *et al.*, 2009). An 80 % reduction in the rate of photodegradation has been reported, whereby 2 h of illumination were required for 80 % substrate decomposition in the first cycle compared to 10 h required for 80 % decomposition in the twentieth cycle (Li *et al.*, 2005). Another study described essentially unchanged photodegradation performance after four cycles (Basha *et al.*, 2011).

Desorption rates in solution have not been investigated in IPCA studies although they have been investigated in studies of AC adsorption which should be applicable to IPCAs. Desorption in terms of the backward rate constant is found to be significantly slower than the adsorption (forwards rate constant) for the adsorption of phenol (Rengaraj *et al.*, 2002). Desorption of microcystin-LR (Lee *et al.*, 2004a, Lee *et al.*, 2004b) using methanol extraction yielded approximately 15 % of the substrate adsorbed on the AC. Desorption from the IPCA was approximately 1 % and the author attributed the difference in desorbed concentration to the photodegradation of the substrate on the IPCA. Given that only a small percentage of the total microcystin-LR desorbed suggests that the degradation rate is either slowed by the need for desorption (as only a small percentage can desorb at a given time) or that only a small percentage of the total adsorption sites can be regenerated. The need for methanol for desorption limits its practicality for IPCAs in typical operating conditions. For 2-methyl-4-chlorophenoxyacetic acid (MCPA) desorption, high temperatures and pressures of 160 - 180°C and 38 bar respectively were able to desorb between 20 % and 60 % of the adsorbed substrate for an AC (Gimeno *et al.*, 2003). These studies suggest that the total regeneration of the adsorption capacity of the AC is impossible. The papers listed at the start of this section indicate that an IPCA can be reused from five to twenty times while maintaining varying levels of performance. This opposing evidence can be reconciled by considering that many studies lack necessary controls (Appendix A and B) and could be inaccurate because they are measuring residual adsorption by the IPCA rather than achieving total saturation of the AC surface before regenerating it. In addition adsorption is occurring at the same time as photodegradation in IPCA studies compared to the dark adsorption conditions where ACs are used and then regenerated usually ex-situ (outside of the reactor) after

reaching saturation. IPCAs might demonstrate the ability to repeatedly degrade organic pollutants and still not be able to recover their original dark adsorption capacity.

For regenerating IPCAs several processes have been investigated either as an alternative to, or supplement to UV light. A hybrid ultrasound (from an ultrasonic bath) and UV system was used to regenerate an IPCA utilised for removing colour compounds from treated wastewater (Zhu and Zou, 2009). Regeneration using UV light alone required 16 h, UV light and hydrogen peroxide required 3 h but regeneration using UV and ultrasound required only 30 min and achieved the highest regeneration levels. This study did not consider the effect of ultrasound on the stability of the activated carbon. Separate research using ultrasound to regenerate GAC has shown that the percentage of particles smaller than what could be considered GAC (<2.5 mm) increased from 0 to 4.6 % after 1 h of sonication (Lim and Okada, 2005). While it was noted that this is smaller than the loss of GAC in thermal reactivation of approximately 10 % it is a disadvantage of ultrasonic regeneration. This is especially relevant to IPCAs as ultrasonication may not only affect particle size but may also loosen the deposited TiO_2 on the IPCA surface. Another study compared the efficiency of regenerating a coated chitosan ACF IPCA using UV light and Fenton reagent (Liu *et al.*, 2010). In six subsequent adsorption/regeneration cycles the removal rate of the UV regenerated and Fenton regenerated IPCAs remained above 82 % and 86 % respectively, while the removal rate of the IPCA that was not regenerated declined from 91 % initially to 51 % after six cycles of adsorption/regeneration. Although the Fenton reagent performed marginally better the structure of the IPCA could be damaged (Liu *et al.*, 2010).

Ultrasonic irradiation results in the formation and collapse of micro scale bubbles and generation of local high temperatures and is an alternative to UV light as an energy source for creating electron holes in TiO_2 particles (Kubo *et al.*, 2005). Ultrasonic irradiation of water causes acoustic cavitation i.e. microscale bubbles are formed. The collapse of these bubbles causes locally high temperatures and extreme pressure (up to 5000K and 1000 ATM) that can decompose water to create hydroxyl radicals, which degrade organic compounds. In ultrasonification studies using an ultrasonic probe immersed in the test solution, 90 g/L of IPCA degraded 1 mol/L of phenol in 180 min and 1.5 g/L IPCA degraded 0.6 mol/L of phenol in 540 min (Kubo *et al.*, 2007). Increasing catalyst loadings markedly increased phenol degradation rates

and it was noted that this would not be possible using photocatalysis due to light penetration problems. However the effect of ultrasonication on the stability of the IPCA and consequent changes in adsorption behaviour were not investigated.

1.4.7 IPCAs and photocatalytic reactor design

Conventional photocatalysis test systems typically use either a suspension of TiO_2 (Karpova *et al.*, 2007, Molinari *et al.*, 2008, Zhang *et al.*, 2007) or an immobilised layer (Blanco *et al.*, 2009, Byrne *et al.*, 1998, Guillard *et al.*, 2004) of unmodified TiO_2. In order to treat wastewaters effectively the TiO_2 must be kept under constant illumination. Under illumination from a 125 W Hg lamp, up to 28 h were required for complete mineralisation of a 47 mg/L solution of gemfibrozil with 0.4 g/L of photocatalyst (Yurdakal *et al.*, 2007) although mineralisation times for gemfibrozil in a membrane photoreactor (with 1 g/L photocatalysts) can be as short as 150 min for 97 % mineralisation (Molinari *et al.*, 2008). In contrast, an IPCA can concentrate the pollutant in a smaller area improving efficiency by increasing substrate contact time with the photocatalyst (Augugliaro *et al.*, 2006) which is important when the pollutant concentration is very low in the µg/L or ng/L range. Moreover, a photocatalysis system using a suspension of TiO_2 (or a PAC based IPCA) requires that the suspension be removed from the water after the photocatalysis step is finished. In a water treatment plant this may be done via filtration or coagulation limiting the possibility of recovery of the catalyst and increasing the cost of treatment. This problem can be overcome by using a GAC, EAC or ACF based IPCA which can be readily filtered from the water or used in a fixed or fluidised bed arrangement obviating the need for separation.

An alternative approach is the use of photocatalytic membrane reactors (PMRs) which filter out the TiO_2 after the photocatalysis step (Mozia *et al.*, 2007a). While PMRs remove the TiO_2 suspension and allow its reuse, they do not overcome the low adsorption and constant illumination problems of TiO_2 suspensions. Systems that use immobilised thin films of unmodified TiO_2 do not have the removal problems of suspensions of TiO_2; however they are limited by their low surface to volume ratio and therefore require large capacities (Ochuma *et al.*, 2007). The use of

microstructured reactors is being investigated to overcome these problems (Coyle and Oelgemöller, 2008, Matsushita *et al.*, 2007).

Magnetic separation represents an innovative solution to liquid-catalyst separation. It involves applying TiO_2 to an inert silica or activated carbon support that had been impregnated with magnetic magnetite particles (Ao *et al.*, 2008c, Ao *et al.*, 2009, Kostedt *et al.*, 2005, Wang and Zhou, 2010). The resulting composites are used in photocatalytic reactors where a magnetic field is used to both stir and recover the catalyst.

IPCAs generally have reaction rates higher than unmodified or virgin TiO_2 (Section 1.4.5) and the use of IPCAs with larger particle sizes allows the use of IPCAs in fluidised bed type reactors which are simpler and do not require active filtration thus reducing reactor costs.

1.5 Conclusions

IPCAs are effective for degrading a wide variety of organic pollutants. IPCAs are more effective than either AC or TiO_2 separately and the proposed mechanism to explain this synergy is the concentration of the substrate at the TiO_2 surface by the AC. A wide variety of IPCA preparation methods are available that centre around sol-gel methods and the ultrasonication of the raw materials.

1.6 Project aims

1. Investigation of the capacity the capacity of IPCAs, commercial AC and TiO_2 to adsorb and photodegrade pharmaceuticals.
2. The potential for synergy between AC and TiO_2 for the removal of pharmaceuticals.

1.7 Project objectives

This work has the following objectives:

1. Preparation of IPCAs using activated carbon and titanium dioxide.
2. Characterisation of IPCAs using SEM, FESEM and XRD.
3. Determine the adsorption kinetics of IPCAs, commercial AC and TiO_2 for famotidine and solifenacin succinate.
4. The adsorption capacity of IPCAs, commercial AC and TiO_2 for famotidine and solifenacin succinate in deionised water at different initial pHs.
5. The adsorption capacity of IPCAs, commercial AC and TiO_2 for different initial concentrations of famotidine and solifenacin succinate in deionised water.
6. The photolysis of famotidine and solifenacin succinate under light from a medium pressure mercury lamp.
7. The ability of IPCAs, commercial AC and TiO_2 to photodegrade famotidine and solifenacin succinate.
8. The potential for synergy between AC and TiO_2 for the removal of famotidine and solifenacin succinate.

Chapter 2 Materials and Methods

2.1 Materials

The materials used in this work are listed in Table 2-1. The properties of the activated carbon are given by its manufactures in Table 2-2.

Table 2-1 Source and description of materials and apparatus used.

Product	**Description**	**Source**
TiO_2 (AEROXIDE P25)	Manufactured by Evonik Industries	National Chemical Company of Ireland
Pall nylon filters	0.2 μm pore size 47mm diameter	Sigma-Aldrich, Germany
Formic acid	>98 %	Fluka, Buchs, Switzerland
0.22μm nylon syringe filters		Phenomenex Inc., United Kingdom
HPLC grade methanol and water		Fisher Scientific, Ireland
Amber HPLC vials		
Parafilm laboratory film		
90mm diameter glass fibre filter paper	(FB59077 equivalent to Whatman no. 3)	
Quartz cuvette	CXA-145-050W (Hellma)	
Stainless steel stubs and carbon tabs		Agar Scientific, Essex, United Kingdom.
Famotidine		Astellas Pharma Co. Ltd., Dublin, Ireland
Solifenacin succinate		
Apparatus (analytical instruments included)		
Ultrasonic cleaner	5510 E-Mt	Bransonic
Tube furnace	CTF 31 600	Carbolite
1L photochemical reactor with a 290mm long immersion well (Schlenk flask)	model 7841-06 model 7857	Ace glass, 1430 N West Blvd Vineland, NJ 08360, United States
125W Medium pressure Hg lamp	TQ 150	Heraeus Noblelight
Scanning electron microscopy	S-3000N VP	Hitachi
Field emission scanning electron microscopy	Hitachi 5500	Hitachi
HPLC	Agilent 1100	Agilent Technologies
X-ray diffractometer	D8 Advance GX002002	Brüker
pH meter	Wissenschaflich Technische Werksatatten pH522/ Jenway Model 3510	

Table 2-2 Activated carbon specification provided by manufacturer.

Properties / Carbon name:	AquaSorb 2000 (Aqua 2k)
Surface area (m^2/g)	1050
Particle size (mm)	0.425-1.70
Iodine number (mg/g)	>1000
Pore volume (cm^3/g)	1.04
Ash content (%)	<15 %
Moisture content (wt. %)	<5
AC type	GAC
pH	8-11
Typical application	Water treatment
Donated by	ENVA Water Treatment, Cork, Ireland

2.2 Methods:

2.2.1 IPCA preparation

2.2.1.1 Initial IPCA preparation method.

AquaSorb 2000 (6 g) was added to a 0.2 L solution of deionised water with 0.6 g of P25 corresponding to a P25: AquaSorb 2000 wt. ratio of 1:10. This IPCA is therefore denoted the 1:10 IPCA. This mixture was then ultrasonicated (Bransonic 5510 E-Mt) for 1 h. The ultrasonicated IPCA solution was oven dried (at 80°C). The IPCA was then washed by adding 0.02 L - 0.03 L of deionised water to the dried IPCA which was then stirred and the water – now containing loose TiO_2 - was decanted using a Pasteur pipette. This process was repeated five times to remove loose TiO_2. Deionised water was then added to the beaker containing the IPCA until it reached the 0.05 L mark. This suspension was oven dried at 110°C. The dried IPCA was collected and stored in sealed glass vials before use. The same procedure was used for the 1:1, 1:1.33, 1:2, 1:4, 1:5, 1:40, 1:20, 1:13, 1:100 and 1:200 IPCAs with the only difference being that the ratios of TiO_2 to activated carbon were adjusted to match the IPCA name.

2.2.1.2 IPCA prepared for heat treated IPCAs

Heat treated IPCAs used the same method for the preparation as the 1:10 IPCA (Section 2.2.1.1) with the following heat treatment conditions. Four grams of 1:10 IPCA were placed evenly inside an alumina ceramic–"boat" type crucible 100 mm x 20 mm x 20 mm (Length x width x depth) in size. The crucible was placed in the centre of a horizontal tube furnace (Carbolite CTF 31 600). The temperature increase rate (ramp rate) for the furnace was 10°C a minute with a treatment time (after the desired temperature was reached) of 2 h for all samples. At 200°C the IPCA samples were heat treated in air. For the 500°C / 600°C / 700°C IPCA samples the 1:10 IPCA was heat treated at 500°C / 600°C / 700°C in an argon atmosphere. The furnace was purged of air with argon for five minutes after insertion of the sample and an argon flow rate of approximately 16 cm^3 per second was maintained until the sample was removed. Samples were heat treated for 2 h and then left to cool for 1 h.

2.2.1.3 Improved IPCA preparation method

AquaSorb 2000 (10 g) was added to a 0.4 L solution of deionised water with 1 g of P25 corresponding to a P25: AquaSorb 2000 wt. ratio of 1:10. This mixture was then ultrasonicated (Bransonic 5510 E-Mt) for 1 h. The ultrasonicated IPCA solution was oven dried (at 80°C), washed in deionised water and then poured onto glass fibre filter paper. The IPCA grains were washed off the filter paper with deionised water into a separate 0.05 L beaker. The smaller TiO_2 particles remained bound to the filter paper. The IPCA was then washed by adding 0.02 L - 0.03 L of deionised water to the dried IPCA which was then stirred and the water – now containing loose TiO_2 - was decanted using a Pasteur pipette. This process was repeated three times to remove loose TiO_2. Deionised water was then added to the beaker containing the IPCA until it reached the 0.05 L mark. This solution was oven dried at 110°C. The dried IPCA was collected and stored in sealed glass vials before use.

2.2.2 Characterisation methods for P25, AC and IPCAs

2.2.2.1 Scanning electron microscopy

The surface structures of AC and IPCAs were analysed by scanning electron microscopy (SEM) using a Hitachi S-3000N VP SEM with a tungsten filament electron gun and Oxford INCA EDS system. The samples were adhered onto stainless steel stubs using carbon tabs. EDX analysis was performed on the 1:2 IPCA (Figure 3-2) at 20 kV and processed using INCA software. All SEM micrographs of the AC (Figure 3-3) and 1:10 IPCA (Figure 3-4) were captured at 20 kV using the secondary electron detector at x30,000 magnification. EDX analysis of the 1:10 IPCA was performed at 20 kV and processed using INCA software.

2.2.2.2 Field emission scanning electron microscopy

Field emission scanning electron microscopy (FESEM) studies used a Hitachi 5500 FESEM equipped with a cold field emission tungsten source with built-in anode heater and an Oxford INCA EDS system. The sample was adhered onto a copper grid using PVC glue before it was placed on the stage for analysis. Only the 1:10 IPCA was used for FESEM analysis. All FESEM images were processed by the "*noise reduction*" feature of the FESEM software. The accelerating voltage varied from 20 kV to 25 kV during image capture using the secondary electron and dark field detectors. EDX analysis of the 1:10 IPCA was performed at 20 kV and processed using INCA software.

2.2.2.3 X-ray diffraction

X-ray diffraction (XRD) studies were conducted at room temperature (20°C - 25°C) using a Brüker D8 Advance GX002002 x-ray diffractometer with NaI scintillator detector configured with either a soller slot or a 0.6 mm solid slot. A 0.6 mm slit was placed in front of the 60 kV, 2.2 kW Cu-Kα radiation X-ray source. IPCA samples were adhered onto borosilicate glass slides using two sided pressure sensitive adhesive tape and the TiO_2 was applied using petroleum jelly. The glass

slides and adhesives were analysed separately to provide controls for all samples. Aqua 2k was used as the AC control. The diffraction angle (2-theta) was set to 22 to 80 for all studies. Data processing used Diffrac plus XRD commander version 2.6.0 and EVA Application 8,0,0,2 software. Scan speed was set to nine seconds/step and the increment was set to 0.05.

2.2.2.4 Fourier Transform Infrared Spectroscopy

Infrared spectra of the 1:10 IPCAs were obtained using a Fourier Transform Infrared Spectrophotometer (FTIR GX 2000, Perkin-Elmer). For the FTIR study, 30 mg of finely ground AC and IPCA were pelleted with 300 mg of KBr (Sigma) in order to prepare translucent sample disks. The FTIR samples were sent to the Central Salt and Marine Chemicals Research Institute, Bhavnagar, Gujarat, India for analysis. The FTIR of the KBr AC pellet was made using the transmission method. The FTIR spectra were recorded with 10 scans at a resolution of $4cm^{-1}$. An unused 1:10 IPCA, a 1:10 IPCA used for famotidine dark adsorption and a 1:10 IPCA used for photodegradation were separately analysed. All the experiments were conducted in triplicate and in some cases 4–5 times. However, only the average values are shown in the figures for clarity. The standard deviation in all cases was found to be ±5 %.

2.2.3 Analytical methods for famotidine and solifenacin

High performance liquid chromatography (HPLC) method

Famotidine/ solifenacin concentrations were measured using a high performance liquid chromatography (HPLC) system consisting of an Agilent 1100 (Agilent Technologies, Palo Alto, Ca, USA) low-pressure gradient pump equipped with a UV–Vis detector. This method was based on a combined method for famotidine, solifenacin and tamsulosin determination (Deegan, 2011). The LOD (limit of detection) and LOQ (limit of quantification) for famotidine/ solifenacin was 0.2 mg/L and 1 mg/L respectively. A 150 mm x 4.6 mm, 3.5 μm particle Luna pentaflourophenyl propyl reverse phase column (Phenomenex Inc., United Kingdom) was used for separation of the analyte. The mobile phase used for famotidine analysis consisted of 15 % methanol to 85 % water (purchased from Fisher Scientific Ireland)

with 0.1 % formic acid (Fluka, Buchs, Switzerland). The mobile phase used for solifenacin analysis was 60 % – 70 % methanol to water (purchased from Fisher Scientific Ireland) with 0.1 % formic acid (Fluka, Buchs, Switzerland).

This solution was filtered by 0.22 µm nylon filters (Sigma-Aldrich, Germany) and degassed by ultrasonication (5510 E-Mt Bransonic) for 30 min. The eluent flow rate was 1 mL/min and the injection volume was 50 µL. The wavelength of the detector was set at 205 nm. Data were processed by Agilent Chem Station software B.02.01SR1.

A 1000 mg/L famotidine/ solifenacin stock solution was prepared by dissolving 100mg of famotidine/ solifenacin into a 0.1 L volume flask using the mobile phase prepared for analysis: 15 % methanol: 85 % water with 1 mL formic acid for famotidine and 60 % - 70 % methanol: 40 % - 30 % water with 1 ml formic acid for solifenacin. This stock solution was used to prepare 10 mg/L, 25 mg/L, 50 mg/L, 75 mg/L and 100 mg/L famotidine standards using 0.01 L volumetrics. All samples and standards were placed in amber HPLC vials (Fisher Scientific Ireland) for analysis.

2.2.4 Sorption studies

2.2.4.1 General adsorption method

All adsorption studies used 0.05g of TiO_2/ AC/ 1:10 IPCA in 0.1 L famotidine/ solifenacin solutions in 0.25 L borosilicate glass conical flasks sealed with parafilm and shaken at 150 rpm in the dark in a 15°C+/-2°C temperature controlled room. Solutions of 100 mg/L famotidine or solifenacin were prepared by dissolving 100 mg of pharmaceutical in 1 L of deionised water and ultrasonicating (Bransonic 5510 E-Mt) this solution for 30 min. The pH of the solution was measured at the start and end of each study using a Jenway Model 3510 pH meter. Each study was done in duplicate and separate adsorbent free controls were prepared using the same method. The shaker was stopped to take 1 mL samples from the famotidine/ solifenacin solutions and adsorbent free controls using pasture pipettes.

For TiO_2 studies 3 mL samples were taken from the famotidine/ solifenacin solutions and adsorbent free controls using pasture pipettes. The 3 mLs of sample

solution were filtered with 0.22 μm nylon syringe filters (Phenomenex Inc., United Kingdom) to remove any TiO_2 particles before analysis. The reduction in the volume of solution with sampling was included in any adsorption loading calculations. The filtered samples were analysed using high performance liquid chromatography (HPLC) (see Section 2.2.3).

The adsorbed substrate or adsorption loading, q (mg/g) represents the substrate uptake and was calculated (Dai, 1994, Hameed *et al.*, 2009, Kim *et al.*, 2008) from the difference in substrate concentration in the aqueous phase before and after adsorption, as per following equation:

$$q = \frac{V(C_i - C_f)}{W} \quad (15)$$

where, q is the adsorption loading, V is the volume of substrate in solution (L), C_i and C_f are the initial concentration of substrate in solution (mg/L) and the final concentration of substrate in solution (mg/L) (after a given time typically 22 h) respectively, and W is the mass of AC/IPCA (g).

2.2.4.2 Adsorption kinetic studies

The method detailed in Section 2.2.4.1 was used for adsorption kinetic studies with the following exception: 0.25 mL samples were taken from the famotidine/ solifenacin solutions in the IPCA and AC studies using pasture pipettes.

2.2.4.3 Effect of initial pH

The method detailed in Section 2.2.4.1 was used with the following exceptions. Adjustment of the famotidine/ solifenacin solution to pH 2 used 1 M HCl, adjustment to pH 4 and pH 6 used 0.1 M HCl and adjustment to pH 8 used 0.1 M NaOH (Hameed *et al.*, 2009, Purkait *et al.*, 2007, Putra *et al.*, 2009). The HCl and NaOH were added to the famotidine/ solifenacin solution drop wise using pasture pipettes until the desired pH was achieved. The famotidine or solifenacin solution was stirred while measurements were taken by a pH meter (Wissenschaflich Technische Werksatatten pH522 or Jenway Model 3510 for solifenacin and all P25 adsorption studies). After the desired pH was achieved the adsorbent was added to the famotidine or solifenacin solutions.

2.2.4.4 Effect of initial concentration

The method detailed in Section 2.2.4.1 was used with the following exceptions. One hundred milligrams of famotidine/ solifenacin dissolved in 0.1 L of the mobile phase used for analysis was used to prepare a 1000 mg/L stock solution of famotidine. The initial concentrations studied were 20 mg/L, 40 mg/L, 50 mg/L, 60 mg/L, 80 mg/L, 100 mg/L and 150 mg/L. The initial concentrations were prepared by adding 2 mL, 4 mL, 5 mL, 6 mL, 8 mL, 10 mL and 15 mL of stock solution to 0.1 L volumetric flasks and making up to the mark with deionised water. For solifenacin AC/ IPCA studies, 10 mg/L and 30 mg/L concentrations were also used. These 0.1 L solutions were added to the 0.25 L conical flasks after 0.05g P25/ AC/ IPCA were weighted into them. For P25 studies the 0.1 L solutions were added to the 0.25 L conical flasks after 0.05 g P25 was weighted into them. The 0.1 L solutions were used to wash the P25 from the weigh boat into the conical flask. The pH of the solution was measured after the P25/ AC/ 1:10 IPCA was added - and at the end of the study - while the solution was stirred.

2.2.4.5 Desorption studies

0.2 g of AC was weighted into 0.2 L solutions in 0.5 L borosilicate glass beakers sealed with parafilm and shaken at approximately 100 rpm in the dark. Solution pH and ambient temperature was also monitored during sample removal. pH of the solution was not adjusted, therefore the natural pH of the solution (pH 6 - 8) was used for all studies. Desorption studies can be divided into two parts: the adsorption stage followed by the desorption stage.

In the adsorption stage the AC is contacted with a famotidine / solifenacin solution to allow the AC to become loaded with pharmaceutical. In the desorption stage the AC that was contacted with famotidine/ solifenacin was placed in 0.2 L of deionised water. When the solution was changed the solution was decanted and the AC was washed with deionised water by adding 25 mLs of deionised water to the AC and then decanting it. This process was repeated three times. After the AC was washed the 0.5 L beaker was filled with a 0.2 L 100 mg/L famotidine/ solifenacin solution. All samples were analysed by HPLC (Section 2.2.3).

Two types of desorption experiments were undertaken, where the AC had different levels of saturation in each. The procedure of both is detailed below:

1. One cycle of saturation – The AC was placed in a 100 mg/L famotidine/ solifenacin solution and shaken for 24 h. After 24 h of adsorption the famotidine/ solifenacin solution was decanted and the AC washed. 0.2 L deionised water was added and then 1ml samples were taken to measure desorption from the AC. After a period of time the deionised water solution was changed and the AC washed.
2. Three cycles of saturation – The AC was placed in a 100 mg/L famotidine/ solifenacin solution (0 h). Samples were taken after 24 h (48 h) and the famotidine/ solifenacin solution was decanted and the AC washed. A fresh 0.2 L, 100 mg/L famotidine/ solifenacin solution was added and a sample was taken after 24 h (72 h) of desorption. The AC was washed and then placed in 0.2 L of deionised water (0 h) signifying the start of the desorption phase. pH measurements were make during the taking of 1ml samples from the famotidine/ solifenacin solutions. After 48 h of desorption the solution was decanted and the AC washed and immersed in a 0.2 L deionised water solution. Samples were taken after 24 h intervals at 72 h and 96 h.

2.2.5 Models used for adsorption analysis

2.2.5.1 Intraparticle diffusion model

The intraparticle diffusion model (Arivolia *et al.*, 2009, Hameed *et al.*, 2009, Hameed, 2009, Hossain and McLaughlan, 2011, Kumar *et al.*, 2003, Thirumal and Kaliappan, 2011, Önal, 2006) can be expressed by the following equation:

$$qt = k_{int} t^{0.5} + C \quad (16)$$

Where qt is adsorption loading (mg/g) at a given time (days), k_{int} is the intraparticle diffusion rate constant (mg/g $day^{-1/2}$) and C is the intercept and indicates the presence of boundary layer diffusion and t is time (days).

2.2.5.2 Bangham equation

Bangham equation (Önal, 2006) is given as:

$$\log\left(\log\left(\frac{C_0}{C_0 - qtm}\right)\right) = \log\left(\frac{k_b m}{2.303V}\right) + \alpha\log(t) \qquad (17)$$

Where C_0 is the initial concentration of the adsorbate in solution (mg/L), V the volume of solution (L), qt is the amount of dye adsorbed (mg/g) at time t, t is time (days), m the weight of the adsorbent used (g/L). α (which must be <1) and k_b, the pore diffusion rate (mL/(g/L)) are the constants (Tütem *et al.*, 1998, Önal, 2006). For a plot of Log Log (C_i/C_i-m*qt) vs. log (t), α is the slope of the line and k_b is equal to 10^intercept(2.303V/m).

2.2.6 Models used for isotherm studies

2.2.6.1 Langmuir

The Langmuir equation (Langmuir, 1916) is expressed as:

$$q_{22h} = \frac{q_m K_L C_{22h}}{1 + K_L C_{22h}} \qquad (18)$$

Where q_{22h} is the adsorption loading (mg/g) after 22 h, q_m (mg/g) is the maximum amount of the adsorbate per unit weight of the adsorbent to form a complete monolayer on the surface (monolayer adsorption capacity), C_{22h} is the concentration in solution after 22 h adsorption, K_L (L/mg) is the Langmuir constant related to the affinity of the binding sites (free energy of adsorption).

2.2.6.2 Freundlich

The Freundlich isotherm model (Freundlich, 1907, Mohan and Singh, 2002) is expressed as:

$$q_{22h} = K_F C_{22h}^{\frac{1}{n}} \qquad (19)$$

Where q_{22h} is the adsorption loading (mg/g) after 22 h, C_{22h} is the concentration in solution after 22 h adsorption, K_F (l/mg), 1/n are Freundlich

constants related to sorption capacity and sorption intensity of the adsorbent, which represent the quantity of sorbate adsorbed onto the IPCAs and AC for an equilibrium concentration.

2.2.6.3 Temkin isotherm

The Temkin isotherm (Hameed *et al.*, 2009, Kundu and Gupta, 2006, Lataye *et al.*, 2008) is expressed in linear form as:

$$q_{22h} = B\ln(A) + B\ln(C_{22h}) \quad (20)$$

Where q_{22h} is the adsorption loading (mg/g) after 22 h, C_{22h} is the concentration in solution after 22 h adsorption, B = RT/b, B is the Temkin energy constant (J mol^{-1}) R the universal gas constant (J mol^{-1} K^{-1}), T the absolute temperature (K), b is the variation of adsorption energy (J mol^{-1}) and A is the equilibrium binding constant (l mg^{-1}) corresponding to the maximum binding energy. A plot of q_{22h} versus $\ln C_{22h}$ enables the determination of the isotherm constants, B and A from the slope and intercept of the line respectively (Lataye *et al.*, 2008).

2.2.6.4 Redlich–Peterson (R-P) isotherm

The Redlich and Peterson model (Kumar *et al.*, 2003, Kumar *et al.*, 2008, Lataye *et al.*, 2008, Redlich and Peterson, 1959) is usually given as:

$$q_{22h} = \frac{K_{r-p} C_{22h}}{1 + A_{r-p} C_{22h}^{\beta}} \quad (21)$$

Where q_{22h} is the adsorption loading (mg/g) at equilibrium, C_{22h} is the concentration in solution after 22 h adsorption, K_{r-p} and A_{r-p} are the Redlich and Peterson isotherm constants (Aksu and Yener, 2001). The equation was determined using a non-linear regression method (Aksu and Yener, 2001). This equation was calculated using the *Solver* Add-In for Microsoft Excel. The isotherm can also be expressed (Wu *et al.*, 2010) as:

$$q_{22h} = \frac{K_{r-p} A_{r-p} C_{22h}}{1 + A_{r-p} Ce_{22h}^{\beta}} \quad (22)$$

Eq (22) can be transformed into:

$$\frac{C_{22h}}{q_{22h}} = \frac{1}{A_{r-p}K_{r-p}} + \left(\frac{1}{K_{r-p}}\right)C_{22h}^{\beta} \quad (23)$$

There are two limiting behaviors: When β = 1 the equation converts to the Langmuir form (eq 22) and when b = 0 it converts to Henry's law. When $A_{r\text{-}p}$ = 0, it transforms into the Freundlich isotherm equation.

2.2.6.5 Error checking of isotherm studies

The fit of calculated isotherm data to the experimental data was investigated using the sum of the squares of the errors (SSE) test (Eq 24) (Basha *et al.*, 2011, Choy *et al.*, 2004, Kumar *et al.*, 2008, Kundu and Gupta, 2006, Kundu and Gupta, 2006) and the standard error (SE) test (Basha *et al.*, 2010) shown in Eq 25.

$$SSE = \sum_{i=1}^{m} (qcal - qexp)^2 \quad (24)$$

$$SE = \sqrt{\frac{1}{n-p}\sum_{i=1}^{m} (qcal - qexp)^2} \quad (25)$$

Where qcal is the calculated adsorption loading (mg/g) at a given time, qexp is the experimental determined adsorption loading (mg/g) at a given time, n is the number of data points in the data set and p is the number of parameters in the model being tested.

2.2.7 Method for photodegradation studies

Photolysis and photocatalysis studies were conducted using a 1 L borosilicate glass photoreactor (Schlenk flask) manufactured by Ace Glass (model 7841-06) and an immersion well (model 7857); 290 mm in length with water cooling (Figure 2-1). A 125 W medium pressure mercury lamp (TQ 150 Heraeus Noblelight, emission between 248 nm and 579 nm, λmax 366 nm see Appendix D) inserted in the middle of the reactor was used as the light source. All studies were illuminated by this light source for 180 min. Tap water was circulated through the immersion well (water cooling jacket) to keep the solution temperature from rising 2°C - 3°C above room temperature (21°C). The famotidine/ solifenacin solution in the photoreactor was mixed using a magnetic stirrer at 150 rpm. All studies had an equilibrium stage where they were placed in the reactor for a given time (240min to 15min) and not illuminated. Samples taken during the dark adsorption stage are denoted with negative values e.g. samples taken 60 min before illumination are denoted as -60. Samples containing TiO_2 were syringe filtered with 0.22 μm nylon filters to remove any TiO_2 particles in the sample. Samples (3ml) were taken and analysed as described in Section 2.2.3. The catalyst concentrations were 0.2 g/L, 0.3 g/L, 0.4 g/L and 0.5 g/L for TiO_2 catalyst concentration optimisation, 0.4g/L for TiO_2 studies and for IPCA studies 0.4 g/L or 1.5g/L. Two initial concentrations were studied: 50 mg/L and 100 mg/L for famotidine and 45 mg/L and 100 mg/L for solifenacin succinate.

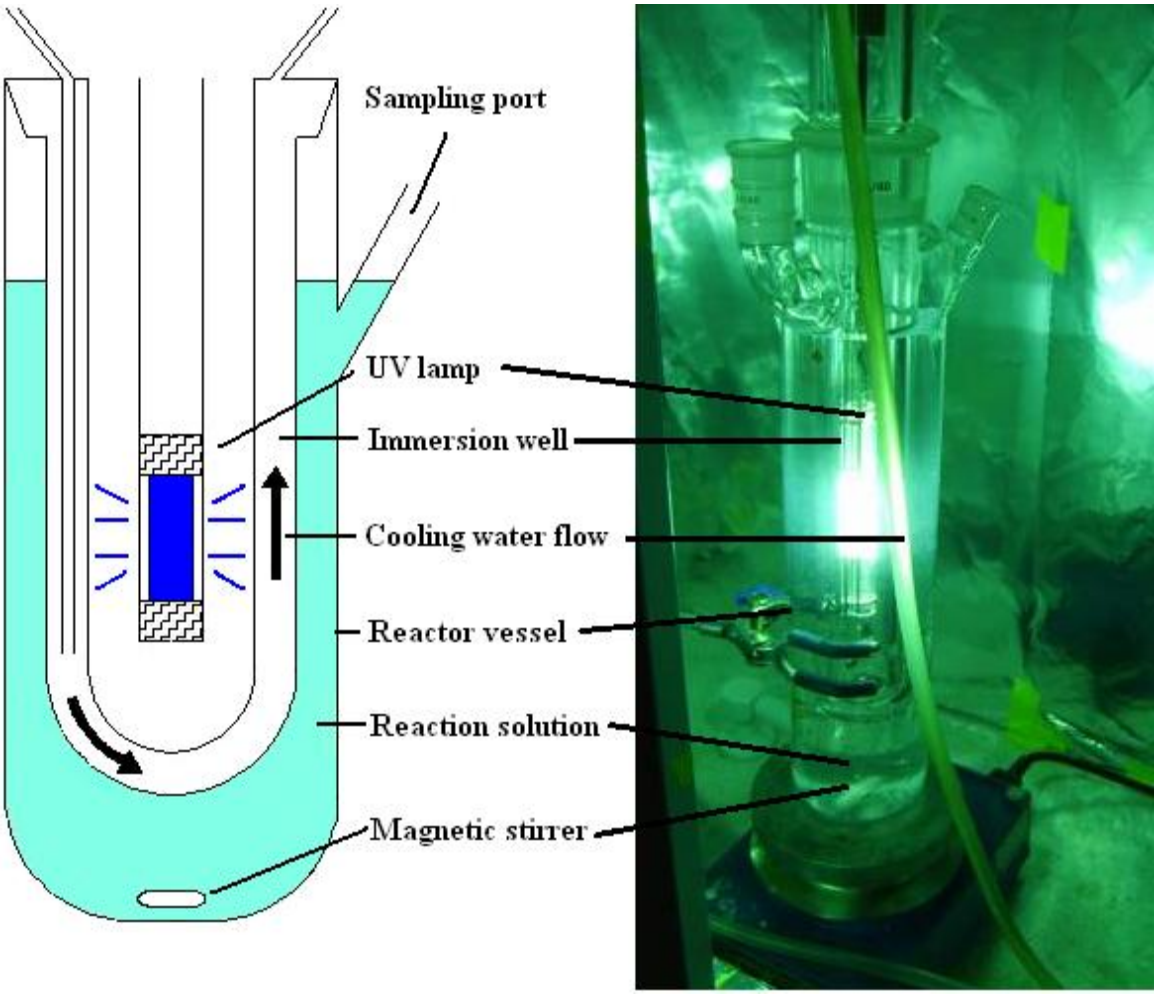

A) **B)**

Figure 2-1 A) Schematic of photochemical reactor, B) Photograph of photochemical reactor using 1:10 IPCA during illumination.

Chapter 3 Characterisation of AC and IPCAs

3.1 Introduction

Physical characterisation methods were used to investigate the properties of the IPCAs. The methods used for the IPCA were also used on the AC and where applicable TiO_2. In this chapter:

- Morphological features of the surface of the AC and IPCAs are determined using SEM and FESEM analysis.
- Energy dispersive x-ray (EDX) is used to analyse the distribution of TiO_2 across the surface of the IPCA and its elemental composition.
- The crystalline structure of the AC and TiO_2 is analysed using X-ray diffraction (XRD).

3.2 Scanning electron microscopy / energy dispersive X-ray of AC and IPCAs.

The texture and morphology of the catalyst are important parameters that influence photocatalytic activity. It is established that small TiO_2 aggregates that are uniformly dispersed, have more reactive sites than agglomerated particles which have a smaller surface area (Foo and Hameed, 2010a). Separate from TiO_2 agglomeration a good dispersion of TiO_2 across the surface of an AC is necessary to create an effective IPCA as large areas without TiO_2 will not have photocatalytic ability, reducing the overall performance of an IPCA.

The first IPCA to be investigated was the 1:2 IPCA (prepared using a ratio of 50% TiO_2 to AC by mass) as its high TiO_2 to AC ratio would likely give more signal response than an IPCA with lower TiO_2 loading. The SEM image of the 1:2 IPCA (Figure 3-1) depicts the granular structure of the carbon surface and shows that it is irregular with some smooth surfaces. EDX analysis of this grain of the 1:2 IPCA (Figure 3-2) shows the presence of titanium (thus titanium dioxide) on the surface of the IPCA. The EDX spectrum also shows the presence of trace levels of Ca, S, Al and Fe. These are likely impurities in the IPCA from Aqua 2k, an AC prepared from bituminous coal which would contain these elements (Xue and Lu, 2008).

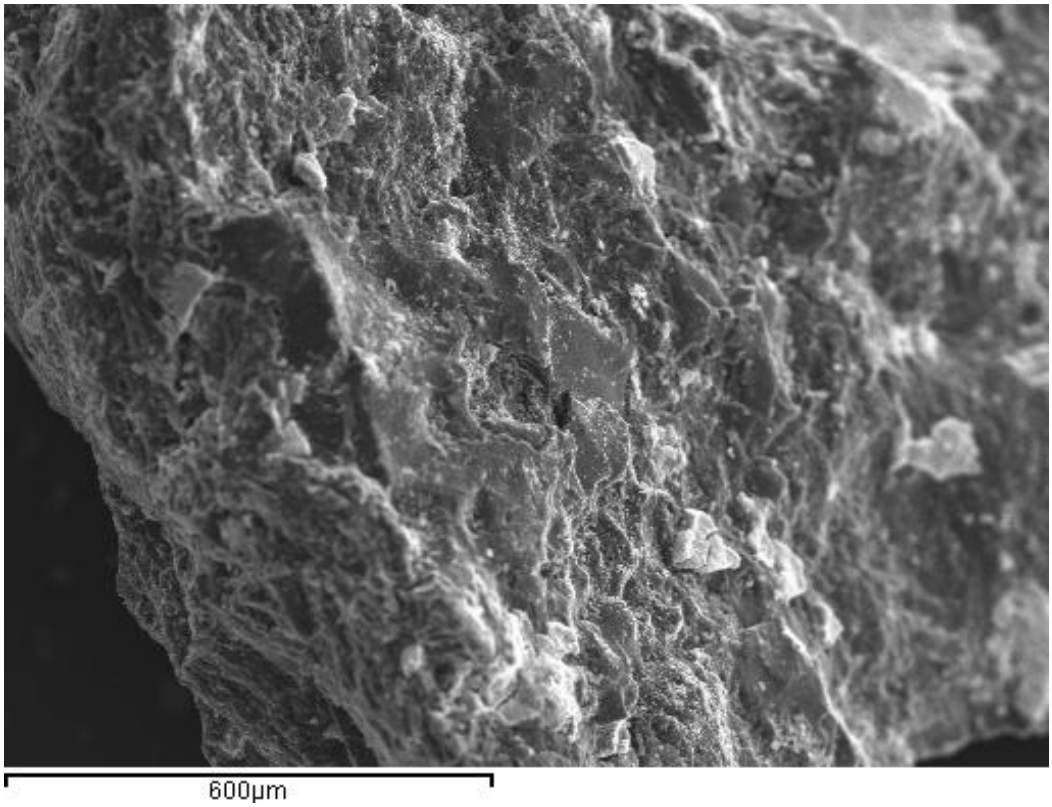

Figure 3-1 SEM image of the 1:2 IPCA surface.

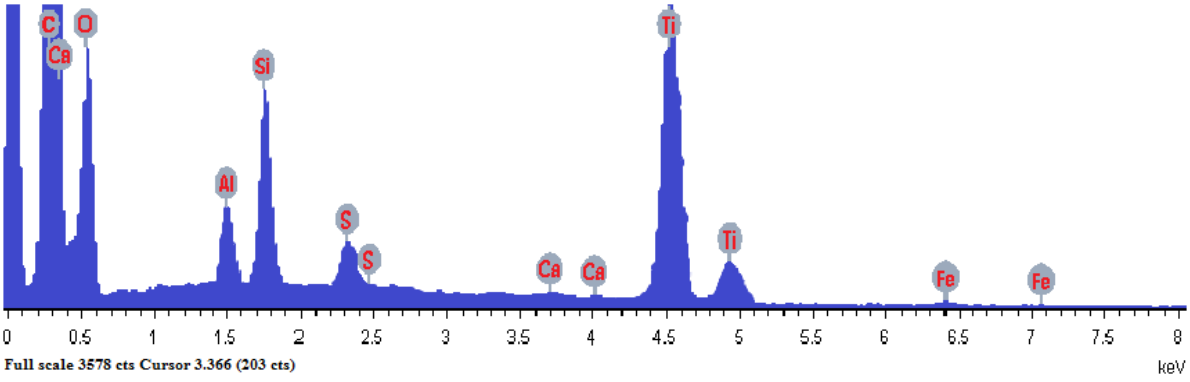

Element	C	O	Al	Si	S	Ca	Ti	Fe
Weight%	69.53	21.81	0.58	1.50	0.40	0.05	5.97	0.16
Atomic%	78.56	18.50	0.29	0.72	0.17	0.02	0.169	0.04

Figure 3-2 SEM - EDX spectrum of 1:2 IPCA.

The SEM image of an AC in Figure 3-3 depicts the carbon surface and shows that it is irregular with some smooth surfaces. The SEM image of a 1:10 IPCA (Figure 3-4) shows a roughened AC surface caused by the homogeneous deposition of aggregates of TiO_2 on the carbon surface, which is in line with comparable studies (Araña *et al.*, 2003b). EDX analysis of a grain of the 1:10 IPCA (Figure 3-5, Figure

3-6) demonstrate a distribution of titanium across its entire surface. The titanium loading appears uneven with some areas of the IPCA displaying notably higher titanium concentrations. While this may be due to irregular distribution of the TiO_2 across the IPCA surface it is more likely caused by emission of X-rays from surfaces of the IPCA that face away from the detector and consequently cannot be detected (Figure 3-7). The areas of the IPCA facing or in proximity to the detector therefore appear to have the highest Ti composition (Eggert 2011).

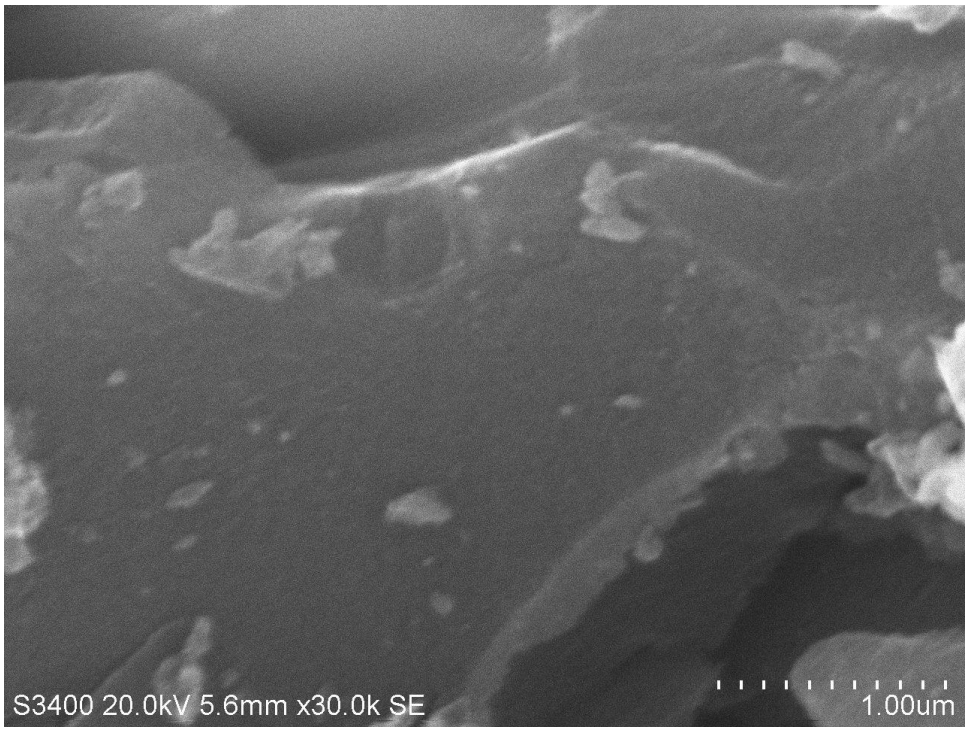

Figure 3-3 SEM micrograph of Aqua 2k AC.

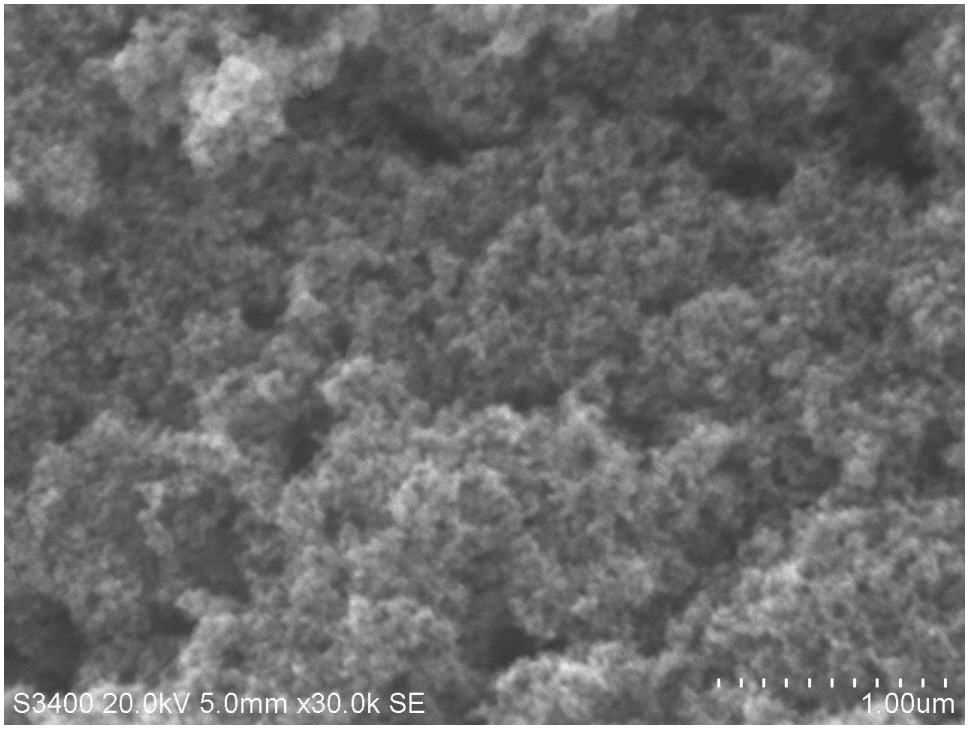

Figure 3-4 SEM micrograph of 1:10 IPCA.

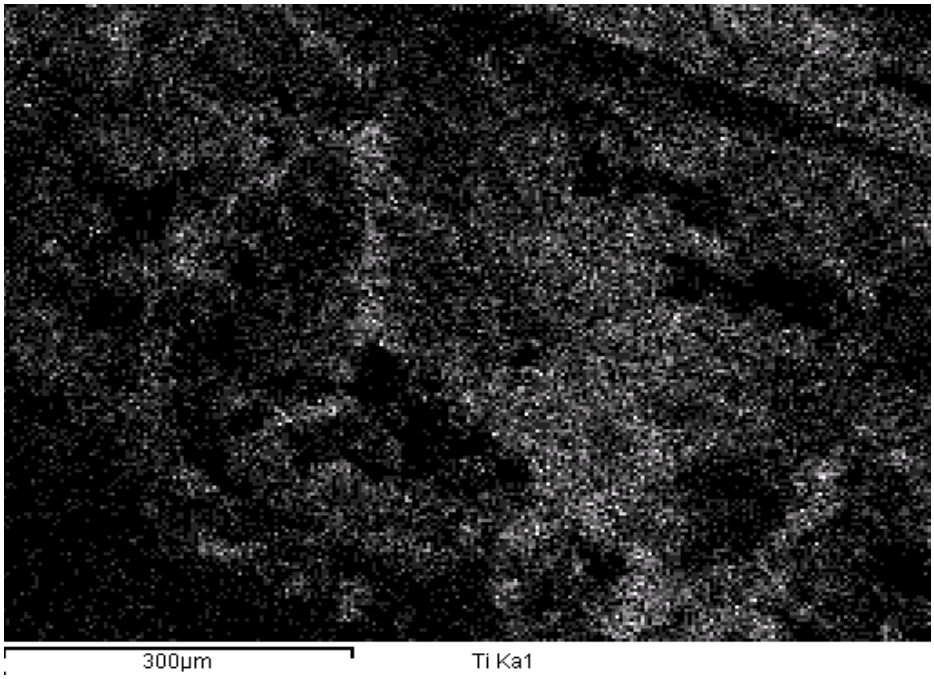

Figure 3-5 EDX analysis of titanium on the 1:10 IPCA surface.

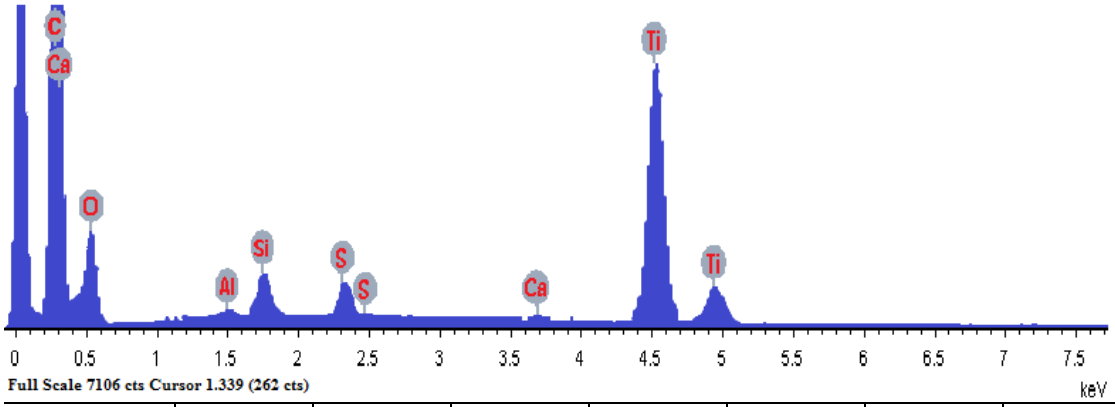

Element	C	O	Al	Si	S	Ca	Ti
Weight%	65.91	20.50	0.11	0.77	0.71	0.09	11.91
Atomic%	77.58	18.11	0.06	0.39	0.31	0.03	3.51

Figure 3-6 EDX spectrum and elemental composition of the 1:10 IPCA surface.

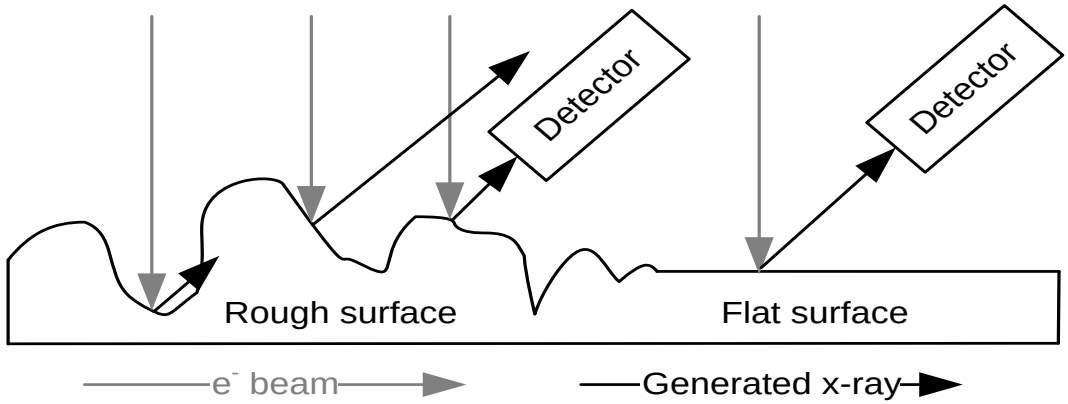

Figure 3-7 Simplified diagram of the emission of X-rays from rough and flat surfaces in EDX.

3.3 Field emission scanning electron microscopy of AC and IPCAs

FESEM uses a field-emission cathode in the electron gun of a SEM to provide narrower probing beams, improving resolution while minimizing sample charging and damage. The improved resolution allows higher magnification than SEM. It was used to provide higher magnifications (180,000 vs. 30,000) of the AC and IPCA surface compared to SEM images.

Figure 3-8 shows the TiO_2 distribution around the surface of a small particle of GAC. Figure 3-9 is a magnification of the centre bottom section of Figure 3-8 and the measurements of the TiO_2 particles are shown. The TiO_2 particles have a diameter in the region of 15 nm – 31 nm. These images demonstrate that TiO_2 can be dispersed effectively across the AC surface by the ultrasonication impregnation method used to prepare the IPCAs. Not every grain of AC was evenly coated with TiO_2 and several larger agglomerations of P25 were also visible indicating that this method does not create an IPCA with a completely even distribution of TiO_2. Figure 3-10 shows the irregular surface of the 1:10 IPCA with heavy deposition of TiO_2 on the top right hand corner, a section of this segment is magnified and shown in Figure 3-11. The agglomerations of TiO_2 are clearly visible and the larger particles of P25 are deposited at the bottom of the TiO_2 layer with smaller grains deposited on top. This effect is caused by the drying procedure during IPCA preparation, the larger and heavier particles should settle first followed by smaller and lighter particles.

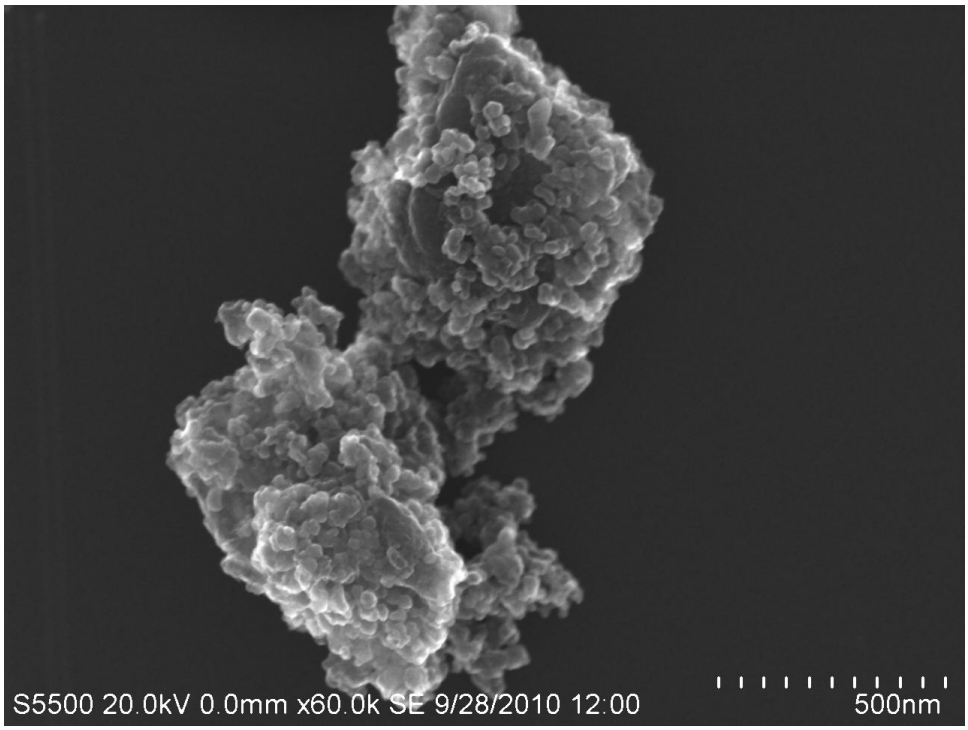

Figure 3-8 FESEM image of a small grain of 1:10 IPCA.

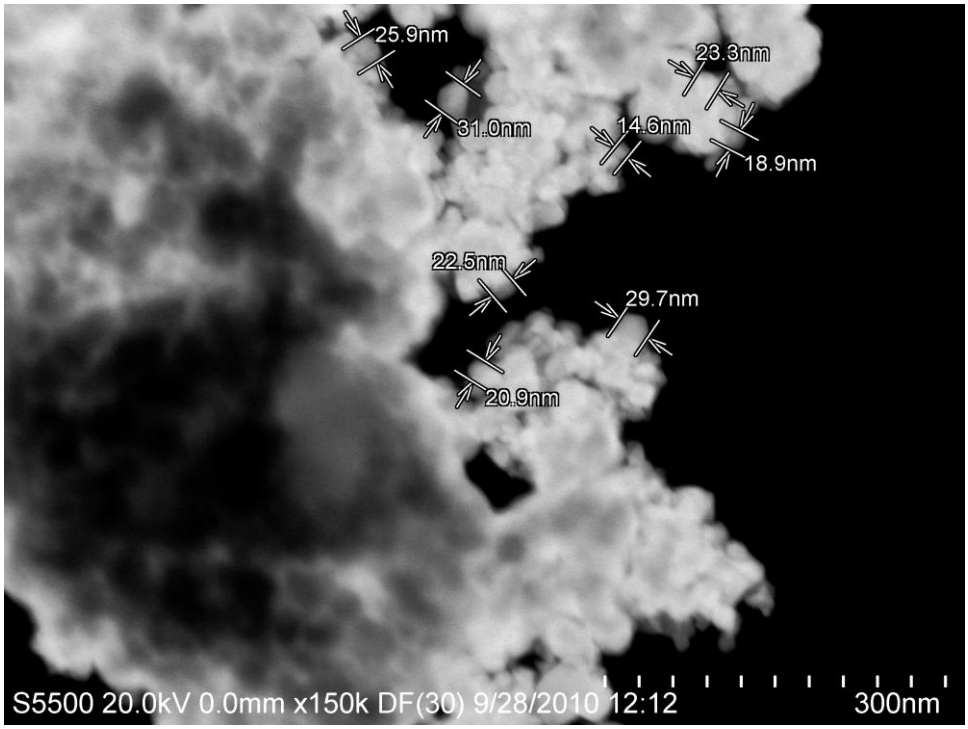

Figure 3-9 FESEM image showing the diameter of TiO_2 particles on the IPCA shown in Figure 3-8.

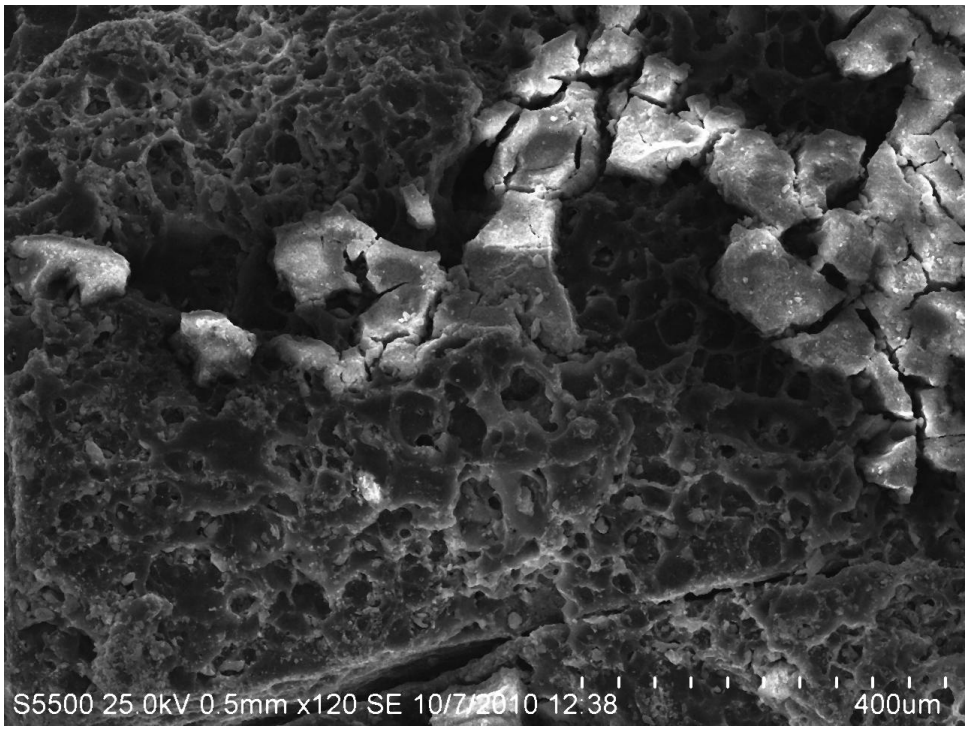

Figure 3-10 FESEM image of a section of 1:10 IPCA.

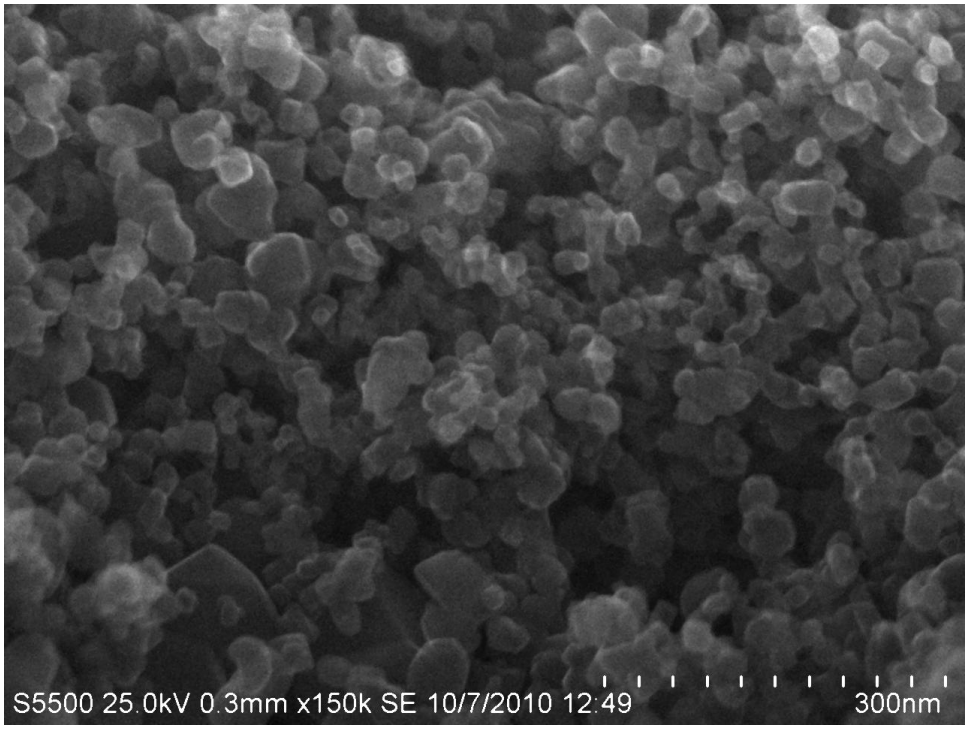

Figure 3-11 Magnified FESEM image of an area of the 1:10 IPCA covered in TiO_2.

A grain of unmodified Aqua 2k AC is shown in Figure 3-12. It has the same irregular macro structure surface as the 1:10 IPCA but without the deposits of TiO_2. The few bright spots on the surface are either a build-up of charge on the AC surface from the electron beam or particles of trace elements in the AC. The surface of the AC shown in Figure 3-13 is at the same magnification as the image of the 1:10 IPCA (Figure 3-11). Figure 3-13 shows an irregular but smooth surface that is fundamentally different to that shown in Figure 3-11. This proves that the agglomerations present in Figure 3-11 are P25 TiO_2 particles and not features of the AC surface. The FESEM results verify the SEM results ensuring agreement of both methods and it indicates the SEM method is able to resolve the P25 effectively, but not at the same resolution as FESEM.

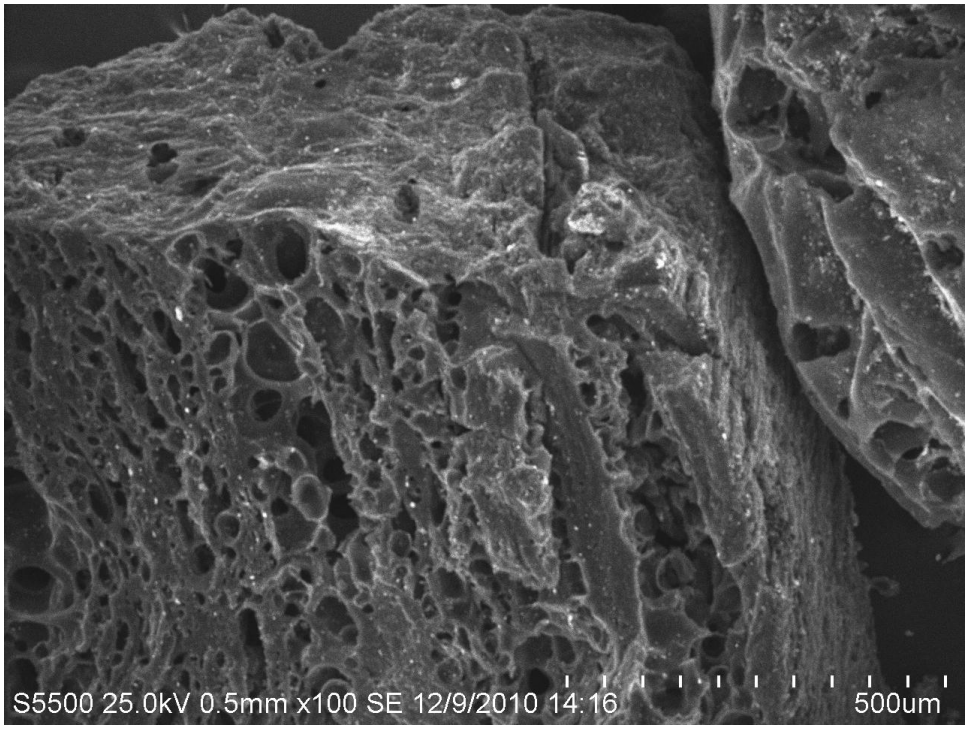

Figure 3-12 FESEM image of a grain of unmodified AC.

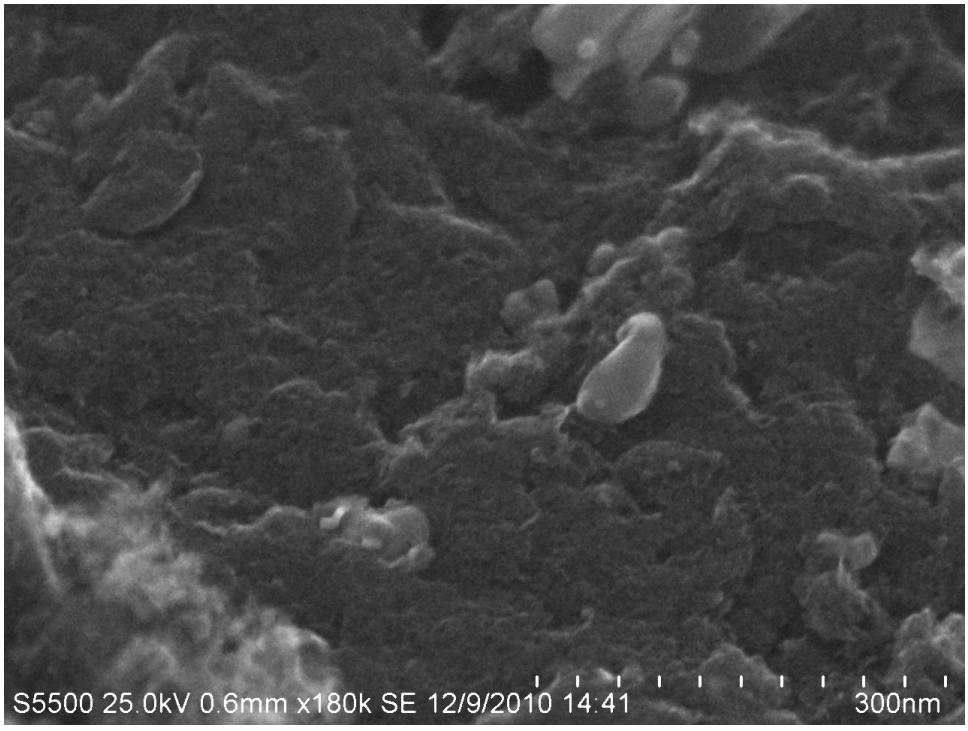

Figure 3-13 High magnification FESEM image of an area of the AC surface.

EDX analysis of the 1:10 IPCA using FESEM yielded similar results to the SEM EDX analysis (Figure 3-5) for the presence of Ti and other trace elements in the AC. Two sites on the 1:10 IPCA were studied and these sites are labelled A (Figure

3-14) and B (Figure 3-16). Site A contains an area of heavy TiO_2 deposition beside an area lacking P25 deposition caused either by wearing off of the TiO_2 or irregular deposition. Two areas of site A were analysed: "*area of IPCA*" which shows a large amount of TiO_2 deposition and "*spot at 20k*" which is a magnification of a smooth section with no apparent TiO_2 deposition. Site B is a separate area of the 1:10 IPCA with little apparent TiO_2 deposition. The % atomic weights are given in Table 3-1. The results for Site B and spot at 20k for Site A indicate that a small quality of P25 is distributed throughout the entire carbon surface. There was significantly more TiO_2 present at the area of IPCA which was visually "roughened" compared to the other "flatter" areas. In terms of % atomic weight Ti represented 1.95 % of the area of IPCA compared to 0.35 % and 0.23 % at the "*spot at 20k*" and Site B respectively.

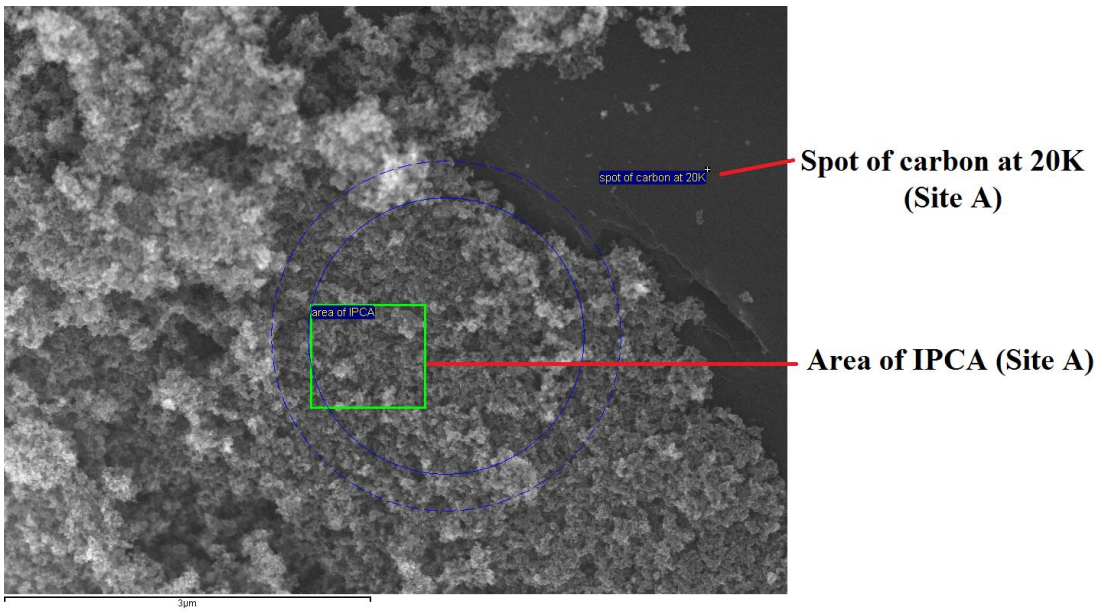

Figure 3-14 FESEM "Site A" of 1:10 IPCA. "Area of IPCA" is in the centre while "spot of carbon at 20k" is in the top right hand corner.

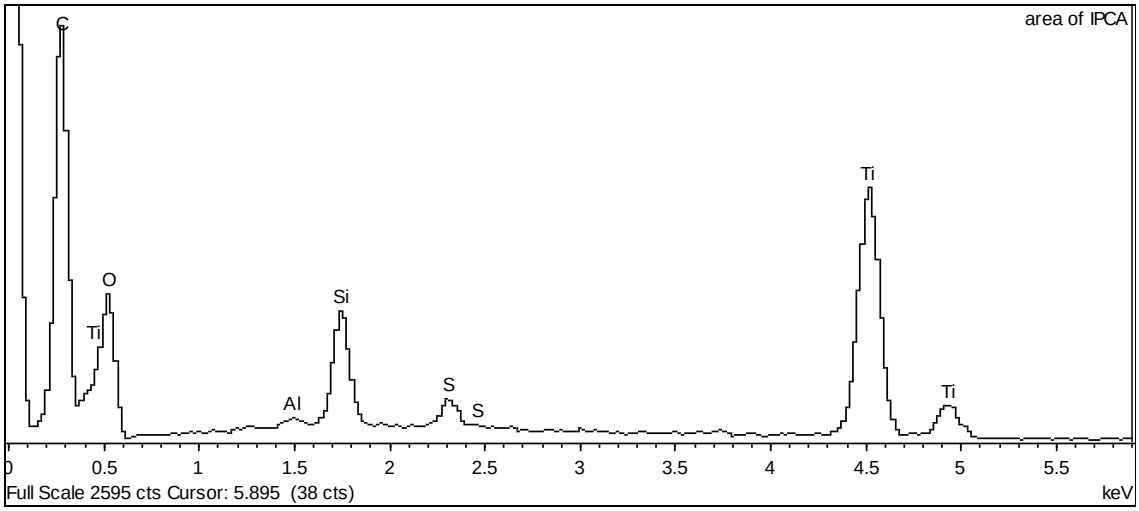

Figure 3-15 FESEM EDX spectrum of "*Area of IPCA*".

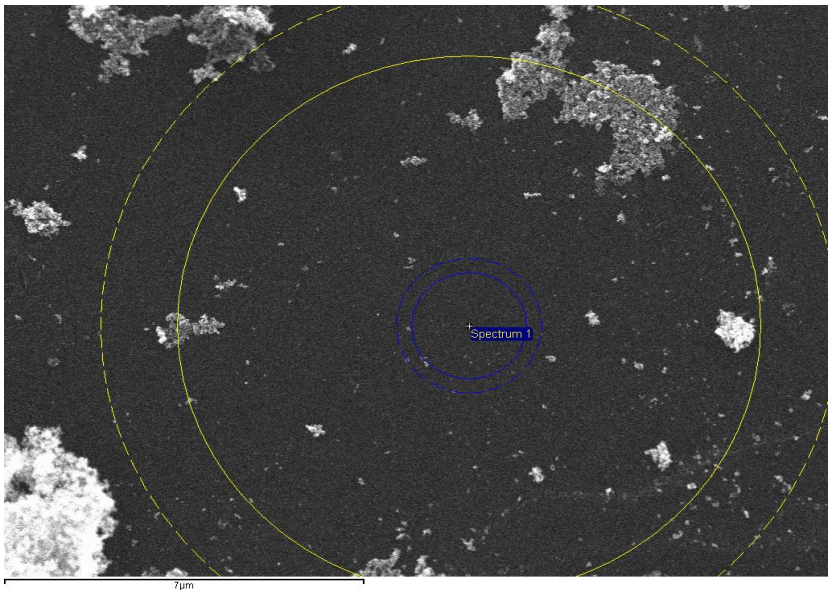

Figure 3-16 FESEM Site B "Spot of carbon".

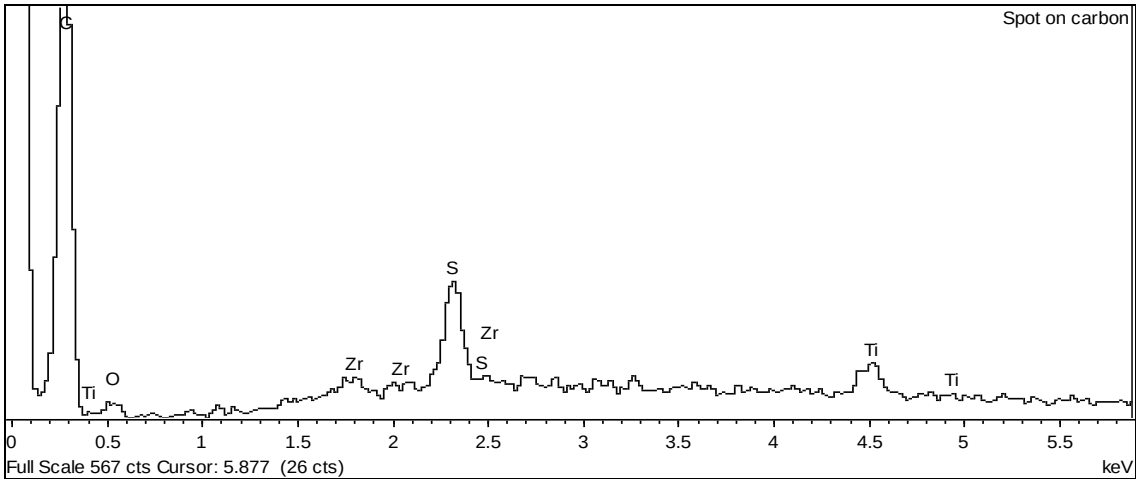

Figure 3-17 FESEM spectrum of "Spot of carbon".

Table 3-1 FESEM, EDX analysis. All elements analysed (Normalised). All results in atomic%.

	C	O	Al	Si	S	TiO_2	Zr
Site A							
Area of IPCA	64.47	32.28	0.09	1.01	0.2	1.95	
Spot at 20k	91.93	7.13		0.5	0.2	0.23	
Site B							
Spot of carbon	94.58	4.02			0.96	0.35	0.09

3.4 X-ray diffraction

XRD is an analytical technique which reveals information about the crystallographic structure and chemical composition of powders and thin films. XRD was used to investigate the crystalline phase of the TiO_2 and the crystalline structure(s) of the AC. Both of these parameters can influence the adsorption and photoactivity of IPCAs and must be monitored especially when an IPCA is heat treated as these properties are changed by heat treatment (see Section 5.4).

The legend names each sample and the type of slot placed over the detector. The glass slides used for mounting the samples were analysed and the results are shown in Figure 3-18. The plain glass slide analysed with the solid slits had a stable baseline with no peaks indicating that the glass slide is inert for this analysis. When the glass is covered with petroleum jelly and analysed with a sollor slot there are no peaks but there is a gradual increase in the baseline at lower 2-theta angles. Petroleum jelly was used to bind the powdered TiO_2 to the glass slide as its viscous nature allows a large amount of TiO_2 to be incorporated onto the slide compared to adhesive tape where the layer of TiO_2 is only a few particles thick. Unlike other adhesives petroleum jelly has no crystalline structure which is important because it will not give any peaks in the XRD spectrum. However, the alkane chains in the petroleum jelly are said to have diffraction peaks close to graphite (Cunningham *et al.*, 2004). Given that there are no peaks at or near the graphite peak at 26.5° this implies that the increase in the baseline is caused by extra x-rays entering the detector through the sollor slot that would be filtered out by the solid slits. It is also possible that it is caused by trace metal impurities in the glass or x-ray interactions with the carbonaceous material in

the petroleum jelly that are too small to be detected using the solid slits. However a baseline with this shape is not observed in the P25 studies (Figure 3-19) which indicates that the petroleum jelly is not the cause and that the rise in the baseline will not interfere with the analysis of other samples.

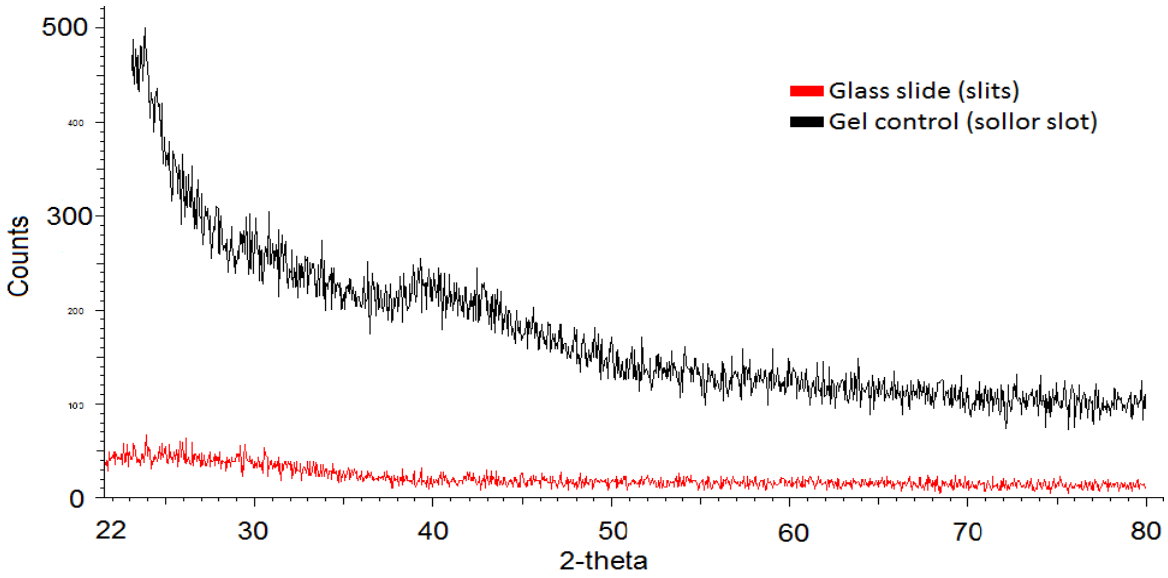

Figure 3-18 XRD spectra of glass slide (with silts) and glass slide covered with petroleum jelly (with sollor slot).

Figure 3-19 shows the XRD spectrum of P25 TiO_2. The sample analysed with solid slits has a lower signal in terms of the number of counts and a higher signal to noise ratio. There is no difference in location of the peaks using either method with the exception of the peaks at 69° and 70.5° which are not visible using solid slits. The reduction in the signal to noise ratio from 11:1 for the solid slits to 7:1 for the sollor slots is a worthwhile trade-off to enhance the signal for smaller peaks which aids the identification of the TiO_2 phases.

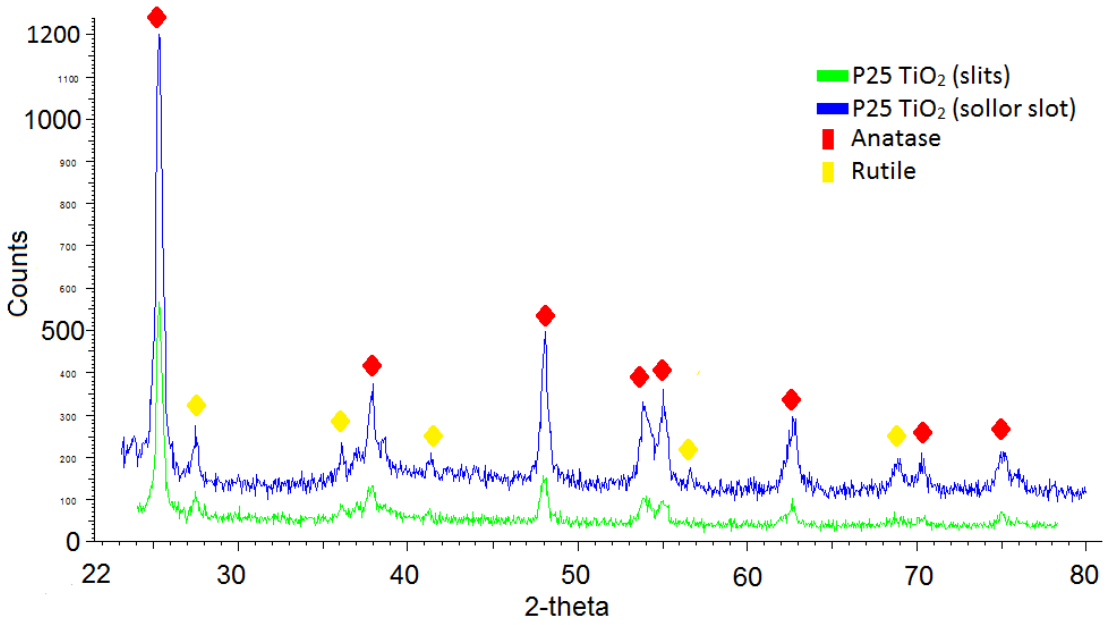

Figure 3-19 XRD spectra of P25 adhered to a glass slide with petroleum jelly with solid slits and a sollor slot.

Figure 3-20 is the same spectrum as Figure 3-19 but the vertical lines correspond to the crystal structure. The peaks at 25°, 38°, 48°, 54°, 55°, 70.5° and 75° correspond to a synthetic anatase phase (SS-NNNN 89-4921). The peaks at 27.5°, 36°, and 41° correspond to the rutile phase (SS-NNNN 89-0553). The peaks at 54.5°, 63° and 69° could refer to either phase due to signal overlap in the case of 69° or insufficient resolution to separate close peaks belonging to both phases for example 54.5° could be a rutile peak or part of the anatase peak at 54°. The rutile phase has an overall weaker signal compared to anatase. This indicates that the P25 is mainly composed of anatase TiO_2 with a smaller concentration of rutile. A calculation based on peak height would indicate that this P25 is approximately 80 % anatase to rutile (Zhao *et al.*, 2010). This value is within the ratio of values found in the literature (Section 1.4.1). The % anatase to rutile in P25 is important because the rutile phase has a lower conducting band potential and may act as an electron sink reducing the recombination of charge carriers. A change in the polymorph ratios could alter the photocatalytic activity.

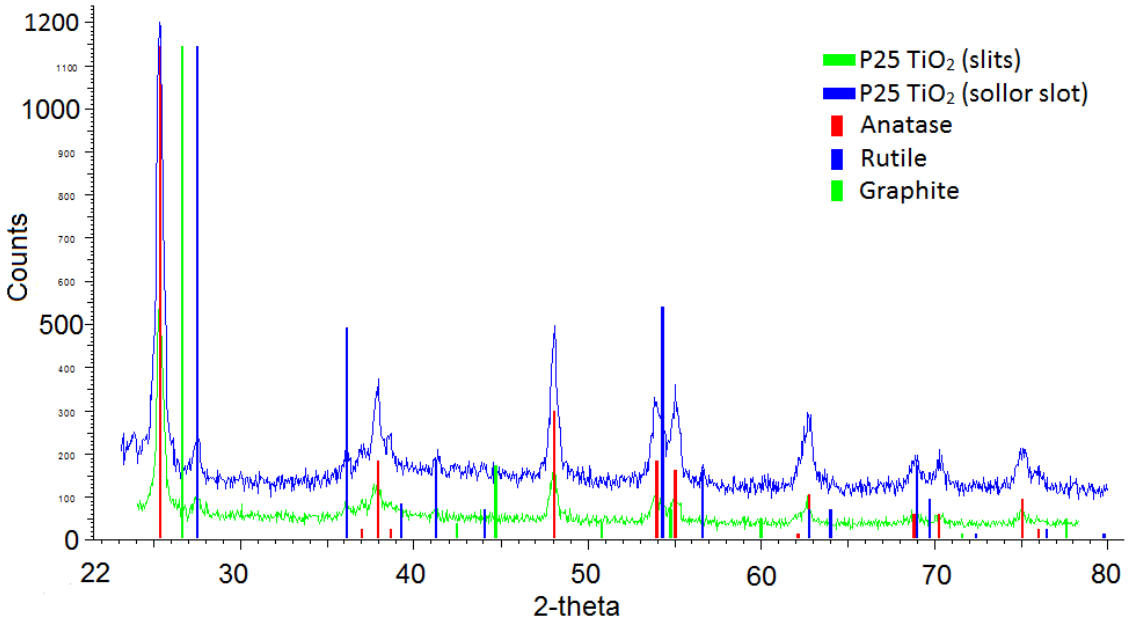

Figure 3-20 XRD spectra of P25 adhered to a glass slide with petroleum jelly with solid slits and a sollor slot. The vertical lines indicate crystalline phase.

The XRD spectrum of the non-heat treated 1:10 IPCA is shown in Figure 3-21). The XRD spectrum of the 1:10 IPCA heat treated at 700°C (see Section 2.2.1.2) is shown in Figure 3-22. The XRD spectrum of unmodified AC is shown in Figure 3-23. There is no noticeable difference between the two 1:10 IPCAs. The AC returns a stronger signal especially in the 40-50° regions. Peaks are visible at 26.5° and 60° for all IPCAs but are absent in the P25 controls (Figure 3-19). These peaks correspond to graphite - the spectra are similar to commercial graphite results reported in the literature (Liang *et al.*, 2003) - which would appear in the XRD spectrum either because it is a constituent of the AC (Zhao *et al.*, 2009) or limited parallelism between the graphene layer of the AC created x-ray scattering that corresponds to graphite (Marsh and Rodríguez-Reinoso, 2006c). The rising baseline at low 2-theta angles is typical of carbonaceous materials (Cunningham *et al.*, 2004) and would be consistent with the defective graphene layer structure of AC and is evident in other studies (Jia *et al.*, 2007, LI *et al.*, 2011, Velasco *et al.*, 2010c). The low concentration of P25 on the surface of the IPCA makes it difficult to resolve the crystalline phase of the TiO_2. The peaks at 25°, 38°, 48°, and the weak signals at 54°, 55° are present in the IPCA but not the AC and correspond to synthetic anatase. Due to the lower response no rutile peaks are visible in contrast to P25 where several were visible. The main rutile peak at 27.5° is not visible due to the rising baseline caused by the AC. For the

unmodified 1:10 IPCA the inability to find rutile is not significant as it can be assumed that the crystalline phase is not changed by ultrasonication. However for the 1:10 IPCA heat treated at 700°C should demonstrate some conversion of the anatase to the rutile phase. However the entire XRD spectrum for both IPCAs is almost identical suggesting that the crystalline structure of the IPCA was not changed by heat treatment.

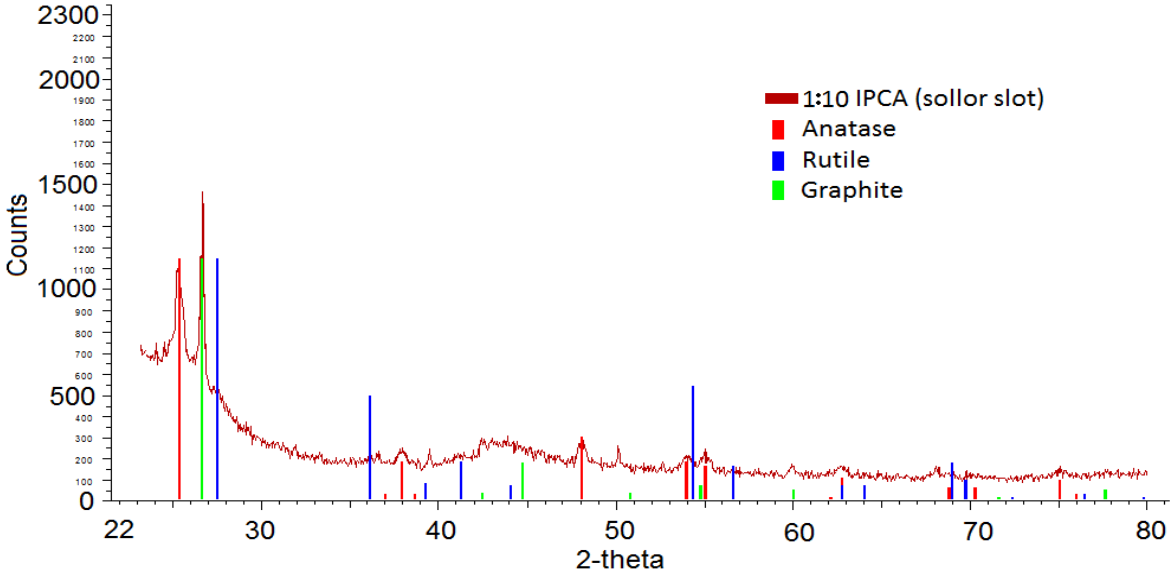

Figure 3-21 XRD spectra of 1:10 IPCA. The vertical lines indicate the crystalline phase.

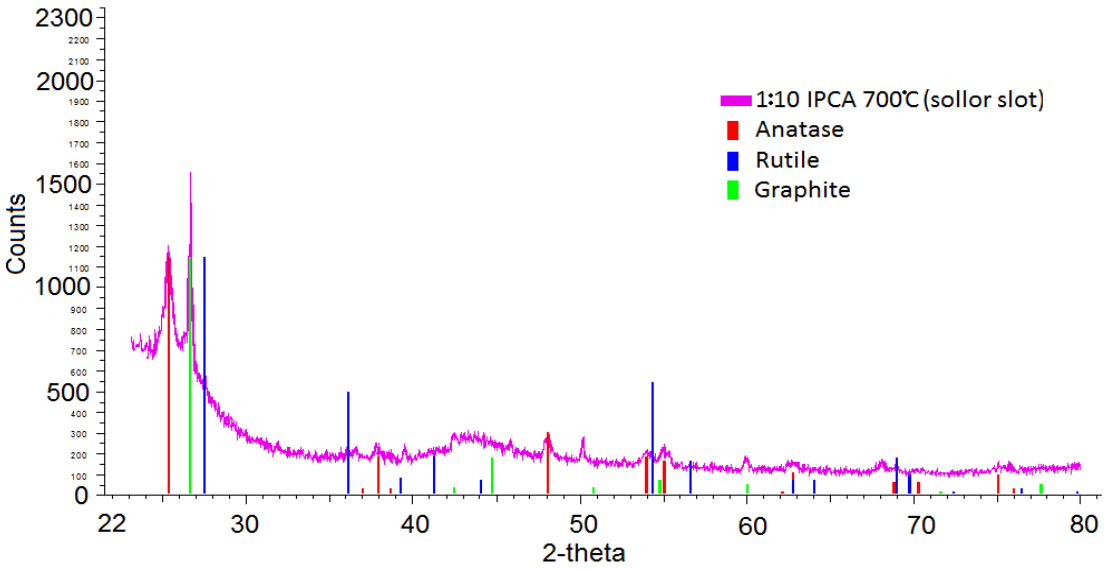

Figure 3-22 XRD spectra of 1:10 IPCA heat treated at 700°C. The vertical lines indicate the crystalline phase.

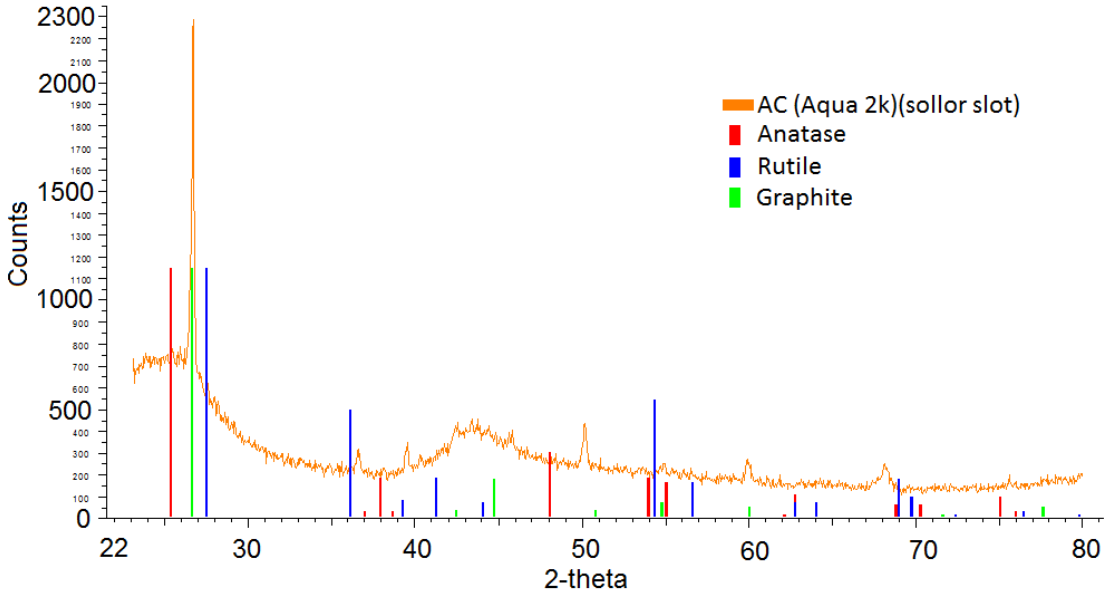

Figure 3-23 XRD spectra of activated carbon. The vertical lines indicate the crystalline phase.

A peak at 50° exists on the IPCA and AC but is absent in the P25 spectrum. Its larger peak height on the AC implies that it is a feature of the AC. Its lower response on the IPCA is possibly due to attenuation of the X-rays by the TiO_2 layer on the IPCA. Attempts to identify this peak were unsuccessful.

3.5 Conclusions

Characterisation of the IPCA confirmed that P25 is distributed across the Aqua 2k surface by the ultrasonication method and that the anatase to rutile ratio in the P25 is 80 %. In conclusion:

- The SEM results confirm that the TiO_2 is distributed across the IPCA surface.
- FESEM studies have shown that the TiO_2 particles typically have a 25 nm particle diameter but are present in larger agglomerations.
- XRD results demonstrated that the AC is graphitic in nature while the TiO_2 is mixed phase with a larger content of the anatase phase to the rutile phase.
- Heat treatment of the IPCA did not cause a noticeable change in the phase of the TiO_2 on the IPCA.

Chapter 4 Adsorption Studies

4.1 Introduction

Adsorption studies of the activated carbon (AC) (Aqua 2k) and TiO_2 provide baseline adsorption properties of the separate materials before they are used to create an IPCA. The adsorption capacities of the IPCAs were studied to determine the effect of adding TiO_2 on the adsorption capacity of the AC surface. The adsorption kinetics of AC and IPCAs in the dark were analysed by the intraparticle diffusion model and Bangham equation. Isotherm data were analysed using the Langmuir, Freundlich, Temkin and Redlich–Peterson models to provide an insight into the interaction between the adsorbent (AC and IPCA) and the adsorbate (famotidine or solifenacin). This chapter will investigate:

- The adsorption kinetics of TiO_2, AC and IPCA.
- The effect of different pHs and initial famotidine and solifenacin concentrations on the adsorption capacity of TiO_2, AC and IPCA.
- The results of isotherm and kinetic models applied to the adsorption data.
- Desorption of adsorbed famotidine and solifenacin from AC into solution to ascertain substrate migration out of the pores of the AC.

4.1.1 Pharmaceuticals under investigation

Two pharmaceuticals: famotidine and solifenacin succinate were selected for photodegradation and adsorption studies using TiO_2, AC and IPCAs. These two pharmaceuticals were selected since they are priority pollutants present in our industrial partner's (Astellas, Dublin) production waste streams.

Famotidine, 3-{[2-(diaminomethyleneamino)-1,3-thiazol-4-yl]-methyl-thio}-N2-sulfamoyl-propionamide is a histamine H_2-receptor antagonist that is a potent inhibitor of gastric and acid secretion in humans (Hassan *et al.*, 1997, Hegedüs *et al.*, 1989). The structure of famotidine is shown in Figure 4-1. It has a molecular weight of 337.449. It contains terminal amino groups and has two well-known crystal structural dimensions (Ferenczy *et al.*, 2000). Its removal from the body has a half-life of 2.5 h to 3.5 h and 65 % to 70 % of the compound is recoverable unchanged in the urine of subjects given famotidine (Lee *et al.*, 2004c). It is discharged from the pharmaceutical industry and partially degraded during conventional water treatment

(Radjenović *et al.*, 2009). Famotidine removal has been studied at three large WWTPs with population equivalents of 74,000, 170,000 and 400,000 (Verlicchi *et al.*, 2012). Famotidine was detected in 19 % of the influent samples and 8 % of the effluent samples. Removal efficiencies were 90 %, 10 % and 85 % with 10 %, 5 % and 15 % adsorption onto the waste activated sludge respectively. The WWTPs with longer solid retention times (SRTs) (10 and 16 days) performed best. These results and the widespread use of famotidine suggest pervasive discharge into the environment via sewage sludge or WWTP effluent. The stability of famotidine in solution and in combination with other drugs has also been investigated (Wu and Fassihi, 2005). Stability varied considerably depending on storage conditions. At pH 2 under light from a "*fluorescent lamp*" at 37°C the half-life of a 10 mg/L deionised water solution of famotidine was 0.65 days while at pH 4 in the dark the same concentration had a half-life of 154 days. Famotidine has a Log D_{ow} (Log distribution coefficient of octanol-water) of -0.64 and a Log P_{ow} (Log partition coefficient of octanol-water) of -2.1 (ChemSpider 2012, Wishart *et al.*, 2012).

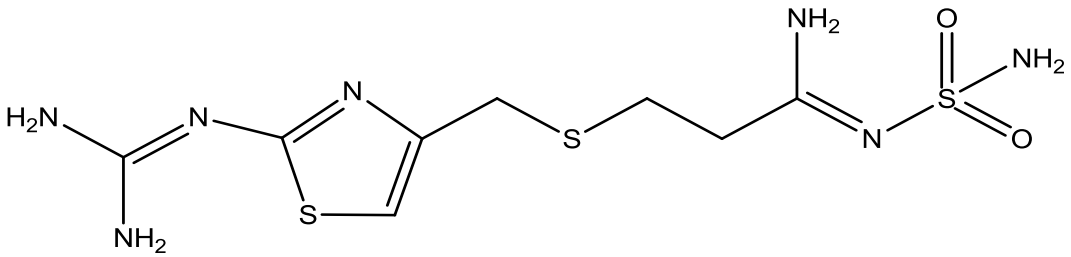

Figure 4-1 Structure of famotidine.

Solifenacin Succinate ((+)-(1S,3_R)-quinuclidin-3_-yl1-phenyl-1,2,3,4-tetrahydroisoquinoline-2-carboxylate monosuccinate) is the succinic acid salt of azabicyclophenyl-isoquinolinecarboxylate and has a molecular weight of 480.55 g. The structure of solifenacin succinate is shown in Figure 4-2. It is a muscarinic receptor antagonist, and has higher selectivity for the urinary bladder than for the salivary gland minimising the dry mouth side effect of similar drugs (Maniscalco *et al.*, 2006, Yanagihara *et al.*, 2007). Solifenacin is weakly basic (pKa 8.5) and is 93 % positively ionized (cationic) at pH 7.4. The Log P_{ow} is 3.96 (ChemSpider 2012, Wishart *et al.*, 2012) and the Log D_{ow} (Log P_{ow} at pH 7) is 1.69, indicating that the octanol: water distribution at pH 7 is 50:1 therefore solifenacin is highly lipophilic

(Maniscalco *et al.*, 2006). It is used for the treatment of overactive bladder syndrome and was shown to improve symptom bother, work productivity, activity participation, and medical care resource utilization in elderly subjects (Zinner *et al.*, 2009). Studies of solifenacin degradation via IPCAs or TiO_2 were not found in the literature.

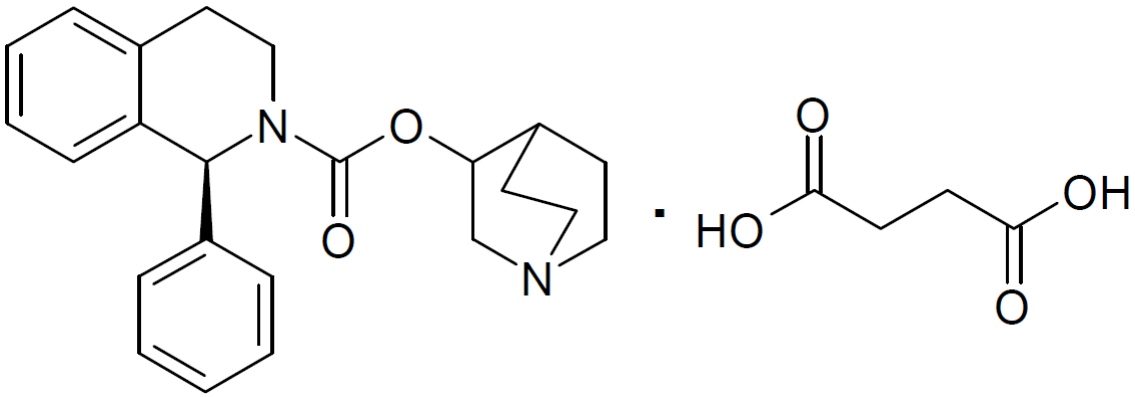

Figure 4-2 Structure of solifenacin succinate.

4.2 TiO_2 adsorption

4.2.1 Famotidine adsorption

4.2.1.1 Kinetics of TiO_2 adsorption

The adsorption of a 100 mg/L concentration of famotidine onto TiO_2 over 72 hours is shown in Figure 4-3. The concentration in the control sample without adsorbent remained constant at 100 mg/L. Equilibrium in the TiO_2 sample appears to have been reached after 7 h, with adsorption of 2 mg - 3 mg of famotidine onto P25 TiO_2. No samples were taken after 72 h. These results in Figure 4-3 demonstrate that the 22 h contact time selected for adsorption studies is adequate for TiO_2 adsorption.

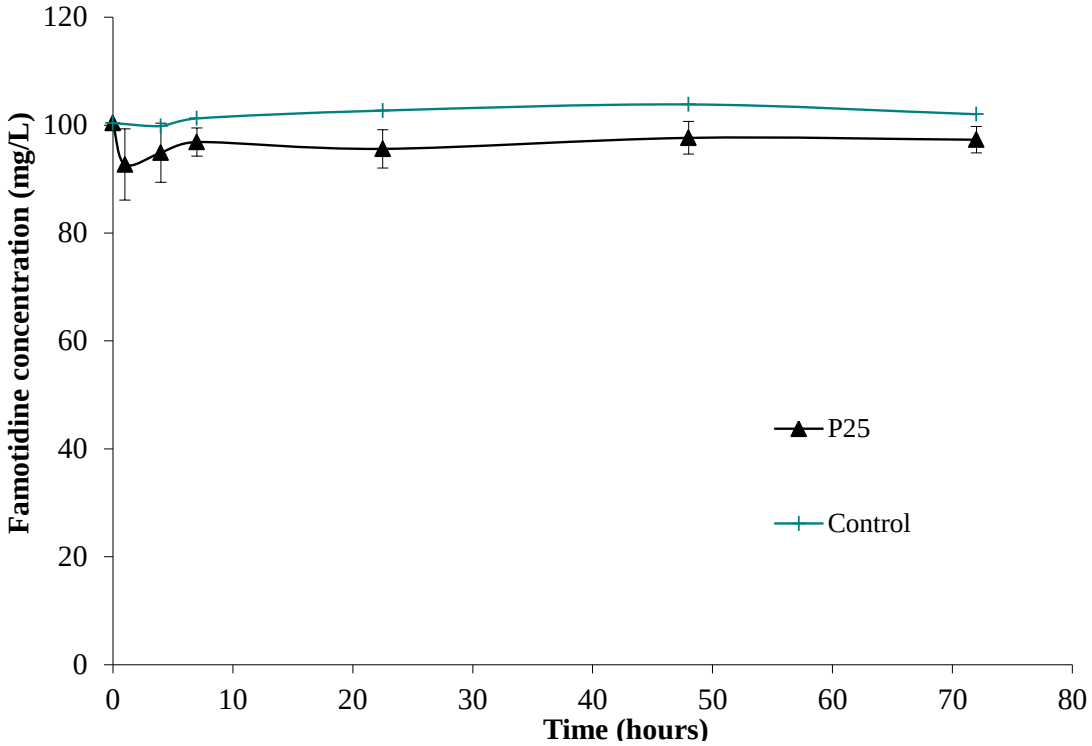

Figure 4-3 Famotidine concentration (mg/L) vs. time (days) for P25 TiO_2 adsorption. Average results shown (N=2), error bars are standard deviation.

4.2.1.2 Effect of initial concentrations on adsorption

The adsorption capability of TiO_2 for famotidine was further investigated using a number of different initial concentrations of famotidine (Figure 4-4). The adsorption of famotidine by TiO_2 was minimal, even at high concentrations. At the highest adsorption loading (2.5 mg/g) the concentration of famotidine was reduced from 40.6 mg/L to 39.3 mg/L.

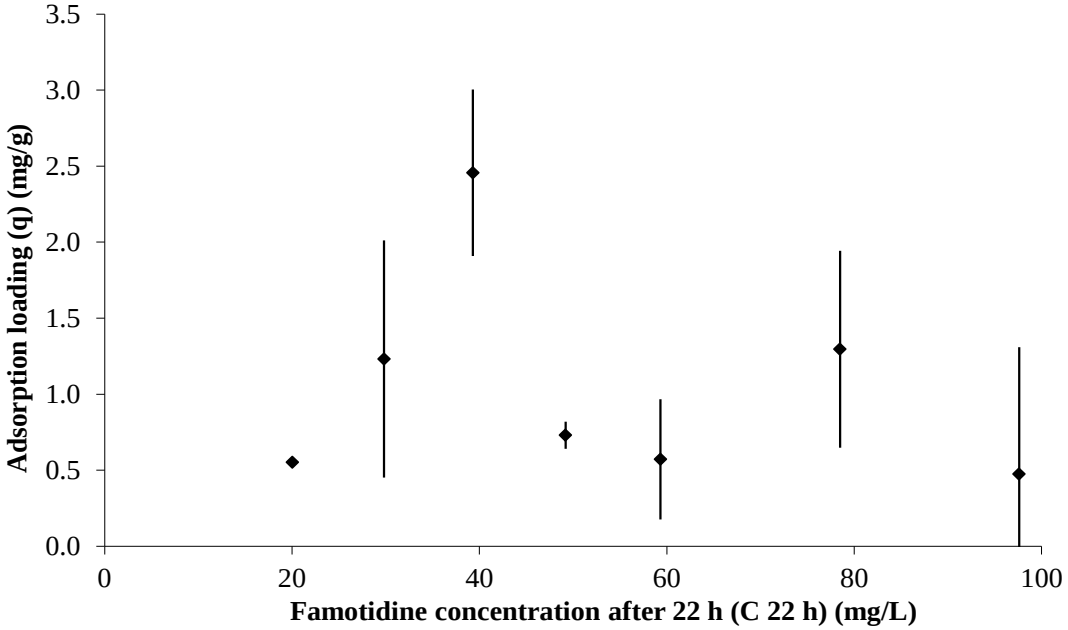

Figure 4-4 Adsorption loading (q) of famotidine onto TiO_2 vs. famotidine concentration after 22 h (C_{22h}). Initial concentrations were 20 mg/L, 30 mg/L, 40 mg/L, 50 mg/L, 60 mg/L, 80 mg/L and 100 mg/L. Average results shown (N=2), error bars are standard deviation.

These results are in agreement with the literature as it is widely reported that TiO_2 (including P25) has little adsorption capacity. The BET surface area of P25 by N_2 adsorption is 44 – 53 m^2/g (Balázs *et al.*, 2008, Velasco *et al.*, 2010b) . No values for pharmaceutical adsorption onto TiO_2 were found in the published literature. However several studies did include adsorption data for other organic compounds such as phenol and heavy metals. These results are summarised in Table 4-1.

Table 4-1 Sample adsorption values for TiO_2 reported in the literature

Photocatalyst	Substrate (C_i)	Solution volume	Result	Ref
50 mg/L P25	2.67 μM As(III), 0.2 mg/L	0.05L	13 μmol/g, 0.97 mg/g	(Liu *et al.*, 2008)
1 g/L P25	100 mg/L Phenol.	0.4L	<3 mg/g "<3 % removal", 31.88 μmol/g	(Velasco *et al.*, 2010a, Velasco *et al.*, 2010c)
0.5 g/L P25	80 mg/L Hg(II)	0.2L	20 mg/g, 250 μmol/g Hg(II) adsorption	(Zhang *et al.*, 2004)
2.5 g/L sol-gel TiO_2	20 mg/L Phenol	0.2L	0.24 mg/g 2.55 μmol/g "3 % adsorption"	(Li *et al.*, 2007)

4.2.1.3 Effect of pH on adsorption

The low adsorption capacity of TiO_2 could be due to the initial solution pH (3.8) of the isotherm studies being unfavourable for adsorption. The point of zero charge (PZC) is defined as the pH at which the net charge is zero (Saepurahman *et al.*, 2010). The PZC of P25 is usually give as 6.5 i.e. at pHs below 6.5 it is positively charged and negatively charged at pHs higher than 6.5. The change on a surface influences its adsorption properties as more cations will be adsorbed on a negatively charged surface (Órfão *et al.*, 2006). The surface charge also influences agglomeration of particles which would lower the particles surface area. Consequently the relationship between initial pH (pH_i) and famotidine adsorption (initial concentration 100 mg/L) in the pH range of 4 to 8 was also evaluated (Figure 4-5). The removal capacity showed no trend as the pH_i value of the solution increased from 4 to 8. Famotidine adsorption rises from pH4 to pH6, however when error bars are considered there is no trend in famotidine adsorption from pH6 to pH8. pH buffers were not used to maintain the solution pH as they might compete with the famotidine for adsorption onto the TiO_2.

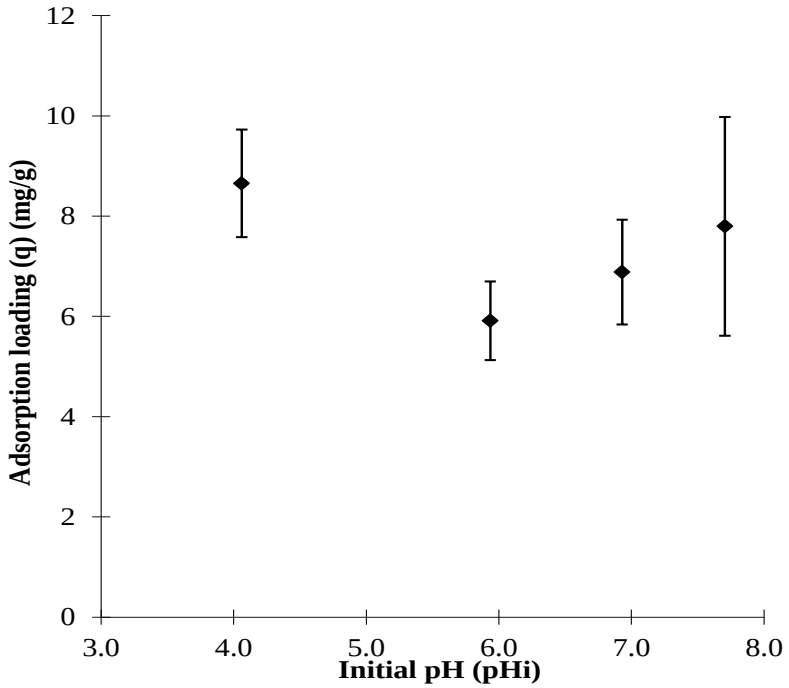

Figure 4-5 Adsorption loading (q) of famotidine onto TiO_2 vs. Initial pH (pH_i). pH_i studied were 4, 6, 6.9 and 7.7. Average results shown (N=2), error bars are standard deviation.

It should be noted that famotidine is unstable at low pHs with a half-life of 0.61 days at pH 2 compared to a half-life of 154 days at pH 4 (Wu and Fassihi, 2005). A series of famotidine controls were used to determine famotidine stability with respect to pH. Figure 4-6 shows the difference in final concentration with the pH_i of the solution. The controls demonstrate stability at all pH_is except pH 2 where the concentration declined by 34 % over 22 hours. For these reasons famotidine adsorption at an initial pH of 2 was not studied.

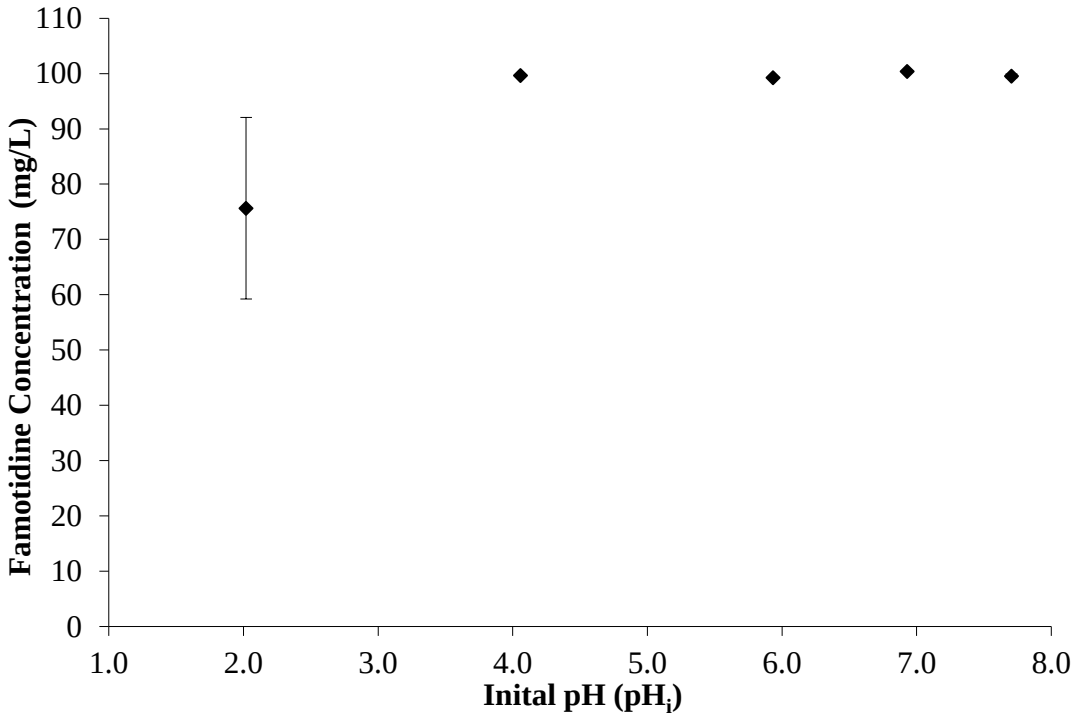

Figure 4-6 Famotidine concentration after 22 h (C_{22h}) vs. initial pH (pH_i) of adsorbent free controls. Initial concentration: 100 mg/L. Average results shown (N=2), error bars are standard deviation.

4.2.2 Solifenacin adsorption

4.2.2.1 Adsorption kinetics of TiO_2

The adsorption of solifenacin onto TiO_2 is shown in Figure 4-7. The concentration in the control sample without adsorbent remained on average constant around 100 mg/L. Similar to the famotidine studies equilibrium appears to have been reached after 7 h. No samples were taken after 72 h. These results demonstrate that

the 22 h contact time selected for adsorption studies is more than adequate for TiO_2 adsorption of solifenacin.

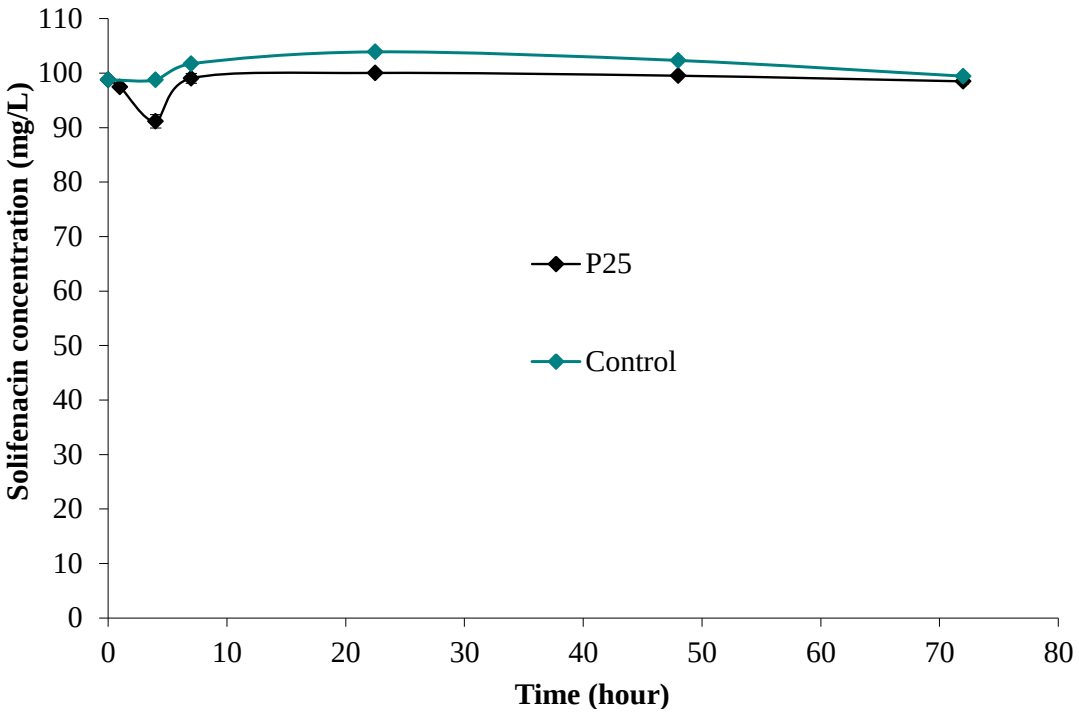

Figure 4-7 Solifenacin concentration (mg/L) vs. time (hours) for P25 TiO_2 adsorption. Average results shown (N=2), error bars are standard deviation.

4.2.2.2 Effect of initial concentration on adsorption

The adsorption of solifenacin onto TiO_2 (Figure 4-8) demonstrates no clear trend with increasing initial concentration (C_i), similar to famotidine adsorption. TiO_2 has a maximum adsorption loading value of 3.5 mg/g at C_i = 150 mg/L and all other adsorption loading values do not exceed 3 mg/g. This result confirms the low adsorption capacity of P25 TiO_2 for solifenacin.

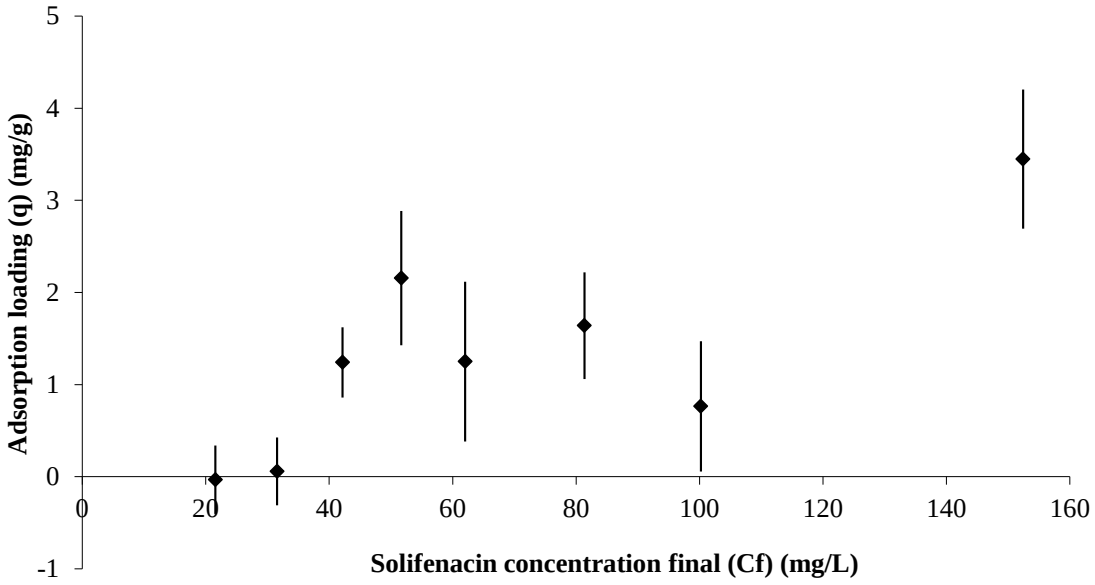

Figure 4-8 Adsorption loading (q) of TiO_2 vs. solifenacin concentration after 22 h (C_{22h}). Initial concentrations studied were 20 mg/L, 30 mg/L, 40 mg/L, 50 mg/L, 60 mg/L, 80 mg/L and 100 mg/L and 150 mg/L. Average results shown (N=2), error bars are standard deviation.

4.2.2.3 Effect of pH on solifenacin adsorption

The effect of pH on the adsorption of solifenacin onto TiO_2 was investigated in pH_i range from 2 to 8 (Figure 4-9). Unlike famotidine, the adsorption capacity of TiO_2 for solifenacin increased with increasing pH over the entire pH range. Maximum solifenacin uptake occurred at initial pH 8 with an adsorption loading of 9 mg/g and the lowest adsorption loading of 1.4 mg/g occurred at initial pH 4. The pH 4 results are similar to the isotherm results at 3.1 - 3.7 (C_i = 100 mg/L) with average adsorption loading values of 1.4 mg/g and 0.8 mg/g respectively (Figure 4-8).

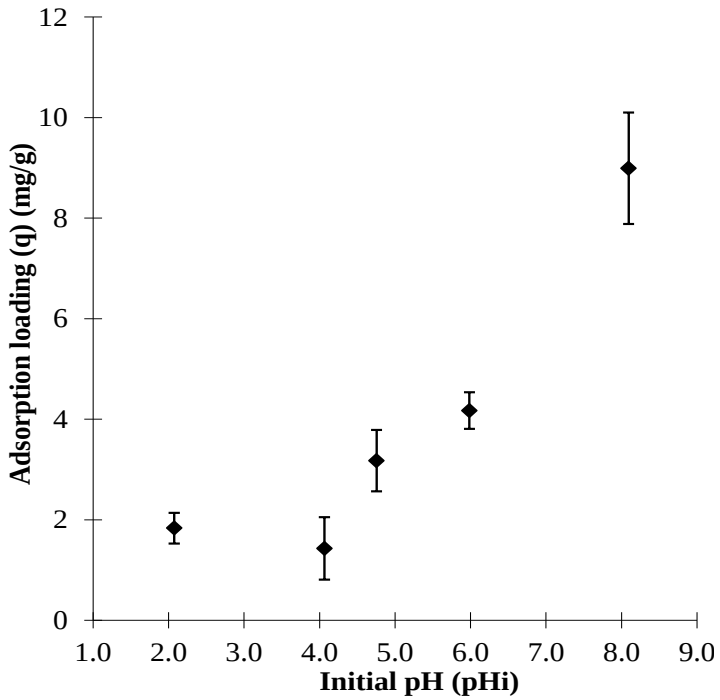

Figure 4-9 Adsorption loading (q) of solifenacin onto TiO_2 vs. initial pH (pH_i). pH_i studied were 2.1, 4.1, 4.8, 6 and 8.1. Average results shown (N=2), error bars are standard deviation.

Solifenacin pH controls are shown in Figure 4-10.

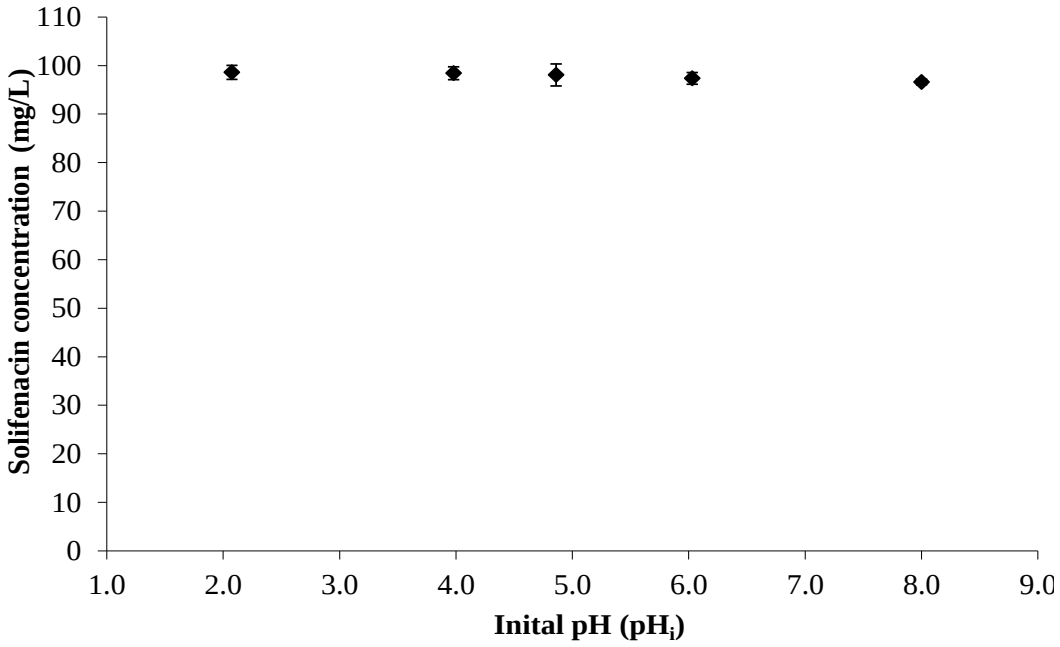

Figure 4-10 Solifenacin concentration after 22 h (C_{22h}) vs. initial pH (pH_i) of adsorbent free controls. Initial concentration: 100 mg/L. Average results shown (N=2), error bars are standard deviation.

These controls were run to determine solifenacin stability with respect to pH. Figure 4-10 shows the difference in C_{22h} vs. the pH_i of the solution. The difference in solifenacin concentration after 22 h in a pH adjusted solution is negligible.

4.3 AC adsorption

4.3.1 Famotidine

4.3.1.1 Adsorption kinetics of AC

The adsorption of famotidine onto AC is shown in Figure 4-11. The famotidine concentration in solution dropped constantly during the study, but the speed decreased with the study time. The concentration in the control sample without adsorbent remained constant at 100 mg/L. Equilibrium during the study period was not reached as the famotidine concentration continued to decline throughout the study. The famotidine concentration in solution dropped below the LOQ (1 mg/L) of the HPLC method by day 21 therefore further samples were not taken.

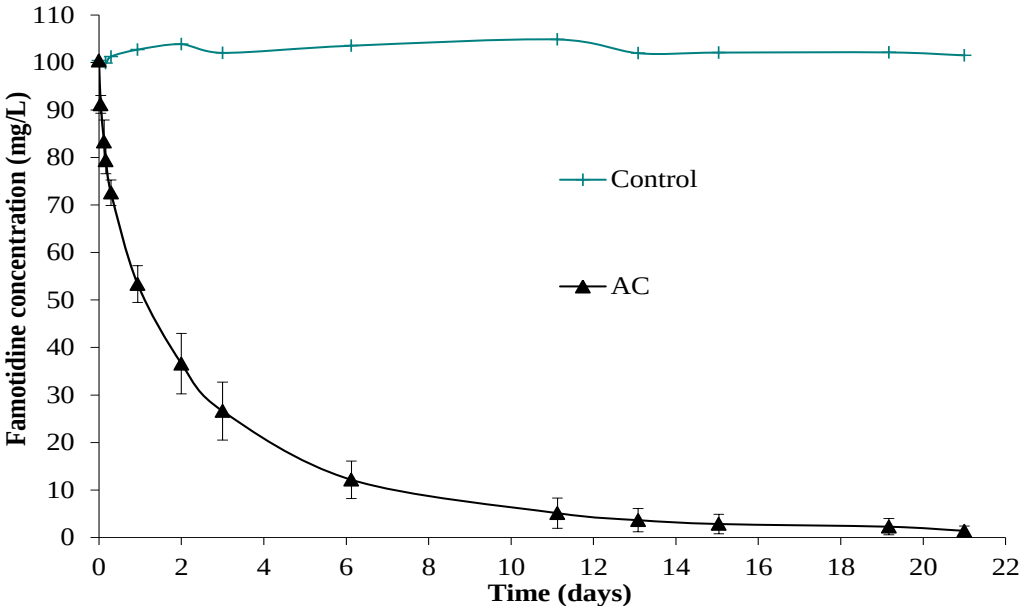

Figure 4-11 Famotidine concentration (mg/L) vs. time (days) for AC. Adsorbent free control is also shown. Average results shown (N=2), error bars are standard deviation.

The constant decline in the famotidine concentration could be due to a very high adsorption capacity of the AC for famotidine. To test this hypothesis the same adsorbents used above were placed in a fresh 100 mg/L famotidine solution and the concentration in solution was monitored over a number of days (Figure 4-12). The adsorption is fastest in the initial part of the study and adsorption gradually declines throughout the study period. Famotidine removal is roughly half that of the first adsorption rate study (Figure 4-11). In the first experiment, after 14 days the AC had reduced the average concentration in solution from 100 mg/L to 3 mg/L while in the second experiment on average the AC reduced the initial concentration from 100 mg/L to 55 mg/L. This indicates that as the adsorption sites on the AC surface were occupied the rate of adsorption of new famotidine molecules from solution decreased. During this experiment equilibrium is not reached (as the concentration in solution is constantly decreasing) demonstrating that famotidine has a very high affinity for the AC and thus a large amount (greater than 250 mg/g) of famotidine can be adsorbed before equilibrium is reached.

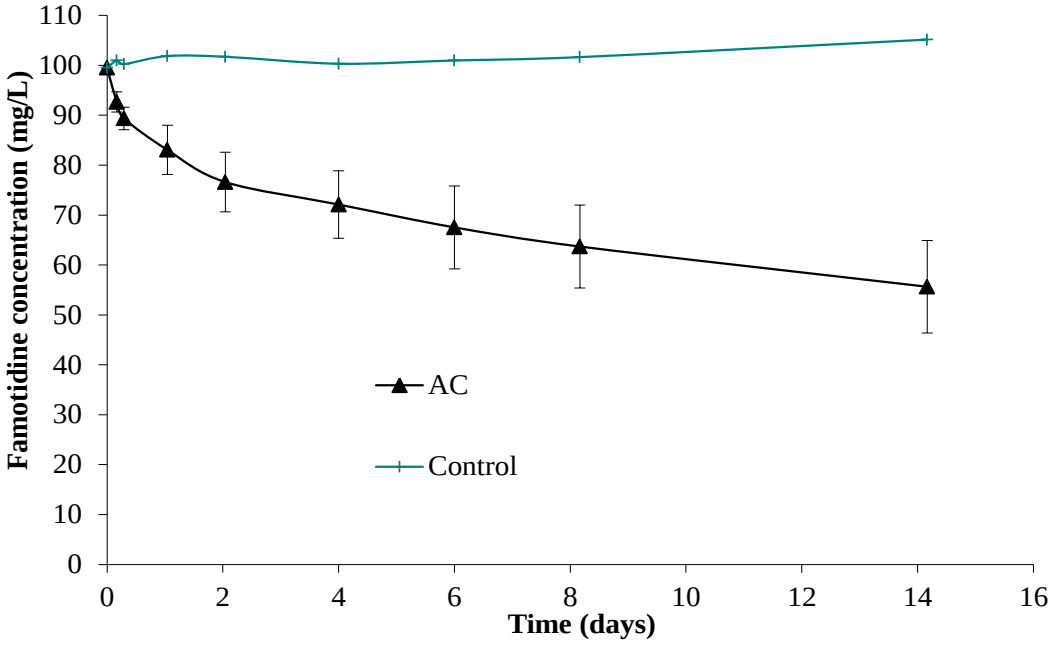

Figure 4-12 Famotidine concentration (mg/L) vs. time (days) for AC. Adsorbent free control is also shown. Average results shown (N=2), error bars are standard deviation.

The adsorption loading (mg/g) of AC is shown in Figure 4-13. For the first adsorption study (1st stage), adsorption levels off suggesting equilibrium is reached at 13 days, however the concentration of famotidine in solution continues to drop (Figure 4-11). The majority of papers in the literature take this pseudo equilibrium as the equilibrium concentration for kinetic analysis (see Table 4-2). The exact time for equilibrium varies between ACs depending on the nature of their pore structure. In the literature surveyed it varied from minutes to greater than 30 days.

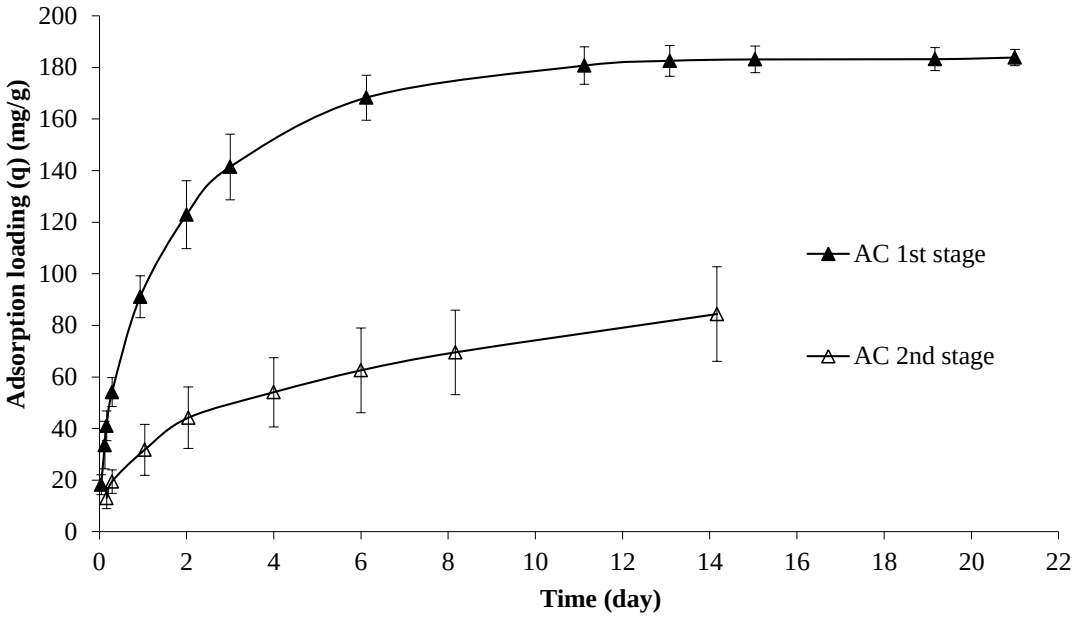

Figure 4-13 Famotidine adsorption (q) loading (mg/g) vs. time (days) for AC for first and second stage famotidine adsorption studies. Average results shown (N=2), error bars are standard deviation.

Table 4-2 Features of adsorption studies

Analyte	Concentration studied	Equilibrium time	Conditions	Models*	Ref
Resorcinol and catechol	500 - 1000 mg/L	48 h (data reported for 25 h)	W= 5 mg/L; V= 0.2 L; pH 7.1; T = 29.9 +/- 0.3°C	L, F, R–P, Radke–Prausnitz, Toth, and Fritz–Schlunder.,	(Kumar *et al.*, 2003)
2,4-D	50 – 400 mg/L	10h (not confirmed)	W= 0.20 g; V = 0.2L; pH 3.6; T=30°C	L,F, T	(Hameed *et al.*, 2009)
17β-estradiol (radio-labelled)	0.5 - 100 ng/L	1-5 h (Studied to 142 h)	W= 2 g/L; V = 0.05 L; pH ?; T = ?°C	None	(Fuerhacker *et al.*, 2001)
Atrazine, Bromoxynil and Diuron	0.259 - 0.499 mg/L, 0.455 - 0.818 mg/L and 0.261 - 0.558 mg/L	3 days (Fully confirmed)	W= 0.7-3.1 mg/L (GAC crushed); V = 2L; pH ?; T = 25°C	F, Differential Column Batch Reactor Kinetics.	(Baup *et al.*, 2000)
Phenol	10 - 60 mg/L	5 h – substrate runs out.	W= 20 500 mg/L; V = 0.1L in 0.25L; pH 2-13; T=27°C	F, First order rate expression.	(Rengaraj *et al.*, 2002)
Amoxicillin	300 mg/L	35 min (concentration graph not shown)	W= 3.5 g (14 g/L); V = 0.25 L in 0.25 L; pH 2.15-7.04; T = 30°C	L,F, pseudo-first and second order models.	(Putra *et al.*, 2009)
Congo red dye (CAS No: 573-58-0)	50 - 545 mg/L	20 - 180 min (not confirmed needs samples at longer intervals)	W= 1g/L; V = 1L; pH 2.15-7.04; T=30°C	L,F, first and pseudo second order models.	(Purkait *et al.*, 2007)
MCPA	14 – 144 mg/L	49, 53 and 72 h (the latter not confirmed)	W= 0.5g (5g/L); V = 0.1L; pH = 7.; T=20°C	L, F, Shrinking-core mass-transfer model.	(Gimeno *et al.*, 2003)
Methyl green, methyl violet	200 - 800 mg/g adsorption	4 - >12 h (not confirmed)	W = 80 – 120 mg (114 - 171 mg/L); V = 0.7 L; pH = 5.6, 5.9, 10.6; T=15 - 26°C	L, first order equation	(Dai, 1994)
2-chlorophenol < 4-chlorophenol < 2, 4-dichlorophenol	20 – 300 mg/L	3 - 11day, 6 days for GAC (not confirmed)	W= 0.01–4g (1-40g/L); V = 0.045-0.1L; pH = 4.5-6.3 no buffer; T=22°C	L, F, pseudo first and second order, intra-particle diffusion	(Hossain and McLaughlan, 2011)
Acid Blue 80, Acid Red 114 and Acid Yellow 117	Not stated probably 50-200 mg/L"	21 days (data not shown)	W= 0.05g (1 g/L); V = 0.05 L; pH = ?; T = 20°C	L, P factor, intra-particle diffusion	(Choy *et al.*, 2004)
Phenol, o-chlorophenol	99 - 204 mg/L	3 to 33 days	W= ?g (1 g/L); V = 0.3 - 0.5L; pH = 7; T = 20°C	F	(Peel and Benedek, 1980)

*L=Langmuir, F=Frendrich, T=Temkin, R-P=Redlich-Peterson

4.3.1.2 Effect of initial pH on famotidine adsorption

The pH of a solution is an important parameter affecting the adsorption process (Lataye *et al.*, 2008, Yao *et al.*, 2010). A change in the pH alters the charge profile of adsorbate species which consequently influences their interactions with the adsorbent (Li *et al.*, 2003). The relationship between initial solution pH (in the pH range of 4 - 8) and famotidine adsorption by the AC was examined (Figure 4-14). Results show that the removal capacity increased as the pH_i value of the famotidine solution increased from 4 to 8. The maximum famotidine uptake of 122 mg/g and was found to occur at pH_i 5.6. The AC and famotidine solution had a pH value of 5.8 in deionised water solutions and famotidine has a pK_a (logarithmic acid dissociation constant) value of 6.9 indicating that famotidine is 93 % protonated at this pH. The solution pH affects the surface charge of the adsorbents and, therefore, the adsorption proceeds through dissociation of functional groups on the active sites of the adsorbent (Lataye *et al.*, 2008, Moreno-Castilla, 2004).

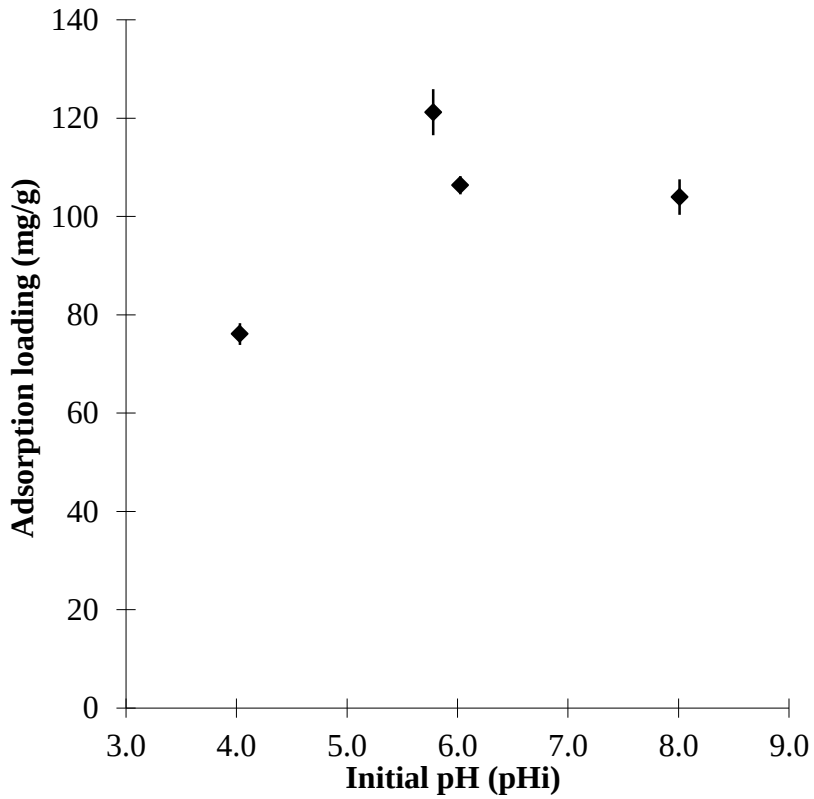

Figure 4-14 Adsorption loading (q) of famotidine onto Aqua 2k vs. initial pH (pH_i). pH_i studied were 4.0, 5.8, 6.0 and 8.0. Average results shown (N=2), error bars are standard deviation.

The famotidine may adsorb onto the AC surface by mechanisms that are not affected by pH: van der waals forces, π-π stacking and hydrophobic interactions. The fact that the adsorption varies with pH suggests other mechanisms may be important. Electrostatic interactions and H bonding (to oxygen groups on the AC surface) would be influenced by pH. The potential chemical interactions of famotidine with the sorbent in this case AC or IPCA may be given by the following equations (Lataye *et al.*, 2008, Moreno-Castilla, 2004). M^+ refers to metal oxides (Al, Si, Ca, Ti oxides) on the AC/ IPCA surface.

$$Fam + H^+ \leftrightarrow FamH^+ \quad (27)$$

$$Fam + AC/\ IPCA \leftrightarrow Fam\text{-}AC/\ IPCA \quad (28)$$

$$Fam\ H^+ + M^+\ AC/\ IPCA \leftrightarrow FamH^+\text{-}AC/\ IPCA + M^+ \quad (29)$$

$$H^+ + FamH^+\text{-}AC/\ IPCA \leftrightarrow H^+\text{-}AC/\ IPCA + FamH^+ \quad (30)$$

$$H^+ + AC/\ IPCA \leftrightarrow H^+\text{-}AC/\ IPCA \quad (31)$$

$$Fam + H^+\text{-}AC/\ IPCA \leftrightarrow FamH^+\text{-}AC/\ IPCA \quad (32)$$

The transition of Fam to $FamH^+$ is dependent on pH, with a maximum amount of $FamH^+$ occurring at low pH ($pH_i \leq 4$), which results in the low adsorption of $FamH^+$ onto the positively charged surface of the AC/ IPCA (AC edges may be positively or negatively charged). At higher pH ($pH_i \geq 5.8$), the Fam molecules are netural in charge and are sorbed onto the adsorbents. The AC (and IPCA) has maximum affinity to Fam and $FamH^+$ for $5.8 \leq pH_i \leq 8$ ($5.6 \leq pH_f \leq 6.8$). As the $FamH^+$ adsorption rate is lower than that of Fam molecules, therefore, the dominant sorption reaction (at pHi ≈8.0) is given by Eq. (28). Other reactions given by Eq. (27) and (29) to (32) play a smaller role in the sorption process as evidenced by the low famotidine adsorption at low pHs and the low metal content on the Aqua 2k surface. Similar pH effects have been observed by other groups (Karimi-jashni and Narbaitz, 1997, Lataye *et al.*, 2008, Nevskaia *et al.*, 1999).

4.3.1.3 Effect of initial concentration on adsorption onto AC

The influence of initial famotidine concentration on adsorption was investigated at concentrations ranging from 20 mg/L to 150 mg/L at pH 3.6. To expedite analysis a 22 h contact time was selected as the largest segment of adsorption (30 %) occurs during this time. After 22 h of adsorption the lowest concentrations (C_i = 20 mg/L) in the isotherm are reduced to approximately 2 mg/L. A longer

equilibrium time would reduce the lower concentrations (or perhaps all concentrations) in solution to less than the limit of quantification of the HPLC detection method (1 mg/L) and as such would not allow the construction of an isotherm. The results are shown in Figure 4-15.

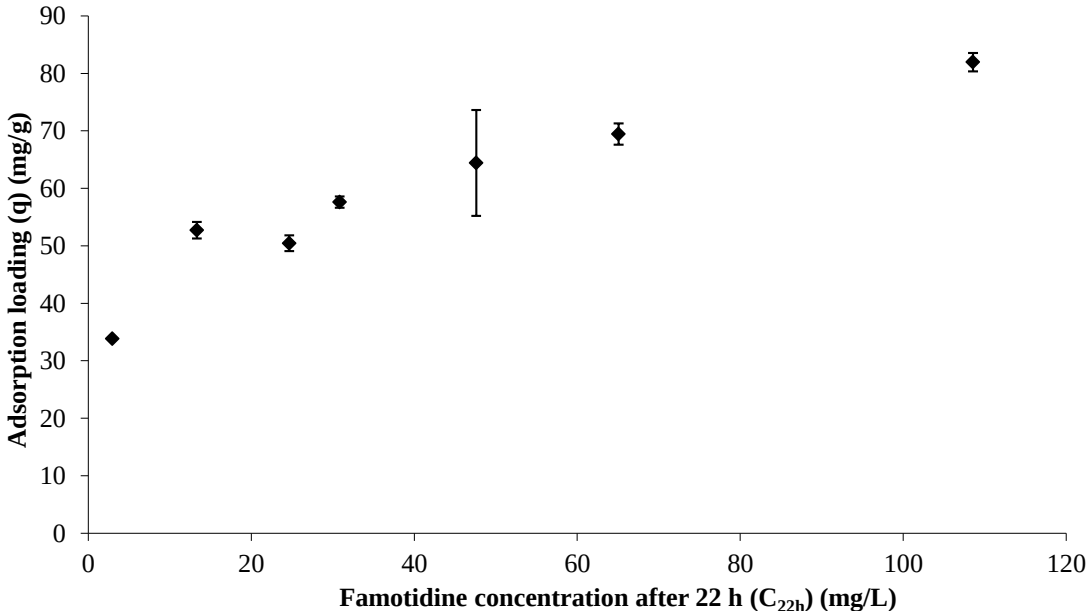

Figure 4-15 Adsorption loading (q) of famotidine on Aqua 2k vs. concentration after 22 h adsorption (C_{22h}). Initial concentrations studied were 20 mg/L, 40 mg/L, 50 mg/L, 60 mg/L, 80 mg/L and 100 mg/L and 150 mg/L. Average results shown (N=2), error bars are standard deviation.

The adsorption capacity initially displayed a steep rise that declined over time. This behaviour reflects saturation on the surface of the AC as the famotidine concentration increased. With the increase of initial famotidine concentration from 20 mg/L to 150 mg/L, the adsorbed famotidine at equilibrium increased from 34 mg/g to 72 mg/g.

4.3.2 Solifenacin

4.3.2.1 Adsorption kinetics of AC

The concentration of solifenacin in solution during the study period is shown in Figure 4-16. The adsorption loading of solifenacin by the AC is shown in Figure 4-17. The concentration in the control sample (without adsorbent) varied slightly from 99 mg/L to 104 mg/L. The concentration in solution dropped constantly but with a gradual slowing of the adsorption process during the course of the experiment. The results demonstrate a tendency towards an equilibrium that is not reached during the 29 day study period. These results are very similar to famotidine with the exception that the adsorption loading (adsorption capacity) is lower. This suggests that the mechanism effecting famotidine is also relevant for solifenacin. Samples were taken for 29 days (1740 h). The equilibrium time reported for solifenacin is outside the majority of values found in the literature (Table 4-2) which contains equilibrium times from minutes to over a month. Some studies will report that equilibrium has been reached when the substrate is completely removed from solution while other studies report equilibrium after a period of time e.g. 24 h (see Table 4-2).

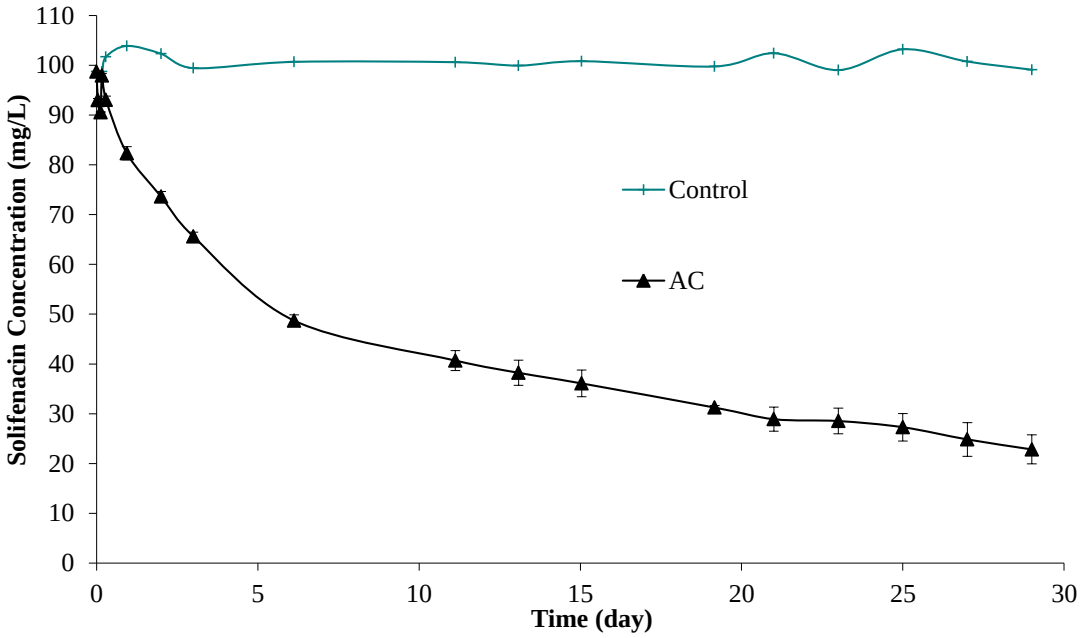

Figure 4-16 Average solifenacin concentration (mg/L) vs. time (day) for AC. Average results shown (N=2), error bars are standard deviation.

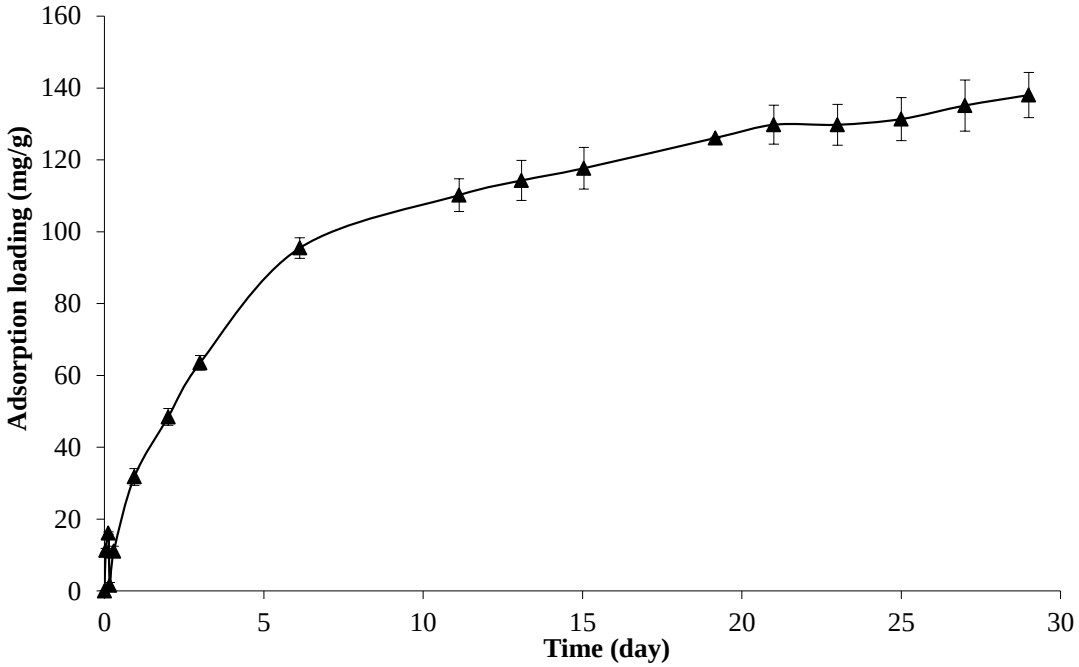

Figure 4-17 Solifenacin adsorption loading (mg/g) vs. time (day) for AC. Average results shown (N=2), error bars are standard deviation.

4.3.2.2 Effect of pH on solifenacin adsorption

The effect of pH on adsorption of solifenacin onto Aqua 2k was investigated in an initial pH range from 2 to 8 (Figure 4-18). The removal capacity of the IPCAs showed no discernible pattern over the entire pH range. Maximum solifenacin uptake occurred at an initial pH of 2 with a adsorption loading of 63 mg/g and the lowest adsorption loading of 41 mg/g occurred at an initial pH of 4. When error bars are included there is an overlap between most of the data points. This indicates that pH does not have a strong effect on solifenacin adsorption onto AC. These results are in contrast to solifenacin adsorption onto P25 where there is increased adsorption with higher initial pHs. Although given the low adsorption capacity of P25 the P25 adsorption results are not reliable. The final pH of the solution is higher than the initial pH for all pHs except pH8 which is in contrast to the results from adsorption of famotidine onto AC.

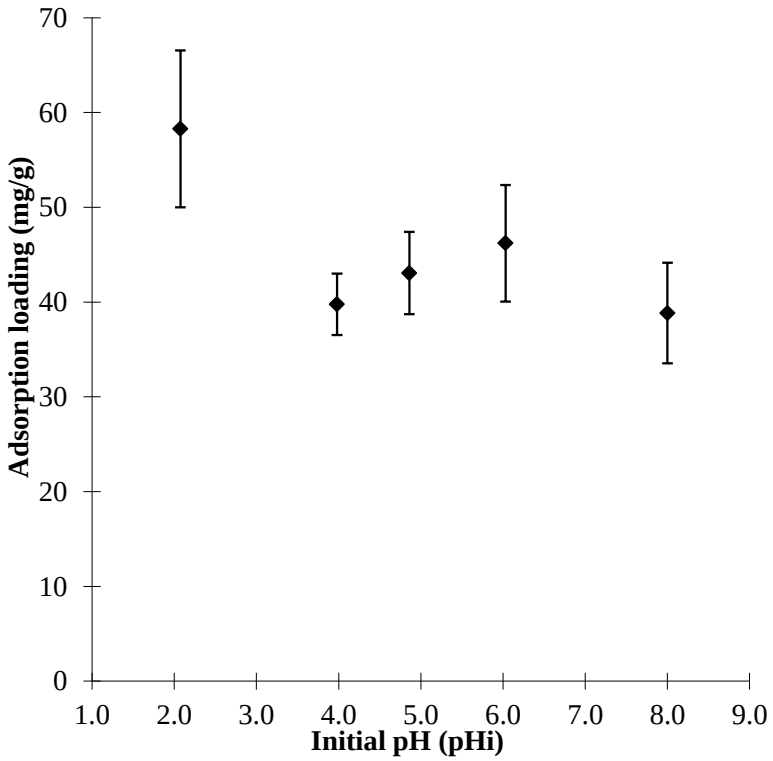

Figure 4-18 Adsorption loading (q) of solifenacin onto Aqua 2k vs. pHi. pH_i studied were 2.1, 4.0, 4.9, 6.0 and 8.0. Average results shown (N=2), error bars are standard deviation.

4.3.2.3 Effect of initial concentration on solifenacin adsorption

The influence of initial solifenacin concentration on the adsorption capacity of Aqua 2k was investigated at concentrations ranging from 10 mg/L to 150 mg/L in the pH range of 3.1 to 3.9 (Figure 4-19). The adsorption loading displayed rose steeply before levelling off. This behaviour reflects saturation on the surface of the AC as the solifenacin concentration increased. The AC adsorbs more solifenacin than P25 with a maximum adsorption loading of 60 mg/g compared to 3.5 mg/g for P25 at an initial concentration of 150 mg/L.

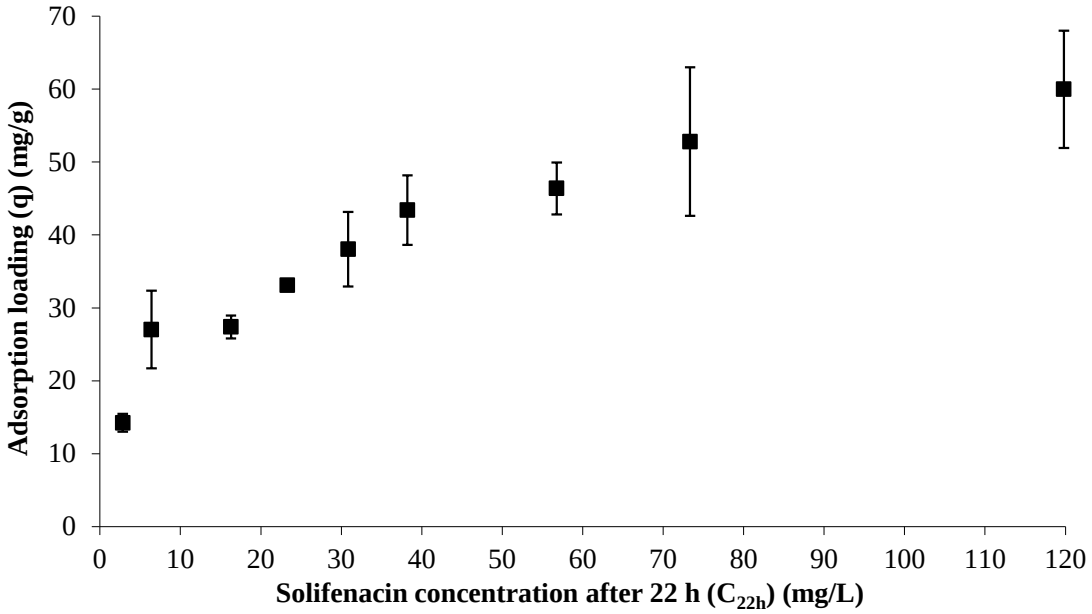

Figure 4-19 Adsorption loading (q) of solifenacin on Aqua 2k vs. concentration after 22 h adsorption (C_{22h}). Initial concentrations studied were 20 mg/L, 30 mg/L, 40 mg/L, 50 mg/L, 60 mg/L, 80 mg/L and 100 mg/L and 150 mg/L. Average results shown (N=2), error bars are standard deviation.

4.4 IPCA adsorption

4.4.1 Famotidine

4.4.1.1 Adsorption kinetics of 1:10 IPCA

The adsorption of famotidine onto AC and 1:10 IPCA is shown in Figure 4-20. The adsorption trend is identical to that of the AC. The famotidine concentration in solution dropped below the LOQ (1 mg/L) of the HPLC method by day 21 therefore further samples were not taken.

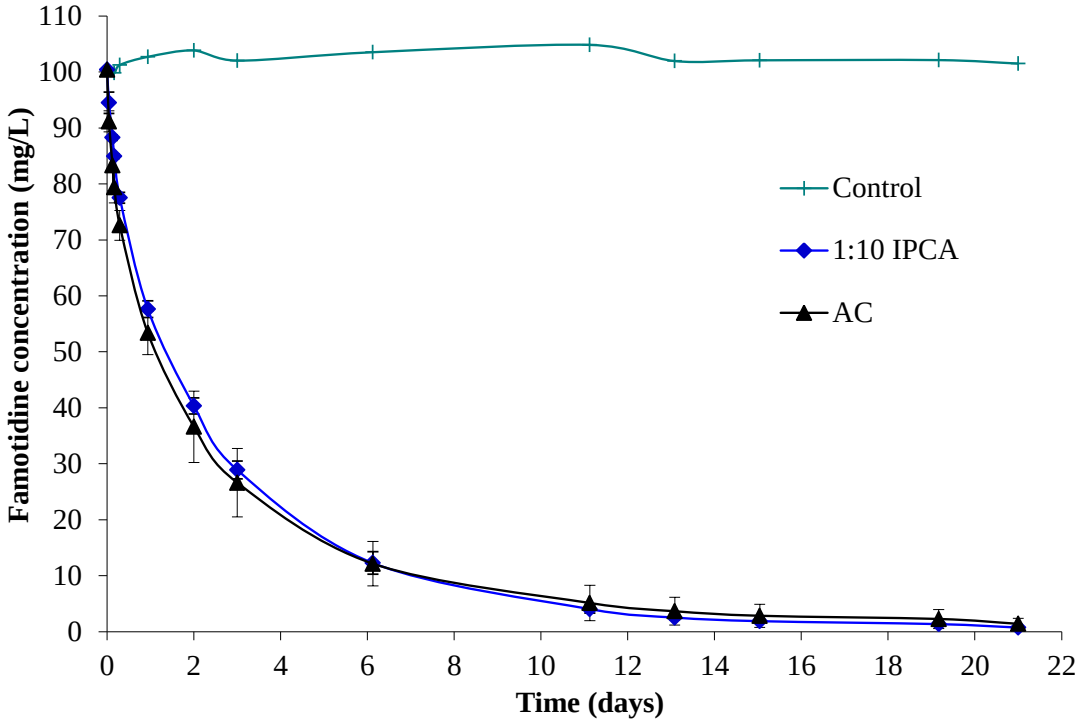

Figure 4-20 Famotidine concentration (mg/L) vs. time (days) for AC and IPCA. Average results shown (N=2), error bars are standard deviation.

The IPCAs were placed in a fresh 100 mg/L famotidine solution and the concentration in solution was monitored over a number of days (Figure 4-21).

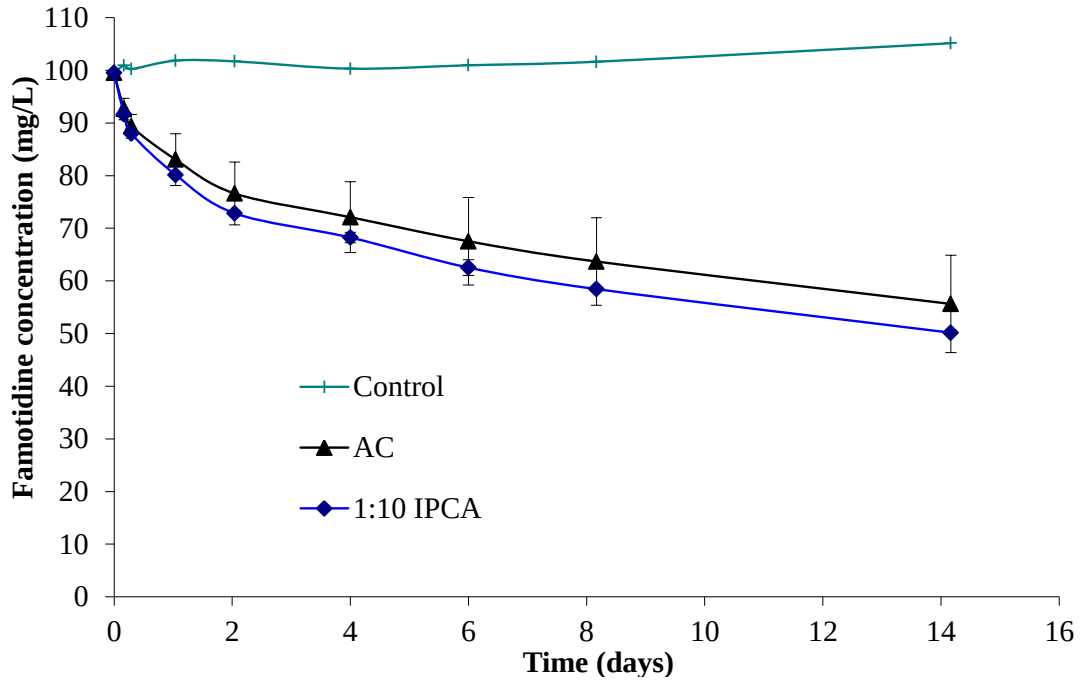

Figure 4-21 Famotidine concentration (mg/L) vs. time (days) for AC and IPCA. Average results shown (N=2), error bars are standard deviation.

The adsorption is fastest in the initial part of the study and adsorption gradually declines throughout the study period. Famotidine removal is roughly half that of the first kinetic study (Figure 4-20). In the first experiment after 14 days the 1:10 IPCA had reduced the average concentration in solution from 100 mg/L to 3 mg/L while in the second experiment on average the 1:10 IPCA reduced the initial concentration from 100 mg/L to 50 mg/L. This indicates that as the adsorption sites on the AC/IPCA surface were occupied the rate of adsorption of famotidine molecules from solution decreased. During this experiment equilibrium is not reached (as the concentration in solution is constantly decreasing) demonstrating that famotidine has a very high affinity for the IPCA and thus a large amount (greater than 270 mg/g) of famotidine can be adsorbed before equilibrium is reached. The adsorption loading (mg/g) of all IPCA and AC samples is shown in Figure 4-22.

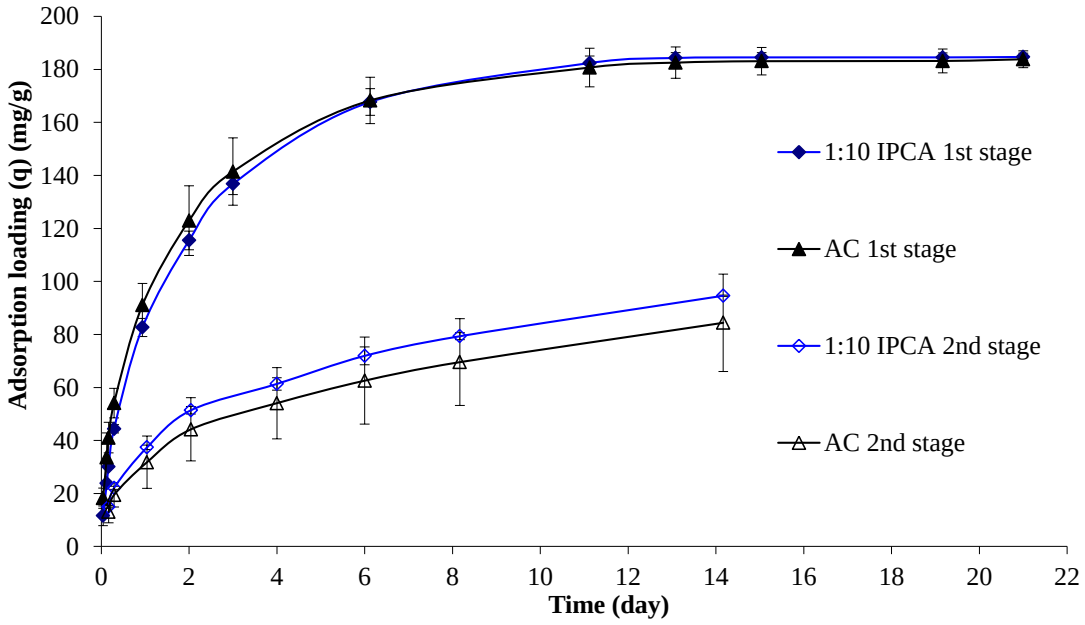

Figure 4-22 Famotidine adsorption (q) loading (mg/g) vs. time (days) for AC and 1:10 IPCA for first and second stage famotidine adsorption studies. Average results shown (N=2), error bars are standard deviation.

For the first adsorption experiment (1st stage), equilibrium appears to be reached at 13 days, however the concentration of famotidine in solution continues to drop (Figure 4-20). The slow adsorption of famotidine suggests that it is retarded by a rate limiting step(s). To investigate this hypothesis the adsorption data were analysed by the intraparticle diffusion model and the Bangham equation. The calculated

parameters and correlation coefficient (R^2) are listed in Table 4-3. For analysis the average concentration of the (1^{st} stage) samples of the IPCA and AC were used. The 2^{nd} stage samples refer to the studies that placed the same AC and IPCA samples in a fresh famotidine solution for the second time.

As noted earlier (Section 1.3, Figure 1-11) adsorption involves four broad steps (1) bulk phase transport of the substrate to the external surface, (2) transport across the boundary layer also known as external mass transfer, (3) transport through the AC by surface diffusion and/or pore diffusion known as intra particle diffusion and (4) adsorption on the surface of the adsorbent. The fourth step is considered instantaneous and given the high stirring rate, volume and initial concentration of the solution, bulk phase transport should not limit the adsorption rate. The rate limiting step would be either the intra-particle diffusion step or transfer across the boundary layer. The former step has been reported in the literature (Kumar *et al.*, 2003) as the rate limiting step. Differential equations containing diffusion terms have shown the fractional uptake of the adsorbate to be a function of the square root of time, ($t^{0.5}$) rather than time t (Choy *et al.*, 2004). This relationship may be used in determining qualitatively the rate controlling step. A fractional uptake diagram of adsorption of famotidine onto AC and 1:10 IPCA in the first stage adsorption experiments are shown in in Figure 4-23.

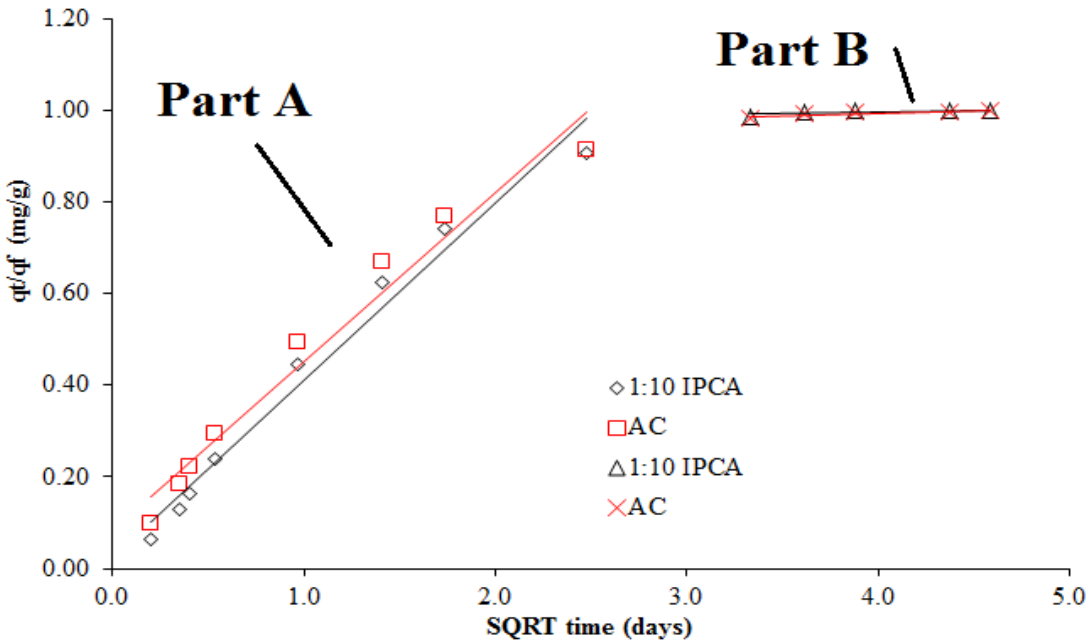

Figure 4-23 Fractional uptake diagram for adsorption of famotidine onto AC and 1:10 IPCA for 1^{st} stage studies.

k_{int} values are determined from the slope of the linear portion of this plot. The values of intercept, C give an idea about the boundary layer thickness, i.e. the larger the intercept, the greater the boundary layer effect. The AC and IPCA display two linear sections that have been labeled "Part A" and "Part B". Part A for both samples demonstrates a linear relationship with the square root of time throughout both experiments. This indicates that intra-particle diffusion is the rate limiting step of the adsorption process. The presence of an intercept value suggests that there is a boundary layer effect slowing the rate of adsorption. The intraparticle diffusion rate constant (k_{int}) is higher for the IPCA than the AC (0.3884 mg/g $day^{0.5}$ vs. 0.3706 mg/g $day^{0.5}$). For Part B of the trend the slope of the line is almost flat (0.0076 mg/g $day^{0.5}$ and 0.011 mg/g $day^{0.5}$ for IPCA and AC respectively) indicating very little intraparticle diffusion. This is likely caused by the reduction in the famotidine concentration in solution. Part B begins after 11 days at which point the famotidine concentration has dropped from 100 mg/L to 4 mg/L. At this point in the study the adsorption process is probably slowed by a lack of substrate which in turn lowers the intraparticle diffusion rate. Results of the 2nd stage studies are shown in Figure 4-25.

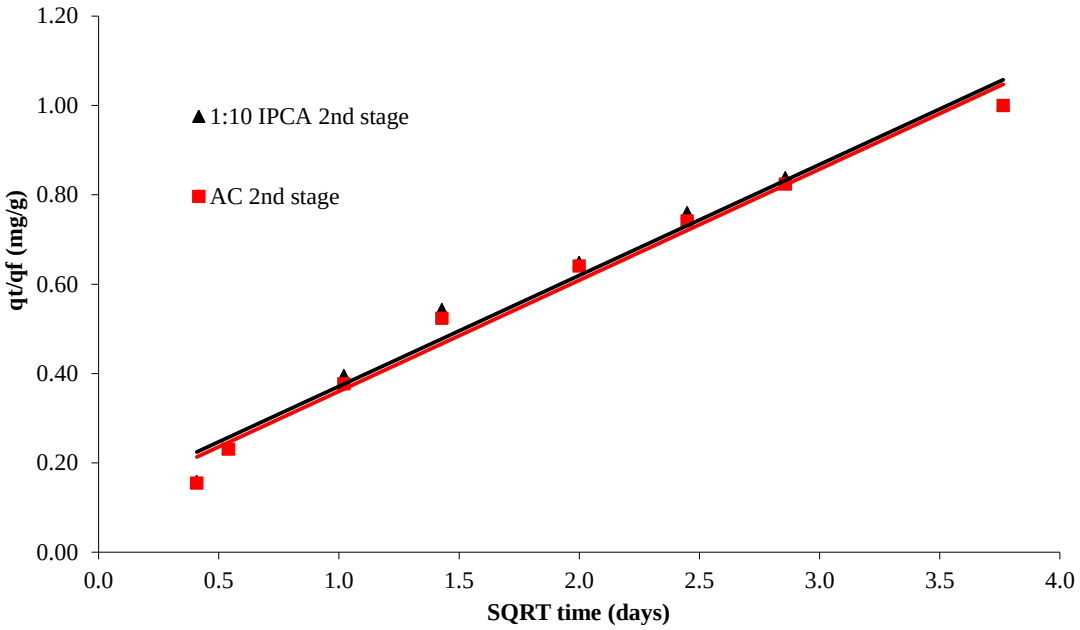

Figure 4-24 Fractional uptake curve for adsorption of famotidine onto AC and 1:10 IPCA for 2nd stage studies.

The 2nd stage studies demonstrate a single linear trend indicating that intraparticle diffusion is rate limiting. The 2nd stage studies have lower k_{int} than the 1st stage studies (Part A) as they do not adsorb as much famotidine. The boundary layer is also larger. Both of these effects are likely caused by the lower adsorption of the famotidine during the 2nd stage studies as the boundary layer effect will be more pronounced when the overall adsorption (and intraparticle diffusion) is lower.

A Bangham equation plot of famotidine adsorption is shown in Figure 4-25. If the Bangham equation produces a straight line then pore or intraparticle diffusion is a limiting factor. A double logarithmic plot linearized the data for famotidine adsorption for the first stage IPCA and AC results with a high degree of correlation (R^2 = 0.9493 and 0.9531). However the second stage IPCA and AC results had higher correlation coefficients (R^2 = 0.9881 and 0.9904). This appears to be due to a plateauing of the famotidine adsorption in the first stage studies from day eleven onwards. At this point the famotidine remaining in solution was almost completely adsorbed (Figure 4-20). The plateauing of the Bangham plot indicates that the intraparticle diffusion rate is no longer the limiting factor at the end of the study period. This is expected as the lack of substrate is limiting the adsorption rate at this stage of the study. The stage two studies do not show this trend as they are not conducted for long enough to adsorb greater than 97 % of the substrate in solution as was the case for the first stage studies. The results of the intraparticle diffusion model and a linear Bangham plot confirm that the diffusion of adsorbate into pores of the adsorbent is a rate-controlling step (Önal, 2006). This result confirms that pore diffusion was the most important factor effecting adsorption with film diffusion (the boundary layer effect) having a small limiting effect. Values of k_b and α (<1) are given in Table 4-3.

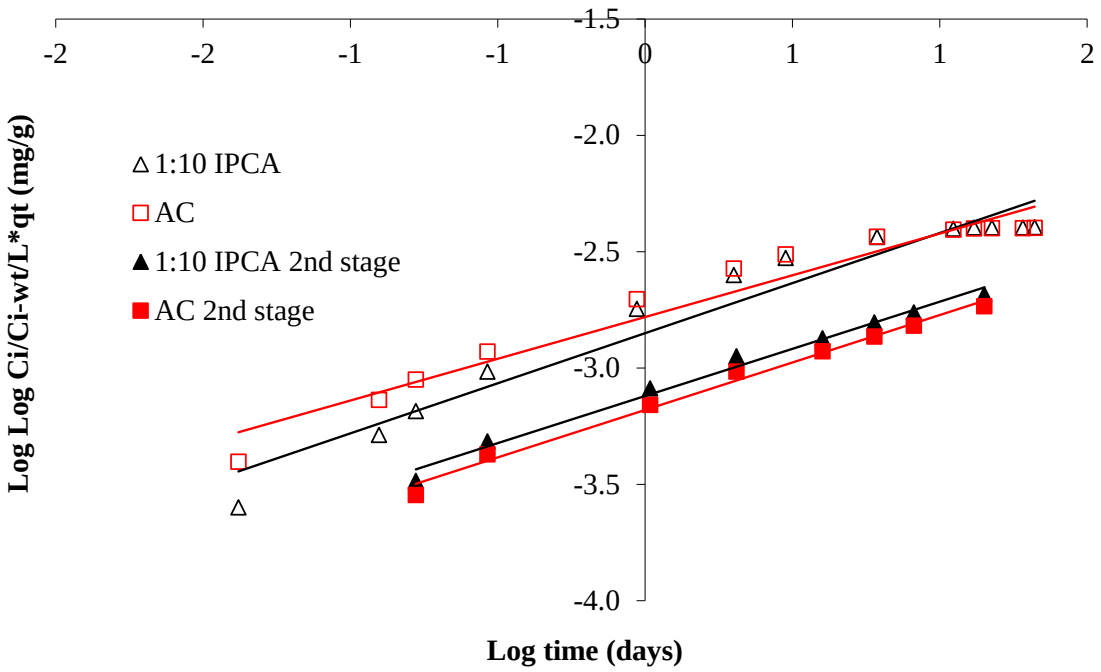

Figure 4-25 Bangham's plot of Log Log (C_i/C_i −qt) vs. Log t for famotidine adsorption.

Table 4-3 Kinetic parameters for adsorption of famotidine onto AC and IPCAs (first and second stage studies)

Model	**Parameters**		
Experimental values			
Sample name	**q (final) (mg/g)**		
1:10 IPCA	184.71		
AC	183.84		
1:10 IPCA (2^{nd} stage)	94.61		
AC (2^{nd} stage)	84.40		
Intraparticle diffusion equation			
	k_{int} (mg/g day$^{0.5}$)	**C (mg/g)**	**R^2**
1:10 IPCA (Part A)	0.3884	0.0215	0.9771
AC (Part A)	0.3706	0.0811	0.9677
1:10 IPCA (Part B)	0.0076	0.9667	0.5799
AC (Part B)	0.011	0.9503	0.7747
1:10 IPCA (2^{nd} stage)	0.0054	0.123	0.9763
AC (2^{nd} stage)	0.0054	0.112	0.9825
Bangham equation			
	α	**k_b (mL/g/L)**	**R^2**
1:10 IPCA	0.4305	0.0649	0.9493
AC	0.359	0.0763	0.9531
1:10 IPCA (2^{nd} stage)	0.4049	0.0349	0.9881
AC (2^{nd} stage)	0.4081	0.0304	0.9904

4.4.1.2 Effect of initial concentration on adsorption

The influence of initial famotidine concentration on IPCA adsorption was investigated using the same conditions as the AC study. IPCAs with TiO_2 to AC ratios from 1:200 to 1:10 were studied so adsorption capacity could be compared to their photocatalytic activity. The results are shown in Figure 4-26.

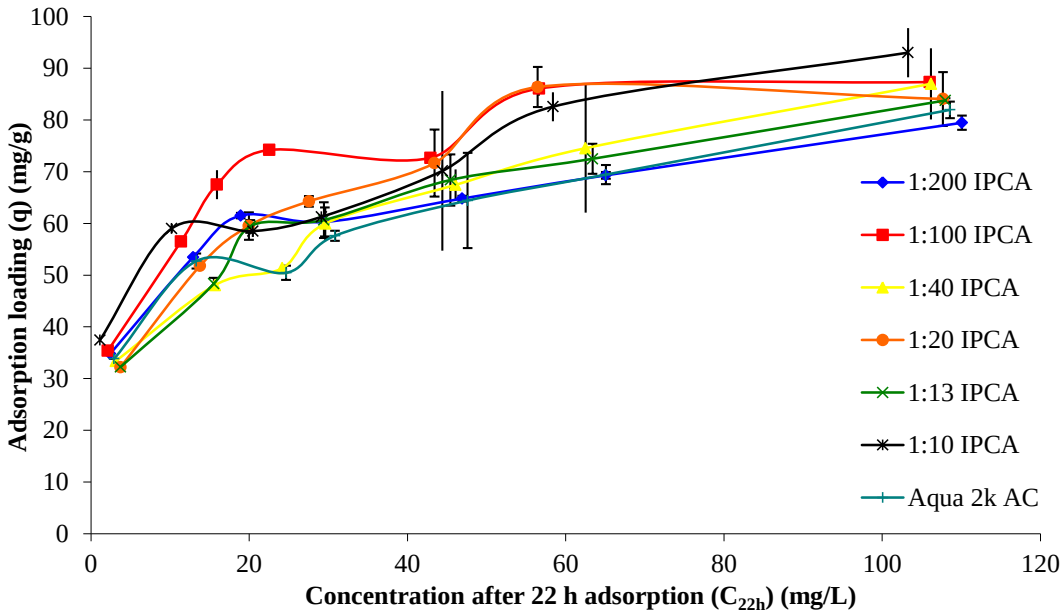

Figure 4-26 Adsorption loading (q) of famotidine on various IPCAs and AC vs. concentration after 22 h adsorption (C_{22h}). Initial concentrations studied were 20 mg/L, 40 mg/L, 50 mg/L, 60 mg/L, 80 mg/L and 100 mg/L and 150 mg/L. Average results shown (N=2), error bars are standard deviation.

The adsorption capacity displays a steep rise with a decline in the rate of increase as the trend starts to plateau. This behaviour was observed for all the adsorbents and reflects saturation of the surface of the adsorbents as the famotidine concentration increased. This shape of isotherm suggests Langmuir-type adsorption between famotidine and the IPCAs and AC. With the increase of initial famotidine concentration from 20 mg/L to 150 mg/L, the adsorbed famotidine after 22 h of adsorption increased from 3 mg/g to 87 mg/g and 34 mg/g to 72 mg/g for the 1:100 IPCA and AC, respectively. The 1:10 IPCA was determined to be the most effective IPCA for famotidine adsorption. With the TiO_2 content in the IPCA increasing from 1:100 to 1:10, the adsorption capacity decreased from 87 mg/g to 75 mg/g due to the higher content of TiO_2 particles on the surface of the AC occupying adsorption sites (Wang *et al.*, 2008).

4.4.1.3 Effect of initial pH on adsorption

The effect of initial pH on famotidine adsorption for the IPCA and AC is shown in Figure 4-27. The IPCA demonstrated an increase in adsorption capacity with increasing pH in contrast to the TiO_2 pH studies that demonstrated no discernible trend. The final pH of both the AC and IPCA are similar providing further confirmation that the adsorption properties of the AC and 1:10 IPCA are quantitatively similar.

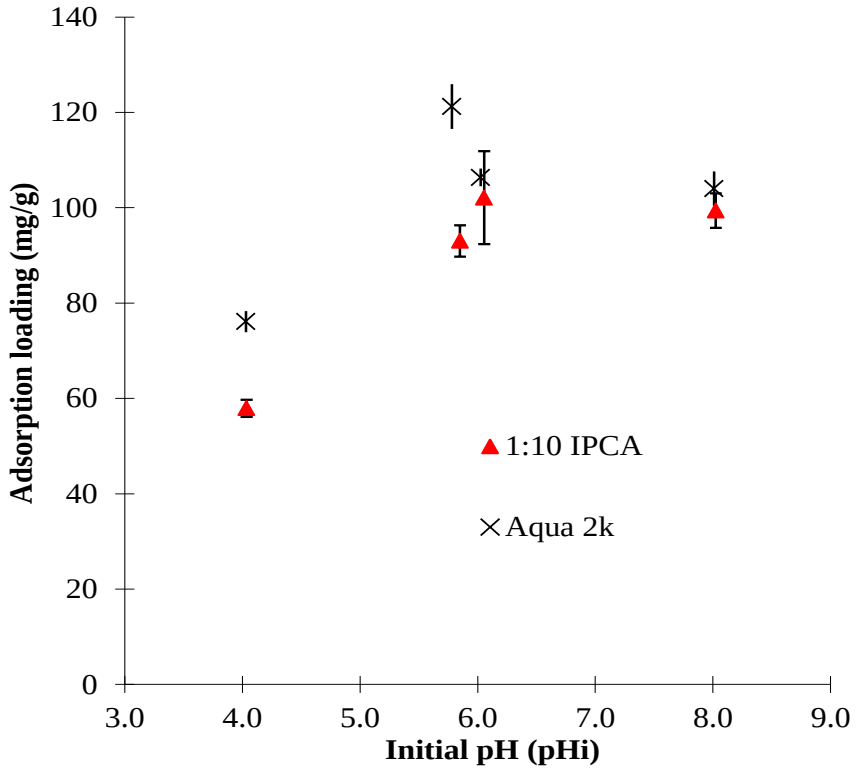

Figure 4-27 Adsorption loading (q) of famotidine onto Aqua 2k and 1:10 IPCA vs. initial pH (pH_i). pH_i studied were 4.0, 5.8, 6.0 and 8.0. Average results shown (N=2), error bars are standard deviation.

4.4.2 Solifenacin

4.4.2.1 Adsorption kinetics of the 1:10 IPCA

The concentration of solifenacin in solution during the study period is shown in Figure 4-28. The adsorption trend is almost identical to the AC suggesting the adsorption mechanisms are the same.

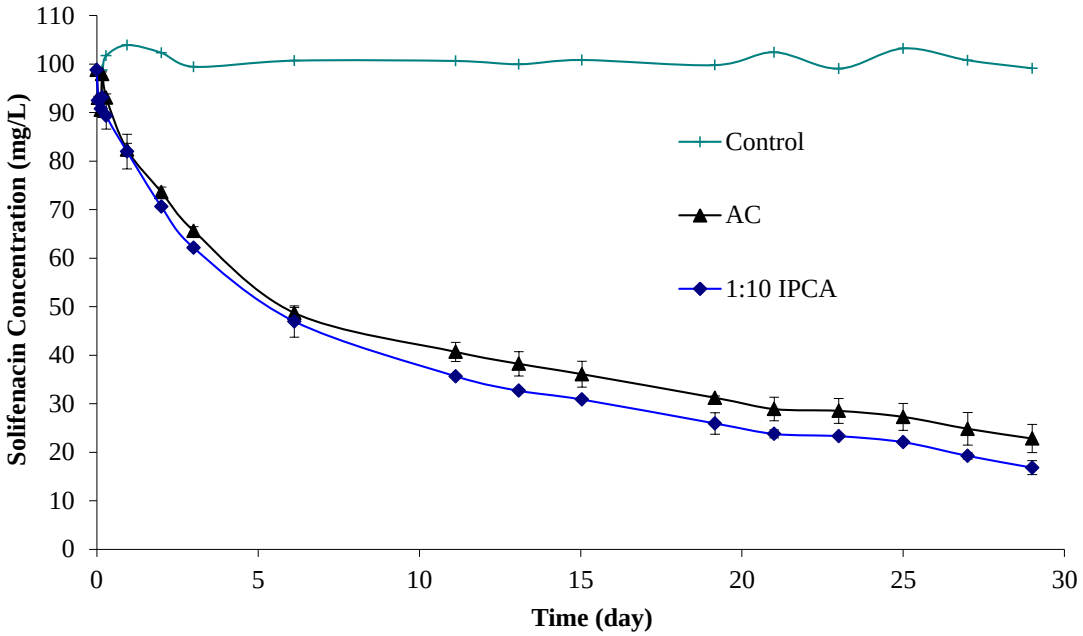

Figure 4-28 Average solifenacin concentration (mg/L) vs. time (day) for AC and IPCA. Average results shown (N=2), error bars are standard deviation.

The adsorption loading of solifenacin by the 1:10 IPCA and AC is shown in Figure 4-29. The same kinetic models used to analyse the famotidine adsorption rate data were also used for solifenacin. A fractional uptake diagram of adsorption of solifenacin onto AC and 1:10 IPCA is shown in Figure 4-30. Figure 4-28 and Figure 4-30 demonstrate that there is multi-linearity in solifenacin adsorption i.e. separate adsorption phases taking place during the course of the experiment. The first stage (Part A) is from day 0 - 6 and has rapid adsorption, the second stage (Part B) from days 6 - 19 has a lower adsorption rate and the third stage (Part C) (days 19 to 29) has an adsorption rate lower than the second stage.

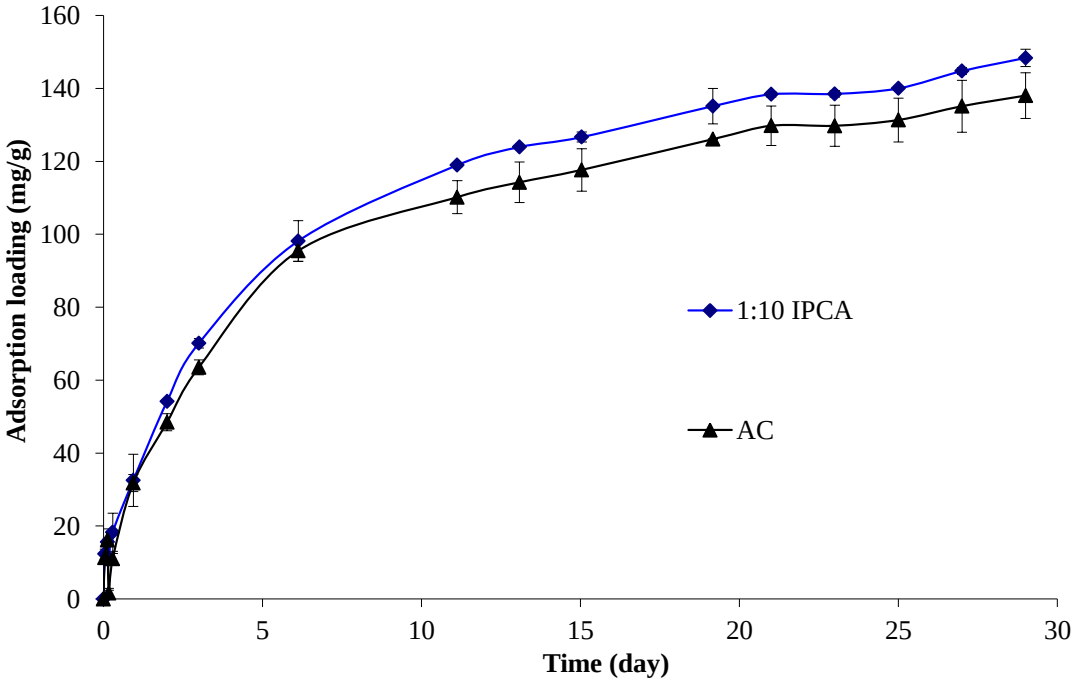

Figure 4-29 Solifenacin adsorption loading (mg/g) vs. time (day) for various adsorbents. Average results shown (N=2), error bars are standard deviation.

Multi-linearity is reported in the literature (Kumar *et al.*, 2003) but the process claimed to be represented by each step varies between researchers. Where the initial part of the plot is linear through the origin (Kumar *et al.*, 2003) - as is the case in this research - the different sections of the curve are attributed to diffusion of the substrates into the macro, meso and micro-pores of the adsorbent. Other researchers attribute the first portion to the diffusion of adsorbate through the solution or the boundary layer diffusion of solute molecules (Arivolia *et al.*, 2009, Önal, 2006). The second portion is described as the intraparticle diffusion stage which is rate limiting and the third portion, if present, is attributed to the final equilibrium stage (Önal, 2006). The large solution volume, concentration of solifenacin in solution and the high stirring rate rules out diffusion through the solution as a rate limiting step. Similarly if the process is controlled by the external resistance (film diffusion) then a plot of lnC vs. t must be linear (Nevskaia *et al.*, 1999).

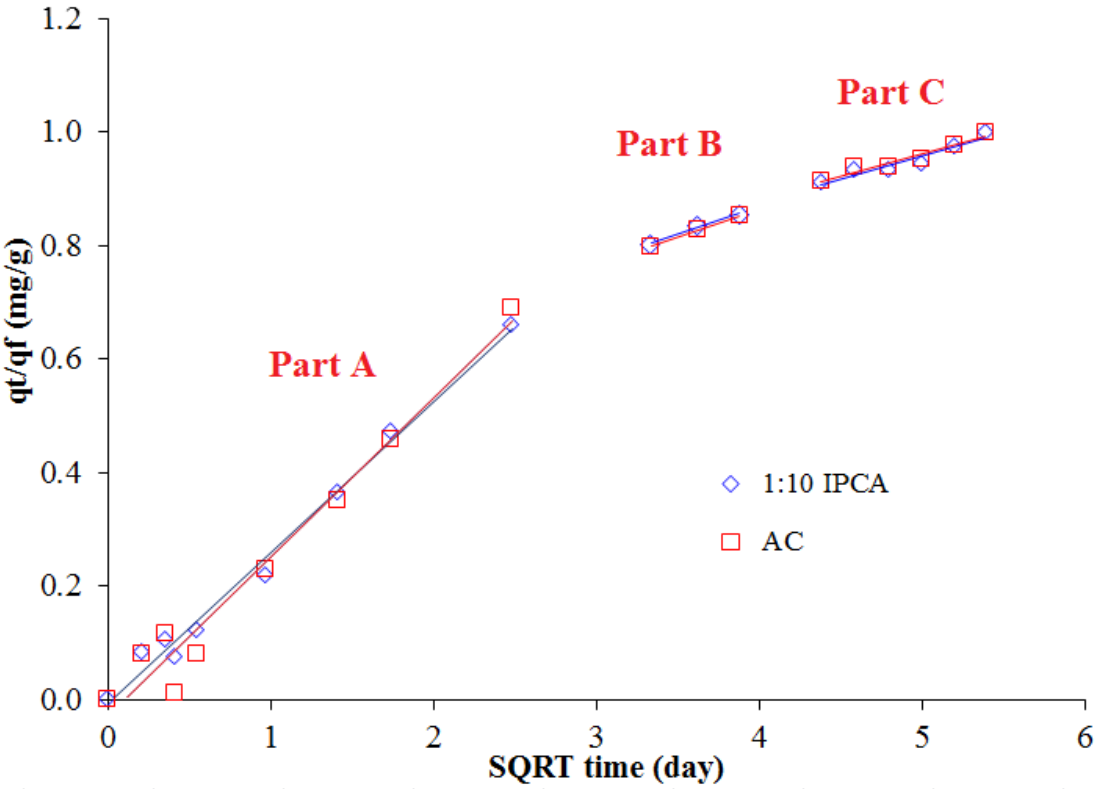

Figure 4-30 Fractional uptake curve of solifenacin for 1:10 IPCA and AC.

However when lnC vs. t was plotted the resulting graph (Figure 4-31) was not linear indicating that it is not a rate limiting step.

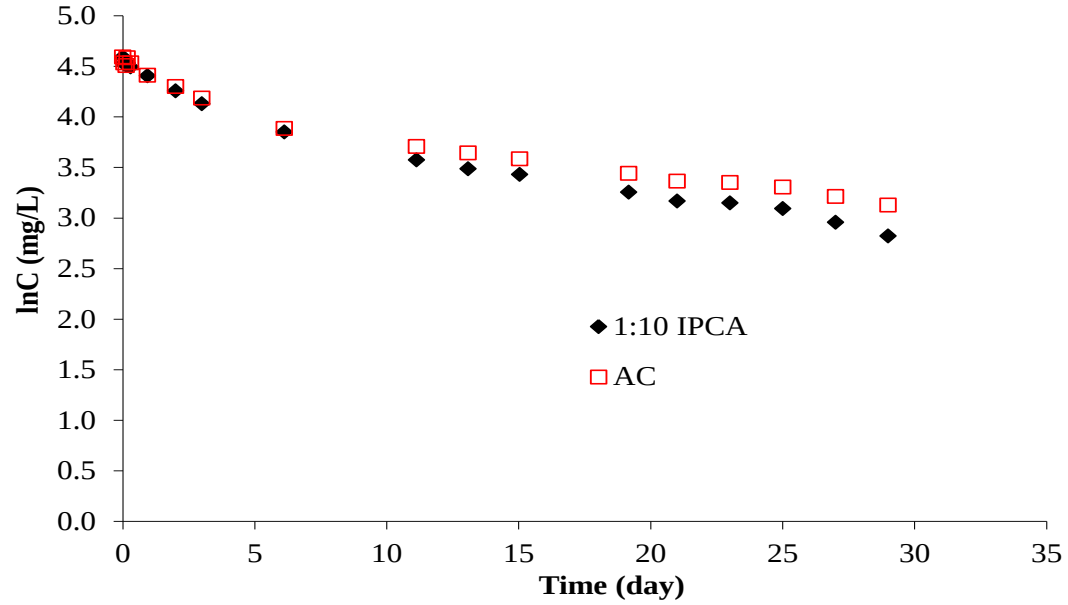

Figure 4-31 lnC (concentration) vs. t for IPCA and AC.

This result is confirmed by the low intercept values for Part A of the graph (0.0062 mg/g and 0.0271 mg/g for the IPCA and AC respectively) which implies a small boundary layer thickness if the boundary layer actually exists. An equilibrium stage is also unlikely as an explanation for the third stage as the studies did not reach equilibrium and at most only removed 87 % of the solifenacin from solution.

A Bangham equation plot of solifenacin adsorption is shown in Figure 4-32. The double logarithmic plot linearized solifenacin adsorption by the IPCA with a high degree of correlation (R^2 = 0.9724). The AC results did not fit as well (R^2=0.8085), however, this is due to an outlier at t = 240min (Log(t) -0.77815). If this point is removed then the R^2 value is much higher (R^2 = 0.9559) and similar to that of the IPCA.

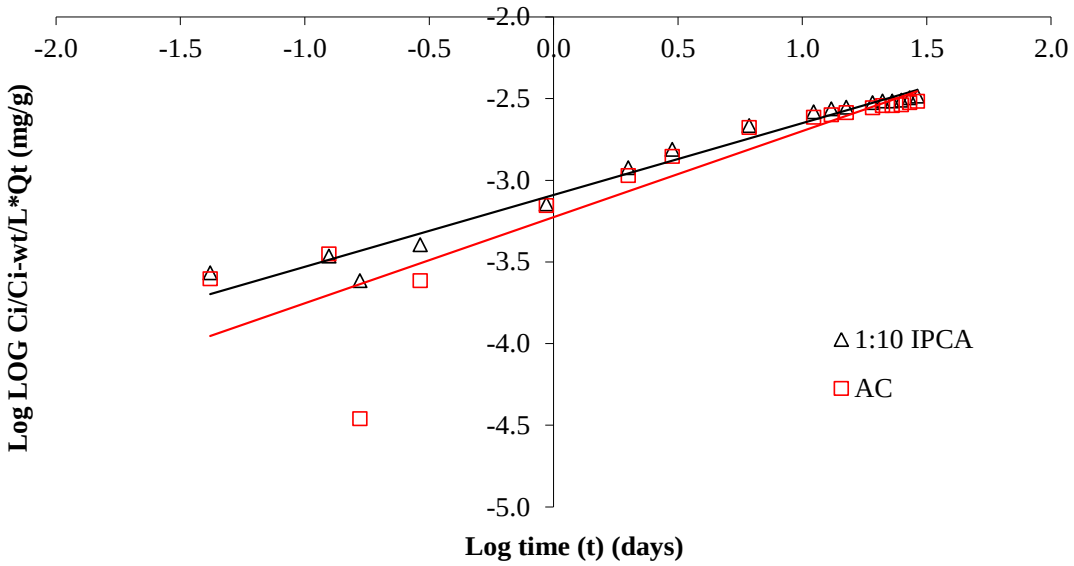

Figure 4-32 Bangham equation for solifenacin.

These results confirm the intraparticle diffusion model i.e. diffusion of solifenacin into the pores of the sorbent is the rate-controlling step. These results are similar to those of famotidine which would be expected since both are being adsorbed onto the same AC. This is possible due to the relatively large size of the famotidine and solifenacin molecules which would hinder their migration through the pore of the AC.

Table 4-4 Kinetic parameters for adsorption of solifenacin onto AC and 1:10 IPCA.

Model	**Parameters**		
Experimental values			
Sample	**q (final) (mg/g)**		
1:10 IPCA	148.37		
AC	138.04		
Intraparticle diffusion equation			
	k_{int} (mg/g day$^{0.5}$)	**C (mg/g)**	**R^2**
1:10 IPCA Part A	0.2669	0.0062	0.9896
AC Part A	0.2801	0.0271	0.9674
1:10 IPCA Part B	0.0958	0.4842	0.9797
AC Part B	0.0998	0.4659	0.9992
1:10 IPCA Part C	0.0822	0.5477	0.9113
AC Part C	0.0788	0.5686	0.9325
Bangham equation			
	α	**K_b (mL/g/L)**	**R^2**
1:10 IPCA	0.4398	0.03747	0.9724
AC	0.5268	0.02740	0.8085

4.4.2.2 Effect of initial concentration on adsorption

The adsorption capacity of the IPCA at different solifenacin initial concentrations was compared to the AC and these results are shown in Figure 4-33. The adsorption loading displayed a steep rise followed by a decline in the rate of adsorption until it plateaued. The values for the AC and IPCA are very similar and are almost identical at initial concentrations of 80 mg/L, 100 mg/L and 150 mg/L (46.4 mg/g, 52.8 mg/g, and 59.9 mg/g vs. 46.2 mg/g, 52.9 mg/g, and 59.6 mg/g for the AC and IPCA respectively). These results confirm that the addition of P25 to the AC (to create an IPCA) did not cause a noticeable reduction in the adsorption capacity of the AC.

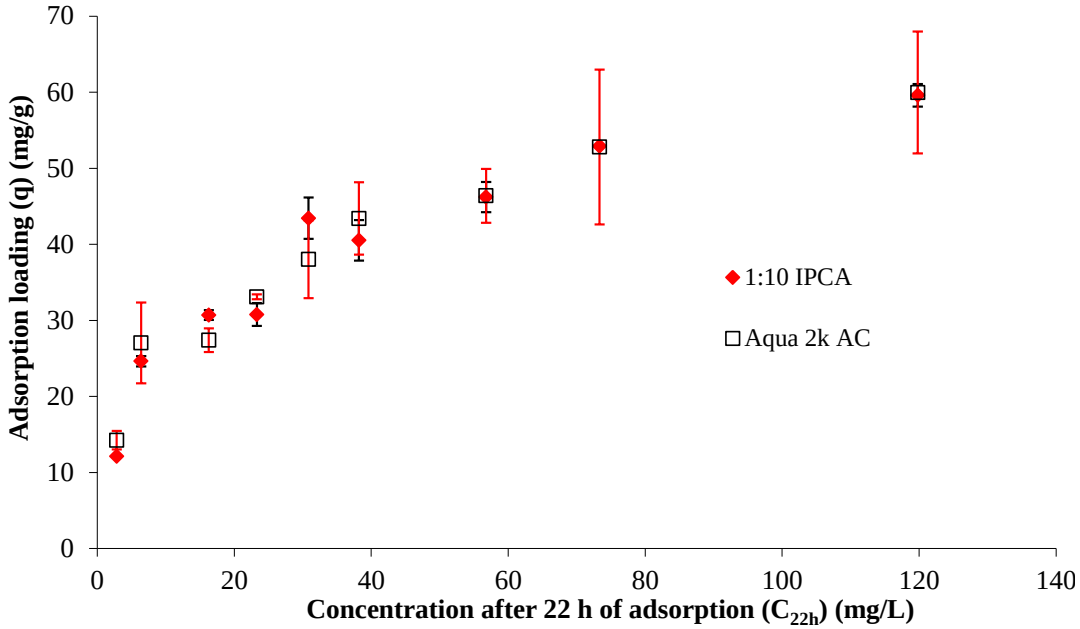

Figure 4-33 Adsorption loading (q) of solifenacin vs. concentration after 22 h (C_{22h}) of adsorption onto Aqua 2k and 1:10 IPCA. Initial concentrations studied were 10 mg/L, 20 mg/L, 30 mg/L, 40 mg/L, 50 mg/L, 60 mg/L, 80 mg/L and 100 mg/L and 150 mg/L. Average results shown (N=2), error bars are standard deviation.

4.4.2.3 Effect of initial pH on adsorption

The effect of pH on solifenacin adsorption for the IPCA and AC control is shown in Figure 4-34. When error bars are included there is not a significant difference between the IPCA and AC in terms of adsorption capacity at different pH_is. There is no clear trend with rising pH for either AC or IPCA adsorption.

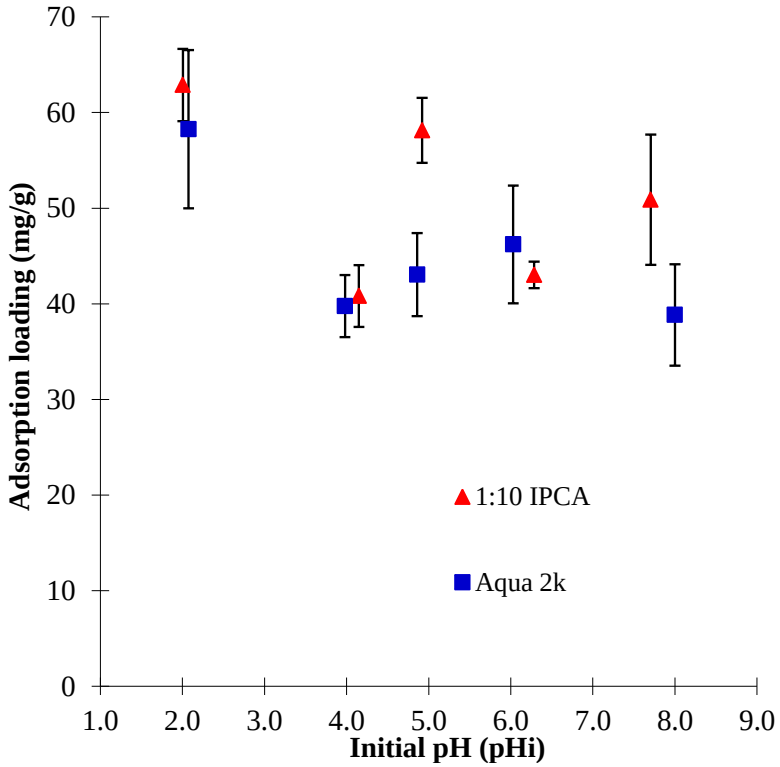

Figure 4-34 Adsorption loading (q) of solifenacin onto Aqua 2k and 1:10 IPCAs vs. initial pH (pHi). pH_i studied for ACs were 2.1, 4.0, 4.9, 6.0 and 8.0. pH_i studied for IPCAs were 2.1, 4.2, 4.9, 6.3 and 7.7. Average results shown (N=2), error bars are standard deviation.

4.5 Isotherm modelling of adsorption onto IPCAs and AC

4.5.1 Famotidine

The relationship between the adsorbed famotidine and the famotidine concentration remaining in solution at equilibrium is described by the adsorption isotherm, characterised by constants whose values express the surface properties and affinity of the adsorbent. To optimise an adsorption system, it is important to establish the most appropriate correlation for the equilibrium plot. Adsorption isotherms namely the Langmuir, Freundlich, Redlich-Peterson and Temkin were applied to the data of famotidine adsorption onto various IPCAs and the unmodified AC. All the statistical parameters and the constants obtained from the models are summarised in Table 4-5.

The experimental data was plotted using different linear forms of the Langmuir isotherm: 1/q vs. $1/C_{22h}$, $(C_{22h}/q)/C_{22h}$, $q/(q/C_{22h})$ and q vs. $1/C_{22h}$ to check for best fit. The plot of $(C_{22h}/q)/C_{22h}$ produced a plot that fitted the experimental data and achieved high R^2 values (0.9739 to 0.9946). The adsorption performances of the various IPCAs and AC were compared by their respective q_m values calculated from fitting the Langmuir isotherm to the experimental data. The sorption performances of IPCAs were higher than that of the AC, and decreased with increasing TiO_2 content of the IPCAs. The 1:40 IPCA showed the highest maximum saturated adsorption (q_m of 96 mg/g) and the 1:10 IPCA had the highest adsorption equilibrium constant (K_L = 0.125 L/mg). The Langmuir constants were used to determine a calculated adsorption loading (q(cal)) which was then compared to the experimental values using the sum of square error (SSE) and standard error (SE) tests (see Section 2.2.6.5). In general the values for both tests will be lower for data that has a higher correlation with the model in question. For simplicity only SSE will be discussed as it is the standard test for the fit of experimental data.

For the C_{22h}/q vs. C_{22h} plot the SSE ranged from between 144.93 to 1064.64, the lowest variance in the data was the 1:20 IPCA. The error values for this model were very high compared to other isotherm models (Table 4-5) indicating that the Langmuir model is a relatively poor fit for the data. The high SSE is due to the Langmuir model not being a good fit for the data at lower famotidine concentrations (Figure 4-35). This can be attributed to the heterogeneous surface of the AC adsorbing a larger proportion of the famotidine at low famotidine concentrations compared to high famotidine concentrations. From a theoretical point of view the Langmuir isotherm is not suitable for use on activated carbons as it is based on three theoretical assumptions (Marsh and Rodríguez-Reinoso, 2006b) that are not applicable to activated carbons:

1. Only monolayer adsorption occurs throughout the whole adsorption process.
2. The adsorption process is localized with no adsorbate-adsorbate interactions.
3. The heat of adsorption is independent of surface coverage i.e. the adsorbent has an energetically homogeneous surface.

The ability of this model to linearise AC isotherms is probably due to assumption (1.) and (3.) compensating for each other. Adsorbate-adsorbate interactions would increase with adsorption while the enthalpies of adsorption

decrease. In spite of these limitations the Langmuir equation is widely used in the published literature.

Table 4-5 Calculated isotherm parameters for famotidine adsorption onto various IPCAs and AC.

Models	**Adsorbents**						
	AC	**1:200 IPCA**	**1:100 IPCA**	**1:40 IPCA**	**1:20 IPCA**	**1:13 IPCA**	**1:10 IPCA**
Langmuir (C_{22h}/q vs. C_{22h})							
q_m (mg/g)	**86.2**	81.9	91.7	96	92.6	88.5	**96**
K_L(L/mg)	**0.087**	0.13	0.17	0.065	0.102	0.125	**0.117**
R^2	**0.9803**	0.9895	0.9946	0.997	0.9922	0.9852	**0.9739**
SSE	**416**	323	212.9	395	144.9	672.7	**1064.64**
SE	**9.12**	8.04	6.53	8.89	5.38	11.60	**14.59**
Freundlich (lnq vs. lnC_{22h})							
K_F (L/g)	**26.7**	30.5	31.99	23.3	22.95	33.4	**36.49**
1/n	**0.2323**	0.2047	0.2356	0.2756	0.3034	0.1985	**0.1891**
n	**4.3048**	4.885	4.244	3.628	3.2959	5.0378	**5.288**
R^2	**0.9764**	0.9606	0.9299	0.9792	0.954	0.9596	**0.9482**
SSE	**682.6**	3114.9	304.96	52.8	242.6	207.96	**174.33**
SE	**11.68**	6.45	7.81	3.25	6.97	6.45	**5.90**
Temkin (q vs. lnC_{22h})							
A (l/g)	**4.4**	10.4	6.8	2	1.7	12.9	**17.8**
B_T (J/mg)	**12.4**	10.9	13.7	15	16.9	11.3	**11.3**
B kJ/mg	**193.5**	219.7	174.4	158.8	141.7	212.4	**211.7**
R^2	**0.8875**	0.9967	0.95	0.9256	0.951	0.9136	**0.8937**
SSE	**74.99**	37.7	243.9	142.9	105.1	138	**208.8**
SE	**3.87**	2.74	6.99	5.35	4.6	5.3	**6.5**
Redlich and Peterson (q vs. C_{22h})							
K_{r-p}	**11760**	71	39.99	20633.9	20641	20647.8	**36373**
A_{r-p}	**447.9**	1.8	0.74	954.96	791.8	626	**1029.9**
β	**0.76**	0.85	0.89	0.70	0.73	0.80	**0.80**
R^2	**0.9874**	0.9850	0.9757	0.9922	0.9597	0.9692	**0.9666**
SSE	**34.5**	34.7	93.9	30.3	171.5	96.9	**129.35**
SE	**2.63**	2.63	4.33	2.46	5.86	4.40	**5.09**

For the Freundlich model the K_F values vary from 22.9 to 36.5 and are highest for the 1:13 and 1:10 IPCAs indicating greater affinity for famotidine adsorption compared to other IPCAs and the AC (Rengaraj *et al.*, 2002). The SSE values for the Freundlich model are similar (range 52.84 to 3114.89 vs. 144.93 to 1064.64) to the Langmuir models indicating that the Freundlich model is not a better fit of the data. The model is a better fit at lower famotidine concentrations than the Langmuir model. The Frendlich model is usually assumed to correspond to a heterogeneous surface so

it would be a better fit of the adsorption data at lower concentrations (Foo and Hameed, 2010b). This is further evidence the Langmuir model is unsuitable.

The Redlich and Peterson isotherm incorporates the features of the Langmuir and Freundlich isotherms into a single equation. The Redlich–Peterson (R-P) isotherm is a good fit for the experimental data as evidenced by high R^2 (0.9562-0.9912) and low SSE values (34.5 to 171.5) for AC and the various IPCAs. β values - β indicates surface heterogeneity - ranged between 0.7 and 0.87. A highly heterogeneous system will have a β value closer to 0 (the Freundlich equation) than 1 (the Langmuir equation) (Basha *et al.*, 2011). This outcome confirms that the adsorption mechanism is closer to Langmuir than Freundlich; however, the presence of surface heterogeneity indicates that Langmuir is not ideal and would suggest that a heterogeneous surface is the reason for the Langmuir isotherm's poor fit of the experimental data at low sorbate concentrations.

The Temkin model provides useful thermodynamic information and is intended for predicting gas phase equilibrium (when organization in a tightly packed structure with identical orientation is not necessary); however more complex liquid-phase adsorption systems cannot always be represented by this model (Foo and Hameed, 2010b). It is a model that is derived from Langmuir and as such assumes monolayer coverage.

The Temkin model demonstrated R^2 values between 0.8875 and 0.9677 with SSE values between 37.7 and 243.9 which are lower than the Langmuir and the Freundlich models. The constant B_T is related to heat of sorption (J/mg), was found to be in the following order: 1:200 IPCA < 1:13 IPCA < 1:10 IPCA < AC < 1:100 IPCA < 1:40 IPCA <1:20 IPCA. A (l/mg) the equilibrium binding constant ranged from 1.7 to 17.8. This suggests differences in the adsorbate - adsorbate interactions on the various IPCAs; however it is likely just variations in the data. In spite of lower R^2 values than the Langmuir model the SSE values of the Temkin model are higher than the Langmuir model which signifies a better fit of the experimental data. Given that the only difference between the Langmuir and Temkin models is that the Temkin model assumes adsorbate – adsorbate interactions. The mechanism suggested for the ability of the Langmuir isotherm to model a heterogeneous solid such as AC is adsorbate – adsorbate interactions compensating for the lowering of adsorption strength with increasing famotidine adsorption. The predicted q values for adsorption of famotidine onto AC are shown in Figure 4-35. The trend seen in this sample is

repeated for all the IPCA samples therefore only the AC, 1:200 IPCA and 1:10 IPCA are shown for clarity.

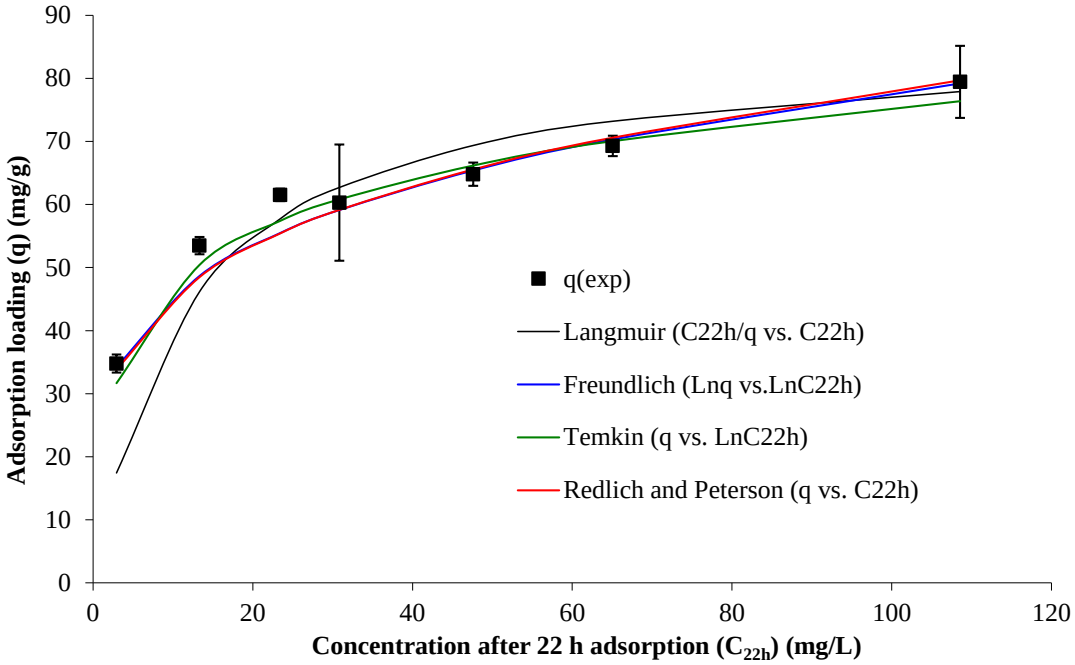

Figure 4-35 Experimental values (q(exp)) and calculated isotherm values of adsorption loading for famotidine adsorption onto AC vs. concentration after 22 h of adsorption (C_{22h}). Average q(exp) results shown (N=2), error bars are standard deviation.

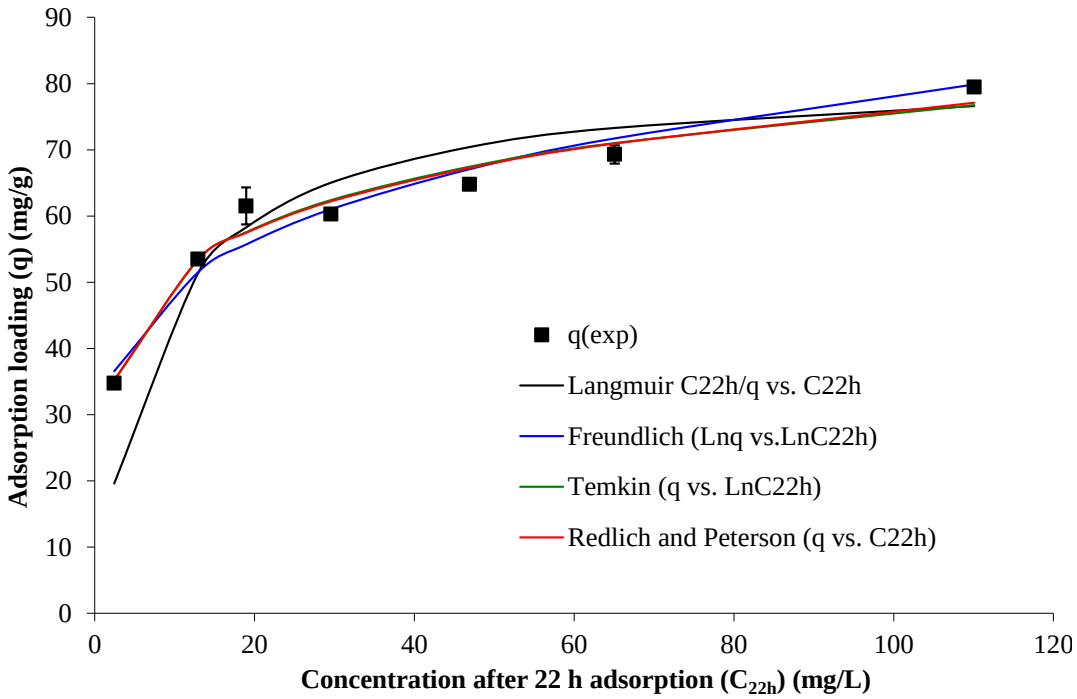

Figure 4-36 Experimental values (q(exp)) and calculated isotherm values of adsorption loading for famotidine adsorption onto 1:200 IPCA vs. concentration after 22 h of adsorption (C_{22h}). Average q(exp) results shown (N=2), error bars are standard deviation.

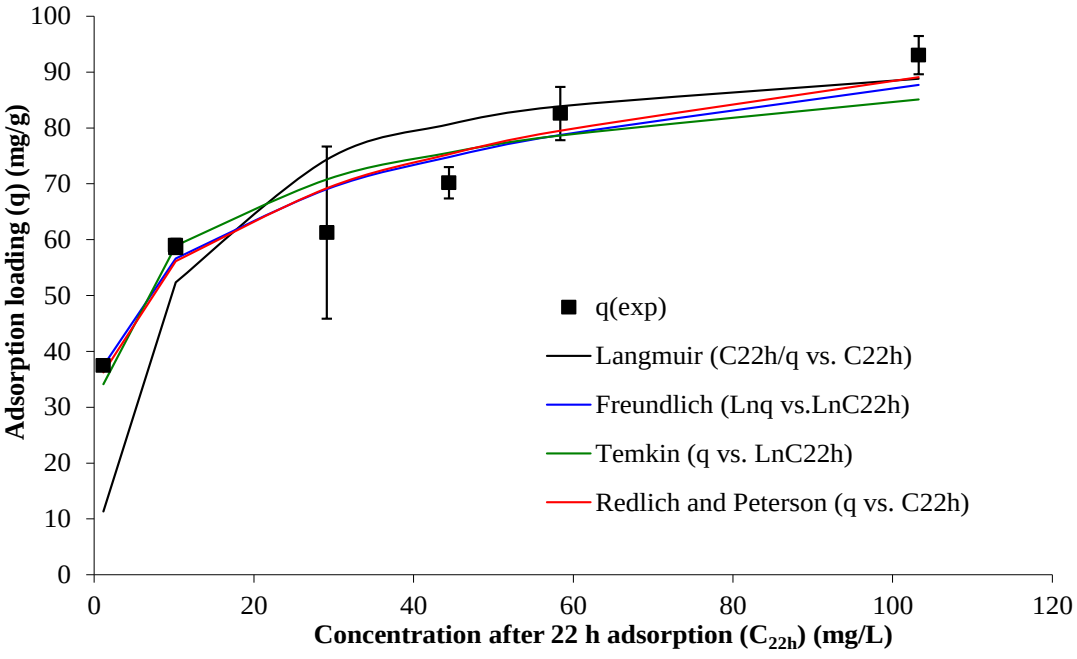

Figure 4-37 Experimental values (q(exp)) and calculated isotherm values of adsorption loading for famotidine adsorption onto 1:10 IPCA vs. concentration after 22 h of adsorption (C_{22h}). Average q(exp) results shown (N=2), error bars are standard deviation.

4.5.2 Solifenacin

The solifenacin adsorption data was modelled using the same methods and models as the famotidine isotherm data (Table 4-6). The fit of this model to the experimental data is shown in Figure 4-38 and Figure 4-39. The statistical parameters and the constants obtained from the models are summarised in Table 4-6.

Like famotidine, only the C_{22h}/q vs. C_{22h} plot of the Langmuir model fitted the data with R^2 values of 0.9751 – 0.9782 for the AC and 1:10 IPCA respectively. The adsorption performances of the 1:10 IPCA and AC were compared by their respective q_m values calculated from fitting the Langmuir isotherm to the experimental data. The sorption performances of the IPCA were higher than that of the AC, which matches the famotidine results. The q_m value for the IPCA and AC were 66.23 mg/g and 68.03 mg/g respectively suggesting similar adsorption performance between both adsorbents.

The Langmuir constants were used to determine a calculated adsorption loading (q(cal)) which was then compared to the experimental values using the SSE and SE tests. For the C_{22h}/q vs. C_{22h} plot the SSE values were 191.3 and 133.9 for the AC and IPCA respectively. The results of the error tests for the Langmuir models were very high compared to other isotherm models (Table 4-6). The Langmuir constants were used to plot the predicted Langmuir isotherms which are shown in Figure 4-38 and Figure 4-39. The predicted Langmuir plots are closer to the experimental values than the famotidine Langmuir plot. This is due to the much better fit of the Langmuir plot to solifenacin adsorption at low solifenacin concentrations especially for the 1:10 IPCA.

For the Freundlich model the K_F (L/g) values were 11.11 and 8.76 for the AC and IPCA respectively indicating greater affinity for solifenacin adsorption onto the AC compared to the 1:10 IPCA (Rengaraj *et al.*, 2002). The SSE values for the Freundlich model are similar to the Langmuir model: 53.11 and 161.97 vs. 191.28 and 133.88 for the AC and IPCA respectively indicating that both models are a good fit of the data.

The Redlich–Peterson (R-P) isotherm models the experimental data well as evidenced by high R^2 (0.9809 and 0.9689) and relatively low SSE (50.79 - 96.39) values for AC and the 1:10 IPCAs (Figure 4-38 and Figure 4-39). β values were 0.67

and 0.79 for the AC and IPCA respectively. These results are similar to those of famotidine suggesting that both famotidine and solifenacin adsorption follow the same adsorption mechanism. The β values of solifenacin adsorption are similar to famotidine which suggests the IPCA has a similarly heterogeneous surface for solifenacin adsorption, although these results could be due to variation in the data.

The predicted q values for adsorption of solifenacin onto AC are shown in Figure 4-38 and the 1:10 IPCA are shown in Figure 4-39.

Table 4-6 Calculated isotherm parameters for solifenacin adsorption onto various IPCAs and AC.

Models	**Adsorbents**				
	AC	**1:10 IPCA**	**Models**	**AC**	**1:10 IPCA**
Langmuir (C_{22h} /q vs. C_{22h})			**Freundlich (lnq vs. ln C_{22h})**		
q_m (mg/g)	66.23	68.03	**K_F (L/g)**	11.11	8.76
K_L(L/mg)	0.0548	0.0504	**1/n**	0.3582	0.4217
			n	2.79	2.37
R^2	0.9751	0.9782	**R^2**	0.9466	0.9087
SSE	191.28	133.88	**SSE**	53.11	161.97
SE	5.23	4.37	**SE**	2.75	4.81
Temkin (q vs. ln C_{22h})			**Redlich and Peterson (q vs. C_{22h})**		
A (l/g)	1.05	0.6869	**K_{r-p}**	66.01	6.947
B_T (J/mg)	11.6	13.128	**A_{r-p}**	5.23	0.288
b (kJ/mg)	206.3	182.5	**β**	0.67	0.79
R^2	0.9377	0.9477	**R^2**	0.9842	0.9735
SSE	274.02	100.37	**SSE**	50.79	96.39
SE	6.26	3.79	**SE**	2.69	3.71

The Temkin model demonstrated R^2 values of 0.9339 and 0.9476 and SSE values of 274 and 100.4 for the AC and IPCA respectively which are similar to the Langmuir and Freundlich models. The Temkin model is derived from the Langmuir equation and it has a similar fit to the Langmuir isotherm in terms of SSE values (Figure 4-38 and Figure 4-39). The main difference between the Langmuir and Temkin model is that the Temkin model assumes adsorbate–adsorbate interactions.

This suggests that interactions between the solifenacin molecules have little influence on the solifenacin adsorption process. This is in contrast to famotidine where the Temkin isotherm - and its assumptions - is the best fit for the data.

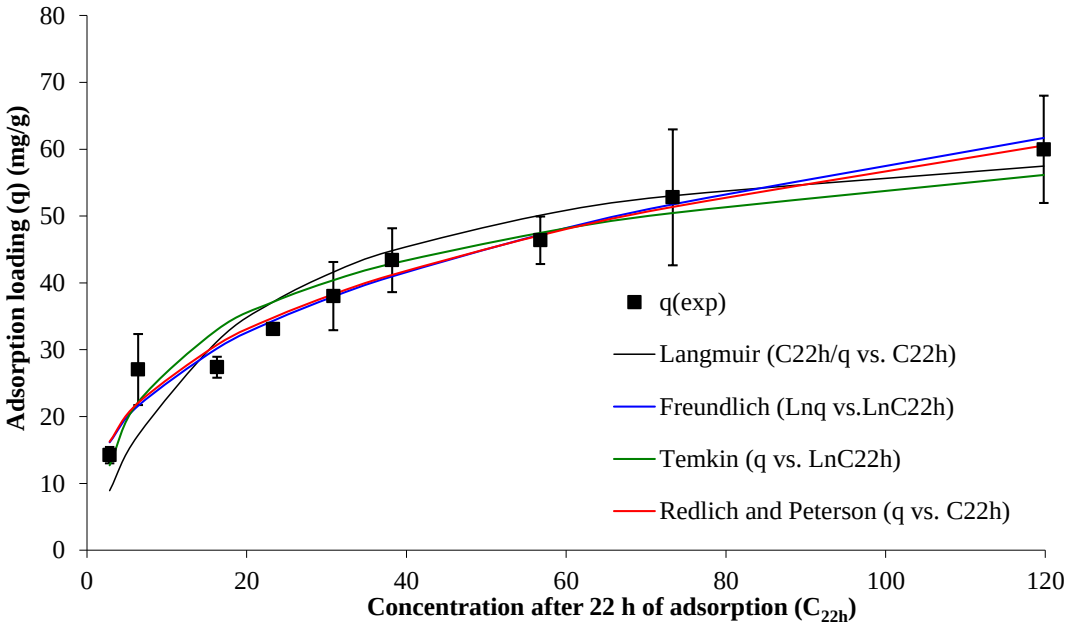

Figure 4-38 Experimental values (q(exp)) and calculated isotherm values of adsorption loading for solifenacin adsorption onto AC vs. concentration after 22 h of adsorption (C_{22h}). Average q(exp) results shown (N=2), error bars are standard deviation.

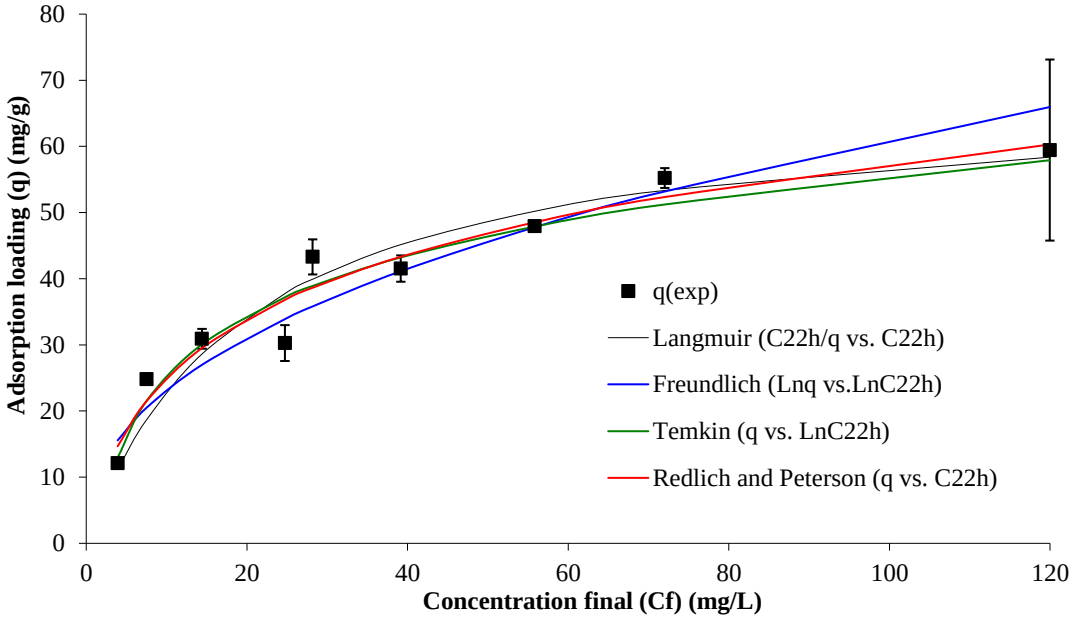

Figure 4-39 Experimental values (q(exp)) and calculated isotherm values of adsorption loading for solifenacin adsorption onto 1:10 IPCA vs. concentration after 22 h of adsorption (C_{22h}). Average q(exp) results shown (N=2), error bars are standard deviation.

4.6 Desorption of famotidine and solifenacin from AC

Desorption is required for photocatalytic regeneration of an IPCA as it is necessary for the transfer of the substrate from the adsorbent (in this case AC) to the TiO_2, where it is photodegraded. Theoretically the bonding of the substrate to the AC is physical as adsorption is a physical rather than chemical process and therefore reversible; however in practice several factors may hinder or prohibit this. The substrate may become stuck inside the micropores of the AC and thus simple desorption will not be able to remove it (Marsh and Rodríguez-Reinoso, 2006a). If the compound is hydrophobic then it will not desorb back into solution in any appreciable way compared to a substrate that is hydrophilic. While some literature imagines the migration of substrate to the TiO_2 as a simple conveyer belt type process (Khan, 2002) in reality it would desorb into solution and via the solution it would migrate towards the TiO_2. Typically AC is not regenerated by desorption into solution i.e. washing of the carbon with clean water either continuously or cyclically over a long period of time. Depending on the application regeneration of the spent up AC usually uses pyrolysis in an oxidizing atmosphere at high temperature (650°C - 1100°C) or

treatment with super-heated steam, CO_2 or both at high temperatures (350°C - 700°C) (Bansal and Goyal, 2005, Mazyck and Cannon, 2000). The regenerated AC can have an adsorption capacity of 90 % to 95 % of the fresh carbon (Bansal and Goyal, 2005) and this process consumes about 1 % – 10 % (Bansal and Goyal, 2005, Lim and Okada, 2005) of the original AC. The lost AC mass is usually made up by the addition of fresh AC.

Desorption studies in the literature typically use a strong acid or base e.g. 0.1N H_2SO_4, 0.1N HNO_3 or 0.1N NaOH (Arivolia *et al.*, 2009, Lataye *et al.*, 2008, Rengaraj *et al.*, 2002) or a solvent e.g. methanol (Lee *et al.*, 2004a) to desorb the substrate from the AC. These methods were not used as strong acids and bases would affect the stability of the IPCA. In addition, the desorption of the substrate from the adsorbent to the photocatalyst creating IPCA synergy is claimed to occur in the reaction solution which would not contain a solvent or be adjusted to a pH favorable for desorption. For this reason desorption in a solution of deionized water is a better test of desorption as IPCAs would be used in these conditions.

First, desorption from ACs with different levels of adsorbed famotidine (famotidine surface area coverage) was investigated. Two types of desorption experiments were undertaken, where the AC had different levels of saturation in each. For the first set the ACs were placed in a 100 mg/L famotidine solution for 24 h (one cycle of adsorption) before it was washed with deionised water and then used for desorption studies. The second set of ACs were placed in 100 mg/L famotidine solutions a total of three times to ensure that they were saturated with famotidine before being used in desorption studies.

The adsorption stage of the study (Table 4-7) showed that 32 % of the famotidine concentration was removed after 90 min and greater than 99 % adsorption occurred after 24 h. The AC saturated with famotidine was then placed in deionised water and a sample was taken at 25 h, the concentration of famotidine was below the limit of detection (0.2 mg/L) indicating that the GAC was adequately washed. Sampling was continued at 24 h, 48 h and 72 h; again no famotidine concentration was detected above the limit of detection. At 72 h the water was changed and samples taken at every hour for four hours. The peak area values increased over each hour but remained below the LOD for all samples.

Table 4-7 Famotidine desorption after 1 adsorption cycle (concentration (mg/L)).

Time / Sample	Adsorption			Desorption			
	0 h	**1.5 h**	**24 h**	**1 h**	**24 h**	**48 h**	**72 h**
Initial	103						
Control		103	110		117.4	128.0	133.3
Aqua 2k (1)		34.5	0.1	0.2	0.1	0.1	0.0
Aqua 2k (2)		31.9	0.0	0.1	0.0	0.0	0.0
Time / Sample	**Desorption**						
	73 h	**74 h**	**75 h**	**76 h**	**96 h**		
Control					140		
Aqua 2k (1)	0.0	0.0	0.0	0.0	0.0		
Aqua 2k (2)	0.0	0.0	0.1	0.0	0.0		

LOQ 1 mg/L LOD 0.2 mg/L. Replacement of the deionised water solution occurred after 0 h and after 72 h.

The samples desorbed no more than 1 % of the adsorbed famotidine and for all the samples the famotidine concentration was lower than the limit of quantification of the detection method. Consequently it was necessary to use more adsorption cycles so that the resulting desorption would be more pronounced and thus easier to detect. The second study saturated the AC with famotidine three times (Table 4-8). Saturation of the adsorption sites on the AC was greater as 98 % of the famotidine is removed by all the ACs in the first adsorption cycle while in the third cycle adsorption of famotidine dropped to 40 %.

This "*adsorbed AC*" was then screened for desorption. Approximately 12 mg/L desorbed from the AC into the solution during the first 24 h in deionised water. When the samples were placed in fresh deionised water for the second time, famotidine was released, although in smaller quantities (6 mg/L) with about 68 % released within 90 min of placing the AC in deionised water. These results indicate that desorption is greater if greater amounts of famotidine are adsorbed onto the surface of the AC. Desorption from Aqua 2k is approximately 3 % in the first desorption cycle and 2 % in the second desorption cycle. A total desorption of 5 % in two cycles with a declining trend suggests that only a small percentage of the

famotidine seems to be mobile under these conditions. Theoretically the famotidine could migrate to the surface of the TiO_2 but this process could take days.

Table 4-8 Famotidine desorption, 3 adsorption cycles (concentration (mg/L)).

Time / Sample	Adsorption				Desorption		Desorption		
	0 h	**24 h**	**48 h**	**72 h**	**24 h**	**48 h**	**49.5 h**	**51 h**	**72 h**
Initial	101.3	107.1	100.0						
Control		101.6	101.9	102.4	102.3	102.2			101.9
Aqua 2k (1)		0.1	26.1	59.8	11.7	8.8	4.5	4.7	6.0
Aqua 2k (2)		0.7	24.6	60.2	11.8	9.4	3.6	4.7	5.9

LOQ 1 mg/L LOD 0.2 mg/L. Replacement of the deionised water solution took place after 0 h and after 48 h.

Similar studies were used to characterise solifenacin desorption. After one cycle of adsorption greater than 96 % of the solifenacin in solution was removed by Aqua 2k (Table 4-9). After 1 h of immersion in fresh deionised water an average concentration of 0.9 mg/L solifenacin desorbed from the AC. When the solutions were placed in fresh deionised water after the 48 h sample the same trend was repeated. The majority of desorption occurs in the first 1 h which indicates that the initial rate of desorption is high, however given the gradual decrease in concentration after 24 h indicates that desorption/adsorption equilibrium is not reached quickly. The equilibrium concentration of solifenacin decreased with each time the AC samples were put in fresh deionised water indicating that desorption rates decreases as the total solifenacin concentration adsorbed on the AC decreases.

Table 4-9 Solifenacin desorption, 1 adsorption cycle (concentration (mg/L)).

Time / Sample	Adsorption		Desorption					Desorption	
	0 h	**24 h**	**1 h**	**2 h**	**3 h**	**24 h**	**48 h**	**72 h**	**96 h**
Initial	98.3								
Control		100.9				101.3	101.0	100.9	101.0
Aqua 2k (1)		3.8	1.2	1.1	1.1	0.3	0.1	0.3	0.2
Aqua 2k (2)		2.2	0.6	0.6	0.6	0.2	0.1	0.3	0.2

LOQ 1 mg/L LOD 0.2 mg/L. The deionised water solution was replaced at time 0 and at time 48 h.

The second study used three adsorption cycles of solifenacin before desorption. These results are shown in Table 4-10. The concentration remaining after the first adsorption cycle was almost identical to the previous study (Table 4-9); however the rate of solifenacin removal drops significantly with each cycle. About two thirds of the desorption over the 24 h period occurred in the first hour before declining from the 24 h to 48 h period in the same trend seen in the famotidine desorption studies and the previous solifenacin study. The solifenacin desorption rate was much higher the first time the ACs were placed in deionised water.

Table 4-10 Solifenacin desorption, 3 adsorption cycles (concentration (mg/L).

Time / Sample	Adsorption				Desorption					Desorption	
	0 h	**24 h**	**48 h**	**72 h**	**1 h**	**2 h**	**3 h**	**24 h**	**48 h**	**72 h**	**96 h**
Initial	96.1	97.1	95.9								
Control		95.6	96.1	96.3				96.4	96.8	96.4	96.7
Aqua 2k (1)		3.2	41.6	68.4	6.5	9.0	10.0	14.0	11.7	4.6	4.5
Aqua 2k (2)		2.8	39.1	66.2	6.6	9.2	10.3	13.3	11.4	5.1	4.8

LOQ: 1 mg/L LOD: 0.2 mg/L. The deionised water solution was replaced at Time = 0 and time = 48 hours.

At 24 h the concentration of solifenacin at equilibrium was 14 mg/L, while 24 h (48 h) after the change of water it had dropped to 5 mg/L. Compared to famotidine, the adsorption loading of solifenacin is much lower but the rate of desorption is also much higher suggesting that the properties of the AC that allow high adsorption capacities also retard desorption. Solifenacin desorption from the AC is approximately 8 % in the first desorption cycle and 3 % in the second desorption cycle. A total desorption of 11 % in two cycles with a declining trend suggests that only a small percentage of the solifenacin is mobile under these conditions. However this rate of total desorption is twice that of the famotidine desorption (5 %) under the same conditions. The difference in adsorption and desorption performance is likely due to the different chemical structures of the substrates (Figure 4-1 and Figure 4-2). The functional groups on famotidine make it very polar which creates strong bonds to the AC surface retarding desorption but enhancing adsorption. By comparison solifenacin has less functional groups (H bond acceptors and H bond donors)

therefore it is easier for it to desorb back into solution. The enhanced desorption could contribute to the synergy in IPCA photodegradation. Faster desorption would lead to more migration to the TiO_2 surface and thus more photodegradation.

4.7 Conclusions

Baseline adsorption studies have demonstrated that AC has a large adsorption capacity for famotidine and solifenacin and is a suitable adsorbent for their removal. Studies of P25 demonstrate that it is an ineffective adsorbent. Isotherm modelling gave some insights into the adsorption process on AC and IPCAs. These results indicate that IPCAs are suitable for adsorbing pharmaceuticals in the dark:

- Intraparticle diffusion is the limiting step for both famotidine and solifenacin adsorption.
- P25 TiO_2 has negligible adsorption capacity.
- The adsorption capacity of AC at 150 mg/L initial concentration is 82 mg/g for famotidine and 60 mg/g for solifenacin. This establishes the adsorption capacity of the AC for the pharmaceuticals under investigation.
- For solifenacin adsorption the IPCA's adsorption capacity (60 mg/g) is not noticeably different to the unmodified AC (60 mg/g). For famotidine adsorption the IPCA (93 mg/g) adsorbed more than the AC (82 mg/g).
- Desorption of famotidine and solifenacin adsorbed on the AC surface was less than 5 % for famotidine and 11 % for solifenacin over a four day period. Indicating that only a small fraction (<12 %) of the API adsorbed on an AC can desorb into solution.
- The Temkin model is the best fit for the famotidine adsorption data, while the Redlich-Peterson model is the best fit for the solifenacin data in terms of R^2 and SSE values.
- These results complete the first part of the first aim of the project: "*The capacity of IPCAs, commercial AC and TiO_2 to adsorb … pharmaceuticals*".

Chapter 5 Photodegradation Studies

5.1 Introduction

Given that IPCAs can adsorb both famotidine and solifenacin, the next step is to determine the IPCA's photocatalytic properties and the photocatalytic properties of the raw materials. Photolysis studies were used to determine the substrate photodegradation due to UV light alone. Photocatalysis studies used unmodified TiO_2 (P25) to demonstrate how much substrate is removed by conventional photocatalysis. Initial screening studies of the IPCAs prepared by ultrasonication were undertaken to determine their photocatalytic properties. This chapter will investigate:

- Photolysis of famotidine and solifenacin using light from a medium pressure mercury lamp.
- Photocatalysis of famotidine and solifenacin using TiO_2, IPCAs and AC.
- If ultrasonication impregnation of Aqua 2k AC and P25 TiO_2 is suitable for preparing photocatalytic IPCAs.
- The optimum TiO_2: Aqua 2k ratio for an IPCA.
- The experimental conditions necessary to determine IPCA photocatalysis
- IPCA dark adsorption, with AC and TiO_2 control studies.
- Photodegradation studies of solifenacin under the same conditions as famotidine.

5.2 Baseline photodegradation studies

No studies of IPCA photodegradation of famotidine were found in the surveyed literature however there is one study on the use of anatase and rutile TiO_2 to degrade famotidine "*compacts*"; compressed mixtures of TiO_2 and famotidine (Kakinoki *et al.*, 2004). This study determined that famotidine discoloured slightly under 300 nm to 450 nm light but discoloured significantly in the presence of irradiated TiO_2 at the same wavelengths.

Initial studies of famotidine and solifenacin photodegradation under UV light were undertaken in the absence of catalysts (photolysis) and in the presence of P25 TiO_2 (photocatalysis). Two concentrations of famotidine were chosen: 50 mg/L and 100 mg/L and 45 mg/L and 100 mg/L for solifenacin.

5.2.1 Photolysis studies

Photolysis of famotidine (no catalyst is used) is shown in Figure 5-1. There is a decline of 15 mg/L famotidine over 180 min of illumination at an initial famotidine concentration of 100 mg/L. At an initial concentration of 50 mg/L the famotidine concentration was reduced by 10 mg/L after 180 min of illumination. These results show that degradation of famotidine (photolysis) occurs in the absence of a catalyst.

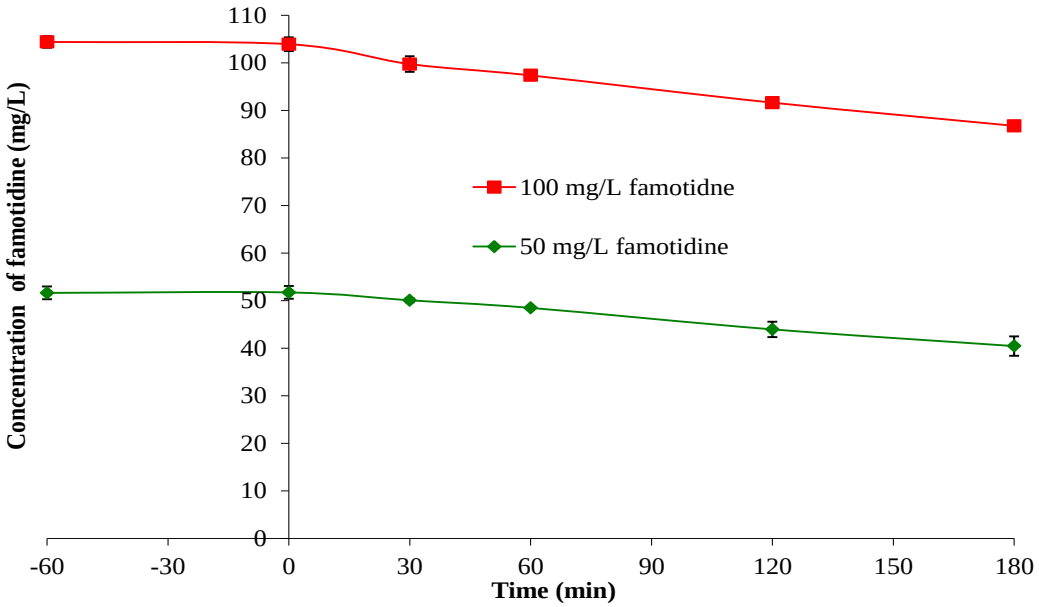

Figure 5-1 Concentration of famotidine vs. time for photolysis studies, t < 0 is the period where famotidine was present in the reactor without illumination. Average results shown (N=2), error bars are standard deviation.

Photolysis studies of solifenacin are shown in Figure 5-2. Solifenacin photolysis is not evident at C_i = 50 mg/L or C_i = 100 mg/L. This indicates that no solifenacin photodegradation occurs in the absence of a photocatalyst.

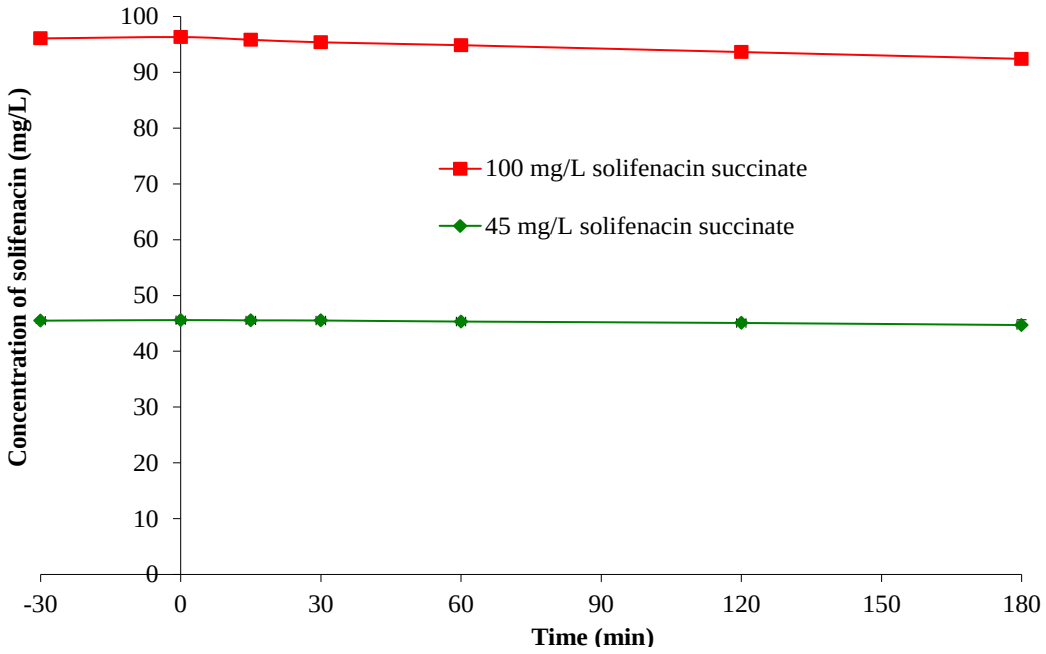

Figure 5-2 Concentration of solifenacin vs. time for photolysis studies, When t < 0 the solifenacin was in the reactor without illumination. Average q(exp) results shown (N=2), error bars are standard deviation.

5.2.2 Photocatalysis studies

5.2.2.1 Photocatalysis catalyst concentration optimisation

For photocatalysis studies it was necessary for the catalyst concentration in solution to be optimised to achieve optimum photocatalysis in solution. The effect of different catalysts concentrations of P25 TiO_2 on the photocatalytic degradation of the 100 mg/L famotidine solution in the borosilicate glass photoreactor used for suspended TiO_2 and IPCA studies is shown in Figure 5-3.

All studies using P25 demonstrate removal of famotidine compared to photolysis. There was no notable difference in famotidine removal for the TiO_2 concentration of 0.2 g/L, 0.3 g/L and 0.4 g/L; however the 0.5 g/L TiO_2 concentration had a slightly higher removal rate. Overall these results are in accordance with previous work (Murphy, 2009) which demonstrated that 0.4 g/L TiO_2 was the optimum catalyst concentration (in the range of 0.1 g/L and 0.6 g/L) at the 0.083 mM (28 mg/L) famotidine concentration investigated.

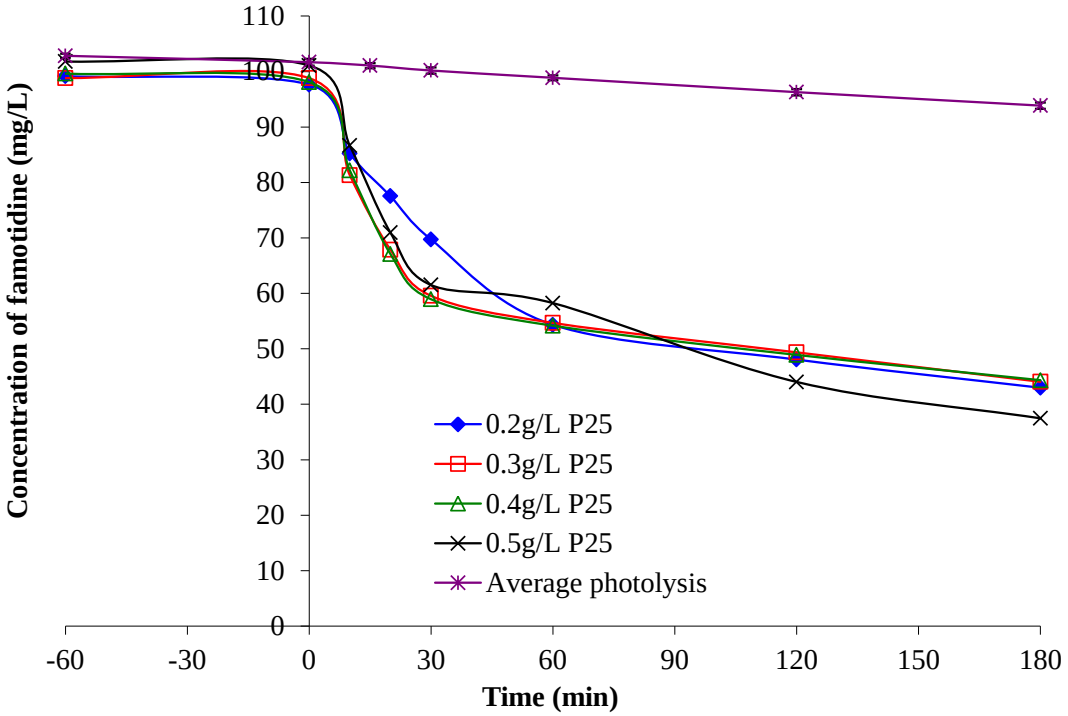

Figure 5-3 Concentration of famotidine vs. time for different P25 catalyst concentrations and photolysis control.

5.2.2.2 Photocatalysis studies for famotidine and solifenacin

The photocatalytic degradation of famotidine by 0.4 g/L TiO_2 at initial concentrations of 50 mg/L and 100 mg/L are shown in Figure 5-4. The shape of each graph is very similar; a fast initial decline in the first 30min of illumination and a slower but steady decline from 30 min onwards. The mass of famotidine removed at both concentrations, after 180 min of irradiation was very similar: 55 mg at C_i = 100 mg/L and 50 mg at C_i = 50 mg/L.

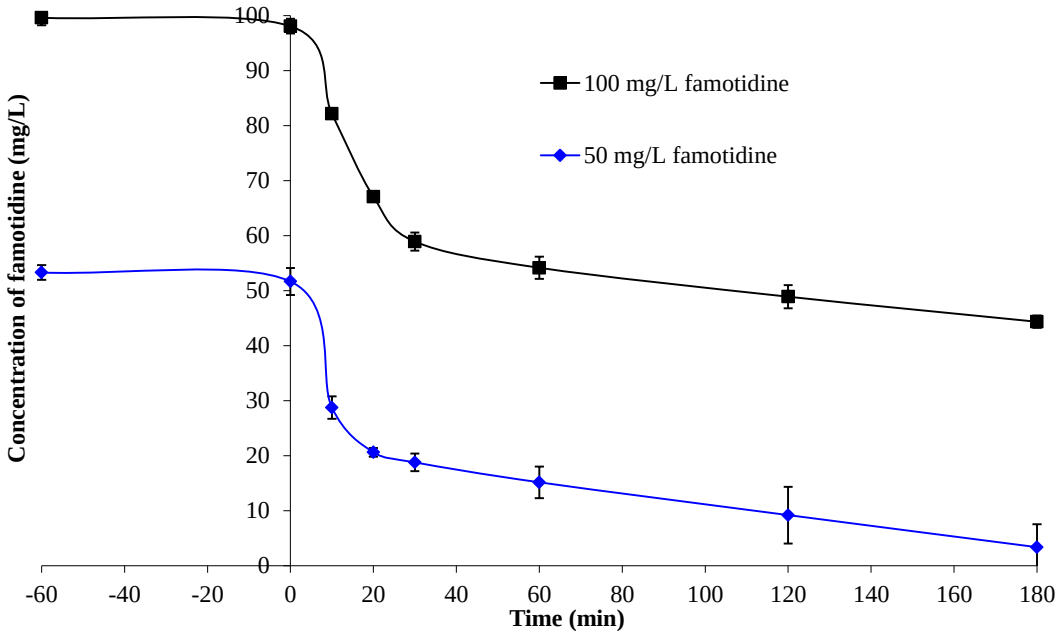

Figure 5-4 Concentration of famotidine vs. time for 0.4g/L P25 photocatalysis studies, t < 0 is the period where famotidine was present in the reactor without illumination. Average q(exp) results shown (N=3), error bars are standard deviation.

The photocatalytic degradation of solifenacin by 0.4 g/L P25 at initial concentrations of 50 mg/L and 100 mg/L are shown in Figure 5-5. The shape of each graph is very similar; a fast initial decline in the first 20min of illumination and a slower but steady decline after that. The mass of solifenacin removed was 24 mg at C_i = 100 mg/L and 30 mg at C_i = 45 mg/L.

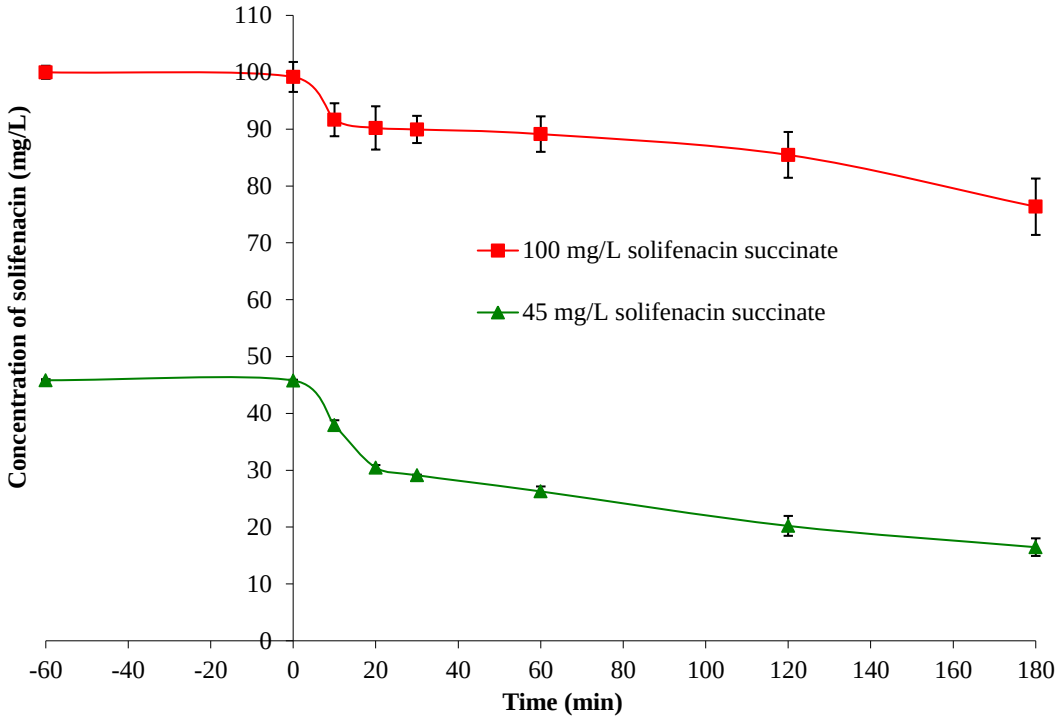

Figure 5-5 Concentration of solifenacin vs. time for 0.4g/L P25 TiO_2 photocatalysis studies, t < 0 is the period where solifenacin was present in the reactor without illumination. Average q(exp) results shown (N=3), error bars are standard deviation.

5.3 Initial IPCA photodegradation studies

These studies used catalyst concentrations of 0.4 g/L of IPCA, the same catalyst concentrations as TiO_2 studies. TiO_2 loadings used to prepare the IPCAs varied from 1:10 to 1:100 (Figure 5-6). A dark adsorption phase of 15 min was included however adsorption equilibrium would take significantly longer (see Section 4.3.1.1). The IPCAs demonstrated limited famotidine removal during the dark adsorption stage while they displayed moderate famotidine removal during the photodegradation stage that exceeded photolysis. The increasing TiO_2 content of the IPCAs had no discernible effect on the photodegradation ability of the IPCA. It was found that TiO_2 loadings above 1:10 demonstrated considerable leaching of TiO_2 particles into solution (Figure 5-7) making it impossible to determine if photodegradation was caused by the IPCA or the free TiO_2 particles in solution. The IPCA concentration in subsequent studies was increased from 0.4 g/L to 1.5 g/L in line with other published IPCA studies (Ao *et al.*, 2008a) to increase photocatalysis.

This new IPCA concentration was shown to be the most effective catalyst concentration for active pharmaceutical ingredient degradation in our group (Basha *et al.*, 2011), thus the study of different IPCA concentrations was not undertaken. Subsequent studies used IPCAs with lower percentage TiO_2 loadings (in the range of 1:100 to 1:2) to limit TiO_2 leaching into solution.

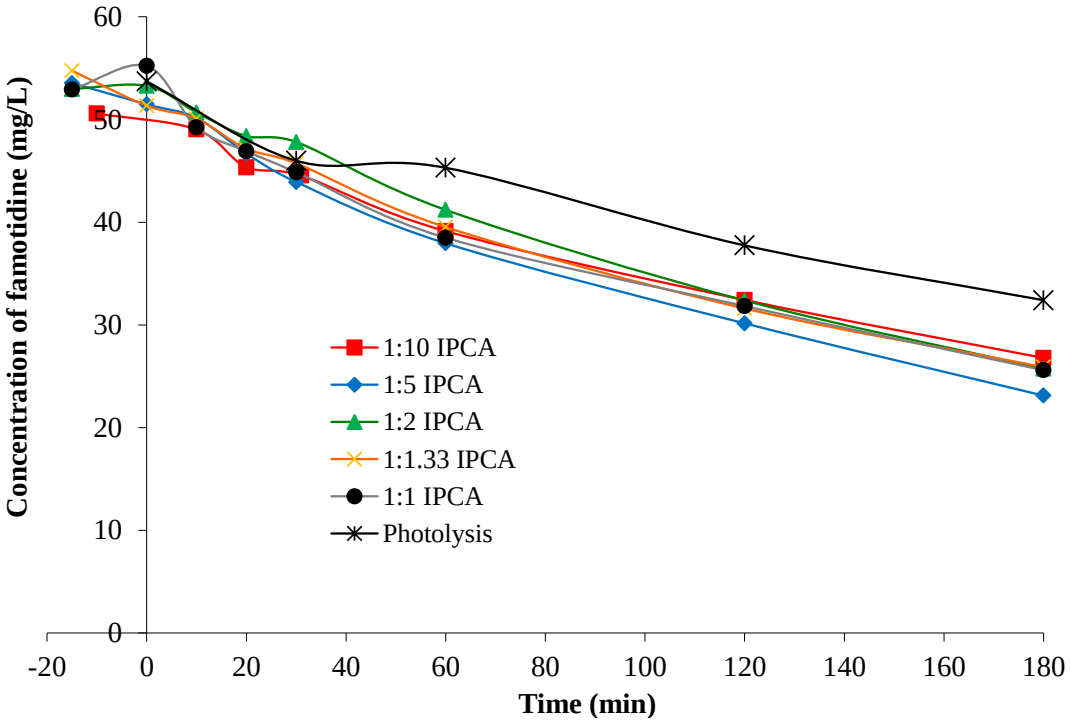

Figure 5-6 Famotidine concentration vs. time of IPCAs prepared by ultrasonication using Aqua 2k with TiO_2 loadings from 1:10 to 1:1. Catalyst concentration 0.4 g/L IPCA. t = -15 to 0 is the dark adsorption phase.

Figure 5-7 1L photoreactor after photodegradation using 1:1 IPCA, loose TiO_2 is visible in solution as a grey cloud. A pH probe is also present in the solution.

The higher catalyst concentration in the photoreactor caused an increase in famotidine sorption during the dark adsorption stage (Figure 5-8) compared to the 0.4 g/L catalyst concentration (Figure 5-6). There was also a more pronounced difference in photodegradation ability in IPCAs prepared with different TiO_2 contents.

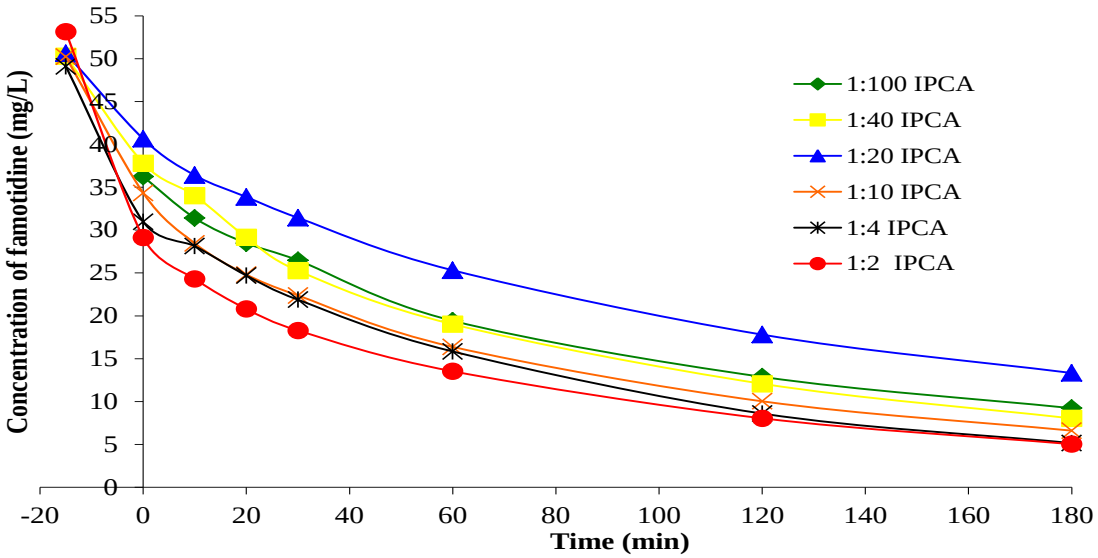

Figure 5-8 Famotidine concentration vs. time of IPCAs prepared by ultrasonication using Aqua 2k with TiO_2 loadings ranging from 1:2 to 1:100. t = -15 to 0 is the dark adsorption phase.

The concentration of famotidine at t = 0 is different for each IPCA. It is necessary to use a kinetic analysis to overcome this limitation. The degradation curves of famotidine exhibit a mono-exponential trend, suggesting that a pseudo-first order reaction model can be applied to describe the kinetic behaviour (Aruldoss *et al.*, 2011, Li *et al.*, 2008b, Yoon et al., 2012, Zhang *et al.*, 2011b). For IPCAs photocatalysis it is necessary for the substrate to adsorb onto the IPCA. A low substrate concentration will have a low adsorption rate which lowers the photodegradation rate. Therefore the initial concentration of famotidine affects the degradation rate, i.e. the kinetic rate constant decreases with decreasing concentration (da Silva and Faria, 2003). Pseudo-first order kinetics with respect to famotidine concentration (C) in solution may be expressed as:

$$-\frac{dC}{dt} = k_{app} C = r \tag{33}$$

Integration of the Eq. 33 leads to following equation.

$$In\left(\frac{C_0}{C}\right) = k_{app} t \tag{34}$$

where, k_{app} is the apparent pseudo-first order rate constant and is affected by famotidine concentration, C_0 is the initial concentration in the bulk solution after dark adsorption, r is reaction rate and t is the reaction time, with the same restriction of $C = C_0$ at t = 0. The values of k_{app} were obtained directly from the regression analysis of the of the plot of Eq. 34 (a plot of $\ln(C_0/C)$ vs. t) for all experiments.

k_{app} values (Table 5-1) for the photodegradation performance of the IPCAs were in the order 1:2 > 1:4 > 1:10 > 1:40 > 1:100 > 1:20. Free TiO_2 particles were present in the 1:4 and 1:2 IPCAs which may be responsible for their higher photodegradation performance. Consequently subsequent studies of IPCAs used P25 loading ratios no greater than 1:10 and additional washing of the IPCAs during and after synthesis to prevent leaching.

Table 5-1 k_{app} values for photodegradation of famotidine using 1:100-1:2 IPCAs.

IPCA type	C_0 (mg/L)	Pseudo-first-order model	
		k_{app} (min^{-1})	Correlation coefficient, R^2
1:100 IPCA	36.25	0.0082	0.9698
1:40 IPCA	37.81	0.0092	0.9728
1:20 IPCA	40.65	0.0066	0.9796
1:10 IPCA	34.33	0.0098	0.9616
1:4 IPCA	30.98	0.0103	0.9961
1:2 IPCA	29.13	0.0104	0.9663

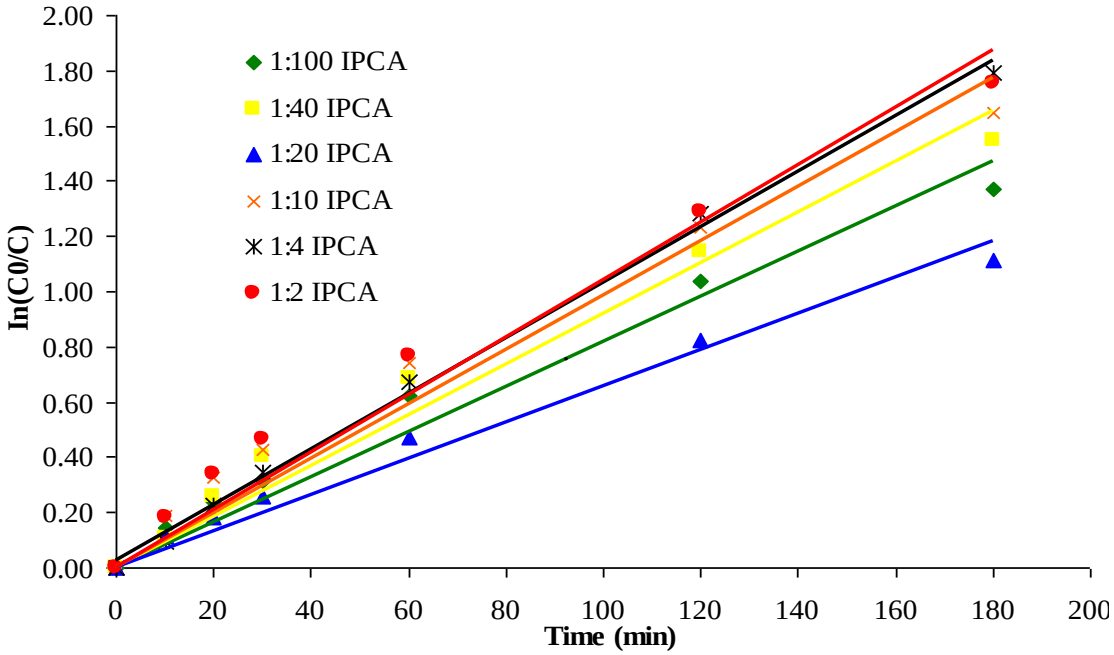

Figure 5-9 Pseudo reaction rates vs. time of IPCAs prepared by ultrasonication using Aqua 2k with P25 TiO_2 loadings from 1:100 to 1:2.

The use of the higher catalyst concentration (1.5 g IPCA/L) demonstrated a more pronounced removal (Figure 5-10) of famotidine, however, the adsorption in the dark adsorption stage is more pronounced with the 1.5 g/L catalyst concentration compared to the 0.4 g/L catalyst concentration. Future studies used a one hour dark adsorption time used in published studies (Liu *et al.*, 2009).

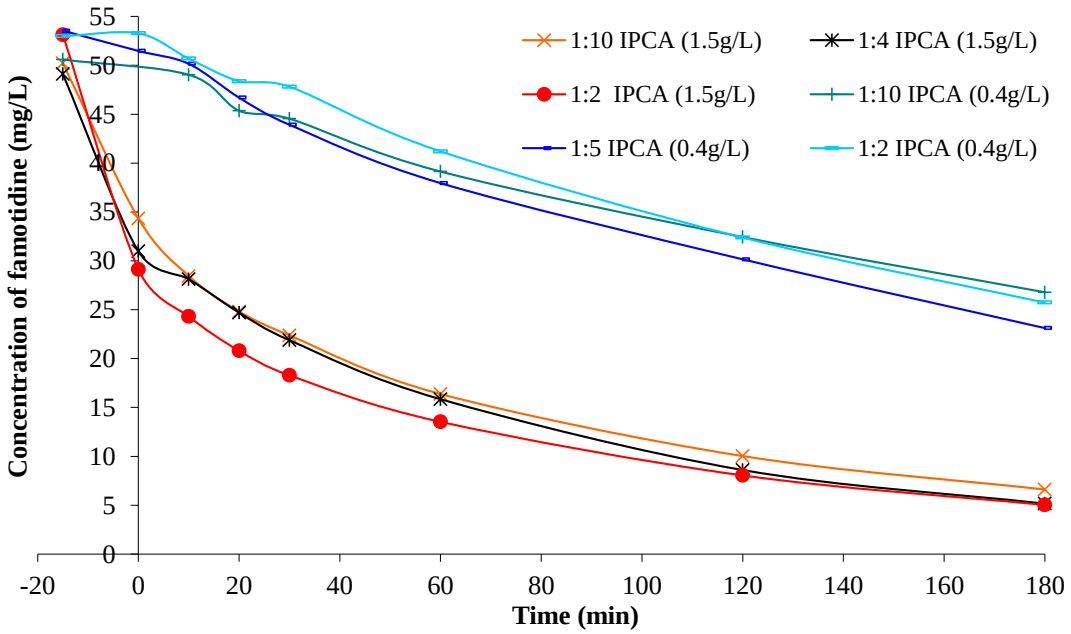

Figure 5-10 Famotidine concentration vs. time of IPCAs with the similar TiO_2 concentrations at 0.4 g/L and 1.5 g/L catalyst concentrations.

5.4 Optimisation of IPCA photodegradation of famotidine

The 1.5 g/L catalyst concentration from previous studies was used and the dark adsorption phase was increased from 15 min to 60 min to help differentiate adsorption from photocatalysis. The stirring rate and illumination time remained the same. The level of removal of famotidine from aqueous solutions by 1:200 to 1:10 IPCAs increased with UV irradiation time after dark adsorption (Figure 5-11, Figure 5-12). Famotidine reduction in photolysis studies was 39 % after 180 min of illumination and was lower than the removal rate of all of the IPCAs and the TiO_2 control. The observed improvement in famotidine removal relative to photolysis and the dark adsorption control was attributed to photocatalytic activity of the TiO_2 particles on the AC. IPCAs containing 10 % TiO_2 (1:10 IPCA) reduced the famotidine concentration faster than the other IPCAs. The relationship between the famotidine degradation rate (in terms of k_{app} values) by the IPCAs follows the sequence: 1:10 > 1:13 > 1:20 > 1:40 > 1:100 > 1:200 > 1:10 (without illumination).

The effect of heat treatment (calcination) on IPCA performance was investigated. Heat treated IPCAs were prepared using the method detailed in Section 2.2.1.2. The removal rates for heat treated 1:10 IPCAs decreased with increasing

calcination temperature in the order: 200°C > 500°C > 600°C > 700°C (Figure 5-13, Table 5-2). The percentage of the famotidine degraded by the 1:10 (non-heat treated) IPCA under UV irradiation was 77 % after 180 min while the 1:10 IPCA heat treated at 200°C degraded 73 % of famotidine. These similar values indicate that heat treatment at 200°C has no significant effect on the catalyst morphology or effectiveness. The reduction in removal efficiency with increasing calcination temperature is shown in Figure 5-13. In published studies it is assumed that both the crystal structure and porosity of the composite catalyst have an influence on its photocatalytic properties (Sun *et al.*, 2009, Sun *et al.*, 2006) i.e. the anatase to rutile structure has changed and this is the cause of the lower photoactivity. The XRD results in Section 6.4 are inconclusive regarding phase change. Further investigation of heat treatment was not undertaken as it was not a promising line of investigation.

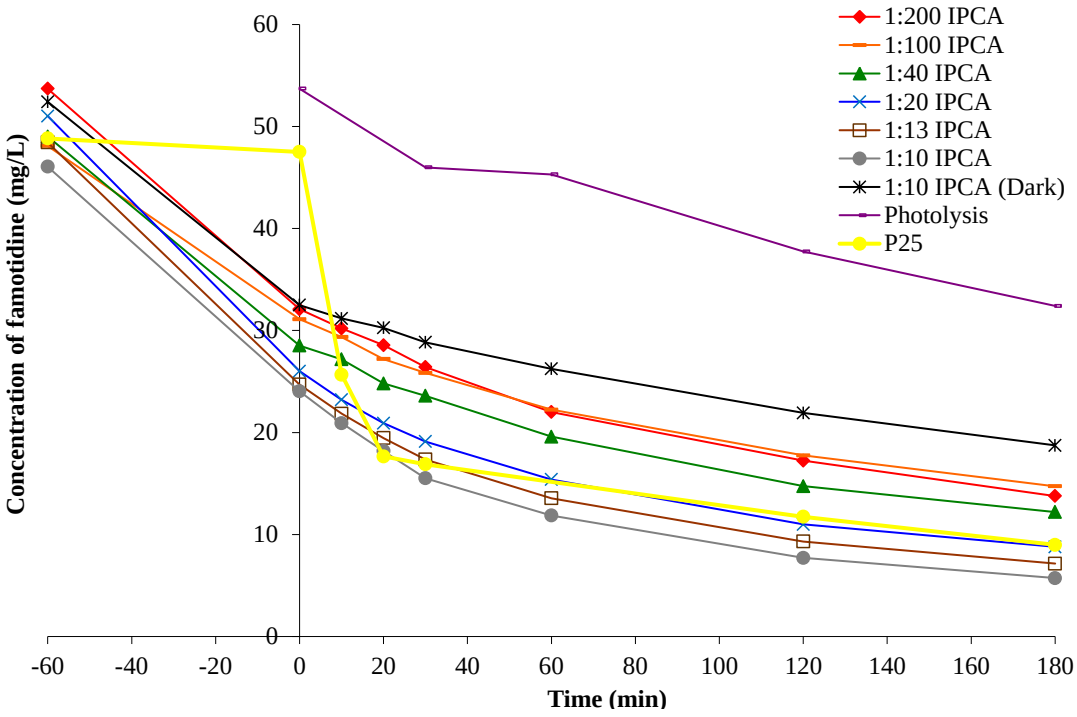

Figure 5-11 Famotidine concentration vs. time for 1:200 IPCA to 1:10 IPCAs including TiO_2, dark adsorption and photolysis controls.

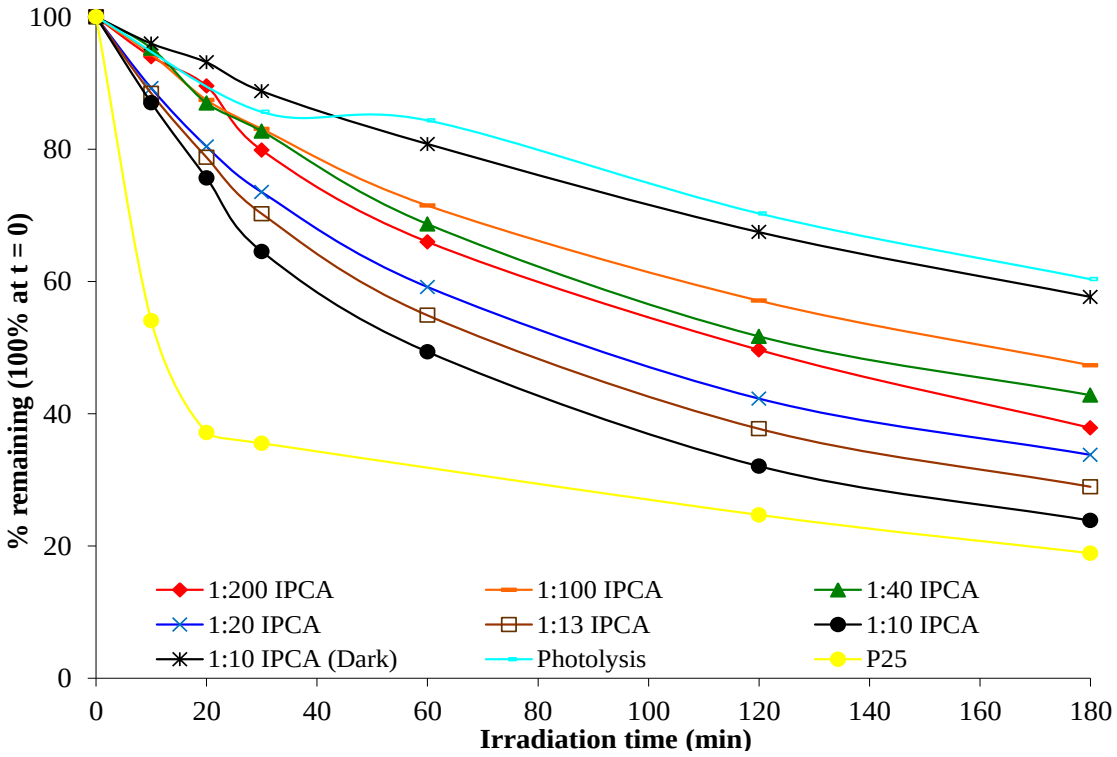

Figure 5-12 Famotidine (%) remaining in solution (100 % at t = 0) using various IPCAs. Non illuminated 1:10 IPCA, TiO_2 and photolysis controls are also shown.

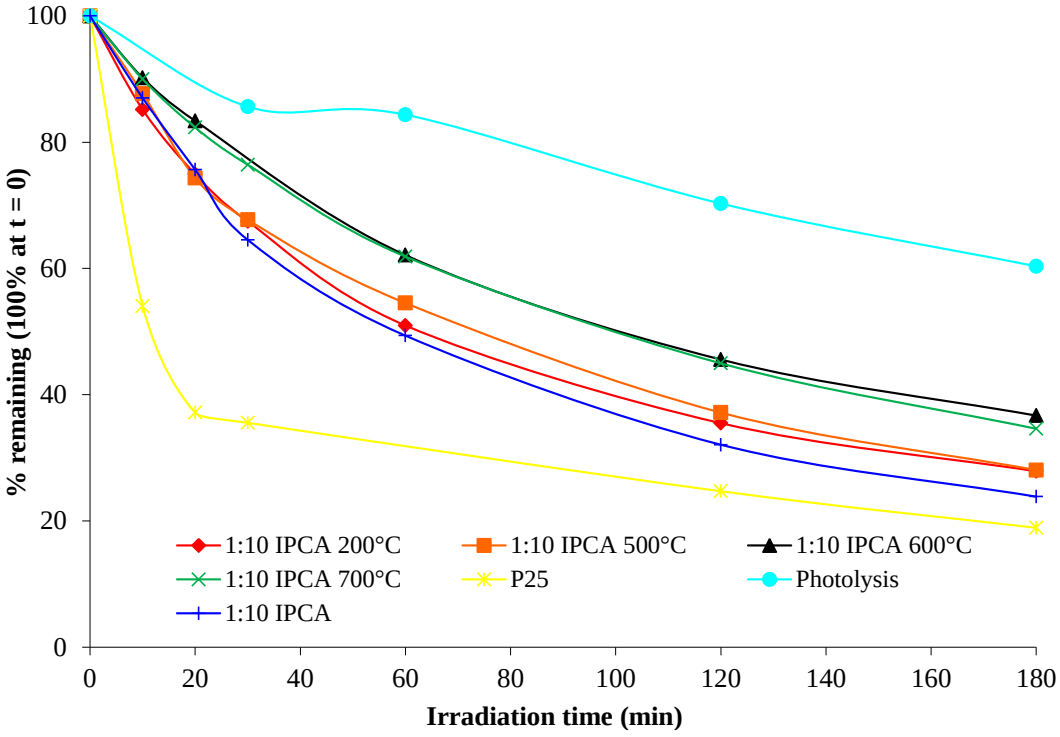

Figure 5-13 Famotidine (%) remaining in solution (100 % at t = 0) using heat treated 1:10 IPCAs. P25 and photolysis controls are included.

The degradation curves of famotidine continue to exhibit a mono-exponential trend and were modelled (Figure 5-14, Figure 5-15) using the same pseudo-first order reaction model as previous studies.

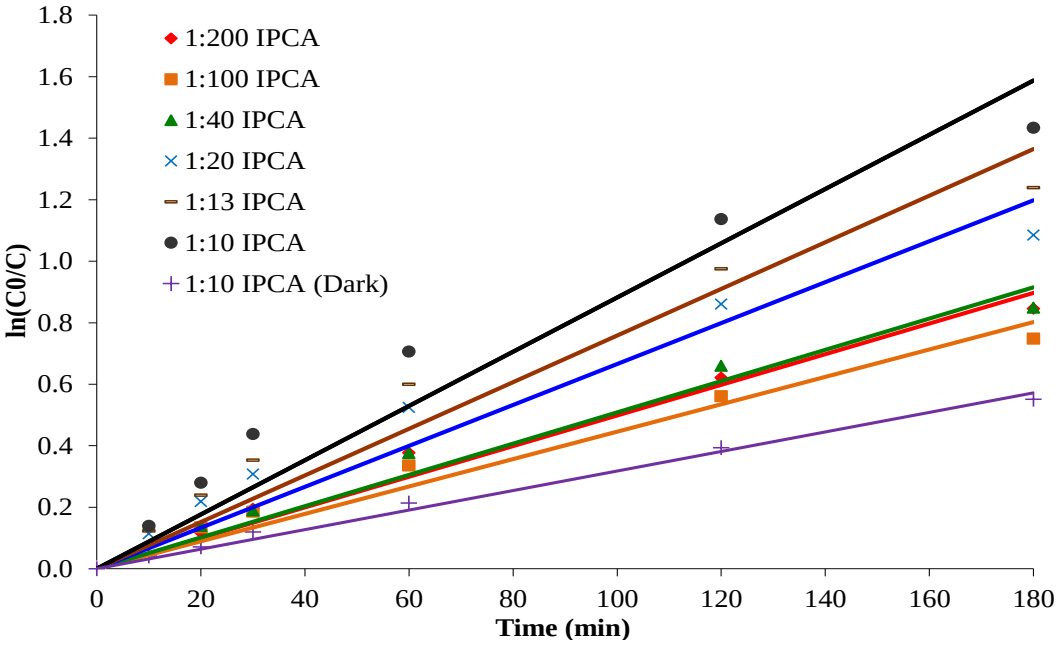

Figure 5-14 Kinetics of famotidine photodegradation (linear transform $\ln(C_0/C)$ vs. t) in photocatalytic experiments using various IPCAs.

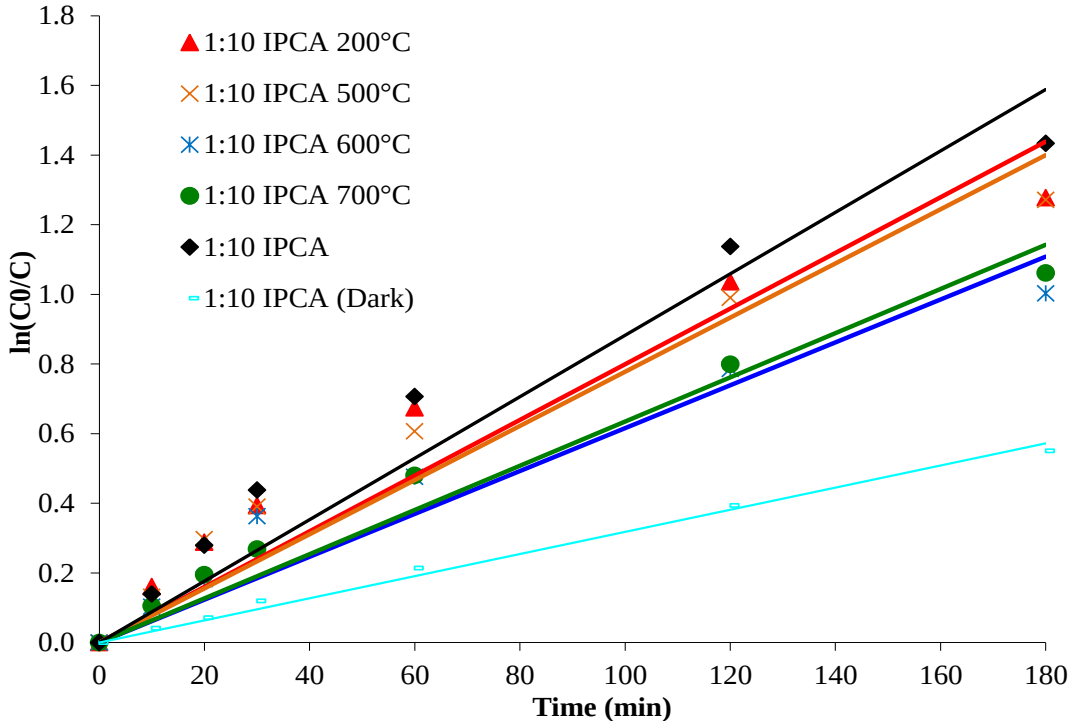

Figure 5-15 Kinetics of famotidine photodegradation (linear transform $\ln(C_0/C)$ vs. t) in photocatalytic experiments using heat treated IPCAs.

Table 5-2 k_{app} values for photodegradation of famotidine using various IPCAs.

IPCA type	Pseudo first-order model		
	C_0 (mg/L)	k_{app} (min^{-1})	Correlation coefficient, R^2
1:200 IPCA	31	0.0045	0.955
1:100 IPCA	31	0.0047	0.947
1:40 IPCA	29	0.0052	0.968
1:20 IPCA	26	0.007	0.915
1:13 IPCA	25	0.0077	0.940
1:10 IPCA	25	0.0091	0.915
1:10 IPCA heat treated at 200°C	26	0.008	0.957
1:10 IPCA heat treated at 500°C	36	0.0078	0.932
1:10 IPCA heat treated at 600°C	29	0.0062	0.924
1:10 IPCA heat treated at 700°C	31	0.0063	0.967

Both the k_{app} values and the photodegradation graphs (Table 5-2 and Figure 5-12) demonstrate that the 1:10 IPCA is the best performing IPCA and that the relative position of each IPCAs in terms of photoactivity (for adsorption performance, see Chapter 4) also corresponds to its TiO_2 loading e.g. the 1:100 and 1:200 IPCA have the lowest TiO_2 loading and photoactivity while the 1:10 IPCA has the opposite. This is in contrast to published studies that demonstrate an optimum TiO_2 loading above which the photocatalytic ability decreases. This is possibly due to the leaching of TiO_2 at higher loading levels into solution because of the preparation method employed in this study. This makes it impossible to identify the optimum loading as the extra photoactivity could also be interpreted as the effect of free TiO_2. The 1:10 IPCA was also found to be the most effective IPCA in other studies in this research group on amoxicillin and indomethacin (Basha *et al.*, 2011, Basha *et al.*, 2010).

5.5 Photodegradation studies of famotidine using 1:10 IPCA and AC control

After the optimum P25: AC ratio was determined and reactor conditions enhanced to allow photodegradation using IPCAs to be observed, more detailed famotidine studies were undertaken. These studies used the 1:10 IPCAs with a 1.5 g/L catalyst concentration (Sections 5.4). The 1:10 IPCA used in this section was prepared using the improved IPCA preparation method (Section 2.2.1.3). To ensure a more pronounced difference between the dark adsorption stage and illuminated stage the dark adsorption stage was extended to 4 h followed by 3 h of photodegradation and the initial concentration before dark adsorption was increased to 100 mg/L in line with the highest concentration used in photolysis studies to ensure that there was a large concentration of famotidine available for degradation after dark adsorption. These conditions were used in an attempt to ensure that the majority of famotidine adsorption would occur before illumination to ensure that it could be separated from photocatalysis. Compared to the previous studies more adsorption will have occurred during the dark phase compared to the photodegradation phase so the results would show more pronounced photodegradation. These results are shown in Figure 5-16.

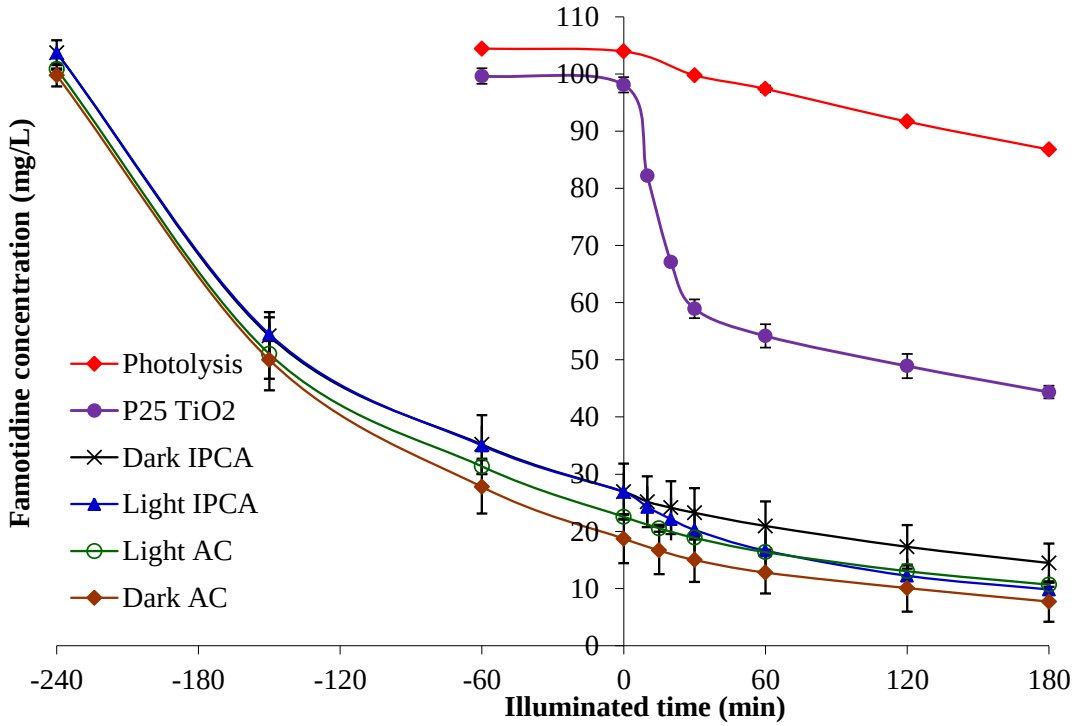

Figure 5-16 Famotidine concentration vs. time for 1:10 IPCAs, AC, P25 and photolysis studies. "Light" studies were illuminated; "Dark" studies were not. Average results shown (N=3), error bars are standard deviation.

The TiO_2 and photolysis controls are the same as those discussed in Section 5.2. The different adsorption rates for each study leaves a different concentration at t = 0 for each adsorbent (light and dark IPCAs and ACs). No discernible pattern can be detected. The dark AC studies remove the most famotidine, while the dark IPCA studies removed the least famotidine of all the adsorbents. When the results are expressed as percentage removed from t = 0 (Figure 5-17) the illuminated IPCA removed the most famotidine, although the dark AC removed the second largest amount of famotidine. When error bars are included and the effect of photolysis is considered there is negligible difference between the illuminated and non-illuminated IPCAs.

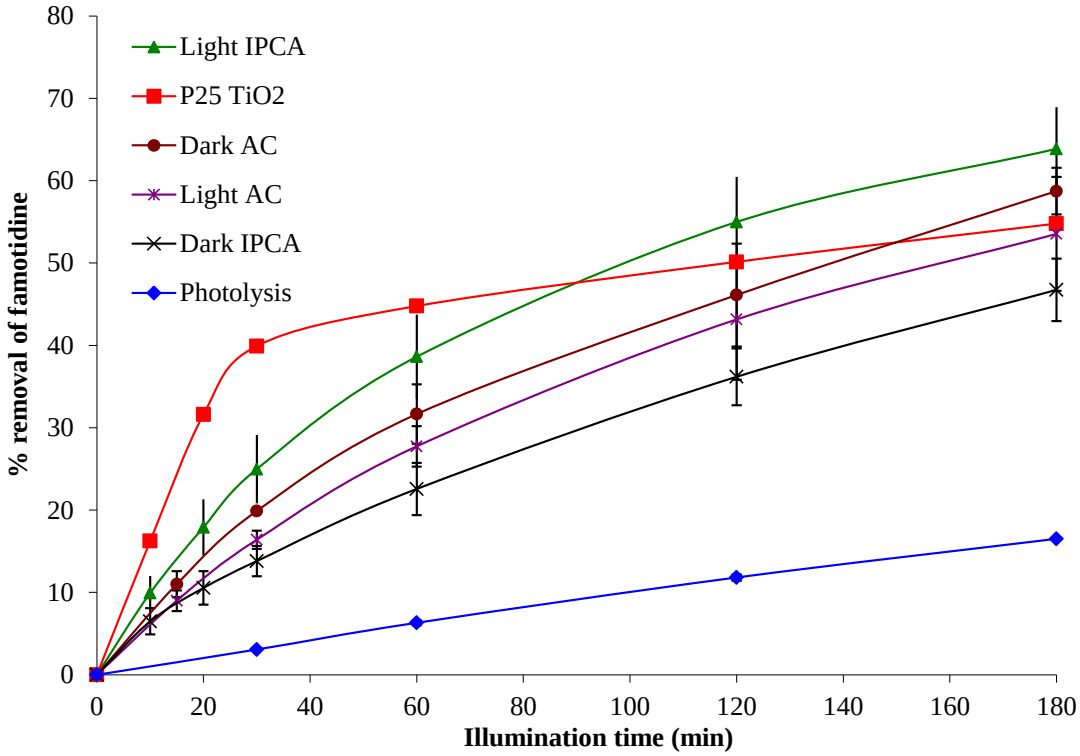

Figure 5-17 Average % remaining of famotidine concentration vs. time for photolysis, P25, illuminated and not illuminated IPCAs and ACs. Average results shown (N=3), error bars are standard deviation.

Further evidence of the lack of photodegradation of famotidine by the IPCA is provided by FTIR. It was used to examine three separate 1:10 IPCAs; one that was unused, another that photodegraded a 50 mg/L famotidine solution and a final sample used for famotidine adsorption in the dark.

The FTIR spectra of the 1:10 IPCA after the adsorption of famotidine in the dark and after photodegradation along with FTIR spectrum of virgin 1:10 IPCA catalyst are shown in Figure 5-18 (a–c). Compared to the raw IPCA (Figure 5-18 (a)) new absorption bands such as 3391, 2918, 1537 and 1089cm^{-1} which appeared on the absorption spectra of the IPCA after famotidine adsorption (Figure 5-18 (b)) can be assigned to O–H stretching, C–H stretch of alkane, N–O stretch of nitro, respectively. Both alcohol and nitro groups were involved in the famotidine adsorption (Figure 5-18 (b)). In general, the famotidine molecule consists of guanidine, thiazole, thioether and sulfamoyl parts (Roeges, 1994). It exhibits strong absorptions in the region 3,550–3,250cm^{-1} as well as 1,500–1,650 and 1,135–1,360cm^{-1} due to NH_2 and SO_2 functional groups (Saepurahman *et al.*, 2010). After irradiation of the famotidine loaded 1:10 IPCA, peaks in the 1,500–1,650 and 1,135–1,360cm^{-1} range decreased

(Figure 5-18 (c)) suggesting that the adsorbed famotidine did not undergo significant – if any - photodegradation. If these peaks were absent then it would indicate that the famotidine was photodegraded.

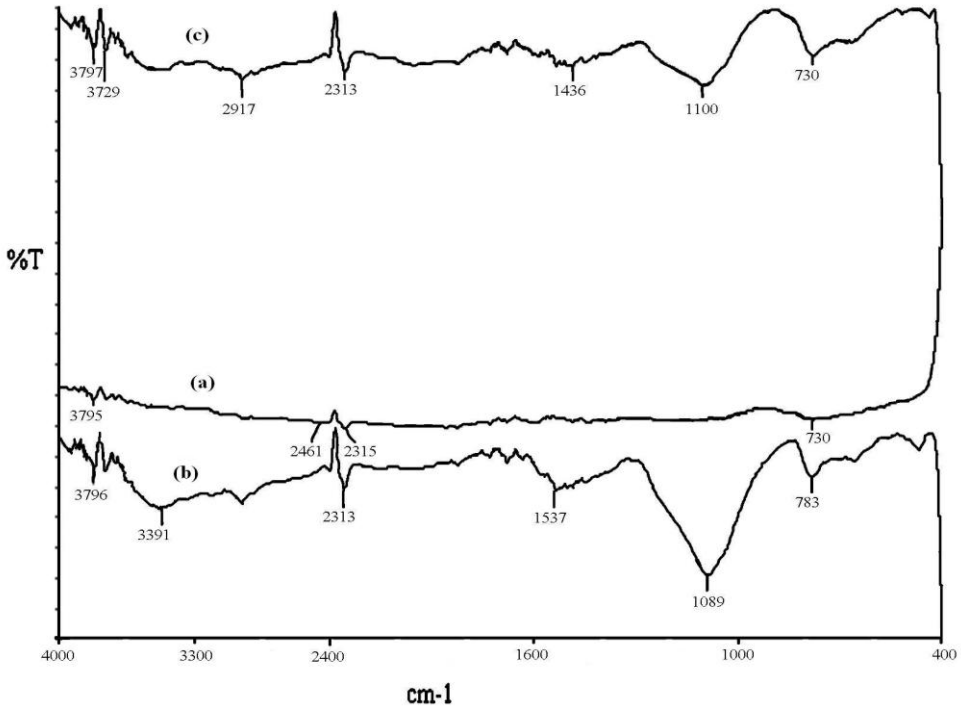

Figure 5-18 FTIR spectra of (a) virgin 1:10 IPCA, (b) 1:10 IPCA after famotidine adsorption and (c) 1:10 IPCA after photodegradation of famotidine.

The limited removal of famotidine at the 50 mg/L famotidine concentration, the negligible removal of famotidine at the 100 mg/L concentration and the FTIR results indicate that IPCAs have a limited ability to photodegrade famotidine. The photodegradation potential of the IPCA for famotidine removal is small compared to its adsorption ability. In conclusion IPCAs are not effective for famotidine photodegradation.

5.6 Photodegradation studies of solifenacin using 1:10 IPCA and AC control

The poor performance of the IPCAs for famotidine degradation casts doubt on the viability of IPCAs for degrading pharmaceuticals. In similar studies using IPCAs (O'Dwyer. 2011) to photodegrade chlorinated pesticides: 2, 4-Dichlorophenoxyacetic acid (2,4-D) and 2-methyl-4-chlorophenoxyacetic acid (MCPA), the illuminated IPCAs removed the same amount of 2,4-D and MCPA as the dark adsorption control. This demonstrates that IPCAs are not effective for chlorinated pesticide removal. They demonstrated no synergy compared to TiO_2 and AC adsorption in the dark. IPCA studies on amoxicillin (antibiotic) and indomethacin (a non-steroidal anti-inflammatory drug) were more successful (Basha *et al.*, 2011, Basha *et al.*, 2010). It was decided to investigate the adsorption and photocatalytic performance of the IPCAs on a different substrate. The pharmaceutical solifenacin succinate was investigated to provide a contrast to famotidine. The IPCAs that were illuminated were labelled "light IPCA" while the IPCAs that were not illuminated were called "dark IPCA". The same naming scheme was also applied to the AC controls. The studies using no catalyst were called "photolysis" and the studies using P25 were labelled "TiO_2".

The 1:10 IPCA used in this section was prepared using the improved IPCA prepation method (Section 2.2.1.3). Initial studies used 40 - 45 mg/L solifenacin in deionised water solutions and are shown in Figure 5-19. Solifenacin removal followed the order light IPCA > dark IPCA > TiO_2 > photolysis. Photolysis had a negligible effect on the solifenacin concentration reducing the concentration by 1 mg/L or 2 %. TiO_2 photocatalysis using P25 reduced the solifenacin concentration by 30 mg/L or 65 % of the solifenacin in solution. The light IPCA was illuminated from t = 0 - 180. It adsorbed and degraded 33 mg/L or 75 % of the solifenacin. Compared to TiO_2 the rate of degradation was identical to the illuminated IPCA from 60 min onwards indicating that the IPCA has robust photocatalytic activity. The dark IPCA removed 20 mg/L of the solifenacin in solution or 50 % and the absence of illuminated means it is due to adsorption. The rate of adsorption moderated during the contact time indicating saturation of the IPCA. A comparison between the light and dark IPCA illustrates the effect of photocatalysis as the illumination dramatically increases the solifenacin

removal rate. There is a large difference between the adsorption rate between the light and dark IPCA during the dark adsorption phase which manifests itself as an average 22 % difference between the initial concentration at t = 0. While the dark IPCAs give consistent results there is a significant difference between the two illuminated IPCA studies. The reproducibility of the light IPCAs are poor as their SD ranges between 2.4 and 4.7 compared to an SD between 0.1 and 1.5 for the dark IPCAs. The poor reproducibility of the light IPCAs is due to different initial concentrations at t = 0 caused by the different adsorption ability of the IPCAs in the t = -180 to 0 stage of the study. Subsequent studies used a higher concentration of solifenacin to confirm the IPCA synergy and to study the photocatalytic and photolysis reactions at higher concentrations.

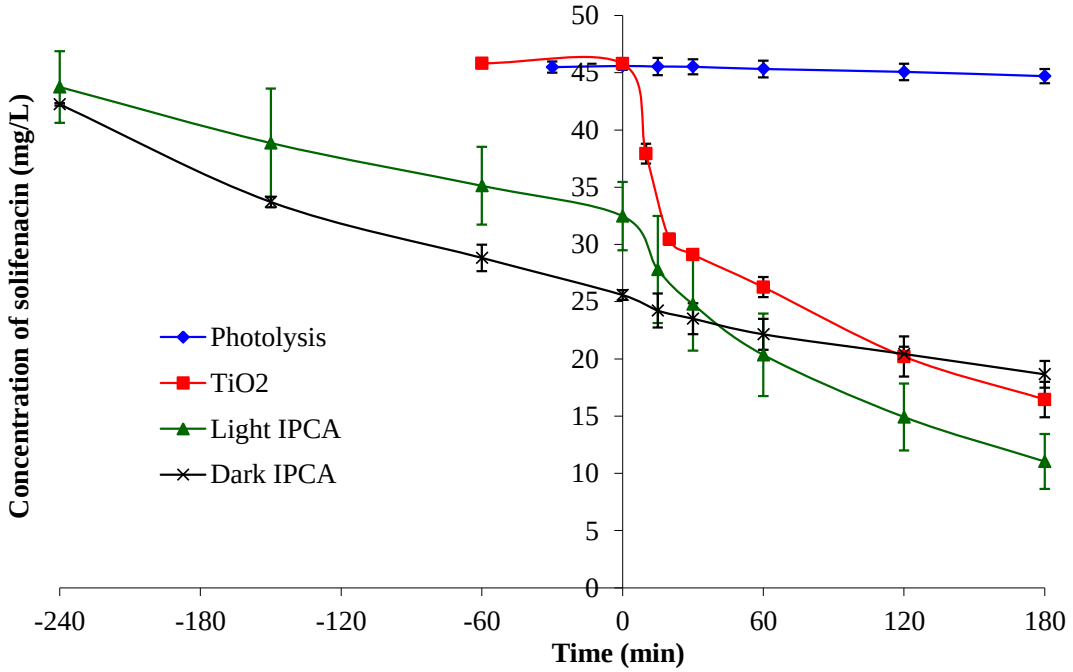

Figure 5-19 Solifenacin concentration vs. time for photolysis, P25 photocatalysts and IPCAs (average results shown). Average results shown (N=2), error bars are standard deviation.

To provide a further comparison with famotidine subsequent studies used a 100 mg/L initial concentration. Both pharmaceuticals have different molecular weights therefore the comparisons can only be used after molar conversion. It is still useful to use a comparison of solifenacin at a "moderate" and then "high" concentration. At the 100 mg/L initial concentration (Figure 5-20) photolysis was

negligible the same as at 40 mg/L, reducing the average solifenacin concentration by 4 mg/L or less than 5 %. Photocatalysis using P25 reduced the solifenacin concentration by 24 mg/L on average or 25 % of the solifenacin in solution. P25 TiO_2 photocatalysis demonstrated a lower % reduction in solifenacin concentration (25 % vs. 65 %) compared to the 40 mg/L initial concentration. Like the 40 mg/L studies the light IPCA shows a considerable increase in solifenacin degradation rates during illumination degrading 43 % of the solifenacin in solution at t = 0 compared to 11 % that was adsorbed by the dark IPCA. The dark IPCA adsorption rate decreases with time and its overall removal rate was lower than the light IPCA due to the absence of photocatalysis.

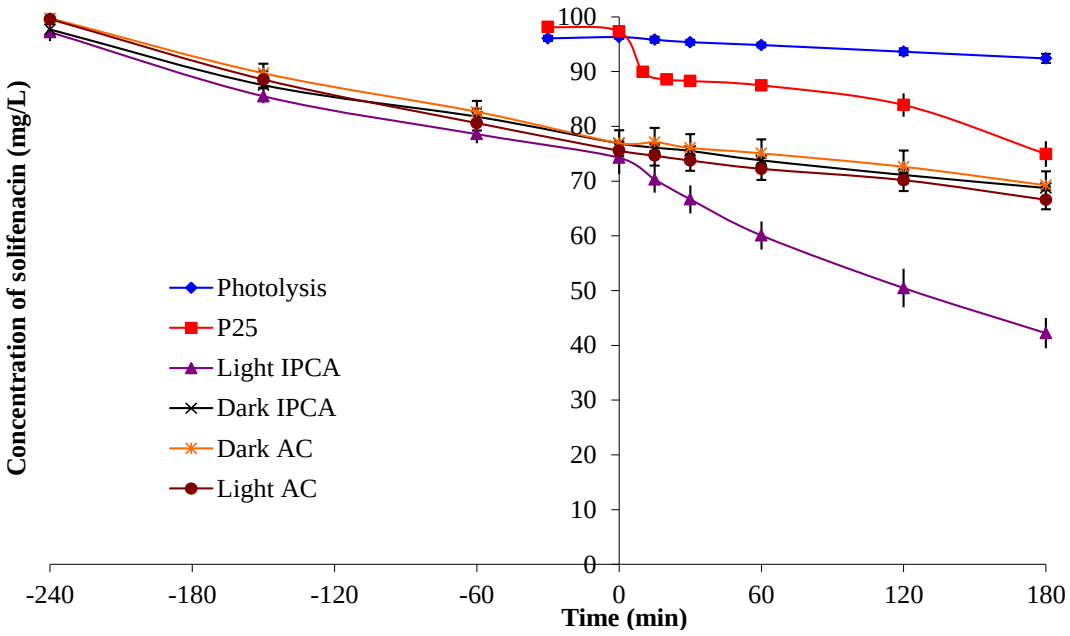

Figure 5-20 Solifenacin concentration vs. time for photolysis, P25 photocatalysts, IPCAs and ACs (average results shown). Average results shown (N=3), error bars are standard deviation.

The light IPCA removed 57 % of the solifenacin compared to 30 % removal by the dark IPCA over the 240 min study period. The AC controls demonstrate no photocatalytic ability. When error bars are considered there is no difference between the illuminated AC, the AC control in the dark and the dark IPCA, as they removed 33 %, 31 % and 30 % of the solifenacin respectively over 420 min. This combined with the negligible photolysis indicates that illuminated IPCAs have considerable synergistic (removal greater than adsorption and photodegradation combined) ability

which cannot be attributed to photolysis plus adsorption as is the case with famotidine studies.

5.7 Conclusions

IPCAs demonstrate the ability to remove famotidine at a faster rate than photolysis at a high catalyst concentration. This confirms that Aqua 2k and P25 can be combined into an IPCA using ultrasonication. In terms of photocatalytic ability and catalyst stability the 1:10 IPCA was determined to be the best IPCA. On investigation with a long (4 h) dark adsorption time famotidine does not demonstrate any convincing photodegradation ability. In contrast, solifenacin photodegradation using IPCAs demonstrates convincing photodegradation ability under the same conditions.

- 1.5 g/L IPCA catalyst concentration is required to achieve high removal of famotidine.
- Removal of famotidine during illumination of the IPCA increases with TiO_2 loading up to a ratio of 1:10.
- IPCAs with TiO_2: AC loadings above 1:10 leach TiO_2 into solution.
- Pseudo first order kinetics can be used to model the famotidine photodegradation reaction at an initial concentration of 50 mg/L.
- Famotidine studies with a 4 h dark adsorption time were unsuccessful as famotidine removal by the illuminated IPCAs was no higher than adsorption by the IPCAs in the dark.
- Solifenacin studies were successful as they demonstrated synergy i.e. the IPCA removed more solifenacin than the AC and TiO_2 combined under illumination.
- The famotidine and solifenacin results represent the realisation of the second project aim: "*The potential for synergy between AC and TiO_2 for the removal of pollutants*".

Chapter 6 Evaluation of Findings

6.1 Introduction

In the reviewed literature in Chapter 1, it is claimed that IPCAs are a robust and effective technology for removing organic pollutants. However, arising from the research for this thesis, it has been found that this is not always the case and synergies between activated carbon and titanium dioxide in the form of an IPCA is not guaranteed. On further evaluation of the literature in this work, many gaps in the research methodologies and experimental conditions reported are used to illustrate that many claimed synergies are flawed. Results from this current work have found synergy in pollutant degradation in the case of solifenacin, but no synergy has been found in the case of famotidine. A possible explanation for this difference is proposed in Section 6.3 arising from the differences in chemical structure of each compound. To test this hypothesis, the degradation of two other pharmaceuticals previously studied within our research group will be compared and contrasted to famotidine and solifenacin with respect to IPCA photodegradation. In summary, this chapter will:

- Critically evaluate the claimed synergy of IPCAs in published literature in the degradation of pollutants (Section 6.2).
- Detail the pharmaceuticals investigated for IPCA synergy and adsorption capacity in this work and in this author's research group (Section 6.3).
- Discuss the contribution of different chemical properties to enhance/inhibit photodegradation and hypothesise as to why synergy is displayed in the degradation of some pharmaceuticals, but not in others (Section 6.4).
- Propose suggestions for future work to determine the mechanisms that enhance/inhibit photocatalytic degradation (Section 6.5).

6.2 Critical assessment of synergy claims in IPCA literature

IPCAs demonstrated synergy (removal greater than adsorption and photodegradation combined) for solifenacin degradation but not famotidine degradation. Famotidine studies demonstrated no removal beyond adsorption and photolysis. This indicates that IPCAs are ineffective for famotidine photodegradation. These famotidine results are in contrast to the majority of the published literature which establishes IPCAs as versatile photocatalysts for organic degradation.

A critical approach was used to re-evaluate IPCA studies included in the literature review and a detailed critique of each study is contained in the "*notes*" column in Appendix A and B. Synergy between the AC and TiO_2 under UV illumination is stated as the key advantage of using IPCAs (Foo and Hameed, 2010a, Khan, 2002, Matos *et al.*, 1998) and warrants more investigation as the evidence used to support claimed synergy is weak or non-existent. In the absence of synergy there is no economic or environmental justification for combining the AC and TiO_2 as they would perform their respective roles as adsorbent and photocatalyst just as efficiently separately.

As it is impossible to review every claim of synergy of TiO_2 and AC (or other adsorbents e.g. zeolite) several of the most cited synergy claims will be discussed. One heavily cited paper that is a proponent of synergy (Matos *et al.*, 1998) used a 50mg: 10mg TiO_2: AC mixture - not a true IPCA as the components are not combined together - denoted as TiO_2+AC to demonstrate synergy for phenol degradation in the mM range (Figure 6-1). Although the graphs legend states μM, the method section in the study refers to the initial concentration in mM. After 30 min of illumination no photolysis was observed. After very rapid adsorption for the first 15 min in contact with the solution the AC and TiO_2+AC displayed no further adsorption. The TiO_2+AC and TiO_2 reduced the substrate concentration during illumination, however TiO_2 on its own displays a higher degradation rate than the TiO_2+AC combination suggesting that the latter has lower photocatalytic performance. The TiO_2+AC mixture reduced the phenol in solution to zero faster due to its lower concentration (at t = 0) after initial dark adsorption. When the degradation curves are linearised and by the outlines it is concluded that the TiO_2 - AC performs better. The lower phenol concentration for the IPCA at time = 0 was not considered in this conclusion.

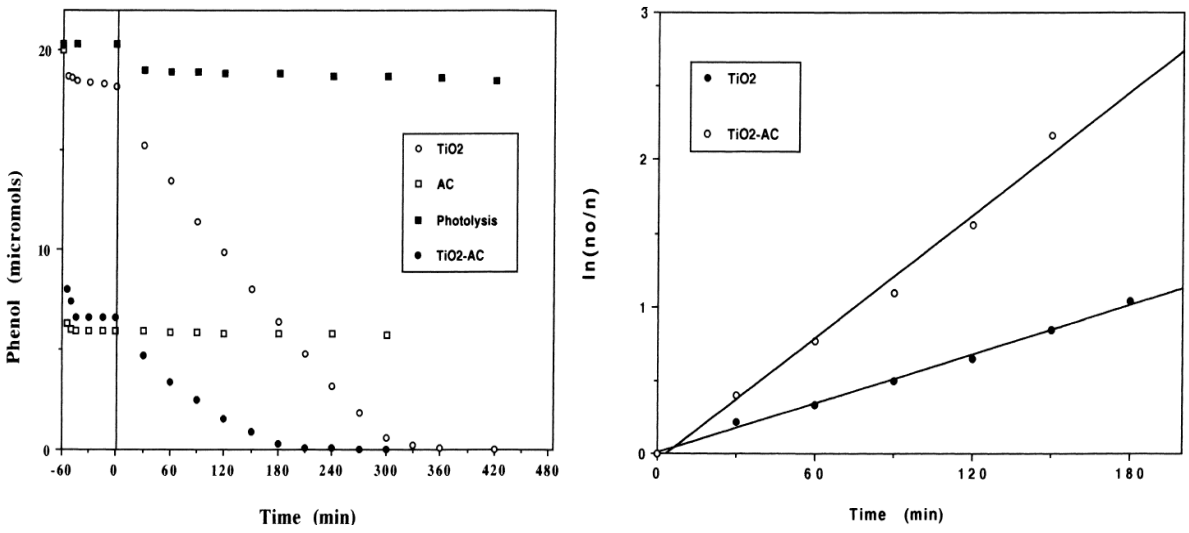

Figure 6-1 "(a) Kinetics of phenol disappearance (b) kinetic curves [sic] of phenol disappearance" (Matos *et al.*, 1998).

AC+TiO_2 mixtures were prepared using a milling technique and ultrasonication and compared to the original mixture described in Figure 6-1. The lower performance of the ultrasonicated mixture could be attributed to the separation of TiO_2 and AC particles, weakening their surface interaction i.e. their synergy (Matos et al. 1998). Changes in adsorption performance and thus a higher initial concentration is a better explanation for the decrease in the apparent rate constant. Discussion of reaction kinetics hides the lack of robust data to support the synergy claim.

It is claimed that the degradation of chemical weapons: soman, VX, and yperite using IPCAs are synergistic (Cojocaru *et al.*, 2009). The degradation of the substrate using IPCAs (1 % – 25 % wt TiO_2 – weight ratios from 1:100 to 1:4 TiO_2 to AC) is greater than unmodified TiO_2 is the only evidence put forward to demonstrate synergy. The lack of an AC and photolysis controls cast doubt on the photodegradation properties of the IPCA. There is N_2 isotherm data in the paper but no empirical data on adsorption so the proposed synergy could be little more than AC adsorption. The N-doped titania prepared for the study does appear to perform better than the unmodified TiO_2 although the N doped TiO_2 was heat treated and the unmodified TiO_2 was prepared using a low temperature method so they are not directly comparable as heat treatment can improve photodegradation performance of a single phase photocatalysis (Fu *et al.*, 2004a, Xu *et al.*, 2008).

In a review titled "*Carbonaceous nanomaterials for the enhancement of TiO_2 photocatalysis*" (Leary and Westwood, 2011) the synergism and photoactivity of AC were attributed to another paper studying phenol. In this paper (Velasco *et al.*, 2010b) the IPCAs were prepared by rotary evaporating a mixture (15:85) of P25 and AC. The study lacks a photolysis control and it is unclear if there was an adsorption phase before UV illumination. The AC performs better than the IPCA under dark adsorption conditions and it removes a higher concentration of phenol under UV illumination than the IPCA. The authors attribute the increased phenol removal by the AC to photoactivity of the AC due to its ash content (11 %). It is proposed that P25 has an antagonistic effect on the AC (Figure 6-2) in the IPCA in the first hour and half of photodegradation that is overcome by the photoactivity of P25. No error bars are given and the experimental method does not mention if the experiments were repeated.

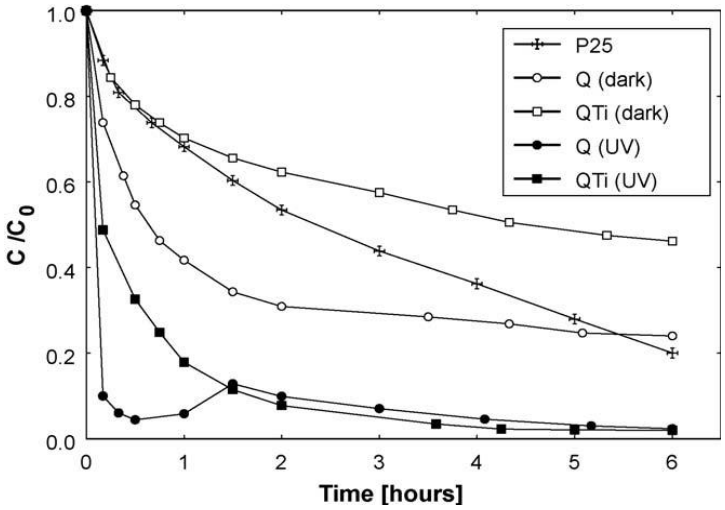

Figure 6-2 "Phenol concentration decay curves of the investigated catalysts under dark adsorption and UV irradiation" "Q" refers to the AC and "QTi" refers to the IPCA (Velasco *et al.*, 2010b).

The IPCAs are claimed to modify the phenol photodegradation pathway as evidenced by the different ratios of intermediates in the IPCA and P25 photodegradation samples (Figure 6-3). It is noted by the author that the difference is probably due to adsorption of intermediates onto the AC.

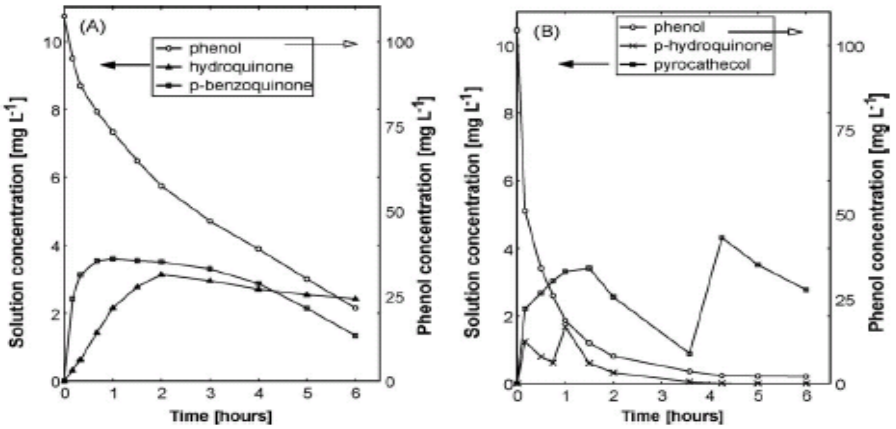

Figure 6-3 "Evolution of phenol decomposition intermediates upon UV irradiation on various materials investigated. (A) commercial titania and (B) carbon/titania composite" (Velasco *et al.*, 2010b).

A review article of IPCAs prepared by chemical vapour deposition (Li Puma *et al.*, 2008) claims IPCA synergy and it subsequently cites the studies listed below. These studies are analysed below and do not offer robust evidence of synergy:

1. Wang *et al.*, (2007) used thirty minutes of dark adsorption and included photolysis and TiO_2 controls. 6 % to 70 % of the dye used as the substrate is removed in the dark adsorption stage and since there is no dark adsorbent control it is impossible to determine if the reaction rate is measuring adsorption or photodegradation.
2. Liu *et al.*, (2007a) also used 30 min of dark adsorption before illumination with no dark adsorption and photolysis controls. Very low adsorption in dark adsorption stage and lack of controls make it difficult to evaluate performance. Photodegradation appears noticeably higher after illumination of the three contaminants.
3. Yoneyama and Torimoto, (2000) notes that mordenite has a high adsorption capacity but its adsorption strength is moderate enough to allow diffusion of adsorbed propionaldehyde to the TiO_2. Adsorbents with high adsorption constants e.g. activated carbon gave lower propionaldehyde decomposition rates presumably due to retardation of the diffusion of the adsorbed propionaldehyde. Experimental data are given but they do not support synergy. None of the examples in the paper have photolysis or adsorbent controls and photodegradation experiments do not seem to use a dark adsorption phase. Although the production of CO_2 would indicate photo-oxidation, with no controls it is impossible to draw firm

conclusions. For AC IPCAs there is a high concentration of catalyst (1 g/L) but the initial substrate concentration of 30 μM in a volume of 10 cm^3 is perhaps too small to evaluate performance. Illumination time is enormous for the comparison of adsorbents >1000 to 2000 min for 100 % CO_2 production. This paper is similar to a previous study by the same author (Torimoto *et al.*, 1996).

A separate review (Foo and Hameed, 2010a) focusing on the photodegradation of textile dyes using IPCAs stated the case for synergy between the AC and TiO_2 although the term is not explicitly used. The authors cited the aforementioned review (Li Puma *et al.*, 2008) as evidence of synergy although this review does not provide any evidence and cites other studies that are listed above. Citing of secondary sources suggests that claims of synergy are taken as an axiom and that the original evidence (or any evidence) of synergy is not subjected to any critical review.

A broad review of IPCAs (Lim *et al.*, 2011) includes a figure to illustrate IPCA synergy. The paper asserts that adsorption is necessary for photodegradation to occur and thus the Langmuir model is widely accepted for modelling equilibrium adsorption. The IPCA photodegradation is enhanced by improved mass transfer, concentrating the target pollutants around the surface of the photocatalyst. These claims are not referenced or supported. The paper documents the method for calculating "*synergy factor*" from Matos *et al.*, (1999). This refers to a letter submitted to the journal Carbon and the results and explanation are essentially the same as a previous paper Matos *et al.*, (1998) discussed above with the exception that the effect of AC surface treatment with acids and bases is investigated.

A film type IPCA prepared using a low temperature sol-gel method was studied for synergy (Ao *et al.*, 2008b). The IPCA film was placed in 20 mls of a 100 mg/L solution of 4-cholophenol for 30 min of dark adsorption followed by illumination for 6 h. While a sol-gel TiO_2 and P25 control were included there was no photolysis and adsorbent controls. The dark adsorption stage was not reported; however, if it was included (as it has been in (Figure 6-4)) it would suggest that the IPCA performance is mainly adsorption.

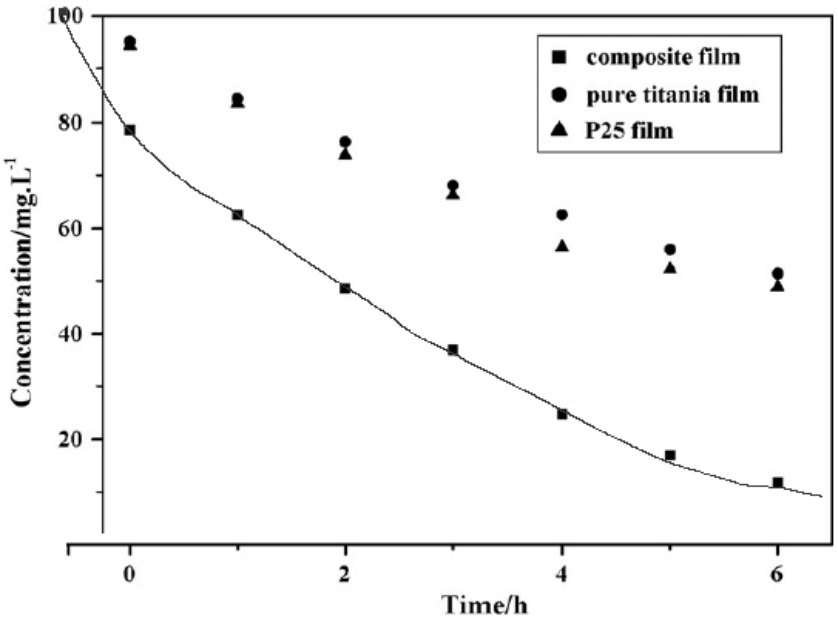

Figure 6-4 Adapted from Ao *et al.*, (2008b): Diagram of degradation of 4-chlorphenol. (The dark adsorption time (black line) of the IPCA is not shown in the original version). Initial concentration of 100 mg/L is stated in the method section.

Linear transformation of the kinetic curves is used to claim that the IPCAs worked better but the curves have different starting points so they are not comparable. Recycling of the composite is detailed but there is no adsorbent or dark control in this study so the IPCA may not have a longer lifespan than the unmodified AC.

A few select studies demonstrated more convincing results. Ao *et al.*, (2008a) used the same sol-gel method as a previous study (Ao *et al.*, 2008b) but with phenol as the substrate. This study lacks a photolysis control and the adsorbent control shows no reduction in phenol after the initial dark adsorption phase. The IPCA removes more phenol from the solution than the TiO_2, however, the slope of the degradation lines are very similar even with the difference in substrate concentrations (Figure 6-5). It suggests an effective photoactive IPCA but not necessarily a synergistic reaction.

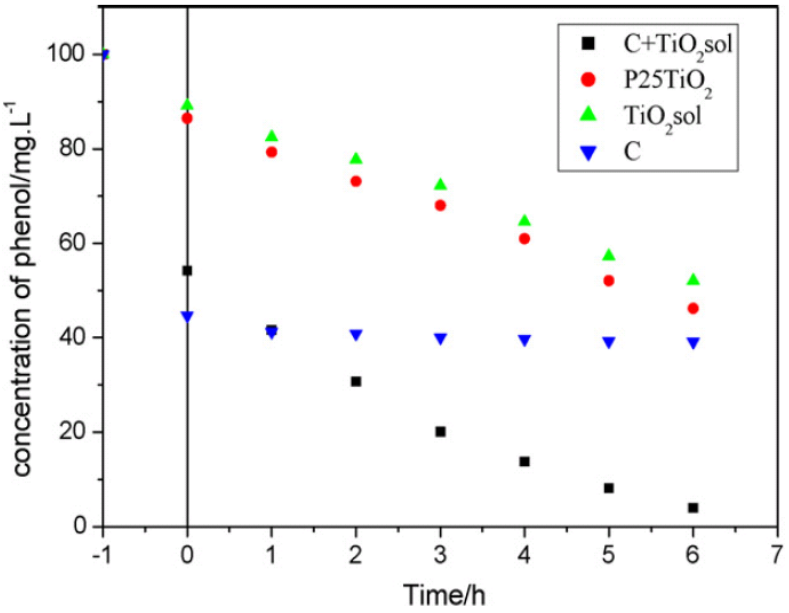

Figure 6-5 "Degradation of phenol in aqueous solutions" (Ao *et al.*, 2008a).

The photodegradation of microcystin-LR in two similar studies from the same author (Lee *et al.*, 2004a, Lee *et al.*, 2004b) demonstrates what appears to be IPCA synergy. Both studies used a closed loop continuous flow fluidised bed reactor and batch photodegradation apparatus. Photolysis is negligible and the illumination of the IPCA causes a significant increase in the removal rate compared to the IPCA that was not illuminated. Seven to fourteen times the amount of substrate could be desorbed from the IPCA that was not illuminated vs. the IPCA that was illuminated. No substrate could be extracted from the IPCA sample that had been illuminated for longer than 30 min. These results suggest that the IPCA can effectively degrade the substrate which is why it cannot be desorbed. The study design does not allow the use of TiO_2 controls which might be more effective at degrading the microcystin-LR, therefore this study does not prove synergy of IPCAs compared to TiO_2 although it does show than an IPCA can perform better than an unmodified AC.

The first studies of IPCAs appeared promising (Torimoto *et al.*, 1996, Torimoto *et al.*, 1997, Yoneyama and Torimoto, 2000), however, they all lack photolysis and dark adsorption controls. CO_2 production is measured and it indicates that something is being mineralised, however, due to a lack of adsorbent controls it is impossible to determine if it is the substrate, AC and/ or functional groups on the AC. The reaction volumes are also very small.

Overall there is some robust evidence of IPCA synergy (see Appendix A and B) in the published literature, however, many of the examples of synergy in the literature are questionable and may not represent IPCAs with any kind of synergetic behaviour. While there are many reports on the increased effectiveness of IPCAs it is not clear if IPCAs can perform better than AC and TiO_2 separately due to a lack of experimental controls in the studies reviewed. The majority of the reviewed studies lack dark adsorption controls therefore it is not certain that the IPCAs remove more substrate under illumination than in darkness. The mechanism by which the IPCA degrades the substrate is also not explicitly explained in most of these adsorption studies. It is generally agreed that the AC concentrates the substrate in the proximity of TiO_2. However it is not clear if the TiO_2 is cleaning the AC by the substrate diffusing towards the TiO_2 from the ACs pores or whether the AC may be concentrating the substrate on the AC surface increasing the substrate contact with TiO_2. In the second case there will be no observable impact on the substrate absorbed in the AC pores. It is also necessary to demonstrate the effectiveness of IPCAs in treating actual water and wastewater samples under typical operating conditions as these conditions are more challenging than bench scale. With the exception of five studies in the published literature, all studies have used a deionised water matrix which is not representative of the solutions that are normally purified with AC.

The limitations of the peer reviewed literature mean that the synergistic behaviour demonstrated by the 1:10 IPCAs for solifenacin degradation is one of the most robust examples of IPCA photocatalytic degradation of an organic pollutant. This is due to the presence of the necessary controls (dark, photolysis and photocatalysis) and a pronounced difference in photodegradation performance between the illuminated and non-illuminated IPCAs.

6.3 Molecules investigated for IPCA photodegradation

The contrast in adsorption and photodegradation performance between famotidine and solifenacin is due to their different chemical structures. With only two substrates it is not possible to draw any conclusions on what features of a chemical structure influence the photodegradation performance of an IPCA. The chemical structure and photocatalytic and adsorption properties of other analytes (indomethacin

and amoxicillin) studied in the Environtech group at DCU (of which this author is a member) will also be considered to try and illuminate any reactivity trends. This section will summarise the structure, adsorption and photocatalysis results of each substrate.

The structure of famotidine is shown in Figure 6-6 and Figure 6-7. Famotidine can be readily photodegraded by TiO_2 but not by the IPCAs, this may be attributed to strong adsorption of famotidine onto AC and negligible desorption.

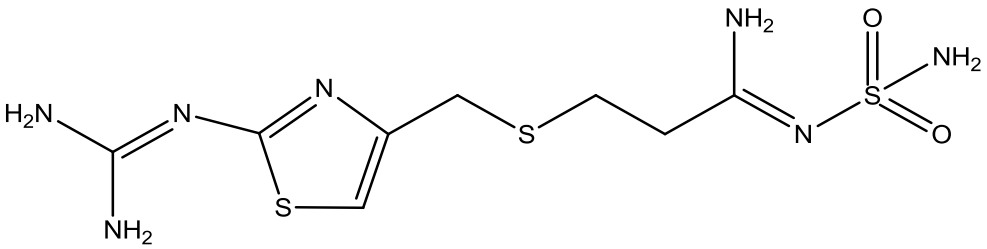

Figure 6-6 Structure of famotidine.

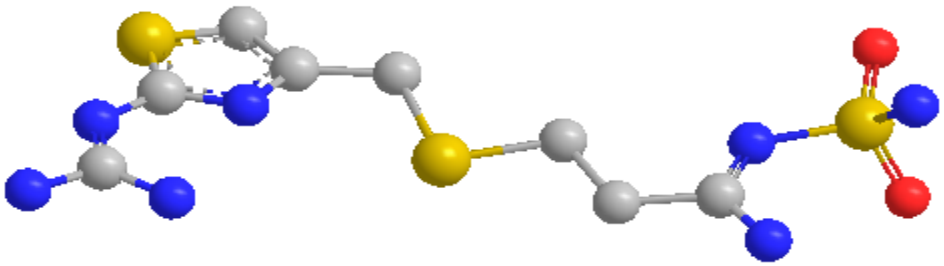

Figure 6-7 3D structure of famotidine.

The structure of solifenacin is shown in Figure 6-8 and Figure 6-9. Unlike famotidine, solifenacin can be readily photodegraded by both TiO_2 and IPCAs. Solifenacin adsorption onto AC was also found to be lower than famotidine; however solifenacin desorption from AC is higher than famotidine (Section 4.6).

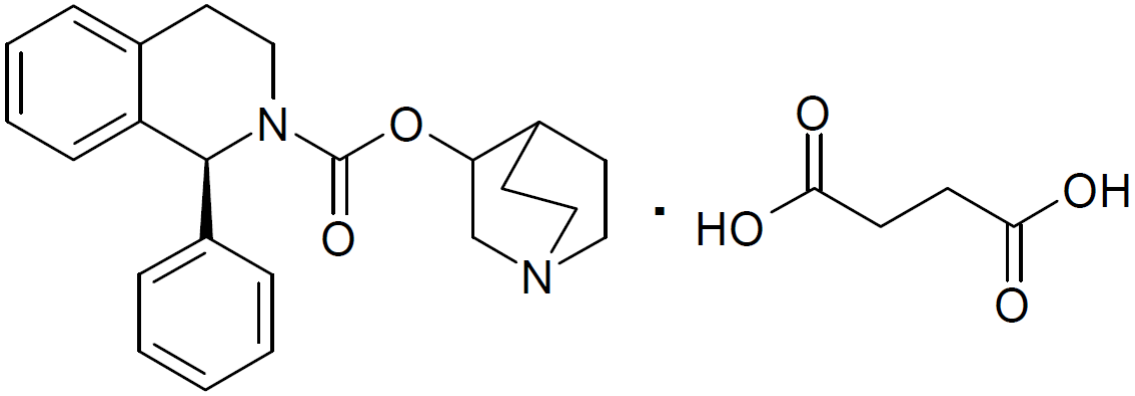

Figure 6-8 Structure of solifenacin.

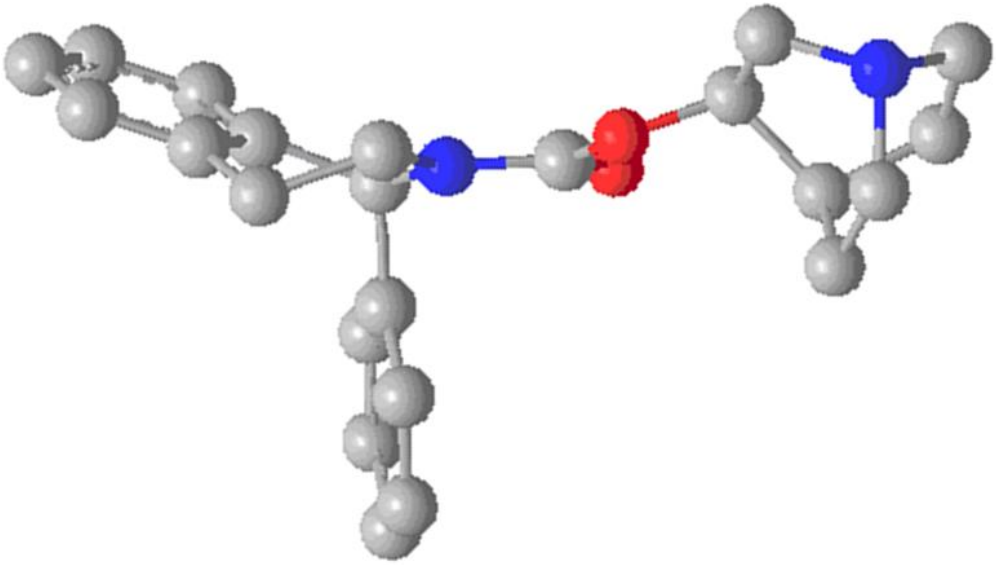

Figure 6-9 3D structure of solifenacin.

The structure of amoxicillin is shown in Figure 6-10 and Figure 6-11. It is a relatively bulky molecule and is readily photodegraded by both TiO_2 and IPCAs (Figure 6-12). Amoxicillin adsorption onto AC is at least four times higher than famotidine and solifenacin, however, desorption from the AC has not been assessed to date.

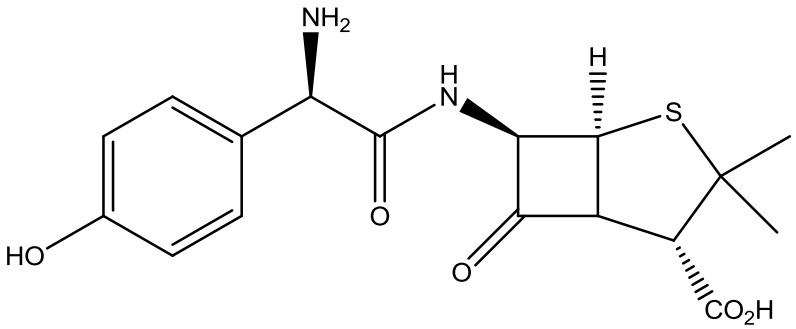

Figure 6-10 Structure of amoxicillin.

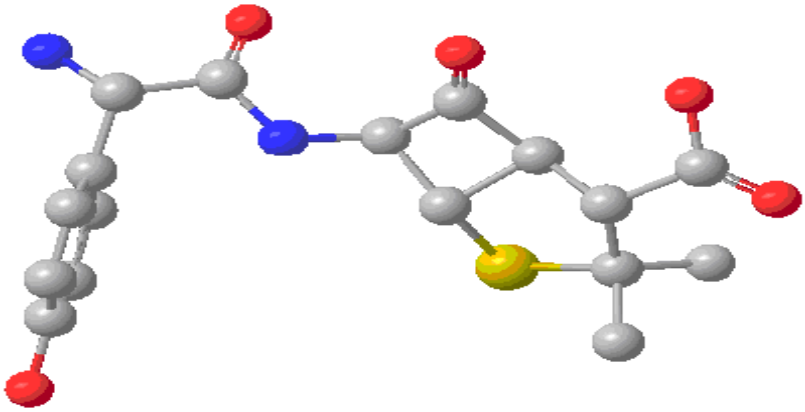

Figure 6-11 3D structure of amoxicillin.

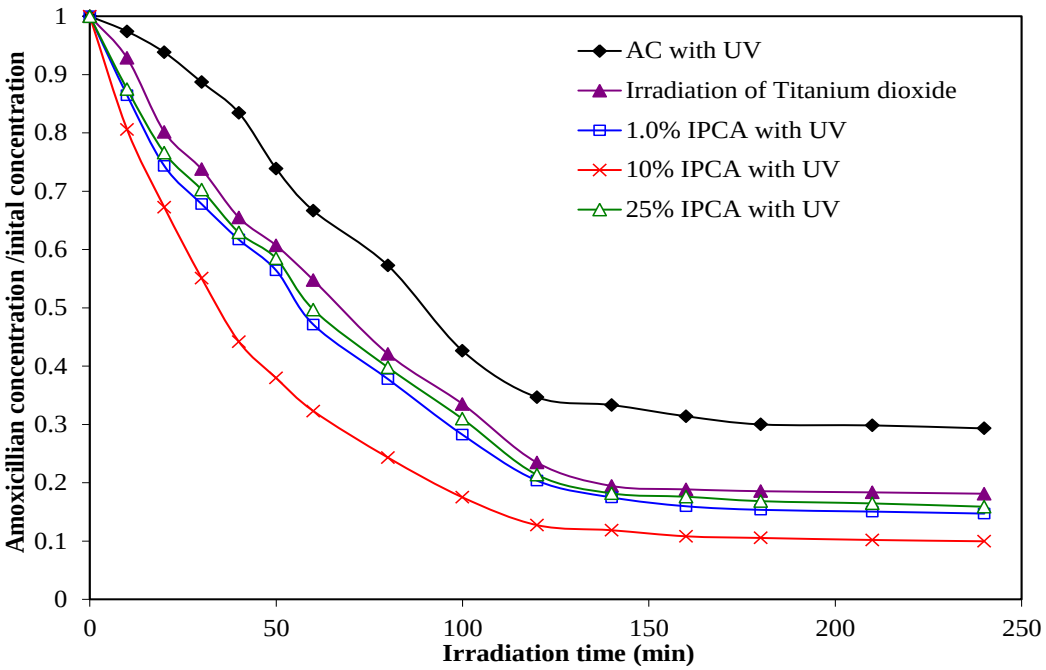

Figure 6-12 Photodegradation and removal of amoxicillin using AC, TiO_2 and IPCAs. Initial concentration 150 mg/L, catalyst concentration 1.5 g/L, 3 h dark adsorption time not shown (Basha *et al.*, 2011).

The structure of indomethacin is shown in Figure 6-13 and Figure 6-14. It is readily photodegraded by TiO_2 and IPCAs (Figure 6-15). Indomethacin adsorption onto AC is higher (max adsorption loading of 100 mg/g) than famotidine and solifenacin (max adsorption loadings of 80 mg/g and 60 mg/g respectively) but lower than amoxicillin (max adsorption loadings of 450 mg/g). Desorption of indomethacin from the AC has not been assessed.

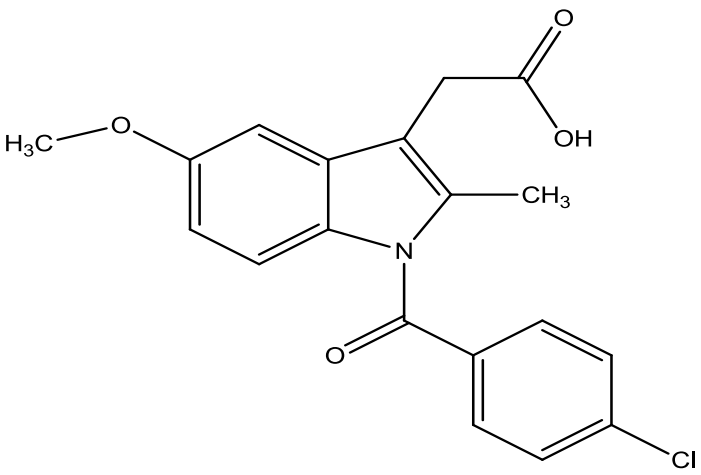

Figure 6-13 Structure of indomethacin.

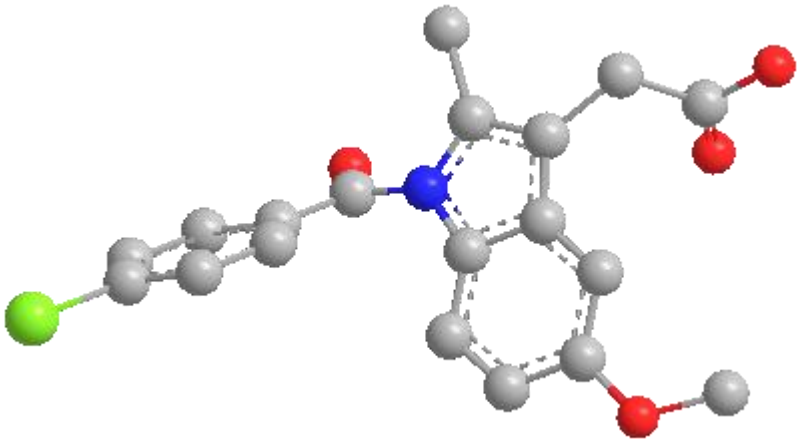

Figure 6-14 3D structure of indomethacin.

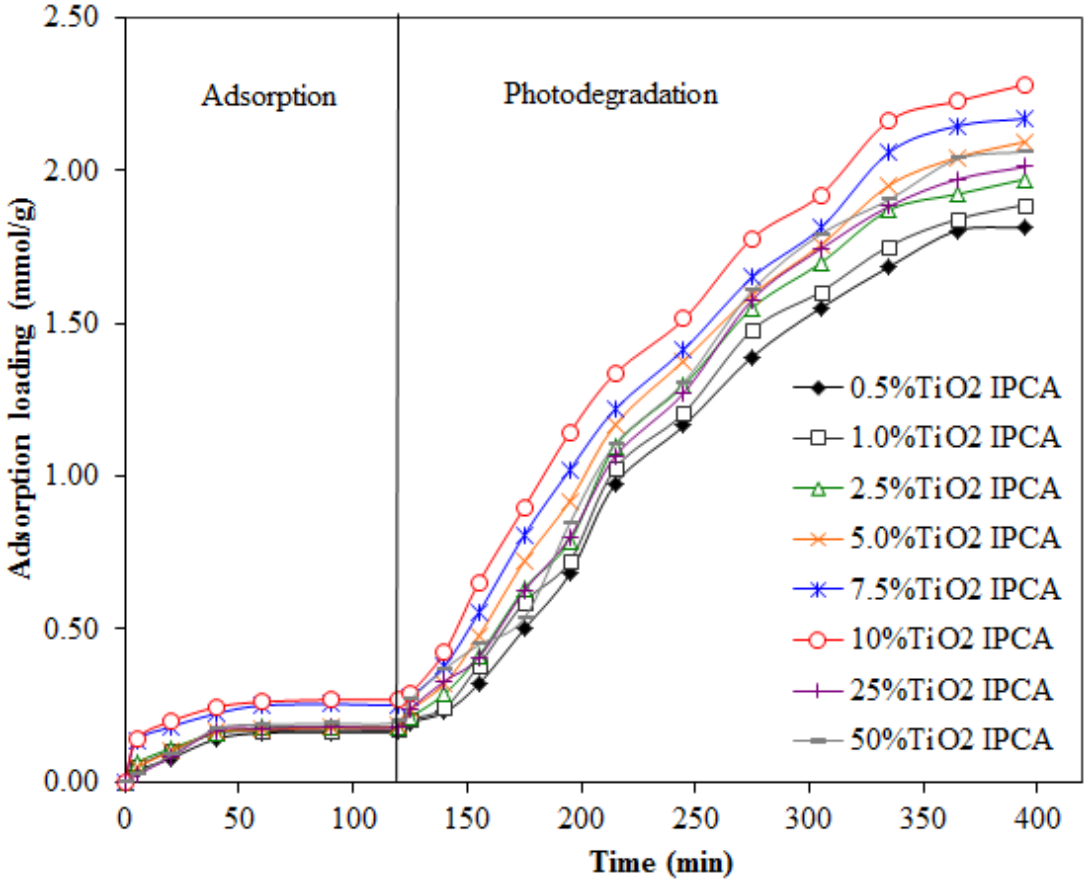

Figure 6-15 Dark adsorption of indomethacin, followed by visible-light photocatalysis kinetic plots for various IPCAs. Initial concentration at t = 0, 0.25 mmol, catalyst concentration is 1.2 g/L. Data from Basha *et al.*, (2010).

6.4 Reasons for success or failure of molecules to be photodegraded by IPCAs

By considering the substrates studied in the Environtech Group at DCU an attempt is made to find what factors influence IPCA photocatalysis. Some of the chemical properties of the APIs investigated for IPCA photodegradation are shown in Table 6-1. While all these substrates have different chemical structures a broad trend can be inferred from their photodegradation with IPCAs. Some factors can be discounted:

1. *Adsorption capacity*. Given that the adsorption of amoxicillin and indomethacin are higher than famotidine it appears that high adsorption on its own is not the cause of the lack of photodegradation of famotidine.

2. *Molecular weight* might not have a significant influence on photodegradation by the IPCAs as solifenacin succinate is heavier than famotidine and photodegrades effectively. In contrast, indomethacin and amoxicillin have a similar molar weight to famotidine and are effectively photodegraded using IPCAs.

Table 6-1 Chemical properties of APIs in IPCA photodegradation studies.

	Famotidine	**Solifenacin**	**Indomethacin**	**Amoxicillin**
CLogP Driver: Mol Refractivity	8.142	10.696	9.505	9.3926
CLogP Driver: Partition Coefficient	-0.513	4.6796	4.1799	2.0318
ACD/LogP:	-0.64	4.159	4.251	0.883
ACD/LogD (pH 5.5)	-2.50	1.2	2.70	-1.64
ACD/LogD (pH 7.4)	-1.27	2.53	0.98	-2.32
#H bond acceptors	9	4	5	8
#H bond donors	8	0	1	5
# freely rotating bonds	7	3	4	6
# of Rule of 5 Violations	1	0	0	1
Molar weight	337.449	480.55	357.787	365.4
Molar Refractivity cm^3	79.06	105.823	94.594	91.475
Molar Volume cm^3	183.554	290.574	269.565	236.218

Source: (ChemSpider 2012)

Famotidine has the lowest molar refractivity, molar volume, Log P and Log D (pH 5.5) values and the highest number of H bond donors and acceptors of the three APIs. In theory the polar nature of famotidine would decrease its adsorption on AC due to repulsion from the nonpolar AC surface. However, as a result of the large number of H bond sites, H bonding occurs between famotidine and the hydroxyl, epoxide and carboxyl groups on the AC surface. Furthermore, the small size of famotidine should minimise steric effects on the AC surface. The combination of

these two effects may explain the high adsorption capacity of the AC for famotidine and hence the low desorption rate that consequently inhibits transfer of the famotidine to the P25 surface for photodegradation.

Solifenacin, indomethacin and amoxicillin, in contrast to famotidine, have larger molar refractivity, molar volume and Log P values and with exception of amoxicillin have half the number of H bond acceptors and H bond donors (for H-bond donors it is at least eight times lower). The less H bonds between the API and the AC surface the lower the binding strength allowing for higher desorption from the surface of the AC. Therefore, in the case of solifenacin and indomethacin reduced H-bond interactions with the AC surface allows for higher desorption to solution followed by migration to the P25 surface of the IPCA resulting in photodegradation, that was observed experimentally.

Amoxicillin presents a challenge to this hypothesis as it has almost the same number of H bond acceptor sites as famotidine (8 vs. 9 respectively) although it has less donor sites (5 vs. 8 respectively). However, the difference in IPCA reactivity between famotidine and amoxicillin may be accounted for by the larger molar volume of amoxicillin, and its branched chain structure would likely cause unfavourable steric interactions with the AC surface of the IPCA. This may lower amoxicillin binding to the AC surface and could increase desorption into solution and thus migration of amoxicillin to the surface of P25 on an IPCA.

The importance of adsorption affinity for the photodegradation of the substrate using IPCA has been suggested in the literature (Yoneyama and Torimoto, 2000). This phenomenon has not been extensively studied and presents an opportunity for future work.

6.5 Future work to confirm mechanism

To confirm that photodegradation using IPCAs is promoted by low substrate affinity to the AC surface caused by a combination of steric effects and low H bonding it would be necessary to study other APIs with similar properties to famotidine. There are two other APIs with a similar structure to famotidine: cimetidine and ranitidine which are also H_2 receptor antagonists. Their chemical

properties are listed (Table 6-2) and structures are shown in Figure 6-16 to Figure 6-19.

Table 6-2 Chemical properties of APIs used in past and future IPCA photodegradation studies.

	Famotidine	**Solifenacin**	**Cimetidine**	**Ranitidine**
ACD/LogP:	-0.64	4.159	0.072	-0.068
ACD/LogD (pH 5.5)	-2.50	1.2	-1.76	-2.73
ACD/LogD (pH 7.4)	-1.27	2.53	-0.25	-1.07
#H bond acceptors	9	4	6	7
#H bond donors	8	0	3	2
# freely rotating bonds	7	3	5	10
# of Rule of 5 Violations	1	0	0	0
Molar weight	337.449	480.55	252.34	314.4
Molar Refractivity cm^3	79.06	105.823	70.7	85.647
Molar Volume cm^3	183.554	290.574	198.2	265.446

Source: (ChemSpider 2012, Lookchem 2012)

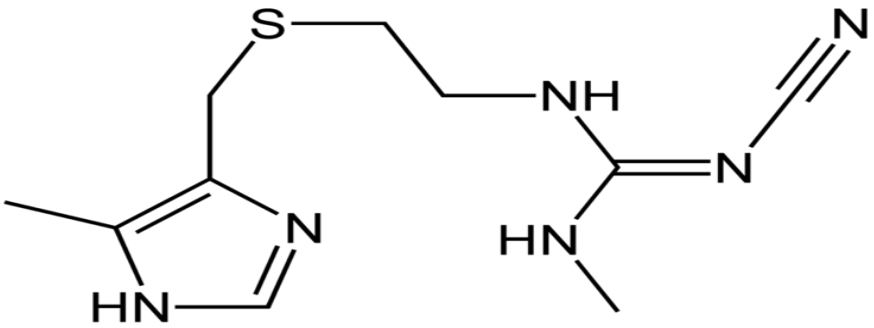

Figure 6-16 Structure of cimetidine.

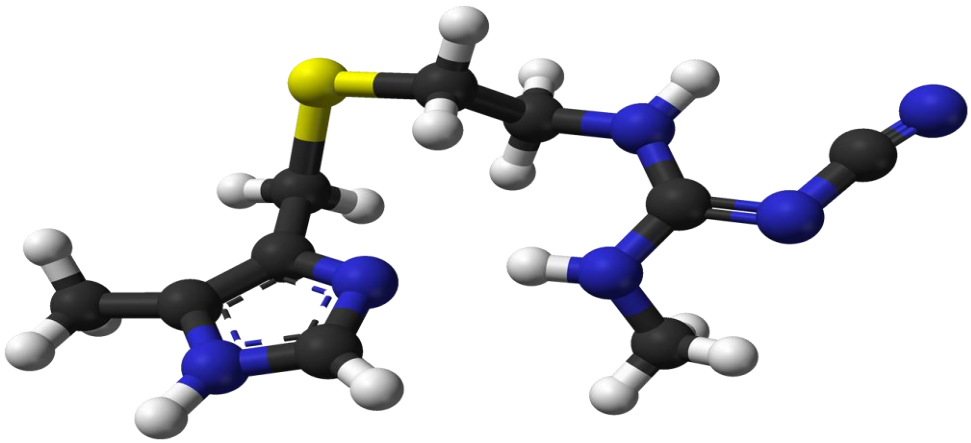

Figure 6-17 3D structure of cimetidine.

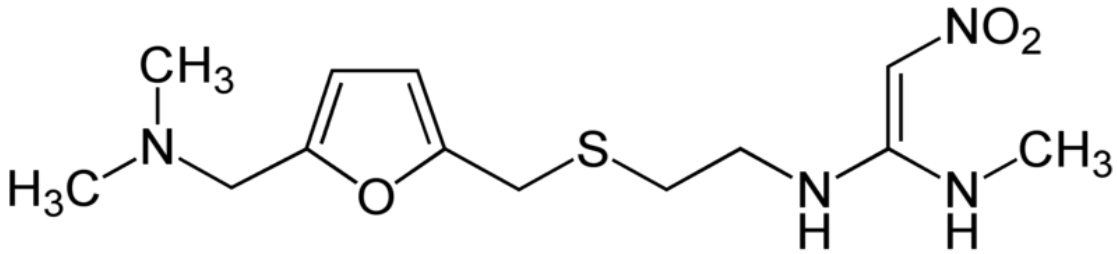

Figure 6-18 Structure of ranitidine.

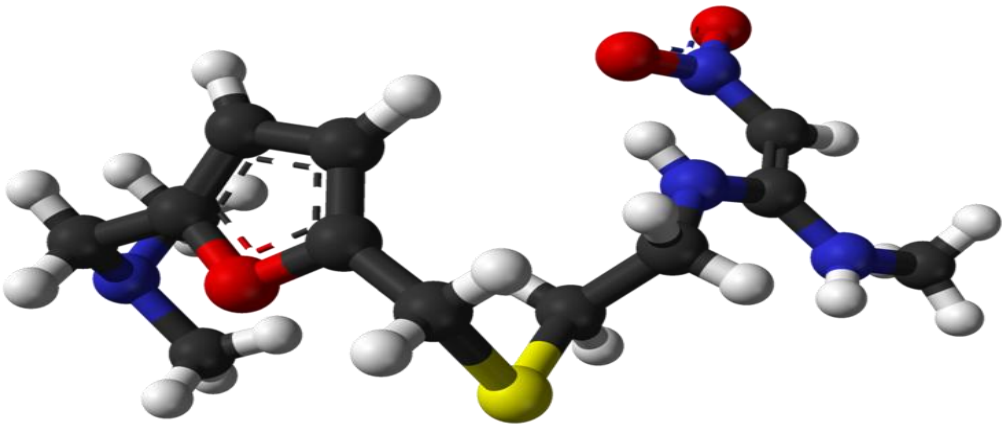

Figure 6-19 3D structure of ranitidine.

If cimetidine and ranitidine are not effectively degraded by IPCAs and have a high adsorption affinity on the AC/IPCA surface (high adsorption capacity and low desorption) then the rate of desorption from the AC surface is vital for photocatalysis. Studies of desorption of amoxicillin and indomethacin from AC would also need to be undertaken to confirm that high desorption rates inhibit API photodegradation.

6.6 Conclusion

The majority of the peer reviewed literature of IPCA photodegradation lacks the necessary controls to confirm IPCA photodegradation. Solifenacin, amoxicillin and indomethacin are effectively degraded by IPCAs while famotidine is not. This difference in photodegradation performance of the IPCA for different APIs is due to steric effects and less H bonding reducing the adsorption affinity of solifenacin, amoxicillin and indomethacin compared to famotidine. The lower adsorption affinity increases desorption and thus migration to the TiO_2 surface allowing photodegradation. IPCA photodegradation studies of cimetidine and ranitidine which have similar chemical structures to famotidine would confirm the proposed mechanism.

Chapter 7 Conclusions and Recommendations

7.1 Conclusions

Arising from shortcomings of existing research, this work investigated and evaluated the following aims:

1. The capacity of IPCAs, commercial AC and TiO_2 to adsorb and photodegrade pharmaceuticals.
2. The synergy between AC and TiO_2 for the removal of pollutants.

The major findings of this work are:

1. The adsorption capacity of AC, IPCA and TiO_2 for solifenacin and famotidine has been determined. Aqua 2k has a high adsorption capacity for famotidine and a lower capacity for solifenacin. This adsorption capacity is not noticeably reduced by the addition of TiO_2 particles to the AC surface to create an IPCA. Baseline photodegradation data for famotidine and solifenacin photolysis and photocatalysis has been gathered. Famotidine is moderately photodegraded by photolysis while there is no photolysis of solifenacin under the same illumination conditions. Famotidine and solifenacin are both degraded by P25 TiO_2; although the photodegradation rate of famotidine is higher.
2. There was no synergy demonstrated between TiO_2 and AC in the photodegradation of famotidine. In contrast solifenacin photodegradation using IPCAs demonstrated more photodegradation than either TiO_2 or AC. The synergy demonstrated in this work by IPCAs for solifenacin degradation is more robust than the vast majority of published literature on IPCA photodegradation.

7.2 Recommendations for future work

- IPCA adsorption and photodegradation studies of cimetidine and ranitidine - which are similar in chemical structure to famotidine - should be undertaken. If IPCAs have a high adsorption capacity and they have no synergy for photodegradation of cimetidine and ranitidine then it would confirm that high adsorption strength inhibits synergistic IPCA photodegradation.
- Studies of APIs that can be photodegraded by IPCAs (solifenacin, amoxicillin and indomethacin) should be undertaken using sunlight as the illumination source.
- The ability of IPCAs to degrade APIs such as solifenacin, amoxicillin and indomethacin should be investigated in real world conditions i.e. in water matrixes that contain natural organic materials and concentration ranges of APIs typically found in wastewater.
- Future studies of API photodegradation using IPCAs should measure desorption as it gives insights into the rate of substrate transfer and influences photodegradation. Desorption of amoxicillin and indomethacin from IPCAs should also be investigated.
- Optimising experimental conditions based on optical modelling of reactor system and materials.

References

Abuzaid, N.S. and Nakhla, G. 1997. Predictability of the homogeneous surface diffusion model for activated carbon adsorption kinetics; formulation of a new mathematical model. *Journal of Environmental Science and Health .Part A: Environmental Science and Engineering and Toxicology,* 32(7), pp.1945-1961.

Aksu, Z. and Yener, J. 2001. A comparative adsorption/biosorption study of mono-chlorinated phenols onto various sorbents. *Waste Management,* 21(8), pp.695-702.

Al-Kdasi, A., Idris, A., Saed, K. and Teong Guan, C. 2004. Treatment of Textile Wastewater by Advanced Oxidation Processes A review. *Global Nest Journal,* 6(3), pp.222-230.

Anpo, M. 2000. Utilization of TiO_2 photocatalysts in green chemistry. *Pure and Applied Chemistry,* 72(7), pp.1265-1270.

Ao, Y., Xu, J., Fu, D. and Yuan, C. 2009. Photocatalytic degradation of X-3B by titania-coated magnetic activated carbon under UV and visible irradiation. *Journal of Alloys and Compounds,* 471(1-2), pp.33-38.

Ao, Y., Xu, J., Fu, D., Shen, X. and Yuan, C. 2008a. Low temperature preparation of anatase TiO_2-coated activated carbon. *Colloids and Surfaces A: Physicochemical and Engineering Aspects,* 312(2-3), pp.125-130.

Ao, Y., Xu, J., Fu, D., Shen, X. and Yuan, C. 2008b. Low temperature preparation of anatase TiO_2-activated carbon composite film. *Applied Surface Science,* 254(13), pp.4001-4006.

Ao, Y., Xu, J., Fu, D., Shen, X. and Yuan, C. 2008c. A novel magnetically separable composite photocatalyst: Titania-coated magnetic activated carbon. *Separation and Purification Technology,* 61(3), pp.436-441.

Ao, Y., Xu, J., Fu, D. and Yuan, C. 2008d. A simple route for the preparation of anatase titania-coated magnetic porous carbons with enhanced photocatalytic activity. *Carbon,* 46(4), pp.596-603.

Araña, J., Doña-Rodríguez, J.M., Tello Rendón, E., Garriga i Cabo, C., González-Díaz, O., Herrera-Melián, J.A., Pérez-Peña, J., Colón, G. and Navío, J.A. 2003a. TiO_2 activation by using activated carbon as a support: Part I. Surface characterisation and decantability study. *Applied Catalysis B: Environmental,* 44(2), pp.161-172.

Araña, J., Doña-Rodríguez, J.M., Tello Rendón, E., Garriga i Cabo, C., González-Díaz, O., Herrera-Melián, J.A., Pérez-Peña, J., Colón, G. and Navío, J.A. 2003b. TiO_2 activation by using activated carbon as a support: Part II. Photoreactivity and FTIR study. *Applied Catalysis B: Environmental,* 44(2), pp.153-160.

Ardee Environment 22 June 2010. *Low Pressure Lamps* [Online]. Available from: http://www.ardeeenvironment.info/low_pressure.html [Accessed 05/26 2012].

Ardee Environment 22 June 2010. *Medium Pressure* [Online]. Available from: http://www.ardeeenvironment.info/medium_pressure.html [Accessed 05/26 2012].

Areerachakul, N., Vigneswaran, S., Ngo, H. and Kandasamy, J. 2008. A continuous photocatalysis system in the degradation of herbicide. *JF: Korean Journal of Chemical Engineering,* 25(4), pp.663-669.

Arivolia, S., Thenkuzhalib, M. and Martin Deva Prasath, P. 2009. Adsorption of rhodamine B by acid activated carbon-Kinetic, thermodynamic and equilibrium studies *Orbital* 1(2), pp. 25/04/12-138-155. Available from: http://www.orbital.ufms.br/index.php/Chemistry/article/view/24

Aruldoss, U., Kennedy, L.J., Judith Vijaya, J. and Sekaran, G. 2011. Photocatalytic degradation of phenolic syntan using TiO_2 impregnated activated carbon. *Journal of Colloid and Interface Science*, 355(1), pp.204-209.

Asiltürk, M. and Şener, Ş. 2012. TiO_2-activated carbon photocatalysts: Preparation, characterization and photocatalytic activities. *Chemical Engineering Journal*, 180(0), pp.354-363.

Augugliaro, V., Litter, M., Palmisano, L. and Soria, J. 2006. The combination of heterogeneous photocatalysis with chemical and physical operations: A tool for improving the photoprocess performance. *Journal of Photochemistry and Photobiology C: Photochemistry Reviews*, 7(4), pp.127-144.

Balázs, N., Mogyorósi, K., Srankó, D.F., Pallagi, A., Alapi, T., Oszkó, A., Dombi, A. and Sipos, P. 2008. The effect of particle shape on the activity of nanocrystalline TiO_2 photocatalysts in phenol decomposition. *Applied Catalysis B: Environmental*, 84(3-4), pp.356-362.

Bansal, R.C. and Goyal, M. 2005. *Activated Carbon Adsorption.* Boca Raton, Florida: CRC Press.

Basha, S., Colin, B., Keane, D., Nolan, K., Morrissey, A., Oelgemöller, M. and Tobin, J.M. 2011. On the adsorption/photodegradation of amoxicillin in aqueous solutions by an integrated photocatalytic adsorbent (IPCA): experimental studies and kinetics analysis. *Photochemical & Photobiological Sciences*, 10(6), pp.1014-1022.

Basha, S., Keane, D., Morrissey, A., Nolan, K., Oelgemöller, M. and Tobin, J. 2010. Studies on the Adsorption and Kinetics of Photodegradation of Pharmaceutical Compound, Indomethacin Using Novel Photocatalytic Adsorbents (IPCAs). *Industrial & Engineering Chemistry Research*, 49(22), pp.11302-11309.

Baup, S., Jaffre, C., Wolbert, D. and Laplanche, A. 2000. Adsorption of Pesticides onto Granular Activated Carbon: Determination of Surface Diffusivities Using Simple Batch Experiments. *Adsorption*, 6pp.219-228.

Begum, N. and Farveez Ahmed, H. 2008. Synthesis of nanocrystalline TiO_2 thin films by liquid phase deposition technique and its application for photocatalytic degradation studies. *Bulletin of Materials Science*, 31(1), pp.43-48.

Benabbou, A.K., Derriche, Z., Felix, C., Lejeune, P. and Guillard, C. 2007. Photocatalytic inactivation of Escherischia coli: Effect of concentration of TiO_2 and microorganism, nature, and intensity of UV irradiation. *Applied Catalysis B: Environmental*, 76(3-4), pp.257-263.

Blanco, J., Malato, S., Fernández-Ibañez, P., Alarcón, D., Gernjak, W. and Maldonado, M.I. 2009. Review of feasible solar energy applications to water processes. *Renewable and Sustainable Energy Reviews*, 13(6-7), pp.1437-1445.

Boorman, G.A., Dellarco, V., Dunnick, J.K., Chapin, R.E., Hunter, S., Hauchman, F., Gardner, H., Cox, M. and Sills, R.C. 1999. Drinking Water Disinfection Byproducts: Review and Approach to Toxicity Evaluation. *Environmental Health Perspectives*, 107(1), pp.207-217.

Byrne, J.A., Eggins, B.R., Brown, N.M.D., McKinney, B. and Rouse, M. 1998. Immobilisation of TiO_2 powder for the treatment of polluted water. *Applied Catalysis B: Environmental*, 17(1-2), pp.25-36.

Cao, X., Oda, Y. and Shiraishi, F. 2010. Photocatalytic and adsorptive treatment of 2,4-dinitrophenol using a TiO_2 film covering activated carbon surface. *Chemical Engineering Journal,* 156(1), pp.98-105.

Cao, X. and Shiraishi, F. 2010. A mechanism of photocatalytic and adsorptive treatment of 2,4-dinitrophenol on a porous thin film of TiO_2 covering granular activated carbon particles. *Chemical Engineering Journal,* 160(2), pp.651-659.

Castiglioni, S., Bagnati, R., Fanelli, R., Pomati, F., Calamari, D. and Zuccato, E. 2006. Removal of Pharmaceuticals in Sewage Treatment Plants in Italy. *Environmental Science & Technology,* 40(1), pp.357-363.

ChemSpider, 26-7-20212. *What is ChemSpider?*[Online]. Available from: http://www.chemspider.com/About.aspx [Accessed 7/26 2012].

Choi, H., Stathatos, E. and Dionysiou, D.D. 2007. Photocatalytic TiO_2 films and membranes for the development of efficient wastewater treatment and reuse systems. *Desalination,* 202(1-3), pp.199-206.

Choy, K.K.H., Porter, J.F. and Mckay, G. 2004. Intraparticle diffusion in single and multicomponent acid dye adsorption from wastewater onto carbon. *Chemical Engineering Journal,* 103(1–3), pp.133-145.

Clara, M., Strenn, B., Gans, O., Martinez, E., Kreuzinger, N. and Kroiss, H. 2005. Removal of selected pharmaceuticals, fragrances and endocrine disrupting compounds in a membrane bioreactor and conventional wastewater treatment plants. *Water Research,* 39(19), pp.4797-4807.

Cojocaru, B., Neatu, s., Pârvulescu, V.I., Somoghi, V., Petrea, N., Epure, G., Alvaro, M. and Garcia, H. 2009. Synergism of Activated Carbon and Undoped and Nitrogen-doped TiO_2 in the Photocatalytic Degradation of the Chemical Warfare Agents Soman, VX, and Yperite. *ChemSusChem,* 2(5), pp.427-436.

Comninellis, C., Kapalka, A., Malato, S., Parsons, S.A., Poulios, I. and Mantzavinos, D. 2008. Advanced oxidation processes for water treatment: advances and trends for R&D. *Journal of Chemical Technology & Biotechnology,* 83(6), pp.769-776.

Cordero, T., Chovelon, J., Duchamp, C., Ferronato, C. and Matos, J. 2007a. Surface nano-aggregation and photocatalytic activity of TiO_2 on H-type activated carbons. *Applied Catalysis B: Environmental,* 73(3-4), pp.227-235.

Cordero, T., Duchamp, C., Chovelon, J., Ferronato, C. and Matos, J. 2007b. Influence of L-type activated carbons on photocatalytic activity of TiO_2 in 4-chlorophenol photodegradation. *Journal of Photochemistry and Photobiology A: Chemistry,* 191(2-3), pp.122-131.

Coyle, E.E. and Oelgemöller, M. 2008. Micro-photochemistry: photochemistry in microstructured reactors. The new photochemistry of the future? *Photochemical and Photobiological Sciences,* 7(11), pp.1313-1322.

Cunningham, N., Dodelet, J.P., Guay, D., Ross, G.G., Hlil, A.R. and Hay, A.S. 2004. RBS and XRD analyses of carbon-coated stainless steel plates. *Surface and Coatings Technology,* 183(2-3), pp.216-223.

da Silva, C.G. and Faria, J.L. 2003. Photochemical and photocatalytic degradation of an azo dye in aqueous solution by UV irradiation. *Journal of Photochemistry and Photobiology A: Chemistry,* 155(1-3), pp.133-143.

Dai, M. 1994. The Effect of Zeta Potential of Activated Carbon on the Adsorption of Dyes from Aqueous Solution: I. The Adsorption of Cationic Dyes: Methyl Green and Methyl Violet. *Journal of Colloid and Interface Science,* 164(1), pp.223-228.

Deegan, A. 2011. *Pharmaceuticals in industrial wastewater and their removal using photo-Fentons oxidation.* Ph.D. Research Thesis. Dublin City University.

Deegan, A., Shaik, B., Nolan, K., Urell, K., Oelgemöller, M., Tobin, J. and Morrissey, A. 2011. Treatment options for wastewater effluents from pharmaceutical companies. *Internation Journal of Environmental Science and Technology,* 8(3), pp.649-666.

Devipriya, S. and Yesodharan, S. 2005. Photocatalytic degradation of pesticide contaminants in water. *Solar Energy Materials and Solar Cells,* 86(3), pp.309-348.

, E., Ordóñez, S., Vega, A. and Coca, J. 2005. Comparison of adsorption properties of a chemically activated and a steam-activated carbon, using inverse gas chromatography. *Microporous and Mesoporous Materials,* 82(1-2), pp.173-181.

Ding, Z., Zhu, H.Y., Greenfield, P.F. and Lu, G.Q. 2001a. Characterization of Pore Structure and Coordination of Titanium in TiO_2 and SiO_2–TiO_2 Sol-Pillared Clay. *Journal of Colloid and Interface Science,* 238(2), pp.267-272.

Ding, Z., Hu, X., Yue, P.L., Lu, G.Q. and Greenfield, P.F. 2001b. Synthesis of anatase TiO_2 supported on porous solids by chemical vapor deposition. *Catalysis Today,* 68(1-3), pp.173-182.

Ding, Z., Hu, X., Lu, G.Q., Yue, P. and Greenfield, P.F. 2000. Novel Silica Gel Supported TiO_2 Photocatalyst Synthesized by CVD Method. *Langmuir,* 16(15), pp.6216-6222.

Djaoued, Y., Brüning, R., Bersani, D., Lottici, P.P. and Badilescu, S. 2004. Sol–gel nanocrystalline brookite-rich titania films. *Materials Letters,* 58(21), pp.2618-2622.

Eggert, F. *The Self Absorption Rough Surfaces / Soft X-Rays* [Online]. Available from: http://microanalyst.mikroanalytik.de/info4.phtml [Accessed 18/10 2011].

Eggins, B.R., Palmer, F.L. and Byrne, J.A. 1997. Photocatalytic treatment of humic substances in drinking water. *Water Research,* 31(5), pp.1223-1226.

El-Sheikh, A.H., Al-Degs, Y.S., Newman, A.P. and Lynch, D.E. 2007. Oxidized activated carbon as support for titanium dioxide in UV-assisted degradation of 3-chlorophenol. *Separation and Purification Technology,* 54(1), pp.117-123.

El-Sheikh, A.H., Newman, A.P., Al-Daffaee, H., Phull, S., Cresswell, N. and York, S. 2004. Deposition of anatase on the surface of activated carbon. *Surface and Coatings Technology,* 187(2-3), pp.284-292.

Enick, O.V. and Moore, M.M. 2007. Assessing the assessments: Pharmaceuticals in the environment. *Environmental Impact Assessment Review,* 27(8), pp.707-729.

Ferenczy, G.G., Párkányi, L., Ángyán, J.G., Kálmán, A. and Hegedus, B. 2000. Crystal and electronic structure of two polymorphic modifications of famotidine. An experimental and theoretical study. *Journal of Molecular Structure: THEOCHEM,* 503(1-2), pp.73-79.

Fitzer, E., Kochling, K.H., Boehm, H.P. and Marsh, H. 1995. Recommended Terminology For the description of carbon as a solid. *Pure and Applied Chemistry,* 67(3), pp.473-506.

Foo, K.Y. and Hameed, B.H. 2010a. Decontamination of textile wastewater via TiO_2/activated carbon composite materials. *Advances in Colloid and Interface Science,* 159(2), pp.130-143.

Foo, K.Y. and Hameed, B.H. 2010b. Insights into the modeling of adsorption isotherm systems. *Chemical Engineering Journal,* 156(1), pp.2-10.

Franz, M., Arafat, H.A. and Pinto, N.G. 2000. Effect of chemical surface heterogeneity on the adsorption mechanism of dissolved aromatics on activated carbon. *Carbon,* 38(13), pp.1807-1819.

Freundlich, H. 1907. Uber die adsorption in Losungen. *Z. Phys. Chem.,* 57pp.385-470.

Fu, P., Luan, Y. and Dai, X. 2004a. Preparation of activated carbon fibers supported TiO_2 photocatalyst and evaluation of its photocatalytic reactivity. *Journal of Molecular Catalysis A: Chemical,* 221(1-2), pp.81-88.

Fu, P., Luan, Y. and Dai, X. 2004b. Preparation of TiO_2 photocatalyst anchored on activated carbon fibers and its photodegradation of methylene blue. *China Particuology,* 2(2), pp.76-80.

Fu, P., Luan, Y. and Dai, X. 2006. Interposition fixing structure of TiO_2 film deposited on activated carbon fibers. *Transactions of Nonferrous Metals Society of China,* 16(4), pp.965-969.

Fuerhacker, M., Dürauer, A. and Jungbauer, A. 2001. Adsorption isotherms of 17β-estradiol on granular activated carbon (GAC). *Chemosphere,* 44(7), pp.1573-1579.

Fujishima, A. and Zhang, X. 2006. Titanium dioxide photocatalysis: present situation and future approaches. *Comptes Rendus Chimie,* 9(5-6), pp.750-760.

Fujishima, A., Rao, T.N. and Tryk, D.A. 2000. Titanium dioxide photocatalysis. *Journal of Photochemistry and Photobiology C: Photochemistry Reviews,* 1(1), pp.1-21.

Fytianos, K., Voudrias, E. and Kokkalis, E. 2000. Sorption–desorption behaviour of 2,4-dichlorophenol by marine sediments. *Chemosphere,* 40(1), pp.3-6.

Gao, B., Yap, P.S., Lim, T.M. and Lim, T. 2011. Adsorption-photocatalytic degradation of Acid Red 88 by supported TiO_2: Effect of activated carbon support and aqueous anions. *Chemical Engineering Journal,* 171(3), pp.1098-1107.

Gao, Y., Liu, H. and Ma, M. 2007. Preparation and photocatalytic behavior of TiO_2-carbon nanotube hybrid catalyst for acridine dye decomposition. *Reaction Kinetics and Catalysis Letters,* 90(1), pp.11-18.

Gernjak, W., Maldonado, M.I., Malato, S., Cáceres, J., Krutzler, T., Glaser, A. and Bauer, R. 2004. Pilot-plant treatment of olive mill wastewater (OMW) by solar TiO_2 photocatalysis and solar photo-Fenton. *Solar Energy,* 77(5), pp.567-572.

Gibs, J., Stackelberg, P.E., Furlong, E.T., Meyer, M., Zaugg, S.D. and Lippincott, R.L. 2007. Persistence of pharmaceuticals and other organic compounds in chlorinated drinking water as a function of time. *Science of the Total Environment,* 373(1), pp.240-249.

Gimeno, O., Plucinski, P., Kolaczkowski, S.T., Rivas, F.J. and Alvarez, P.M. 2003. Removal of the Herbicide MCPA by Commercial Activated Carbons: Equilibrium, Kinetics, and Reversibility. *Industrial & Engineering Chemistry Research,* 42(5), pp.1076-1086.

Gogate, P.R. and Pandit, A.B. 2004. A review of imperative technologies for wastewater treatment I: oxidation technologies at ambient conditions. *Advances in Environmental Research,* 8(3-4), pp.501-551.

Grover, D.P., Zhou, J.L., Frickers, P.E. and Readman, J.W. 2011. Improved removal of estrogenic and pharmaceutical compounds in sewage effluent by full scale granular activated carbon: Impact on receiving river water. *Journal of Hazardous Materials,* 185(2–3), pp.1005-1011.

Guillard, C., Debayle, D., Gagnaire, A., Jaffrezic, H. and Herrmann, J. 2004. Physical properties and photocatalytic efficiencies of TiO_2 films prepared by PECVD and sol–gel methods. *Materials Research Bulletin*, 39(10), pp.1445-1458.

Gültekin, I. and Ince, N.H. 2007. Synthetic endocrine disruptors in the environment and water remediation by advanced oxidation processes. *Journal of Environmental Management*, 85(4), pp.816-832.

Hall, K.R., Eagleton, L.C., Acrivos, A. and Vermeulen, T. 1966. Pore- and Solid-Diffusion Kinetics in Fixed-Bed Adsorption under Constant-Pattern Conditions. *Industrial & Engineering Chemistry Fundamentals*, 5(2), pp.212-223.

Hameed, B.H. 2009. Spent tea leaves: A new non-conventional and low-cost adsorbent for removal of basic dye from aqueous solutions. *Journal of Hazardous Materials*, 161(2-3), pp.753-759.

Hameed, B.H., Salman, J.M. and Ahmad, A.L. 2009. Adsorption isotherm and kinetic modeling of 2,4-D pesticide on activated carbon derived from date stones. *Journal of Hazardous Materials*, 163(1), pp.121-126.

Hamidin, N., Yu, Q.J. and Connell, D.W. 2008. Human health risk assessment of chlorinated disinfection by-products in drinking water using a probabilistic approach. *Water Research*, 42(13), pp.3263-3274.

Haque, F., Vaisman, E., Langford, C.H. and Kantzas, A. 2005. Preparation and performance of integrated photocatalyst adsorbent (IPCA) employed to degrade model organic compounds in synthetic wastewater. *Journal of Photochemistry and Photobiology A: Chemistry*, 169(1), pp.21-27.

Hassan, M.A., Salem, M.S., Sueliman, M.S. and Najib, N.M. 1997. Characterization of famotidine polymorphic forms. *International Journal of Pharmaceutics*, 149(2), pp.227-232.

He, Z., Yang, S., Ju, Y. and Sun, C. 2009. Microwave photocatalytic degradation of Rhodamine B using TiO_2 supported on activated carbon: Mechanism implication. *Journal of Environmental Sciences*, 21(2), pp.268-272.

Heberer, T. 2002. Occurrence, fate, and removal of pharmaceutical residues in the aquatic environment: a review of recent research data. *Toxicology Letters*, 131(1-2), pp.5-17.

Hegedüs, B., Bod, P., Harsányi, K., Péter, I., Kalman, A. and Parkanyi, L. 1989. Comparison of the polymorphic modifications of famotidine. *Journal of Pharmaceutical and Biomedical Analysis*, 7(5), pp.563-569.

Helmig, E.G., Fettig, J.D., Cordone, L., Schoenberg, T.H., DeMarco, M.J. and Suri, R., P.S. 2005. API Removal from Pharmaceutical Manufacturing Wastewater – Results of Process Development, Pilot-Testing, and Scale-Up. *IN: Proceedings of the Water Environment Federation, WEFTEC 2005.* Water Environment Federation.

Hoffmann, M.R., Martin, S.T., Choi, W. and Bahnemann, D.W. 1995. Environmental Applications of Semiconductor Photocatalysis. *Chemical Reviews*, 95(1), pp.69-96.

Hossain, G.S.M. and McLaughlan, R.G. 2011. Sorption of chlorophenols from aqueous solution by granular activated carbon, filter coal, pine and hardwood. *Environmental Technology*, pp.1-8.

Hou, D., Feng, L., Zhang, J., Dong, S., Zhou, D. and Lim, T. 2012. Preparation, characterization and performance of a novel visible light responsive spherical activated carbon-supported and Er^{3+}:$YFeO_3$-doped TiO_2 photocatalyst. *Journal of Hazardous Materials*, 199–200(0), pp.301-308.

Hou, Y., Qu, J., Zhao, X., Lei, P., Wan, D. and Huang, C.P. 2009. Electro-photocatalytic degradation of acid orange II using a novel TiO_2/ACF photoanode. *Science of the Total Environment,* 407(7), pp.2431-2439.

Hrudey, S.E. 2009. Chlorination disinfection by-products, public health risk tradeoffs and me. *Water Research,* 43(8), pp.2057-2092.

Hu, L., Flanders, P.M., Miller, P.L. and Strathmann, T.J. 2007. Oxidation of sulfamethoxazole and related antimicrobial agents by TiO_2 photocatalysis. *Water Research,* 41(12), pp.2612-2626.

Huang, D., Miyamoto, Y., Ding, J., Gu, J., Zhu, S., Liu, Q., Fan, T., Guo, Q. and Zhang, D. 2011a. A new method to prepare high-surface-area N–TiO_2/activated carbon. *Materials Letters,* 65(2), pp.326-328.

Huang, D., Miyamoto, Y., Matsumoto, T., Tojo, T., Fan, T., Ding, J., Guo, Q. and Zhang, D. 2011b. Preparation and characterization of high-surface-area TiO_2/activated carbon by low-temperature impregnation. *Separation and Purification Technology,* 78(1), pp.9-15.

Huang, M., Xu, C., Wu, Z., Huang, Y., Lin, J. and Wu, J. 2008. Photocatalytic discolorization of methyl orange solution by Pt modified TiO_2 loaded on natural zeolite. *Dyes and Pigments,* 77(2), pp.327-334.

Huerta-Fontela, M., Galceran, M.T. and Ventura, F. 2011. Occurrence and removal of pharmaceuticals and hormones through drinking water treatment. *Water Research,* 45(3), pp.1432-1442.

Hurum, D.C., Agrios, A.G., Gray, K.A., Rajh, T. and Thurnauer, M.C. 2003. Explaining the Enhanced Photocatalytic Activity of Degussa P25 Mixed-Phase TiO_2 Using EPR. *The Journal of Physical Chemistry B,* 107(19), pp.4545-4549.

Inagaki, M., Nonaka, M., Kojin, F., Tsumura, T. and Toyoda, M. 2006. Cyclic Performance of Carbon-Coated TiO_2 for Photocatalytic Activity of Methylene Blue Decomposition . *Environmental Technology,* 27(5), pp.521-528.

Jankowska, H., Swiatkowski, A. and Choma, J. 1991. *Active Carbon.* Market Cross House, Cooper Street, Chichester, West Sussex, PO19 1EB, England: Ellis Horwood Limited.

Janus, M., Inagaki, M., Tryba, B., Toyoda, M. and Morawski, A.W. 2006. Carbon-modified TiO_2 photocatalyst by ethanol carbonisation. *Applied Catalysis B: Environmental,* 63(3-4), pp.272-276.

Jia, B., Duan, L., Ma, C. and Wang, C. 2007. Characterization of TiO_2 Loaded on Activated Carbon Fibers and Its Photocatalytic Reactivity. *Chinese Journal of Chemistry,* 25(4), pp.553-557.

Jin, Y., Wu, M., Zhao, G. and Li, M. 2011. Photocatalysis-enhanced electrosorption process for degradation of high-concentration dye wastewater on TiO_2/carbon aerogel. *Chemical Engineering Journal,* 168(3), pp.1248-1255.

Jo, W.K., Shin, S.H. and Hwang, E.S. 2011. Removal of dimethyl sulfide utilizing activated carbon fiber-supported photocatalyst in continuous-flow system. *Journal of Hazardous Materials,* 191(1–3), pp.234-239.

Jo, W. and Yang, C. 2009. Granular-activated carbon adsorption followed by annular-type photocatalytic system for control of indoor aromatic compounds. *Separation and Purification Technology,* 66(3), pp.438-442.

Joakim Larsson, D.G. and Fick, J. 2009. Transparency throughout the production chain—a way to reduce pollution from the manufacturing of pharmaceuticals? *Regulatory Toxicology and Pharmacology,* 53(3), pp.161-163.

Kabir, M.F., Vaisman, E., Langford, C.H. and Kantzas, A. 2006. Effects of hydrogen peroxide in a fluidized bed photocatalytic reactor for wastewater purification. *Chemical Engineering Journal,* 118(3), pp.207-212.

Kakinoki, K., Yamane, K., Teraoka, R., Otsuka, M. and Matsuda, Y. 2004. Effect of relative humidity on the photocatalytic activity of Titanium dioxide and photostability of famotidine. *Journal of Pharmaceutical Sciences,* 93(3), pp.582-589.

Karimi-jashni, A. and Narbaitz, R.M. 1997. Impact of pH on the adsorption and desorption kinetics of 2-nitrophenol on activated carbons. *Water Research,* 31(12), pp.3039-3044.

Karpova, T., Preis, S., Kallas, J. and Torres, A. 2007. Selective photocatalytic oxidation of steroid estrogens in presence of saccharose and ethanol as co-pollutants. *Environmental Chemistry Letters,* 5(4), pp.219-224.

Kasprzyk-Hordern, B., Dinsdale, R.M. and Guwy, A.J. 2009. Illicit drugs and pharmaceuticals in the environment – Forensic applications of environmental data. Part 1: Estimation of the usage of drugs in local communities. *Environmental Pollution,* 157(6), pp.1773-1777.

Kavitha, V. and Palanivelu, K. 2004. The role of ferrous ion in Fenton and photo-Fenton processes for the degradation of phenol. *Chemosphere,* 55(9), pp.1235-1243.

Keane, D., Basha, S., Nolan, K., Morrissey, A., Oelgemöller, M. and Tobin, J. 2010. Photodegradation of Famotidine by Integrated Photocatalytic Adsorbent (IPCA) and Kinetic Study. *Catalysis Letters,* 144(2), pp.300-308.

Khan, A.Y. 2002. *Titanium Dioxide Coated Activated Carbon: A Regenerative Technology For Water Recovery.* Master Of Engineering. Univ Of Florida.

Khetan, S.K. and Collins, T.J. 2007. Human Pharmaceuticals in the Aquatic Environment: A Challenge to Green Chemistry. *Chemical Reviews,* 107(6), pp.2319-2364.

Kim, C.H., Kim, B. and Yang, K.S. 2011. Visible light-induced photocatalytic activity of Ag-containing TiO_2/carbon nanofibers composites. *Synthetic Metals,* 161(11-12), pp.1068-1072.

Kim, S., Ngo, H.H., Shon, H.K. and Vigneswaran, S. 2008. Adsorption and photocatalysis kinetics of herbicide onto titanium oxide and powdered activated carbon. *Separation and Purification Technology,* 58(3), pp.335-342.

Kim, T.Y., Lee, Y., Park, K., Kim, S.J. and Cho, S.Y. 2005. A study of photocatalysis of TiO_2 coated onto chitosan beads and activated carbon. *Research on Chemical Intermediates,* 31(4), pp.343-358.

Klamerth, N., Miranda, N., Malato, S., Agüera, A., Fernández-Alba, A.R., Maldonado, M.I. and Coronado, J.M. 2009. Degradation of emerging contaminants at low concentrations in MWTPs effluents with mild solar photo-Fenton and TiO_2. *Catalysis Today,* 144(1-2), pp.124-130.

Kostedt, W.L., Drwiega, J., Mazyck, D.W., Lee, S., Sigmund, W., Wu, C. and Chadik, P. 2005. Magnetically Agitated Photocatalytic Reactor for Photocatalytic Oxidation of Aqueous Phase Organic Pollutants. *Environmental Science & Technology,* 39(20), pp.8052-8056.

Kubo, M., Fukuda, H., Chua, X.J. and Yonemoto, T. 2007. Kinetics of Ultrasonic Degradation of Phenol in the Presence of Composite Particles of Titanium Dioxide and Activated Carbon. *Industrial & Engineering Chemistry Research,* 46(3), pp.699-704.

Kubo, M., Matsuoka, K., Takahashi, A., Shibasaki-Kitakawa, N. and Yonemoto, T. 2005. Kinetics of ultrasonic degradation of phenol in the presence of TiO_2 particles. *Ultrasonics Sonochemistry,* 12(4), pp.263-269.

Kumar, A., Kumar, S. and Kumar, S. 2003. Adsorption of resorcinol and catechol on granular activated carbon: Equilibrium and kinetics. *Carbon,* 41(15), pp.3015-3025.

Kumar, K.V., Porkodi, K. and Rocha, F. 2008. Comparison of various error functions in predicting the optimum isotherm by linear and non-linear regression analysis for the sorption of basic red 9 by activated carbon. *Journal of Hazardous Materials,* 150(1), pp.158-165.

Kumar, P.M., Badrinarayanan, S. and Sastry, M. 2000. Nanocrystalline TiO_2 studied by optical, FTIR and X-ray photoelectron spectroscopy: correlation to presence of surface states. *Thin Solid Films,* 358(1-2), pp.122-130.

Kun, R., Mogyorósi, K. and Dékány, I. 2006. Synthesis and structural and photocatalytic properties of TiO_2/montmorillonite nanocomposites. *Applied Clay Science,* 32(1-2), pp.99-110.

Kundu, S. and Gupta, A.K. 2006. Arsenic adsorption onto iron oxide-coated cement (IOCC): Regression analysis of equilibrium data with several isotherm models and their optimization. *Chemical Engineering Journal,* 122(1-2), pp.93-106.

Lacey, C., McMahon, G., Bones, J., Barron, L., Morrissey, A. and Tobin, J.M. 2008. An LC–MS method for the determination of pharmaceutical compounds in wastewater treatment plant influent and effluent samples. *Talanta,* 75(4), pp.1089-1097.

Langmuir, I. 1916. The Constitution and Fundamental Properties of Solids and Liquids. Part I. Solids. *Journal of the American Chemical Society,* 38(11), pp.2221-2295.

Lataye, D.H., Mishra, I.M. and Mall, I.D. 2008. Adsorption of 2-picoline onto bagasse fly ash from aqueous solution. *Chemical Engineering Journal,* 138(1-3), pp.35-46.

Leary, R. and Westwood, A. 2011. Carbonaceous nanomaterials for the enhancement of TiO_2 photocatalysis. *Carbon,* 49(3), pp.741-772.

Lee, S. 2004. *Photocatalytic Nanocomposites Based On TiO_2 And Carbon Nanotubes.* PhD. University of Florida.

Lee, D., Kim, S., Cho, I., Kim, S. and Kim, S. 2004a. Photocatalytic oxidation of microcystin-LR in a fluidized bed reactor having TiO_2-coated activated carbon. *Separation and Purification Technology,* 34(1-3), pp.59-66.

Lee, D., Kim, S., Kim, S., Chung, I. and Kim, S. 2004b. Photocatalytic oxidation of microcystin-LR with TiO_2-coated activated carbon. *Chemical Engineering Journal,* 102(1), pp.93-98.

Lee, K.W., Kayser, S.R., Hongo, R.H., Tseng, Z.H. and Scheinman, M.M. 2004c. Famotidine and long QT syndrome. *The American Journal of Cardiology,* 93(10), pp.1325-1327.

Lee, Y., Chang, K., Hu, C. and Lin, K. 2010. Synthesis of activated carbon-surrounded and carbon-doped anatase TiO_2 nanocomposites. *Journal of Materials Chemistry,* 20(27), pp.5682-5688.

Lever,John. 2010. E-mail correspondance from Jacobi Carbons. Personal Communication.

Li Puma, G., Bono, A., Krishnaiah, D. and Collin, J.G. 2008. Preparation of titanium dioxide photocatalyst loaded onto activated carbon support using chemical vapor deposition: A review paper. *Journal of Hazardous Materials,* 157(2-3), pp.209-219.

Li, F., Yuasa, A., Ebie, K. and Azuma, Y. 2003. Microcolumn test and model analysis of activated carbon adsorption of dissolved organic matter after precoagulation: effects of pH and pore size distribution. *Journal of Colloid and Interface Science,* 262(2), pp.331-341.

Li, Y., Chen, J., Liu, J., Ma, M., Chen, W. and Li, L. 2010. Activated carbon supported TiO_2-photocatalysis doped with Fe ions for continuous treatment of dye wastewater in a dynamic reactor. *Journal of Environmental Sciences,* 22(8), pp.1290-1296.

Li, Y., Ma, M., Wang, X. and Wang, X. 2008a. Inactivated properties of activated carbon-supported TiO_2 nanoparticles for bacteria and kinetic study. *Journal of Environmental Sciences,* 20(12), pp.1527-1533.

Li, Y., Sun, S., Ma, M., Ouyang, Y. and Yan, W. 2008b. Kinetic study and model of the photocatalytic degradation of rhodamine B (RhB) by a TiO_2-coated activated carbon catalyst: Effects of initial RhB content, light intensity and TiO_2 content in the catalyst. *Chemical Engineering Journal,* 142(2), pp.147-155.

Li, Y., Zhang, S., Yu, Q. and Yin, W. 2007. The effects of activated carbon supports on the structure and properties of TiO_2 nanoparticles prepared by a sol–gel method. *Applied Surface Science,* 253(23), pp.9254-9258.

Li, Y., Li, X., Li, J. and Yin, J. 2006. Photocatalytic degradation of methyl orange by TiO_2-coated activated carbon and kinetic study. *Water Research,* 40(6), pp.1119-1126.

Li, Y., Li, X., Li, J. and Yin, J. 2005. Photocatalytic degradation of methyl orange in a sparged tube reactor with TiO_2-coated activated carbon composites. *Catalysis Communications,* 6(10), pp.650-655.

Li, Y., Chen, W. and Li, L. 2011. Effects of Surface Areas and Adsorption Strength on the Photoactivity and Decomposition Kinetics of Acid Red 27 over TiO_2-Coated/Activated Carbon Composites. *Acta Physico -Chimica Sinica,* 27(07), pp.1751-1756.

Liang, C., Dai, S. and Guiochon, G. 2003. A Graphitized-Carbon Monolithic Column. *Analytical Chemistry,* 75(18), pp.4904-4912.

Lim, J. and Okada, M. 2005. Regeneration of granular activated carbon using ultrasound. *Ultrasonics Sonochemistry,* 12(4), pp.277-282.

Lim, T., Yap, P., Srinivasan, M. and Fane, A.G. 2011. TiO_2/AC Composites for Synergistic Adsorption-Photocatalysis Processes: Present Challenges and Further Developments for Water Treatment and Reclamation. *Critical Reviews in Environmental Science and Technology,* 41(13), pp.1173-1230.

Liu, G., Zhang, X., Talley, J.W., Neal, C.R. and Wang, H. 2008. Effect of NOM on arsenic adsorption by TiO_2 in simulated As(III)-contaminated raw waters. *Water Research,* 42(8–9), pp.2309-2319.

Liu, J., Yang, R. and Li, S. 2006. Preparation and application of efficient TiO_2/ACFs photocatalyst. *Journal of Environmental Sciences,* 18(5), pp.979-982.

Liu, L.F., Zhang, P.H. and Yang, F.L. 2010. Adsorptive removal of 2,4-DCP from water by fresh or regenerated chitosan/ACF/TiO_2 membrane. *Separation and Purification Technology,* 70(3), pp.354-361.

Liu, L., Chen, F. and Yang, F. 2009. Stable photocatalytic activity of immobilized Fe^0/TiO_2/ACF on composite membrane in degradation of 2,4-dichlorophenol. *Separation and Purification Technology,* 70(2), pp.173-178.

Liu, S.X., Chen, X.Y. and Chen, X. 2007a. A TiO_2/AC composite photocatalyst with high activity and easy separation prepared by a hydrothermal method. *Journal of Hazardous Materials,* 143(1-2), pp.257-263.

Liu, Y., Yang, S., Hong, J. and Sun, C. 2007b. Low-temperature preparation and microwave photocatalytic activity study of TiO_2-mounted activated carbon. *Journal of Hazardous Materials,* 142(1-2), pp.208-215.

Lookchem, 22 August 2012. *Lookchem-Cimetidine* [Online]. Available from: http://www.lookchem.com/Cimetidine/ [Accessed 8/22 2012].

Lu, M., Chen, J. and Chang, K. 1999. Effect of adsorbents coated with titanium dioxide on the photocatalytic degradation of propoxur. *Chemosphere,* 38(3), pp.617-627.

Maekawa, K., Chiyoda, O., Ohshiro, S., Okada, S., Anpo, M. and Yamashita, H. 2006. Photocatalytic degradation of organic pollutants diluted in water using TiO_2 loaded on fluoride-modified hydrophobic mesoporous silica. *Comptes Rendus Chimie,* 9(5-6), pp.817-821.

Mahadwad, O.K., Parikh, P.A., Jasra, R.V. and Patil, C. 2011. Photocatalytic degradation of reactive black-5 dye using TiO2-impregnated activated carbon. *Environmental Technology,* 33(3), pp.307-312.

Mahmoodi, N.M., Arami, M. and Zhang, J. 2011. Preparation and photocatalytic activity of immobilized composite photocatalyst (titania nanoparticle/activated carbon). *Journal of Alloys and Compounds,* 509(14), pp.4754-4764.

Malato, S., Blanco, J., Vidal, A. and Richter, C. 2002. Photocatalysis with solar energy at a pilot-plant scale: an overview. *Applied Catalysis B: Environmental,* 37(1), pp.1-15.

Maniscalco, M., Singh-Franco, D., Wolowich, W.R. and Torres-Colón, R. 2006. Solifenacin succinate for the treatment of symptoms of overactive bladder. *Clinical Therapeutics,* 28(9), pp.1247-1272.

Markandya, A., Taylor, T., Longo, A., Murty, M.N., Murty, S. and Dhavala, K. 2008. Counting the cost of vulture decline—An appraisal of the human health and other benefits of vultures in India. *Ecological Economics,* 67(2), pp.194-204.

Marsh, H. and Rodríguez-Reinoso, F. ,2006a. Chapter 9 - Production and Reference Material *IN:* Marsh, H. and Rodríguez-Reinoso, F. (eds.) *Activated Carbon.* Oxford Elsevier Science Ltd, pp.454-508.

Marsh, H. and Rodríguez-Reinoso, F. ,2006b. Introduction to the Scope of the Text *IN:* Marsh, H. and Rodríguez-Reinoso, F. (eds.) *Activated Carbon.* Oxford Elsevier Science Ltd, pp.1-12.

Marsh, H. and Rodríguez-Reinoso, F. ,2006c. Chapter 2 - Activated Carbon (Origins) *IN:* Marsh, H. and Rodríguez-Reinoso, F. (eds.) *Activated Carbon.* Oxford Elsevier Science Ltd, pp.13-86.

Marsh, H. and Rodríguez-Reinoso, F. ,2006d. Chapter 4 - Characterization of Activated Carbon *IN:* Anonymous*Activated Carbon.* Oxford Elsevier Science Ltd, pp.143-242.

Matos, J., Laine, J., Herrmann, J.M., Uzcategui, D. and Brito, J.L. 2007. Influence of activated carbon upon titania on aqueous photocatalytic consecutive runs of phenol photodegradation. *Applied Catalysis B: Environmental,* 70(1-4), pp.461-469.

Matos, J., Laine, J. and Herrmann, J.M. 1999. Association of activated carbons of different origins with titania in the photocatalytic purification of water. *Carbon,* 37(11), pp.1870-1872.

Matos, J., Laine, J. and Herrmann, J. 1998. Synergy effect in the photocatalytic degradation of phenol on a suspended mixture of titania and activated carbon. *Applied Catalysis B: Environmental,* 18(3-4), pp.281-291.

Matsushita, Y., Ichimura, T., Ohba, N., Kumada, S., Sakeda, K., Suzuki, T., Tanibata, H. and Murata, T. 2007. Recent progress on photoreactions in microreactors. *Pure and Applied Chemistry,* 79(11), pp.1959-1968.

Mazyck, D.W. and Cannon, F.S. 2000. Overcoming calcium catalysis during the thermal reactivation of granular activated carbon: Part I. Steam-curing plus ramped-temperature N_2 treatment. *Carbon,* 38(13), pp.1785-1799.

Ménesi, J., Körösi, L., Bazsó, É., Zöllmer, V., Richardt, A. and Dékány, I. 2008. Photocatalytic oxidation of organic pollutants on titania–clay composites. *Chemosphere,* 70(3), pp.538-542.

Mills, A. and Le Hunte, S. 1997. An overview of semiconductor photocatalysis. *Journal of Photochemistry and Photobiology A: Chemistry,* 108(1), pp.1-35.

Mills, L.J. and Chichester, C. 2005. Review of evidence: Are endocrine-disrupting chemicals in the aquatic environment impacting fish populations? *Science of the Total Environment,* 343(1-3), pp.1-34.

Mo, D. and Ye, D. 2009. Surface study of composite photocatalyst based on plasma modified activated carbon fibers with TiO_2. *Surface and Coatings Technology,* 203(9), pp.1154-1160.

Mo, S. and Ching, W.Y. 1995. Electronic and optical properties of three phases of titanium dioxide: Rutile, anatase, and brookite. *Physical Review B,* 51(19), pp.13023-13032.

Mohan, D. and Singh, K.P. 2002. Single- and multi-component adsorption of cadmium and zinc using activated carbon derived from bagasse—an agricultural waste. *Water Research,* 36(9), pp.2304-2318.

Molinari, R., Caruso, A., Argurio, P. and Poerio, T. 2008. Degradation of the drugs Gemfibrozil and Tamoxifen in pressurized and de-pressurized membrane photoreactors using suspended polycrystalline TiO_2 as catalyst. *Journal of Membrane Science,* 319(1-2), pp.54-63.

Mompelat, S., Le Bot, B. and Thomas, O. 2009. Occurrence and fate of pharmaceutical products and by-products, from resource to drinking water. *Environment International,* 35(5), pp.803-814.

Moreno-Castilla, C. 2004. Adsorption of organic molecules from aqueous solutions on carbon materials. *Carbon,* 42(1), pp.83-94.

Mounir, B., Pons, M.N., Zahraa, O., Yaacoubi, A. and Benhammou, A. 2007. Discoloration of a red cationic dye by supported TiO_2 photocatalysis. *Journal of Hazardous Materials,* 148(3), pp.513-520.

Mozia, S., Tomaszewska, M. and Morawski, A.W. 2007a. Photocatalytic membrane reactor (PMR) coupling photocatalysis and membrane distillation—Effectiveness of removal of three azo dyes from water. *Catalysis Today,* 129(1-2), pp.3-8.

Mozia, S., Toyoda, M., Inagaki, M., Tryba, B. and Morawski, A.W. 2007b. Application of carbon-coated TiO_2 for decomposition of methylene blue in a photocatalytic membrane reactor. *Journal of Hazardous Materials,* 140(1-2), pp.369-375.

Muranaka, C.T., Julcour, C., Wilhelm, A., Delmas, H. and Nascimento, C.A.O. 2010. Regeneration of Activated Carbon by (Photo)-Fenton Oxidation. *Industrial & Engineering Chemistry Research,* 49(3), pp.989-995.

Murphy, S. 2009. *Photocatalytic Degradation of Pharmaceuticals in Aqueous Solutions.* Transfer thesis. DCU.

Nagaoka, S., Hamasaki, Y., Ishihara, S., Nagata, M., Iio, K., Nagasawa, C. and Ihara, H. 2002. Preparation of carbon/TiO_2 microsphere composites from cellulose/TiO_2 microsphere composites and their evaluation. *Journal of Molecular Catalysis A: Chemical,* 177(2), pp.255-263.

Nevskaia, D.M., Santianes, A., Muñoz, V. and Guerrero-Ruíz, A. 1999. Interaction of aqueous solutions of phenol with commercial activated carbons: an adsorption and kinetic study. *Carbon,* 37(7), pp.1065-1074.

Neyens, E. and Baeyens, J. 2003. A review of classic Fenton's peroxidation as an advanced oxidation technique. *Journal of Hazardous Materials,* 98(1-3), pp.33-50.

Ni, M., Leung, M.K.H., Leung, D.Y.C. and Sumathy, K. 2007. A review and recent developments in photocatalytic water-splitting using TiO_2 for hydrogen production. *Renewable and Sustainable Energy Reviews,* 11(3), pp.401-425.

Nieuwenhuijsen, M.J., Toledano, M.B., Eaton, N.E., Fawell, J. and Elliott, P. 2000. Chlorination disinfection byproducts in water and their association with adverse reproductive outcomes: a review. *Occupational and Environmental Medicine,* 57(2), pp.73-85.

Oaks, J.L., Gilbert, M., Virani, M.Z., Watson, R.T., Meteyer, C.U., Rideout, B.A., Shivaprasad, H.L., Ahmed, S., Iqbal Chaudhry, M.J., Arshad, M., Mahmood, S., Ali, A. and Ahmed Khan, A. 2004. Diclofenac residues as the cause of vulture population decline in Pakistan. *Nature,* 427(6975), pp.630-633.

Ocampo-Pérez, R., Sánchez-Polo, M., Rivera-Utrilla, J. and Leyva-Ramos, R. 2011. Enhancement of the catalytic activity of TiO_2 by using activated carbon in the photocatalytic degradation of cytarabine. *Applied Catalysis B: Environmental,* 104(1-2), pp.177-184.

Ochuma, I.J., Osibo, O.O., Fishwick, R.P., Pollington, S., Wagland, A., Wood, J. and Winterbottom, J.M. 2007. Three-phase photocatalysis using suspended titania and titania supported on a reticulated foam monolith for water purification. *Catalysis Today,* 128(1-2), pp.100-107.

O'Dwyer,R. (2011) Development of titanium dioxide composites for the removal of pesticides from water and wastewater using photocatalysis. Transfer Thesis, Dublin City University.

Oh, W., Zhang, F., Chen, M., Lee, Y. and Ko, W. 2009. Characterization and relative photonic efficiencies of a new Fe-ACF/TiO_2 composite photocatalysts designed for organic dye decomposition. *Journal of Industrial and Engineering Chemistry,* 15(2), pp.190-195.

Ohno, T., Sarukawa, K., Tokieda, K. and Matsumura, M. 2001. Morphology of a TiO_2 Photocatalyst (Degussa, P-25) Consisting of Anatase and Rutile Crystalline Phases. *Journal of Catalysis,* 203(1), pp.82-86.

Olympus Microscopy Resource Center, 06 June 2012. *Non-Coherent Light Sources for Confocal Microscopy* [Online]. Available from: http://www.olympusmicro.com/primer/techniques/confocal/noncoherentsources.html [Accessed 06/06 2012].

Önal, Y. 2006. Kinetics of adsorption of dyes from aqueous solution using activated carbon prepared from waste apricot. *Journal of Hazardous Materials,* 137(3), pp.1719-1728.

Órfão, J.J.M., Silva, A.I.M., Pereira, J.C.V., Barata, S.A., Fonseca, I.M., Faria, P.C.C. and Pereira, M.F.R. 2006. Adsorption of a reactive dye on chemically modified activated carbons—Influence of pH. *Journal of Colloid and Interface Science,* 296(2), pp.480-489.

Oulton, R.L., - Kohn, T. and - Cwiertny, D.M. 2010. Pharmaceuticals and personal care products in effluent matrices: A survey of transformation and removal during wastewater treatment and implications for wastewater management. *Journal of Environmental Monitoring,* 12(11), pp.1956-1978.

Ovenstone, J. and Yanagisawa, K. 1999. Effect of Hydrothermal Treatment of Amorphous Titania on the Phase Change from Anatase to Rutile during Calcination. *Chemistry of Materials,* 11(10), pp.2770-2774.

Parson, S., Jefferson, B. and Christopher, N. ,2007. Sustainable Water: Chemical Science Priorities Summary Report *IN:* Hardy, J. (ed.) London Royal Society of Chemistry,

Peel, R.G. and Benedek, A. 1980. Attainment of equilibrium in activated carbon isotherm studies. *Environmental Science & Technology,* 14(1), pp.66-71.

Peralta-Hernández, J.M., Manríquez, J., Meas-Vong, Y., Rodríguez, F.J., Chapman, T.W., Maldonado, M.I. and Godínez, L.A. 2007. Photocatalytic properties of nano-structured TiO_2-carbon films obtained by means of electrophoretic deposition. *Journal of Hazardous Materials,* 147(1-2), pp.588-593.

Pfeffer, R., Dave, R.N., Wei, D. and Ramlakhan, M. 2001. Synthesis of engineered particulates with tailored properties using dry particle coating. *Powder Technology,* 117(1-2), pp.40-67.

Phillips, P.J., Smith, S.G., Kolpin, D.W., Zaugg, S.D., Buxton, H.T., Furlong, E.T., Esposito, K. and Stinson, B. 2010. Pharmaceutical Formulation Facilities as Sources of Opioids and Other Pharmaceuticals to Wastewater Treatment Plant Effluents. *Environmental Science & Technology,* 44(13), pp.4910-4916.

Purkait, M.K., Maiti, A., DasGupta, S. and De, S. 2007. Removal of congo red using activated carbon and its regeneration. *Journal of Hazardous Materials,* 145(1-2), pp.287-295.

Putra, E.K., Pranowo, R., Sunarso, J., Indraswati, N. and Ismadji, S. 2009. Performance of activated carbon and bentonite for adsorption of amoxicillin from wastewater: Mechanisms, isotherms and kinetics. *Water Research,* 43(9), pp.2419-2430.

Qourzal, S., Assabbane, A. and Ait-Ichou, Y. 2004. Synthesis of TiO_2 via hydrolysis of titanium tetraisopropoxide and its photocatalytic activity on a suspended mixture with activated carbon in the degradation of 2-naphthol. *Journal of Photochemistry and Photobiology A: Chemistry,* 163(3), pp.317-321.

Radjenović, J., Petrović, M. and Barceló, D. 2009. Fate and distribution of pharmaceuticals in wastewater and sewage sludge of the conventional activated sludge (CAS) and advanced membrane bioreactor (MBR) treatment. *Water Research,* 43(3), pp.831-841.

Ravichandran, L., Selvam, K. and Swaminathan, M. 2010. Highly efficient activated carbon loaded TiO_2 for photo defluoridation of pentafluorobenzoic acid. *Journal of Molecular Catalysis A: Chemical,* 317(1-2), pp.89-96.

Redlich, O. and Peterson, D.L. 1959. A Useful Adsorption Isotherm. *The Journal of Physical Chemistry,* 63(6), pp.1024-1024.

Rengaraj, S., Moon, S., Sivabalan, R., Arabindoo, B. and Murugesan, V. 2002. Agricultural solid waste for the removal of organics: adsorption of phenol from water and wastewater by palm seed coat activated carbon. *Waste Management,* 22(5), pp.543-548.

Rizzo, L., Meric, S., Kassinos, D., Guida, M., Russo, F. and Belgiorno, V. 2009. Degradation of diclofenac by TiO_2 photocatalysis: UV absorbance kinetics and process evaluation through a set of toxicity bioassays. *Water Research,* 43(4), pp.979-988.

Rodríguez-Reinoso, F. and Molina-Sabio, M. 1998. Textural and chemical characterization of microporous carbons. *Advances in Colloid and Interface Science,* 76-77pp.271-294.

Roeges, N.P.G. 1994. *A Guide to the Complete Interpretation of Infrared Spectra of Organic Structures.* Chichester: John Wiley & Sons, Ltd.

Rolando M.A., R. 2007. *Adsorption and Diffusion in Nanoporous Materials.* First Edition ed. Boca Raton, Florida USA: CRC Press.

Rouquerol, F., Rouquerol, J. and Sing, K. 1999. *Adsorption by Powders and Porous Solids Principles, Methodology and Applications.* 1st ed. London: ACADEMIC PRESS.

Rouquerol, J., Avnir, D., Fairbridge, C.W., Everett, D.H., Haynes, J.M., Pernicone, N., Ramsay, J.D.F., Sing, K.S.W. and Unger, K.K. 1994. Recommendations for the characterization of porous solids (Technical Report). *Pure and Applied Chemistry,* 66(8), pp.1739-1758.

Ryu, J. and Choi, W. 2008. Substrate-Specific Photocatalytic Activities of TiO_2 and Multiactivity Test for Water Treatment Application. *Environmental Science & Technology,* 42(1), pp.294-300.

Saepurahman, Abdullah, M.A. and Chong, F.K. 2010. Preparation and characterization of tungsten-loaded titanium dioxide photocatalyst for enhanced dye degradation. *Journal of Hazardous Materials,* 176(1-3), pp.451-458.

SEN Lights Corporation 25 August 2011. *Low-Pressure Mercury Lamps* [Online]. Available from: http://www.senlights.com/lamp/lplamp/lamp.htm [Accessed 05/26 2012].

Serpone, N. 2006. Is the Band Gap of Pristine TiO_2 Narrowed by Anion- and Cation-Doping of Titanium Dioxide in Second-Generation Photocatalysts? *The Journal of Physical Chemistry B,* 110(48), pp.24287-24293.

Shankar, M.V., Anandan, S., Venkatachalam, N., Arabindoo, B. and Murugesan, V. 2006. Fine route for an efficient removal of 2,4-dichlorophenoxyacetic acid (2,4-D) by zeolite-supported TiO_2. *Chemosphere,* 63(6), pp.1014-1021.

Shen, W., Li, Z. and Liu, Y. 2008. Surface Chemical Functional Groups Modification of Porous Carbon. *Recent Patents on Chemical Engineering,* 1pp.27-40.

Shi, J., Zheng, J., Wu, P. and Ji, X. 2008. Immobilization of TiO_2 films on activated carbon fiber and their photocatalytic degradation properties for dye compounds with different molecular size. *Catalysis Communications,* 9(9), pp.1846-1850.

Shi, J. 2009. Preparation of Fe(III) and Ho(III) co-doped TiO_2 films loaded on activated carbon fibers and their photocatalytic activities. *Chemical Engineering Journal,* 151(1-3), pp.241-246.

Shi, L. and Weng, D. 2008. Highly active mixed-phase TiO_2 photocatalysts fabricated at low temperatureand the correlation between phase compositionand photocatalytic activity. *Journal of Environmental Sciences,* 20(10), pp.1263-1267.

Sirtori, C., Zapata, A., Oller, I., Gernjak, W., Agüera, A. and Malato, S. 2009. Decontamination industrial pharmaceutical wastewater by combining solar photo-Fenton and biological treatment. *Water Research,* 43(3), pp.661-668.

Slimen, H., Houas, A. and Nogier, J.P. 2011. Elaboration of stable anatase TiO_2 through activated carbon addition with high photocatalytic activity under visible light. *Journal of Photochemistry and Photobiology A: Chemistry,* In Press, Accepted Manuscript

Smith, S.J., Stevens, R., Liu, S., Li, G., Navrotsky, A., Boerio-Goates, J. and Woodfield, B.F. 2009. Heat capacities and thermodynamic functions of TiO_2 anatase and rutile: Analysis of phase stability. *American Mineralogist,* 94(2-3), pp.236-243.

Snyder, S.A., Adham, S., Redding, A.M., Cannon, F.S., DeCarolis, J., Oppenheimer, J., Wert, E.C. and Yoon, Y. 2007. Role of membranes and activated carbon in the removal of endocrine disruptors and pharmaceuticals. *Desalination,* 202(1-3), pp.156-181.

Spectroscopy TV 27 May 2012. *LED Measurement Using an Integrating Sphere* [Online]. Available from: http://spectroscopytv.com/2009/02/13/led-measurement-using-an-integrating-sphere/ [Accessed 05/27 2012].

Sreekanth, D., Sivaramakrishna, D., Himabindu, V. and Anjaneyulu, Y. 2009. Thermophilic treatment of bulk drug pharmaceutical industrial wastewaters by using hybrid up flow anaerobic sludge blanket reactor. *Bioresource Technology,* 100(9), pp.2534-2539.

Suman Raj, D.S. and Anjaneyulu, Y. 2005. Evaluation of biokinetic parameters for pharmaceutical wastewaters using aerobic oxidation integrated with chemical treatment. *Process Biochemistry,* 40(1), pp.165-175.

Sun, J., Wang, X., Sun, J., Sun, R., Sun, S. and Qiao, L. 2006. Photocatalytic degradation and kinetics of Orange G using nano-sized Sn(IV)/TiO_2/AC photocatalyst. *Journal of Molecular Catalysis A: Chemical,* 260(1-2), pp.241-246.

Sun, J., Wang, Y., Sun, R. and Dong, S. 2009. Photodegradation of azo dye Congo Red from aqueous solution by the WO_3–TiO_2/activated carbon (AC) photocatalyst under the UV irradiation. *Materials Chemistry and Physics,* 115(1), pp.303-308.

Sun, Q. and Xu, Y. 2010. Evaluating Intrinsic Photocatalytic Activities of Anatase and Rutile TiO_2 for Organic Degradation in Water. *The Journal of Physical Chemistry C,* 114(44), pp.18911-18918.

Tao, Y., Wu, C. and Mazyck, D.W. 2006. Removal of methanol from pulp and paper mills using combined activated carbon adsorption and photocatalytic regeneration. *Chemosphere,* 65(1), pp.35-42.

Taylor, P.J. 2005. Matrix effects: the Achilles heel of quantitative high-performance liquid chromatography–electrospray–tandem mass spectrometry. *Clinical Biochemistry,* 38(4), pp.328-334.

Ternes, T.A., Stumpf, M., Mueller, J., Haberer, K., Wilken, R.-. and Servos, M. 1999. Behavior and occurrence of estrogens in municipal sewage treatment plants — I. Investigations in Germany, Canada and Brazil. *Science of the Total Environment,* 225(1–2), pp.81-90.

Ternes, T.A., Meisenheimer, M., McDowell, D., Sacher, F., Brauch, H., Haist-Gulde, B., Preuss, G., Wilme, U. and Zulei-Seibert, N. 2002. Removal of Pharmaceuticals during Drinking Water Treatment. *Environmental Science & Technology,* 36(17), pp.3855-3863.

Thirumal, J. and Kaliappan, S. 2011. Equilibrium, Kinetic and Thermodynamic behavior of Perchlorate Adsorption Onto the Activated Carbon. *European Journal of Scientific Research,* 64(3), pp.365-376.

Torimoto, T., Okawa, Y., Takeda, N. and Yoneyama, H. 1997. Effect of activated carbon content in TiO_2-loaded activated carbon on photodegradation behaviors of dichloromethane. *Journal of Photochemistry and Photobiology A: Chemistry,* 103(1-2), pp.153-157.

Torimoto, T., Ito, S., Kuwabata, S. and Yoneyama, H. 1996. Effects of Adsorbents Used as Supports for Titanium Dioxide Loading on Photocatalytic Degradation of Propyzamide. *Environmental Science & Technology,* 30(4), pp.1275-1281.

Treschev, S.Y., Chou, P., Tseng, Y., Wang, J., Perevedentseva, E.V. and Cheng, C. 2008. Photoactivities of the visible-light-activated mixed-phase carbon-containing titanium dioxide: The effect of carbon incorporation. *Applied Catalysis B: Environmental,* 79(1), pp.8-16.

Tryba, B., Morawski, A.W. and Inagaki, M. 2003a. A new route for preparation of TiO_2-mounted activated carbon. *Applied Catalysis B: Environmental,* 46(1), pp.203-208.

Tryba, B., Morawski, A.W. and Inagaki, M. 2003b. Application of TiO_2-mounted activated carbon to the removal of phenol from water. *Applied Catalysis B: Environmental,* 41(4), pp.427-433.

Tsumura, T., Kojitani, N., Umemura, H., Toyoda, M. and Inagaki, M. 2002. Composites between photoactive anatase-type TiO_2 and adsorptive carbon. *Applied Surface Science,* 196(1-4), pp.429-436.

Tütem, E., Apak, R. and Ünal, Ç.F. 1998. Adsorptive removal of chlorophenols from water by bituminous shale. *Water Research,* 32(8), pp.2315-2324.

Vaisman, E., Kabir, M., Kantzas, A. and Langford, C. 2005. A fluidized bed photoreactor exploiting a supported photocatalyst with adsorption pre-concentration capacity. *Journal of Applied Electrochemistry,* 35(7), pp.675-681.

Velasco, L.F., Tsyntsarski, B., Petrova, B., Budinova, T., Petrov, N., Parra, J.B. and Ania, C.O. 2010a. Carbon foams as catalyst supports for phenol photodegradation. *Journal of Hazardous Materials,* 184(1-3), pp.843-848.

Velasco, L.F., Parra, J.B. and Ania, C.O. 2010b. Role of activated carbon features on the photocatalytic degradation of phenol. *Applied Surface Science,* 256(17), pp.5254-5258.

Velasco, L.F., Parra, J.B. and Ania, C.O. 2010c. Phenol Adsorption and Photo-oxidation on Porous Carbon/Titania Composites. *Adsorption Science & Technology,* 28(8), pp.727-738.

Verhoeven, J.W. 1996. Glossary Of Terms Used In Photochemistry. *Pure and Applied Chemistry,* 68(12), pp.2223-2286.

Verlicchi, P., Al Aukidy, M. and Zambello, E. 2012. Occurrence of pharmaceutical compounds in urban wastewater: Removal, mass load and environmental risk after a secondary treatment—A review. *Science of the Total Environment,* 429(0), pp.123-155.

Vieno, N.M., HÃ¤rkki, H., Tuhkanen, T. and Kronberg, L. 2007. Occurrence of Pharmaceuticals in River Water and Their Elimination in a Pilot-Scale Drinking Water Treatment Plant. *Environmental Science & Technology,* 41(14), pp.5077-5084.

von Gunten, U. and Hoigne, J. 1994. Bromate Formation during Ozonization of Bromide-Containing Waters: Interaction of Ozone and Hydroxyl Radical Reactions. *Environmental Science & Technology,* 28(7), pp.1234.

Wahi, R.K., Yu, W.W., Liu, Y., Mejia, M.L., Falkner, J.C., Nolte, W. and Colvin, V.L. 2005. Photodegradation of Congo Red catalyzed by nanosized TiO_2. *Journal of Molecular Catalysis A: Chemical,* 242(1-2), pp.48-56.

Wang, C., Deng, Z. and Li, Y. 2001. The Synthesis of Nanocrystalline Anatase and Rutile Titania in Mixed Organic Media. *Inorganic Chemistry,* 40(20), pp.5210-5214.

Wang, C., Lee, C., Lyu, M. and Juang, L. 2008. Photocatalytic degradation of C.I. Basic Violet 10 using TiO_2 catalysts supported by Y zeolite: An investigation of the effects of operational parameters. *Dyes and Pigments,* 76(3), pp.817-824.

Wang, H., Wang, H., Jiang, W. and Li, Z. 2009a. Photocatalytic degradation of 2,4-dinitrophenol (DNP) by multi-walled carbon nanotubes (MWCNTs)/TiO_2 composite in aqueous solution under solar irradiation. *Water Research,* 43(1), pp.204-210.

Wang, R., Fan, K. and Chang, J. 2009b. Removal of acid dye by $ZnFe_2O_4/TiO_2$-immobilized granular activated carbon under visible light irradiation in a recycle liquid–solid fluidized bed. *Journal of the Taiwan Institute of Chemical Engineers,* 40(5), pp.533-540.

Wang, S. and Zhou, S. 2010. Titania deposited on soft magnetic activated carbon as a magnetically separable photocatalyst with enhanced activity. *Applied Surface Science,* 256(21), pp.6191-6198.

Wang, W., Silva, C.G. and Faria, J.L. 2007. Photocatalytic degradation of Chromotrope 2R using nanocrystalline TiO_2/activated-carbon composite catalysts. *Applied Catalysis, B: Environmental,* 70(1-4), pp.470-478.

Wang, X., Hu, Z., Chen, Y., Zhao, G., Liu, Y. and Wen, Z. 2009a. A novel approach towards high-performance composite photocatalyst of TiO_2 deposited on activated carbon. *Applied Surface Science,* 255(7), pp.3953-3958.

Wang, X., Liu, Y., Hu, Z., Chen, Y., Liu, W. and Zhao, G. 2009b. Degradation of methyl orange by composite photocatalysts nano-TiO_2 immobilized on activated carbons of different porosities. *Journal of Hazardous Materials,* 169(1-3), pp.1061-1067.

Watkinson, A.J., Murby, E.J. and Costanzo, S.D. 2007. Removal of antibiotics in conventional and advanced wastewater treatment: Implications for environmental discharge and wastewater recycling. *Water Research,* 41(18), pp.4164-4176.

Wishart, D.S., Knox, C., Guo, A.C., Cheng, D., Shrivastava, S., Tzur, D., Gautam, B. and Hassanali, M. 30/06/2012. *DrugBank: a knowledgebase for drugs, drug actions and drug targets (Famotidine).*[Online]. Available from: http://www.drugbank.ca/drugs/DB00927 [Accessed 07/09 2012].

Wishart, D.S., Knox, C., Guo, A.C., Cheng, D., Shrivastava, S., Tzur, D., Gautam, B. and Hassanali, M. 27/06/2012. *DrugBank: a knowledgebase for drugs, drug actions and drug targets (Solifenacin).*[Online]. Available from: http://www.drugbank.ca/drugs/DB01591 [Accessed 07/09 2012].

Woan, K., Pyrgiotakis, G. and Sigmund, W. 2009. Photocatalytic Carbon-Nanotube-TiO_2 Composites. *Advanced Materials,* 21(21), pp.2233-2239.

Wu, C., Nguyen, J., Cai, M., Ruthkosky, M., Rogers, J., Feng, L., Watano, S. and Yoshida, T. 2003. Surface Enhancement of Al_2O_3 Fiber With Nanosized Al_2O_3 Particles Using A Dry Mechanical Coating Process. *Journal of Engineering Materials and Technology,* 125(2), pp.163-169.

Wu, F., Liu, B., Wu, K. and Tseng, R. 2010. A new linear form analysis of Redlich–Peterson isotherm equation for the adsorptions of dyes. *Chemical Engineering Journal,* 162(1), pp.21-27.

Wu, H., Wang, Q., Yao, Y., Qian, C., Zhang, X. and Wei, X. 2008. Microwave-Assisted Synthesis and Photocatalytic Properties of Carbon Nanotube/Zinc Sulfide Heterostructures. *The Journal of Physical Chemistry C,* 112(43), pp.16779-16783.

Wu, Y., Zhang, J., Xiao, L. and Chen, F. 2010. Properties of carbon and iron modified TiO_2 photocatalyst synthesized at low temperature and photodegradation of acid orange 7 under visible light. *Applied Surface Science,* 256(13), pp.4260-4268.

Wu, Y. and Fassihi, R. 2005. Stability of metronidazole, tetracycline HCl and famotidine alone and in combination. *International Journal of Pharmaceutics,* 290(1-2), pp.1-13.

Xia, X., Jia, Z., Yu, Y., Liang, Y., Wang, Z. and Ma, L. 2007. Preparation of multi-walled carbon nanotube supported TiO_2 and its photocatalytic activity in the reduction of CO_2 with H_2O. *Carbon,* 45(4), pp.717-721.

Xu, D., Huang, Z., Kang, F., Inagaki, M. and Ko, T.-. 2008. Effect of heat treatment on adsorption performance and photocatalytic activity of TiO_2-mounted activated carbon cloths. *Catalysis Today,* 139(1-2), pp.64-68.

Xu, J., Ao, Y., Chen, M., Fu, D. and Yuan, C. 2010. Photocatalytic activity of vanadium-doped titania–activated carbon composite film under visible light. *Thin Solid Films,* 518(15), pp.4170-4174.

Xu, J., Ao, Y., Fu, D. and Yuan, C. 2008. Synthesis of fluorine-doped titania-coated activated carbon under low temperature with high photocatalytic activity under visible light. *Journal of Physics and Chemistry of Solids,* 69(10), pp.2366-2370.

Xue, G., Liu, H., Chen, Q., Hills, C., Tyrer, M. and Innocent, F. 2011. Synergy between surface adsorption and photocatalysis during degradation of humic acid on TiO_2/activated carbon composites. *Journal of Hazardous Materials,* 186(1), pp.765-772.

Xue, Q. and Lu, S. 2008. *Microstructure of ferrospheres in fly ashes: SEM, EDX and ESEM analysis.* Zhejiang University Press, co-published with Springer

Yamabi, S. and Imai, H. 2002. Crystal Phase Control for Titanium Dioxide Films by Direct Deposition in Aqueous Solutions. *Chemistry of Materials,* 14(2), pp.609-614.

Yamashita, H., Kawasaki, S., Yuan, S., Maekawa, K., Anpo, M. and Matsumura, M. 2007. Efficient adsorption and photocatalytic degradation of organic pollutants diluted in water using the fluoride-modified hydrophobic titanium oxide photocatalysts: Ti-containing Beta zeolite and TiO_2 loaded on HMS mesoporous silica. *Catalysis Today,* 126(3-4), pp.375-381.

Yamashita, H., Maekawa, K., Nakao, H. and Anpo, M. 2004. Efficient adsorption and photocatalytic degradation of organic pollutants diluted in water using fluoride-modified hydrophobic mesoporous silica. *Applied Surface Science,* 237(1-4), pp.393-397.

Yan, X., Ohno, T., Nishijima, K., Abe, R. and Ohtani, B. 2006. Is methylene blue an appropriate substrate for a photocatalytic activity test? A study with visible-light responsive titania. *Chemical Physics Letters,* 429(4-6), pp.606-610.

Yanagihara, T., Aoki, T., Soeishi, Y., Iwatsubo, T. and Kamimura, H. 2007. Determination of solifenacin succinate, a novel muscarinic receptor antagonist, and its major metabolite in rat plasma by semi-micro high performance liquid chromatography. *Journal of Chromatography B,* 859(2), pp.241-245.

Yang, H., Liu, L., Yang, F. and Yu, J. 2008. Fibrous TiO_2 prepared by chemical vapor deposition using activated carbon fibers as template via adsorption, hydrolysis and calcinations. *Journal of Zhejiang University - Science A,* 9(7), pp.981-987.

Yang, J., Sliva, A., Banerjee, A., Dave, R.N. and Pfeffer, R. 2005. Dry particle coating for improving the flowability of cohesive powders. *Powder Technology,* 158(1-3), pp.21-33.

Yao, S.H., Jia, Y.F. and Zhao, S.L. 2012. Photocatalytic oxidation and removal of arsenite by titanium dioxide supported on granular activated carbon. *Environmental Technology,* 33(9), pp.983-988.

Yao, S., Li, J. and Shi, Z. 2010. Immobilization of TiO_2 nanoparticles on activated carbon fiber and its photodegradation performance for organic pollutants. *Particuology,* 8(3), pp.272-278.

Yao, Y., Li, G., Ciston, S., Lueptow, R.M. and Gray, K.A. 2008. Photoreactive TiO_2/Carbon Nanotube Composites: Synthesis and Reactivity. *Environmental Science & Technology,* 42(13), pp.4952-4957.

Yap, P. and Lim, T. 2011. Effect of aqueous matrix species on synergistic removal of bisphenol-A under solar irradiation using nitrogen-doped TiO_2/AC composite. *Applied Catalysis B: Environmental,* 101(3-4), pp.709-717.

Yap, P., Lim, T. and Srinivasan, M. 2011. Nitrogen-doped TiO_2/AC bi-functional composite prepared by two-stage calcination for enhanced synergistic removal of hydrophobic pollutant using solar irradiation. *Catalysis Today,* 161(1), pp.46-52.

Yap, P., Lim, T., Lim, M. and Srinivasan, M. 2010. Synthesis and characterization of nitrogen-doped TiO_2/AC composite for the adsorption–photocatalytic degradation of aqueous bisphenol-A using solar light. *Catal Today,* 151(1-2), pp.8-13.

Ye, S., Tian, Q., Song, X. and Luo, S. 2009. Photoelectrocatalytic degradation of ethylene by a combination of TiO_2 and activated carbon felts. *Journal of Photochemistry and Photobiology A: Chemistry,* 208(1), pp.27-35.

Yoneyama, H. and Torimoto, T. 2000. Titanium dioxide/adsorbent hybrid photocatalysts for photodestruction of organic substances of dilute concentrations. *Catal Today,* 58(2-3), pp.133-140.

Yoon, J., Baek, M., Hong, J., Lee, C. and Suh, J. 2012. *Photocatalytic degradation of azo dye using TiO_2 supported on spherical activated carbon.* Springer New York

Yu, Y., Yu, J.C., Chan, C., Che, Y., Zhao, J., Ding, L., Ge, W. and Wong, P. 2005. Enhancement of adsorption and photocatalytic activity of TiO_2 by using carbon nanotubes for the treatment of azo dye. *Applied Catalysis B: Environmental,* 61(1-2), pp.1-11.

Yuan, R., Guan, R., Liu, P. and Zheng, J. 2007. Photocatalytic treatment of wastewater from paper mill by TiO_2 loaded on activated carbon fibers. *Colloids and Surfaces A: Physicochemical and Engineering Aspects,* 293(1-3), pp.80-86.

Yuan, R., Guan, R., Shen, W. and Zheng, J. 2005a. Photocatalytic degradation of methylene blue by a combination of TiO_2 and activated carbon fibers. *Journal of Colloid and Interface Science,* 282(1), pp.87-91.

Yuan, R., Guan, R. and Zheng, J. 2005b. Effect of the pore size of TiO_2-loaded activated carbon fiber on its photocatalytic activity. *Scripta Materialia,* 52(12), pp.1329-1334.

Yuan, R., Zheng, J., Guan, R. and Zhao, Y. 2005c. Surface characteristics and photocatalytic activity of TiO_2 loaded on activated carbon fibers. *Colloids and Surfaces A: Physicochemical and Engineering Aspects,* 254(1-3), pp.131-136.

Yurdakal, S., Loddo, V., Augugliaro, V., Berber, H., Palmisano, G. and Palmisano, L. 2007. Photodegradation of pharmaceutical drugs in aqueous TiO_2 suspensions: Mechanism and kinetics. *Catalysis Today,* 129(1-2), pp.9-15.

Zaleska, A. 2008. Doped-TiO_2: A Review. *Recent Patents on Engineering,* 2pp.157-164.

Zarezade, M., Ghasemi, S. and Gholami, M.R. 2011. *The effect of multiwalled carbon nanotubes and activated carbon on the morphology and photocatalytic activity of TiO_2/C hybrid materials.* The Royal Society of Chemistry

Zhang, F., Nriagu, J.O. and Itoh, H. 2004. Photocatalytic removal and recovery of mercury from water using TiO_2-modified sewage sludge carbon. *Journal of Photochemistry and Photobiology A: Chemistry,* 167(2-3), pp.223-228.

Zhang, W., Zou, L. and Wang, L. 2011a. A novel charge-driven self-assembly method to prepare visible-light sensitive TiO_2/activated carbon composites for dissolved organic compound removal. *Chemical Engineering Journal,* 168(1), pp.485-492.

Zhang, W., Li, Y., Wang, C. and Wang, P. 2011b. Kinetics of heterogeneous photocatalytic degradation of rhodamine B by TiO_2-coated activated carbon: Roles of TiO_2 content and light intensity. *Desalination,* 266(1-3), pp.40-45.

Zhang, X. and Lei, L. 2008. Effect of preparation methods on the structure and catalytic performance of TiO_2/AC photocatalysts. *Journal of Hazardous Materials,* 153(1-2), pp.827-833.

Zhang, X. and Lei, L. 2007. A kinetic model for describing effect of the external surface concentration of TiO_2 on the reactivity of eggshell activated carbon supported TiO_2 photocatalyst. *Chinese Science Bulletin,* 52(24), pp.3339-3345.

Zhang, X., Zhou, M. and Lei, L. 2006. TiO_2 photocatalyst deposition by MOCVD on activated carbon. *Carbon,* 44(2), pp.325-333.

Zhang, X., Zhou, M. and Lei, L. 2005a. Preparation of an Ag–TiO_2 photocatalyst coated on activated carbon by MOCVD. *Materials Chemistry and Physics,* 91(1), pp.73-79.

Zhang, X., Zhou, M. and Lei, L. 2005b. Preparation of photocatalytic TiO_2 coatings of nanosized particles on activated carbon by AP-MOCVD. *Carbon,* 43(8), pp.1700-1708.

Zhang, X., Zhou, M. and Lei, L. 2005c. Enhancing the concentration of TiO_2 photocatalyst on the external surface of activated carbon by MOCVD. *Materials Research Bulletin,* 40(11), pp.1899-1904.

Zhang, X., Wu, F., Wu, X., Chen, P. and Deng, N. 2008. Photodegradation of acetaminophen in TiO_2 suspended solution. *Journal of Hazardous Materials,* 157(2-3), pp.300-307.

Zhang, Y., Zhou, J.L. and Ning, B. 2007. Photodegradation of estrone and 17β-estradiol in water. *Water Research,* 41(1), pp.19-26.

Zhang, Y., Xiong, X., Han, Y., Yuan, H., Deng, S., Xiao, H., Shen, F. and Wu, X. 2010. Application of titanium dioxide-loaded activated carbon fiber in a pulsed discharge reactor for degradation of methyl orange. *Chemical Engineering Journal,* 162(3), pp.1045-1049.

Zhao, J., Yang, L., Li, F., Yu, R. and Jin, C. 2009. Structural evolution in the graphitization process of activated carbon by high-pressure sintering. *Carbon,* 47(3), pp.744-751.

Zhao, W., Bai, Z., Ren, A., Guo, B. and Wu, C. 2010. Sunlight photocatalytic activity of CdS modified TiO_2 loaded on activated carbon fibers. *Applied Surface Science,* 256(11), pp.3493-3498.

Zhou, H. and Smith, D.W. 2002. Advanced technologies in water and wastewater treatment. *Journal of Environmental Engineering and Science,* 1(4), pp.247-264.

Zhu, Z.P., Huang, K.L. and Zhou, Y. 2007. Preparation and Characterization of New Photocatalyst Combined MWCNTs with TiO_2 Nanotubes. *Transactions of Nonferrous Metals Society of China,* 17pp.1117-1121.

Zhu, B. and Zou, L. 2009. Trapping and decomposing of color compounds from recycled water by TiO_2 coated activated carbon. *Journal of Environmental Management,* 90(11), pp.3217-3225.

Zhu, Y., Fu, Y. and Ni, Q. 2011. Preparation and performance of photocatalytic TiO_2 immobilized on palladium-doped carbon fibers. *Applied Surface Science,* 257(6), pp.2275-2280.

Zinner, N., Noe, L., Rasouliyan, L., Marshall, T., Christopher Runken, M. and Seifeldin, R. 2009. Impact of solifenacin on quality of life, medical care use, work productivity, and health utility in the elderly: An exploratory subgroup analysis. *The American Journal of Geriatric Pharmacotherapy*, 7(6), pp.373-382.

Zwiener, C. and Frimmel, F.H. 2000. Oxidative treatment of pharmaceuticals in water. *Water Research*, 34(6), pp.1881-1885.

Appendix A, IPCAs Prepared by Wet Methods

Preparation method	Adsorbent (catalyst loading)	Photocatalyst	Substrate (initial concentration)	Irradiation source	Controls	Notes	Ref
Sol-gel method used to prepare TiO_2 and magnetic particles solution. Impregnated using refluxing and ultrasonication.	Magnetic activated carbon: (PAC containing magnetic magnetite particles). (0.2 g/L)	Anatase TiO_2	X-3B (50 mg/L)	0.25L breaker irradiated with UV: 200W, Visible: halogen 500W lamp	Adsorbent (UV&Vis), no control for the recycle.	The adsorbent shows little photocatalytic action compared to the IPCA. Dark adsorption (30min) of the IPCA is a third higher. Without a dark IPCA control it is impossible to determine if the enhanced X-3B removal (over 80min) is due to photodegradation.	(Ao *et al.*, 2009)
As above.	Magnetic activated carbon (PAC) (1.5g/L)	Anatase TiO_2	Phenol (100 mg/L)	0.5L cylindrical stainless steel photoreactor with a 20W UV lamp (365nm) covered by a quartz glass sleeve.	TiO_2 and P25, no control for recycle.	Without adsorbent controls the photodegradation of the IPCAs could be simple adsorption.	(Ao *et al.*, 2008c)
Preparation methods as above with the exception that some of the samples were calcined at 350 or 450°C in a N_2 atmosphere for 2h.	Magnetic activated carbon (PAC) (0.8 g/L)	Anatase TiO_2	Phenol (100 mg/L)	0.5L glass beaker (containing 400ml solution) covered in silver paper with an 8W UV lamp (365nm).	P25, no control for the recycle.	Dark adsorption stage (1h) not shown suggests that phenol decrease is residual adsorption.	(Ao *et al.*, 2008d)
Separate sol gel methods were used to prepare TiO_2 and magnetic ferrite particles. The ferrite and TiO_2 particles in the sol-gel solution were then applied to the AC using ultrasonication.	Magnetic ferrite activated carbon (PAC) (0.4g/L)	Anatase and rutile (P25 as reference)	Methyl orange (20 mg/L)	0.5L cylindrical glass reactor with a UV lamp (365nm) and circulating water jacket. Aeration: 0.6 L/min	P25, TiO_2 and no control for the recycle. Photolysis not shown	30min dark adsorption time not shown and photodegradation is expressed in % removal at t=0. Without an adsorbent control it is impossible to determine if removal is photocatalytic.	(Wang and Zhou, 2010)
Sol gel method was used to prepare a TiO_2 solution. Impregnation used ultrasonication and dip coating onto glass plates.	PAC coated on a glass plate (not stated)	Anatase TiO_2 (P25 as reference)	4-cholophenol (100 mg/L)	Cylindrical silica reactor (volume not stated) with 200W UV lamp (365nm, 9 mW cm^{-2}).	None, None for recycling	The dark adsorption stage was not shown however if it was added it would suggest that the IPCA performance is mainly adsorption. Linear transform of the kinetic curves is used to claim that the IPCAs worked better but the curves have different starting points so they are not comparable.	(Ao *et al.*, 2008b)

Sol gel method was used to prepare a TiO_2 solution and ultrasonication was used for impregnation.	PAC (1.5g/L)	Anatase TiO_2	Phenol (100 mg/L)	0.5L cylindrical photoreactor with 20W UV lamp, (peak 365nm).	Adsorbent, none for recycle	Adsorbent control: no reduction in phenol after the initial dark adsorption phase. The IPCA removes more phenol from the solution than the TiO_2's however the slope of the degradation curves appears very similar before accounting for the different in substrate concentrations.	(Ao *et al.*, 2008a)
TiO_2 was synthesised using a sol gel method and a "dip coating method" and ultrasonication for impregnation.	GAC (2g/L)	Anatase TiO_2	Phenol (10 mg/L)	0.05L photoreactor excited by electrode-less discharge lamp (EDL) excited by microwave irradiation (254-579nm, output not stated).	None	Extensive characterisation information used to compare solutions prepared with and without microwaves. Looks at the effect of heat treatment but finds no effect.	(Liu *et al.*, 2007b)
As above.	PAC (1.5g/L P25/IPCA, 0.1g/L AC)	Anatase TiO_2	Rhodamine B (RhB) (30 mg/L)	0.05L solution irradiated in a microwave with a MW-EDML (MicroWave-Electrodeless Discharge Mercury Lamp) output not stated.	Photolysis,TiO_2, P25 & adsorbent	40min of dark adsorption not shown 14% of solution removed by P25, 20% by the IPCA and 39% by the smaller quantity of AC suggesting IPCA adsorption is low. Dark IPCA control is not shown. The IPCAs improved performance over P25 could be adsorption.	(He *et al.*, 2009)
TiO_2 prepared using a sol gel method. Impregnation added GAC to this solution, followed by calcination.	GAC (2g/L)	Anatase TiO_2, (P25 as reference)	Methyl orange (50 mg/L)	0.5L cylindrical glass (0.25L solution) reactor inside equipped with an UV lamp (365nm, output not stated) with aeration.	Mixtures of TiO_2 and P25. None for recycling	The most effective IPCA (heat treated) is only marginally more effective than a mixture of P25 and AC suggesting the IPCA is ineffective. Uses pre-saturation but not a dark adsorption phase. The lack of a dark or adsorbent control means it is unclear if the removal is adsorption or photodegradation.	(Wang *et al.*, 2009a)
Sol gel method used to prepare TiO_2 solution. Varying amounts of GAC were added to this solution which underwent hydrothermal treatment at 180°C for 8h. Calcination at 600°C for 2h was the final step in IPCA calcination.	GAC (2g/L)	Anatase TiO_2	Methyl orange (50 mg/L)	0.5L cylindrical glass (0.25L solution) reactor using a central UV lamp (365nm, 300W) with aeration of 0.6 L/min.	Mixture of TiO_2 + AC	Mixture of TiO_2 and AC has mid range performance compared to the other IPCAs. Includes adsorption data that shows adsorption in 60min. No dark adsorption stage after	(Wang *et al.*, 2009b)

						pre-saturation. It is likely that MO removal is slow adsorption after pre-sat as degradation is expressed as C/C_0.	
Sol gel method used to prepare TiO_2. Impregnation using ultrasonication followed by heat treatment.	GAC (1.79g/L)	Anatase and rutile TiO_2	Methyl orange (5 x 10^{-3} mole L^{-1} and 3,6,7,12,15 x 10^{-3} mole/L)	0.28L Photoreactor with 10 - 40W UV lamp (135 mW/cm^2, λ 320–400 nm, peak: 365 nm) and aeration of 56 ml min^{-1}.	Mixture of TiO_2 + AC, TiO_2, AC control for recycling (20 cycles)	Dark adsorption (1h) not shown but based on the data in the text the 25% reduction in 1h the "photodegradation" is in fact residual adsorption. This relationship is expressed as "Remnant rate%". Not clear that the mixture performs better than IPCA. Not clear that the AC recycle control was illuminated.	(Li *et al.*, 2005)
As above.	GAC (2.5g/L)	Anatase /rutile TiO_2, % ratios 1:0 and 35:65	Methylene blue (20 mg/L)	As above	TiO_2 and IPCA dark and light.	No photolysis control weakens case for IPCA action. The similar adsorption performance of the IPCA and TiO_2 suggests the IPCA has very poor adsorption.	(Li *et al.*, 2007)
Sol gel method was used to prepare TiO_2. Impregnation using stirring followed by calcination.	GAC (2g/L)	Anatase and rutile TiO_2	Methyl orange (1 x 10^{-3} mol/L)	0.28L cynical Pyrex reaction cell (1.2cm inter diameter, 28cm height) containing 0.25L solution equipped with an air-aerated stopcock, 40W UV lamp, fixed in the middle of the quartz cell.	TiO_2.	No adsorbent control. Photolysis claimed to be 4%. Dark adsorption (30min) not shown and may explain "photodegradation".	(Li *et al.*, 2006)
As above.	GAC (3.5g/L)	Anatase to rutile TiO_2 in the ratio of 2.3.	Rhodamine B (RhB) (1, 2.5, 5, 8 and 10 mmol/L)	UV Light intensity in 0.25L Pyrex photoreactor: 0, 15, 25, 40 and 60mWcm^{-2} with aeration (56mls^{-1})	None	No "*raw data*" all kinetics. 30min dark adsorption.	(Li *et al.*, 2008b)
As above.	GAC (2g/L)	Anatase and/or rutile phase	Escherichia coli (1 × 10^7 cfu/ml.) (E. coli, NCIMB 8277)	IPCA was suspended in sterilised water using ultrasonication and stirred. Irradiation using a black light fluorescent lamp. Volume not given.	Photolysis & TiO_2	Seems to decrease survivability. Results expressed as survival rate could mean that cfu's were still high after irradiation time. Biofouling of AC ?	(Li *et al.*, 2008a)

Sol gel method using a rotary evaporator was used to prepare the IPCA.	GAC (0.19 g/L)	TiO_2 (phase not stated)	Microcystin-LR (cyanobacteria endotoxin) (50 -200 mg/L)	Cylindrical continuous flow fluidized bed reactor (65cm h x 68cm inside diameter) with a 4W black light lamp (370nm, 0.6mW/cm^2) containing 4.5kg IPCA/AC.	Photolysis, Light & dark adsorbent and IPCA	The comparison between adsorption and illumination appears convincing. However the TiO_2 could be leaching. Analysis section mentions CO_2 measurement but nothing in the results about it.	(Lee *et al.*, 2004a)
As above.	GAC (1 g/L)	Anatase TiO_2	Microcystin-LR (200 mg/L)	1L glass cylinder with a water jacket for cooling. Irradiation was provided by a 4W black light lamp (370nm, 0.6mW cm^{-2}).	Photolysis, Light & dark adsorbent and IPCA	Almost identical paper to the one above paper. Uses desorption to claim mineralisation.	(Lee *et al.*, 2004b)
Commercial TiO_2 was loaded onto an ACF using an epoxy resin followed by calcination.	ACF (5.7 g/L, 2.9 g/L TiO_2 – assumed volume of solution, not explicitly stated)	P25 (30 nm)	Paper mill effluent	0.35L cylindrical photoreactor with water cooling jacket, 500W high-pressure Hg lamp (365nm) and aeration	P25, photolysis. None for recycle.	Measures colour and COD removal. Dark adsorption not shown. Could be adsorption not photodegradation.	(Yuan *et al.*, 2007)
As above.	ACF (IPCA not stated, P25 same as above)	P25 (30 nm)	b-cyclodextrin ($(C_2H_{10}O_5)_7$) (200 mg/L)	As above	P25, dark adsorption. None for recycle.	P25 only compared to one IPCA for COD removal. P25 has reasonably similar (but more erratic) degradation rate compared to the IPCA. Dark adsorption and photolysis not shown. IPCA adsorption better than photodegradation but does not continue.	(Yuan *et al.*, 2005b)
As above.	ACF (1 g/L)	P25 (30 nm)	Methylene blue (85 mg/L)	As above	P25 & dark adsorption. None for recycle.	No dark adsorption, the first cycle of P25 is as effective as the IPCA. Under illumination COD decreases very quickly initially. Initial adsorption is also very pronounced.	(Yuan *et al.*, 2005a)
50mg: 10mg TiO_2 :AC were added in a suspended mixture. **Not strictly an IPCA it is a synergistic mixture**.	PAC (0.6-2.4 g/L)	P25	Phenol (20 μM)	0.1L pyrex photoreactor illuminated from below with a 125 W high pressure Hg. Circulating water cell with >349 cut off filter provided water cooling.	TiO_2, photolysis and adsorbent	The TiO_2+AC and TiO_2 display photodegradation however the TiO_2 displays a much steeped degradation curve than the TiO_2+AC. However the latter degrades the phenol	(Matos *et al.*, 1998)

						quicker due to its lower initial concentration from the dark adsorption stage. The author then linearies the degradation curves and concludes that the TiO_2-AC performs better without accounting for the lower initial concentration.	
Sol gel method was used to prepare TiO_2 solution. Impregnation involved mixing followed by heat treatment.	PAC, powdered silica, mordenite (1 g/L)	TiO_2 (phase not stated most likely anatase)	Propyzamide (7.8 mg/L)	Pyrex reaction cell with a 400W Xe lamp and UV cut-off filter (λ > 300nm, 135mW cm^{-2}).	TiO_2	As below	(Torimoto *et al.*, 1996)
Sol-gel method.	PAC, powdered silica, mordenite, zeolite (varying 1 g/L)	TiO_2 (phase not stated most likely anatase)	Propionaldehyde (1.2-30 µM)	Illuminated with 10W black lamp for 15cm^3 volume. 5-400W xenon lamp for air-saturated 10cm^3 suspension. No apparent water cooling.	TiO_2	Experimental data are given but do not support synergy or ensure that the "*rate of photooxidation is enhanced*". Photodegradation experiments do not use a dark adsorption phase. Although the production of CO_2 would indicate photo-oxidation. With no controls it is impossible to draw firm conclusions. Illumination time is enormous for the comparison of adsorbents >1-2000 minutes for 100% CO_2 production. Reaction volume very small	(Yoneyama and Torimoto, 2000)
As above.{gaseous degradation)	PAC (0.2 g/L)	TiO_2 (phase not stated most likely anatase)	Dichloromethane, trichloromethane, tetrachloromethane (1.0 mmol dm^{-3}).	Reaction cell with l0W fluorescent black lamp (300 nm to 430 nm, peak of 352 nm, 1.8 mW cm^{-2}).	TiO_2, dark TiO_2 & IPCA.	Measured CO_2 appears convincing. No photolysis control.	(Torimoto *et al.*, 1997)
Coating of commercial TiO_2 with a carbon based precursor. The mixture was then carbonised at 700°C.	Carbon coated TiO_2 (0.525 g/L)	ST-01, Anatase TiO_2, (traces of rutile)	Methylene blue (2.94 x 10^{-4} mol L^{-1}) and heavy oil.	10 W/m^2 UV irradiation from a "*black light*" for MB and 16.4 W/m^{-2} UV irradiation for the heavy oil.	Dark IPCA, TiO_2	Results suggest photodegradation is mainly adsorption.	(Tsumura *et al.*, 2002)

Sol gel method used to apply TiO_2 to the surface of Poly(Vinyl Butyral) (PVB) followed by heat treatment.	Poly(Vinyl Butyral) (PVB) carbonised to form an AC. (0.6 g/L)	Anatase and rutile TiO_2 in the ratio of 1-0.3	Phenol (50 mg/L).	Degradation experiments were carried out under illumination from six UV lamps with 20 W power.	Photolysis, Dark adsorbent, P25	IPCA adsorption is very low. No TiO_2 control. Degradation is comparatively slow. P25 is more effective than the best IPCA. AC stops TiO_2 phase change.	(Tryba *et al.*, 2003a)
Sol gel method was used to prepare a TiO_2 solution and impregnation used stirring, followed by calcination.	PAC (0.6 g/L)	Anatase and Rutile TiO_2 (depending on calcination temperature.)	Phenol (50 mg/L)	Six lamps UV lamps were used to irradiate the solution from the top.	Photolysis, light adsorbent	The unmodified AC is almost as effective as the best performing IPCA. "	(Tryba *et al.*, 2003b)
Carbon precursor applied to P25. The composite was then dehydrated and carbonised at 600°C.	Cellulose/TiO_2 microsphere composites (not stated)	P25 (20 nm), ST-01 (7 nm)	Acetaldehyde (2000 mg/L)	Cell containing 3 cm^3 reactant illuminated with two 4 W black lights λ 300–400 nm)	Dark IPCA, TiO_2, P25, mixture	No dark adsorption phase and photolysis control. After the first thirty minutes the IPCAs performance is little more than photolysis and adsorption.	(Nagaoka *et al.*, 2002)
As above.	ACF (not stated)	Anatase and rutile TiO_2	Methylene blue (concentration not stated)	Not stated (looks at reuse of an IPCA)	None for experiments and none of recycle	Lots of characterisation but no robust data.	(Fu *et al.*, 2006)
Sol-gel method used to prepare TiO_2. Impregnated onto the activated carbon cloth by dip coating followed by calcination.	Activated carbon cloths (1.5 cm x 1.5 cm)	Anatase and rutile TiO_2.	Methylene blue (2.94 x 10^{-4} mol/L)	"*UV irradiation*" from a 365nm black light of 100 ml solution	None	Pre-saturation. Isotherms but no raw data.	(Xu *et al.*, 2008)
Sol gel method was used to prepare the pure TiO_2 and impregnate the AC. The solutions were then dried and calcined at different temperatures.	PAC (1 g/L TiO_2 and IPCA containing the same amount of TiO_2)	Anatase and rutile TiO_2 (P25 as reference)	Chromotrope 2R (10-80 mg/L)	0.8L photoreactor with low pressure Hg vapour lamp (Lamda max = 253.7 nm, 3 W radiant flux)	Photolysis and TiO_2	30 min dark adsorption. Between 6-70% of dye is removed in the dark adsorption stage and with no dark adsorbent control it is impossible to determine if the k_{app} is measuring adsorption or photodegradation.	(Wang *et al.*, 2007)
The IPCA's were prepared by several methods, mechanofusion using a theta composer and boiling impregnation (boiling dry a solution of TiO_2 and AC).	PACs and GACs prepared by different activation methods. (50-30 mg/L, mass in continuous flow system not stated)	P25	Methylene blue (0.5-30 mg/L), Procion red MX-B5 (reactive red 2) (10-20 mg/L)	4-Watt low-pressure Hg UV lamp (approx 0.37 mW/cm^2 for batch studies and 2 mW/cm^2 for column studies)	Light adsorbent. None for recycle.	Only measures decolourisation. No photolysis or P25 control. Information seems patchy. On p80 claims synergy. Claims IPCA works better after regeneration.	(Khan, 2002)
Sol gel method used to prepare a TiO_2 solution, which was drip coated onto the ACF and calcined at 600 or 800°C in an N_2 atmosphere.	ACF (2 g/L)	Anatase TiO_2	Methyl orange and acid fuchsine (120 mg/L)	0.25 L cylindrical photoreactor and water-cooled quartz jacket with 500	TiO_2 & dark adsorption. None for	TiO_2 is almost as effective as the IPCA in the first cycle and is not used in	(Shi *et al.*, 2008)

				W high-pressure Hg lamp (365 nm, 12.5 mW cm^{-2}) and aeration.	recycle.	subsequent cycles. Adsorption data is incomplete. Suggests IPCA performance is adsorption and photolysis	
The WO_3–TiO_2 photocatalyst was prepared by a sol gel method. Impregnation involved stirring and calcination.	GAC (20 g ? not stated)	WO_3–TiO_2 (Anatase TiO_2)	Congo Red (10-50 mg/L with H_2O_2 addition.)	2.5 L "*fluidized bed photoreactor*" containing 2 L solution with 500 W high-pressure Hg-vapour lamp and aeration (0.2 m^3 h^{-1})	None.	Mentions photodegradation efficiency. Impossible to determine if substrate removal is photodegradation or adsorption.	(Sun *et al.*, 2009)
P25 was added to an epoxy resin solution and drip coated onto an ACF and then calcined.	ACF (1 g/L TiO_2, 6.4 g ACF not incl TiO_2 loading)	P25	Methylene blue (85 mg/L)	0.35L cylindrical photoreactor with a water-cooled quartz jacket and 500W high-pressure Hg lamp (365nm)	P25, none of recycle.	Reproducibility seems poor. P25 as effective as the IPCA.	(Yuan *et al.*, 2005c)
Various quantities of commercial TiO_2 and AC were mixed in an aqueous solution and stirred for 1 hr before filtration.	Activated carbon (form not stated) (2 g/L TiO_2 & "proportionate AC concentration was used for the other catalyst)	P25	Phenol, salicylic acid, 4-aminophenol or p-nitrophenol (100 mg/L)	0.25L photoreactor(s) with air sparging (100ml min^{-1}) and irradiated with a "UV lamp". Natural sunlight was also used (no further information given)	TiO_2	No raw data all linear transforms. No photolysis control. TiO_2 is compared for sun and UV light. FTIR data convincing however.	(Araña *et al.*, 2003a, Araña *et al.*, 2003b)
Sol gel a method was used to prepare the IPCA. Impregnation involved stirring and was followed by calcination.	PAC (1 g/L)	Anatase TiO_2 (P25 as reference)	Phenol, methyl orange (MO) and Cr(VI) (Concentration not stated)	Cylindrical quartz photoreactor containing 0.25 L solution (with water cooling jacket) and an 8W UV lamp (365 nm) position.	TiO_2,, TiO_2 control for recyle.	30 min dark adsorption, results expressed as C/C_0. Very low adsorption in dark adsorption stage. Photodegradation appears noticeably higher after the start of illumination for the three contaminants.	(Liu *et al.*, 2007a)
Commercial TiO_2 powder was carbon coated by mixing with polyvinyl alcohol in different mass ratios. The resulting IPCA was then calcined.	Carbon-coated anatase powders (0.5 g/L)	Anatase TiO_2 (ST-01)	Methylene blue (3.2×10^{-5} mol dm^{-3})	Photocatalytic membrane reactor (PMR) with direct contact membrane distillation and Hg UV lamp (355 nm, 146.1 W m^{-2} at irradiation plate).	Photolysis, TiO_2 for 2 recycle.	No error bars so it appears that ST-01 is nearly as effective as the best performing IPCA with and without membrane distillation.	(Mozia *et al.*, 2007b)
The Fe was added to the ACF by dip coating. The Fe-ACF was then added to a solution of TiO_2 precursor and stirred followed by vaporisation and calcination at 700°C.	Fe-ACF (5 g/L)	Mixture of anatase and rutile TiO_2	Methylene blue (1.0 x 10^{-5} mol/L)	UV lamp above the solution (20 W, 365 nm)	Adsorbent, IPCA.	Dark adsorption not shown and consist of 3 mins of sonication. MB removal is not clear as it the shows UV spectrum and not concentration.	(Oh *et al.*, 2009)

Liquid phase deposition used to apply TiO_2 to the ACF. The ACF was then dried and annealed at high temperature.	ACF (weight not stated – 3 mm thick)	Anatase TiO_2	Acid Orange II (AOII) (50-200 mg/L)	Photoreactor consisting of quartz reactor irradiated by a 15W germicidal lamp (90% output at 253.7nm). The IPCA was used as the photoanode, Pt wire used as the counter electrode.	Photolysis, dark and light IPCA, electrochemical oxidation & combined photo and electro chem	Dark adsorption of TOC and substrate is half as effective as IPCA. Combined process is additive and not synergetic. Intermediate removal via HPLC. No dark adsorption stage and no error bars.	(Hou *et al.*, 2009)
A sol gel method was used to prepare carbon coated TiO_2. The resulting solution was dried, pulverised and calcined.	Carbon coated TiO_2 (0.33 g/L)	Anatase and rutile TiO_2	Methylene blue (1.6 x 10^{-5} M).	UV light bulb (0.5 mW/cm^2, 364 nm) and visible light from an incandescent light bulb (13.6 mW/cm^2). LEDs used to provide lighting for NO degradation	Visible and UV photolysis, TiO_2.	Measures decolouring of MB, adsorption peak shifts significantly over time. Amount of MD irritated is tiny. Degradation is measured using UV-vis spec at a single wavelength for linearised results.	(Treschev *et al.*, 2008)
Electrophoretic deposition was used to apply a suspension of P25 and AC to a conductive glass plate electrode. The electrodes were then placed in an oven and heated in air at 450°C for 30 min.	PAC (not stated)	P25	Orange-II (OG-II) (50 mg/L)	Glass reactor with direct illumination by a low-pressure mercury vapour UV lamp (75 mW/cm^2, λ = 365 nm).	TiO_2.	No dark adsorption, removal rate of IPCA small (30%) likely due to adsorption. Measures H_2O_2 production.	(Peralta-Hernández *et al.*, 2007)
Commercial TiO_2 was carbon coated by exposing it to ethanol vapours for 1hr in temperature ranging from 150 to 400°C.	Carbon coated TiO_2 (0.1 g/L)	Tytanpol A11 (Police, Poland) and P25 (Degussa, Germany)	Phenol (100 mg/L)	Artificial solar light was provided by using a 100 W lamp (354W/m^2 visible, 0.09 W m^{-1} UV) and UV light was provided by 6, 20 W UV lamps (100 W/m^2 visible, 154 W m^{-2} UV)	P25, A11 in visible and UV.	15min dark adsorption. Does not show phenol decomposition v time (24h vis/5h UV). Measures functional group decomposition. Under UV no decomposition reaction is higher than 50%. Photolysis seems as effective as the IPCA.	(Janus *et al.*, 2006)
A sol gel method was used to prepare TiO_2/ACF composite. The gel was then dried and then calcined.	ACF (weight not stated)	Anatase and rutile TiO_2	Toluene (20mg/L)	Solution was irritated with a 500 W high pressure mercury lamp (380 nm).	TiO_2, adsorbent.	Measures TOC. Adsorbent has 80% of the effectiveness of the IPCA since photolysis is not shown it is likely there is no synergy.	(Liu *et al.*, 2006)
A sol gel method was used to prepare F doped TiO_2. Impregnation used ultrasonication.	PAC (1 g/L)	F doped anatase TiO_2 (brookite traces)	Phenol (25mg/L)	0.2 L silica photoreactor with 250 W halogen lamp with a light filter cutting <400 nm (11.3 mW cm^{-2})	P25, TiO_2, F-TiO_2 doped IPCAs, Photolysis (not shown)	Regular IPCA no more effective than P25. 30min dark adsorption. Concentration as C/C_0 based on the adsorption data in the text the F-IPCA has more adsorption capacity causing the "photodegradation"	(Xu *et al.*, 2008)

Commercial TiO_2 was impregnated on the ACF by stirring and then ultrasonication. The resulting IPCA was then calcined.	ACF (not stated)	Anatase TiO_2	Methylene blue (100 mg/L)	Lamp fitted along reaction cell and the ACF was fixed horizontally along the reaction cell (no information on power output or lamp type).	Photolysis, dark adsorption, No control for recycle.	No synergy, IPCA performance has the same shape as photolysis plus adsorption.	(Jia *et al.*, 2007)
Commercial TiO_2 was impregnated onto the PAC using ultrasonication. N doped IPCA was prepared by adding saturated urea to the TiO_2 suspension and then following the procedure outlined above.	PAC (200 g/L)	Anatase TiO_2	Soman, VX, and Yperite (concentration not stated)	Photoreactor (size not stated) consisting of a closed quartz tube flushed with air ($50cm^3min^{-1}$), 125W high-pressure black-bulb lamp (λ365 nm, 3.0W UVA λ 315–400 nm).	TiO_2	The degradation of the substrate over IPCAs (1-25% wt TiO_2) is greater than unmodified TiO_2 is the only evidence put forward to demonstrate synergy. There is N_2 isotherm data in the paper but no empirical data on adsorption so the proposed synergy could be little more than AC adsorption. The N-doped titania appears to perform better than the unmodified TiO_2 although it was heat treated and the unmodified TiO_2 was not so they are not directly comparable	(Cojocaru *et al.*, 2009)
Commercial TiO_2 powder was coated with Poly(vinyl alcohol) and then carbonised. The powder was then adhered onto organic adhesive tape or a film using an organic binder.	Carbon coated TiO_2 (not stated)	Anatase TiO_2 (ST-01)	Methylene blue (2.94 x 10^{-5} mol/L)	3x20 W UV light bulbs where placed 200mm from the IPCA tape or film.	None for recycle.	No controls and results expressed as C/C_0. Impossible to determine anything.	(Inagaki *et al.*, 2006)
Commercial TiO_2 was applied to the GAC using ultrasonication. Commercial TiO_2 was added to a chitosan solution and cast into beads by a "*phase-inversion technique*".	GAC (0.25-1.5 g/L)	Anatase TiO_2	Salmonella choleraesuis subsp. ATCC 14028 (10^8 cfu ml^{-1})	1L batch photoreactor with 20W high pressure mercury lamp (320–400 nm)	Dark TiO_2, Photolysis, TiO_2, dark adsorbent	Removal using TiO_2 is slightly more effective than either IPCA. No mention of dark adsorption.	(Kim *et al.*, 2005)
Sol gel method was used to prepare the entire IPCA followed by heat treatment at 200°C in air.	GAC (50 g fluidised bed system)	Anatase TiO_2, rutile and brookite traces	Colour (organics absorption at 254 nm)	Adsorption was carried out separately. UV regeneration using six 18 W UV-A or UV-C lamps and/or ultrasonic bath	Adsorbent control for adsorption. No fresh or used AC for Recycle.	No photolysis control, regeneration experiments do not prove anything due to a lack of controls. Only demonstrates adsorption by the IPCAs and ACs.	(Zhu and Zou, 2009)
Sol gel processes was used to prepare separate solutions of $ZnFe_2O_4$ and TiO_2. The latter solution was added drop wise to the $ZnFe_2O_4$. GAC was then added to the combined solution and shaken for 12h and dried. The samples were then calcined at 500°C for 2 h.	GAC (20-40 g)	Anatase TiO_2 doped with $ZnFe_2O_4$	Acid dye - brillred-RH (5-20 mg/L)	"*Recycle fluidized bed reactor*" with 150 W visible light source.	Adsorbent.	No raw data, all linearisied results. GAC is almost as effective as IPCA.	(Wang *et al.*, 2009b)
CdS P25 was prepared by a sol gel and a precipitation method. These catalysts were applied to ACFs using an adhesive and dip coating.	ACFs (not explicitly stated)	CdS doped P25	Methylene blue (50 mg/L)	75mm x 50mm piece of the IPCA were put 100mL flasks and exposed to sunlight for 5h	TiO_2	CdS doping of the TiO_2 increased its absorbance in the visible spectrum and the doped IPCA performed	(Zhao *et al.*, 2010)

						better than the P25 IPCA. However a comparison of plain and doped TiO_2 under illumination from sunlight was not reported so it is impossible to know if the doping created a more effective TiO_2 under solar illumination conditions.	
Sol gel method used to prepare the doped TiO_2. This solution was added drop wise to the ACF. Followed by calcined at 600 - 800°C in N_2.	ACF (not stated)	Fe(III) and Ho(III) doped TiO_2	Methyl orange (120 mg/L)	0.25L cylindrical vessel with a water-cooled quartz jacket with a 500-W high-pressure Hg (365 nm). Aeration was used.	None, none for recycle.	Raw data expressed as C/C_0. No proof.	(Shi, 2009)
Sol-gel method used to prepare Fe(0) doped TiO_2. ACF was dip coated using this solution and calcined at 200°C for 2h.	ACF (not stated)	Fe(0) TiO_2 (phase not stated)	2,4-dichlorophenol (10-100 mg/L)	Cylindrical quartz tube 30cm×3cm (height×diameter) with a 20W germicidal low-pressure Hg lamp (λmax 254 nm, 92 W/cm^2 at 365 nm)	TiO_2, Fe(0). None for 7 recycles.	Photolysis is not shown but it would seem to be very effective. 60min dark adsorption. Photodegradationand TOC removal likely adsorption.	(Liu *et al.*, 2009)
The IPCAs were obtained by mixing P25 and activated carbon at different proportions in water and stirred for 3 h followed by filtering and drying.	PAC (1g/L)	P25	Pentafluorobenzoic acid (100-600 mg/L)	175 cm^3 immersion type photoreactor with either a 16 W low pressure Hg lamp (λ 253.7 nm, photon flux: 2.54×10^{-5} Einstein $L^{-1}s^{-1}$) or 8 W medium pressure Hg lamp (λ 365 nm, photon flux: 2.08×10^{-6} Einstein L^{-1} s^{-1}). Aeration 8.1 mLs^{-1}	AC+P25, P25, two wavelength used.	Only measures defluoridation. No dark adsorption or photolysis. P25 as effective at 254nm.	(Ravichandran *et al.*, 2010)
A commercial solution of amorphous TiO_2 was applied to either a plain PET film or a PET film with GAC adhered to it using a silicon binder. The GAC film was sprayed with the TiO_2 and dried a total of five times.	GAC (not stated)	Anatase TiO_2	2,4-dinitrophenol (1 to 250 mg/L)	Batch-recirculation flow system with 6 W blacklight blue fluorescent lamp (λ 300–400 nm).	TiO_2, light & dark AC and IPCA. None for recycle.	No photolysis, no synergy, IPCA only delivers a minuscule improvement in performance compared to AC. Looks at the effect of temperature.	(Cao *et al.*, 2010)
As above	As above (not explicitly stated - TiO_2 content between 0.09 and 0.12 g)	As above	2,4-dinitrophenol (5-80 mmol/m^3)	As above	TiO_2	Looks at degradation products, no significantly new data. No synergy although it is claimed.	(Cao and Shiraishi, 2010)
Sol gel method used to prepare a TiO_2 solution. The ACF was impregnated with TiO_2 by immersing it in this solution for 1h followed by calcination at 500°C in an Ar atmosphere.	ACF (1-3 g/L)	Anatase TiO_2	Phenol, methyl orange (7-80 and 120 mg/L respectively)	Quartz reactor with Hg UV lamp (300 W,λmax 365 nm)	TiO_2, light and dark adsorbent. None for	No photolysis control. Suggests that IPCA is more effective than TiO_2 although synergy is not	(Yao *et al.*, 2010)

					recycle	proven. 60min dark adsorption, results given as C/C_0 or % removal.	
P25 was added to an acetone and epoxy solution and stirred vigorously. Prewashed GAC was added to this solution. The suspension was filtered, washed and dried. Followed by calcination at 500°C for 2h in an N_2 atmosphere. These processes were repeated once to yield the final IPCA.	GAC (2.5 g/L)	P25	Rhodamine B (5×10^{-3} mol/L)	Photodegradation experiments used a Pyrex reaction cell aerated at 0.6 L/min. A UV lamp was fixed in the middle of the quartz cell (light intensity varied between 50-200W).	None	Extended discussion of kinetics of IPCA action. Contains no raw data (only linearised graphs) and the kinetic examples incorporate no photolysis, TiO_2 or adsorbent controls.	(Zhang *et al.*, 2011b)
Catalyst I: TiO_2 deposited on cellulose fibers. Catalyst II: A composite of a layer of cellulose fibers with deposited TiO_2, a layer of carbon fibers and a layer of cellulose fibers. Both catalysts were rinsed for 12 h by deionised water	Commercial photocatalyst fibres from Ahlstrom (France) (not stated)	Commercial TiO_2 (type not stated)	Basic red 46 (10 and 25 mg/L)	PTFE (polytetrafluoroethylene) coated flat plate photoreactor inclined at 30° with two 15W UV lamps (emission λ= 365 nm) or 2 visible light lamp. Natural sunlight was also used (180 - 190 W/m^2).	None	Results expressed as decolourisation.	(Mounir *et al.*, 2007)
Sol-gel method used to prepare TiO_2. The ACF was then added to this solution and stirred vigorously for 1h. The IPCA was then dried and calcined at 900°C for 2h in an N_2 atmosphere.	ACF (1.25 g/L)	TiO_2 (type not stated)	Methyl orange (80 mg/L)	0.2 L pulsed discharge reactor with aeration (oxygen flow rate of 96 L h^{-1}). UV light generated by the pulse discharges, irradiating a suspended ACF IPCA.	Photolysis	No comparison except that the IPCA increased system efficiency by 58% compared to photolysis.	(Zhang *et al.*, 2010)
Sol-gel method was used to prepared Fe doped TiO_2 using $Fe(NO_3)_3$ and tetrabutyl orthotitanate. Ultrasonic impregnation was used to apply the doped TiO_2 to the AC. The dried IPCA was calcined at 250°C in air and then 500°C in N_2.	GAC (2-12 g/L)	Fe-TiO_2 (anatase and rutile TiO_2)	Wastewater (from a "*dye factory*", municipal wastewater was also used)	Continuous flow 6.3 L stainless steel cylindrical photoreactor with 2 UV lamps mounted in the centre. Aeration (56 mL/sec) was used.	TiO_2. None for recycle.	Results expressed as COD or colour remnant %. TiO_2 is quite effective. Dark adsorption is not mentioned. No control, no proof.	(Li *et al.*, 2010)
Boiling impregnation was used to apply commercial TiO_2 to the adsorbent. These were then heat treated at 550°C	GAC, glass beads, zeolite, brick, quartz. (1.2 g/L)	P25	Propoxur ($4.78\text{x}10^{-4}$ M)	1 L double-jacked vessel with a quartz cover. UV irradiation was provided by three 10 W low pressure Hg lamps (peak λ: 254 nm) above the reactor.	Dark and light adsorbent.	Results expressed as C/C_0. No TiO_2 and photolysis controls. Unclear if IPCA is actually an adsorbent.	(Lu *et al.*, 1999)
V doped titania (VTO) was prepared using a sol gel method. Ultrasonic impregnation was used to apply the VTO to PAC. This IPCA was then applied using dip coating to a glass plate.	PAC (not explicitly stated)	V-doped titania	X-3B (50 mg/L)	1.2 L cylindrical silica batch photoreactor system with 250 W halogen lamp (filter cutting off <400 nm) and vertical aeration with IPCA placed on the bottom of the reactor.	Photolysis, P25, doped TiO_2	30min dark adsorption. Results expressed as C/C_0. Dark adsorption not shown. IPCA performance could be adsorption.	(Xu *et al.*, 2010)
Solution of P25 was applied to the AC and carbon foam by mixing in a rotary evaporator followed by drying. Carbon form prepared by acid modification of coal tar pitch followed by heat treatment at 600°C in N_2 and then stream activation at 800°C for 1h	"*Carbon foams*" & GAC (1 g/L)	P25	Phenol (100 mg/L)	0.4 L photoreactor with 125 W high pressure Hg lamp vertically suspended in a cylindrical quartz cooling jacket.	Light and Dark IPCAs, P25.	No photolysis control. Results expressed as C/C_0 Comparison table of other work. No dark adsorption, unclear if IPCA actually	(Velasco *et al.*, 2010a)

						photodegrades. Includes intermediate analysis.	
IPCA prepared by rotary evaporating a mixture (15:85) of P25 and AC. All samples were washed with DI water and dried at 110°C	GAC (1 g/L)	P25	Phenol (10 mg/L)	0.4 L photoreactor with 125 W a high pressure Hg lamp vertically suspended in a cylindrical, double-walled quartz cooling jacket.	Adsorbent (light and dark), TiO_2, Photolysis	The study lacks a photolysis control and it is unclear if there was an adsorption phase before UV illumination. The AC performs better in the dark than the IPCA, however it performs better under UV illumination. The author attributes this to photoactivity of the unmodified AC possibly due to its ash content (11%). It is proposed that P25 has an antagonistic effect on the AC (Fig 3.) in the IPCA in the first hour and half of irradiation that is overcome by the photoactivity of P25. No error bars are given and the experimental method does not mention if the experiments were repeated. The authors claim that IPCAs "modify the phenol photodegradation pathway" as evidenced by the different ratios of intermediates in the IPCA and P25 photodegradation samples. It is noted however, that the difference is probably due to absorption of intermediates onto the AC.	(Velasco *et al.*, 2010b)
As above	GAC (1 g/L)	P25	As above	As above	Light and Dark IPCAs, P25.	Graphs are expressed differently however raw data appears the same.	(Velasco *et al.*, 2010c)
A sol-gel method was used to prepare N doped TiO_2. PAC was then added to this solution and stirred followed by filtration to remove the IPCA which was calcined at 400°C in N_2	PAC (0.25 g/L)	Anatase TiO_2 with traces of brookite.	Bisphenol-A (36 mg/L)	0.25 L solar simulator equipped with a 150W Xe arc lamp (Light intensity 1000 W/m^2, UV/Vis intensity approx 6.5%/40%). Additional light filters used to	TiO_2, P25.	Results expressed as C/C_0 or efficiency (%). 1.5h dark adsorption not shown. No photolysis or dark IPCA controls. Effectiveness of different	(Yap *et al.*, 2010)

				control certain wavelengths.		light wavelengths compared.	
Chitosan/ACF composite films were prepared by adding the ACF to a chitosan and pore forming agent solution. A separate sol gel TiO_2 solution was prepared and applied to the Chitosan/ACF using dip coating.	Chitosan/ACF (Not explicitly stated)	TiO_2 (phase not stated)	2,4–Dichlorophenol (1-50 mg/L)	On-site regeneration: 0.1L solution irritationed with 20W UV light (λ 254nm). Off-site regeneration: IPCA was dipped in distilled water in a shallow tank reactor under the same light source. Fenton reagent was also investigated for regeneration	Membrane and C/ACF. Membrane control included for recycle.	Results expressed %removal. No TiO_2 or photolysis control. The adsorbent without TiO_2 is almost as effective as the IPCA.	(Liu *et al.*, 2010)
Prepared by a one-step carbonization (at 450°C under vacuum) of a self-assembled matrix consisting of titanium tetra-isopropoxide and a triblock copolymer.	Form not stated (0.25 g/L)	C doped Anatase TiO_2	Methylene blue (10 mg/L)	0.025 L (w/ 20 ml solution) quartz photochemical reactor with 150 W Xe lamp (180 $mWcm^{-2}$) with UV-cut off filter (<400 nm)	None	Comparison between dark adsorption and the start of illumination appears convincing but there are no controls.	(Lee *et al.*, 2010)
Ultrasonication used to apply P25 to GAC followed by oven drying, filtering and washing.	GAC (1.2 g/L)	P25	Indomethacin (0.1 to 1.5 mmol/L)	1 L photoreactor and water cooled immersion well with 125 W medium pressure Hg lamp.	Photolysis, None for recycle.	No P25 control. Convincing comparison between dark adsorption and photodegradation.	(Basha *et al.*, 2010)
Ultrasonication used to apply P25 to GAC followed by oven drying, filtering and washing. Heat treatment between 200°C - 700°C.	GAC (1.5 g/L)	P25	Famotidine (50 mg/L)	1 L photoreactor and water cooled immersion well with 125 W medium pressure Hg lamp.	Photolysis.	No P25 and dark adsorbent control. Results expressed as remnant%, no error bars.	(Keane *et al.*, 2010)
Two methods a conventional sol-gel method using a triethylamine as a visible light sensitiser and a self assembly method using poly(sodium styrene sulfonate) to modify the AC surface and then adding N-TiO_2 that was treated to have the opposite charge.	PAC (0.3 g/L)	Anatase TiO_2	Humic acid (molecular weight >2000 Da) (11.2 mg/L)	0.2 L cylindrical photoreactor with 100 W Xe lamp (420-630 nm, 570 mW)	TiO_2s, Dark IPCA. None for recycle.	Results expressed as C/C_0. Useful XRD information. Lacks necessary controls. IPCAs and TiO_2 results appear to be expressed the same way using different notation. Places great emphasis on surface chemistry, the self assembly IPCA works much better than the sol gel.	(Zhang *et al.*, 2011a)
Sol-gel method used to prepare TiO_2. The AC was dipped in the TiO_2 solution followed by drying and calcining at 300°C in N_2 for 2h. This procedure was repeated up to 5 times, prior and a final cycle where the temperature, was held at 500°C.	GAC (2 g/L IPCA, 0.4 g/L TiO_2)	Anatase TiO_2	Humic acid (15 mg/L -5.04 mg/L TOC, TOC 1.7-19.4 mg/L)	Photoreactor containing 0.5 L solution with a water-cooled quartz jacket and a 500 W mercury lamp (major emission at 365 nm, 12.5 mW/cm^2)	Photolysis, Mixture, TiO_2	Results expressed as C/C_0 or % remnant. IPCA seems to perform better than the mixture and TiO_2 however there is no dark adsorption and photolysis is not on the same graph. It appears convincing however the difference in TOC between the IPCA and TiO_2 is 20% or about 1mg/L so it may	(Xue *et al.*, 2011)

						not be significant. The demonstration of "synergy" is not robust. Separate adsorption studies. L-M model.	
Sewage sludge was activated by 5M $ZnCl_2$ and pyrolysed in N_2 atmosphere at 650ºC for 60min followed by treatment with 1M HNO_3 solution and washing with distilled water Mixture of 0.1 to 10 g/L AC and 0.001 to 8 g/L P25, **Not IPCA, synergistic mixture.**	GAC (0.1 to 10 g/L,)	P25	Hg(II) 10-120 mg/L	0.2 L cylindrical quarts bottle irradiated with 16-light Rayonet Photochemical Reactor (253.7 nm)	Light and dark TiO_2, AC and IPCA.	No photolysis or illuminated AC controls. Mixture appears more effective than TiO_2 or AC.	(Zhang *et al.*, 2004)
Mixture of TiO_2 and AC, **not IPCA synergistic mixture.**. 5mg TiO_2:5mg AC approximately 334mg/L IPCA.	PAC (167 mg/L)	P25	Cytarabine (50 mg/L) (Antineoplastic pharmaceutical**)**	0.03 L solution irradiated with a 700 W medium pressure Hg lamp (238-334 nm, $I_0 = 3.75\times10^{-7}$ Einstein s^{-1}).		(measures Pzc bubbles N_2 through the solution) Results expressed as C/C_0. Degradation of combined system is very effective, no robost demonstration of synergy.	(Ocampo-Pérez *et al.*, 2011)
The IPCA impregnation method applied a Ti precursor to the AC which was then placed in water vapour. For comparison a sol–gel method was also used to apply TiO_2 to the AC. Both methods were followed by calcination at 400°C for 3h in vacuum.	PAC (0.04 g/L TiO_2 and approx 0.5 g/L IPCA containing 8% TiO_2)	Anatase TiO_2 (N doped TiO_2 prepared in another paper(Huang *et al.*, 2011a))	Methylene blue (1×10^{-3} mol/L)	0.1 L of solution illuminated with a halogen lamp (no other information given)	Photolysis, TiO_2	10h dark adsorption, Only one comparison and no error bars. No adsorption time after a new solution was added after dark adsorption. It is likely that the photodegradation is in fact residual adsorption.	(Huang *et al.*, 2011b)
Commercial TiO_2 powder was dissolved by hydrofluoric acid. The precipitate was mixed with PAC. A separate phenol solution was prepared and added to the TiO_2/AC. Formaldehyde was added to the phenol carbon titania slurry followed by calcinations at 500°C for 5h in N_2.	PAC (10 g/L)	Commercial TiO_2 (SD fine chemicals)	Phenolic syntan (50-1000 mg/L)	0.5 L quartz tube filled with 0.1 L solution illuminated by five 25 W UV lamps (λ 254 nm)	Photolysis	Results are average values. No TiO_2 or adsorbent control. 8h pre-saturation but no dark adsorption time.	(Aruldoss *et al.*, 2011)
Ultrasonication used to apply P25 to GAC followed by oven drying, filtering and washing.	GAC (1-2.5 g/L)	P25	Amoxicillin (149.6–151.1 mg/L)	1 L photoreactor and water cooled immersion well with 125 W medium pressure Hg lamp.	TiO_2, light AC, None for recycle.	Convincing comparison between dark adsorption and photodegradation. Leaching from IPCA.	(Basha *et al.*, 2011)
Sol gel method used to prepare the TiO_2. The AC was added to the solution and the coating was repeated twice. Finally the vacuum-dried precipitates were calcined using a variety of temperatures and atmospheres.	PAC (0.25 g/L)	Anatase and rutile	Bisphenol-A (36 mg/L)	0.25 L "*solar simulator*" with a 150 W Xe arc lamp.	P25, Dark adsorption	Aeration not used because it can cause evaporation. Looks at effect of aqueous matrix species on BPA photodegradation in terms of k_{app}. Greater than 90% removal occurred in 8h. No raw data.	(Yap and Lim, 2011)

As above	PAC (0.15-0.35 g/L)	As above	As above	As above, dichroic mirrors were used to control light λ to 280–400 nm and visible-light illumination (420–630 nm).	Photolysis, Sunlight, dark adsorption. None for controls.	Results of C/C_0. No adsorbent or TiO_2 controls.	(Yap *et al.*, 2011)
Carbon fibre was activated with nitric acid followed by washing. The carbon fibres were then dipped into a Pd solution followed by a $SnCl_2$ solution. TiO_2 sol was prepared using a sol gel method with dip-coating for impregnation. The coated carbon fibre was calcined in N_2 at 600°C	PAN carbon fibre (not explicitly stated)	Anatase TiO_2	Acid orange II (100 mg/L)	0.025 L Pyrex tube irradiated with a 500 W Hg lamp.	Non-doped IPCA, None for controls.	No photolysis or adsorbent controls. Photodegradation mainly takes place in the first 15min so is likely adsorption as there is no dark adsorption time.	(Zhu *et al.*, 2011)
Sol gel method used to prepare $Sn(IV)TiO_2$. Tin tetrachloride was added to Ti precursor followed by AC (activated by nitric acid) addition. After drying the IPCA were calcined between 450-600°C. The dip coating followed by calcination was repeated twice. The IPCA was then cleaned using ultrasonication	GAC (5-15 g/L)	Anatase and rutile TiO_2	Orange G (azo dye) (10-60 mg/L)	2 L fluidized bed photoreactor with 300 W high-pressure Hg (λ max at 365 nm). 2.5L solution flowed through at 0.3L/min with H_2O_2 addition. Aeration of 0.2 m^3/h. at a flow rate of 0.3 L/min.	None.	Dark adsorption and error bars not shown. No controls no evidence. H_2O_2 addition complicates interpretation of the results.	(Sun *et al.*, 2006)
Sol gel method was used to prepare the TiO_2. AC was added to this solution and mixed for impregnation. The IPCA was then dried and ground down and calcined 4-600°C different temperatures under N_2 atmosphere.	PAC (0.5 g/L)	Anatase TiO_2	Acid Red 88 (azo dye) (not stated ?)	0.3 L photoreactor with 9W black-light (max λ 365 nm). In organic ions were added as sodium salts at 1×10^{-4} mol/L.	None, None for recycle.	Overnight pre-saturation not shown. Results expressed as % removal. Addition of inorganic ions is interesting as they decrease performance.	(Gao *et al.*, 2011)
Laboratory prepared AC. TiO_2 nanoparticles were mixed with the AC and applied to the inside of the photoreactor using a UV resistant binder.	PAC (not stated)	Commercial TiO_2	Basic Red 18 and Basic Red 46 (azo dye) (0.128 mM and 0.120 mM)	5 L Pyrex photoreactor with two 15 W UVC lamps (200–280 nm). IPCA was adhered to inside surface.	TiO_2, UV spec.	Results expressed as C/C_0. No control for H_2O_2 addition. Measurement of intermediates and anions.	(Mahmoodi *et al.*, 2011)
Sol gel method was used to prepare TiO_2. Impregnation using stirring followed by calcination at 500°C. Butyl alcohol used as a "plugging agent".	Not stated	Mixed phase TiO_2	Acid Red 27 (not stated)	0.28 L cynical Pyrex reaction cell (1.2 cm inter diameter, 28 cm height) containing 0.25 L solution equipped with an air-aerated stopcock, 40 W UV lamp, fixed in the middle of the quartz cell.	TiO_2, P25	Dark adsorption not shown. No dark IPCA control. Results expressed as % remaining after t=0. No evidence of synergy.	(LI *et al.*, 2011)
Sol gel TiO_2 applied using ultrasonication. Followed by ageing and calcination at 350 - 600°C for 5h.	PAC, GAC and MWCNT	Mixed phase TiO_2	Acid Blue 92 (AC and MWCNTs) Wastewater Concentration not stated	Pyrex reactor with 125 W high-pressure Hg lamp) with cooling water jacket.	None	Dark adsorption time not shown. No controls for dye or wastewater studies. No proof of photodegradation.	(Zarezade et al., 2011)
TiO_2 prepared using sol gel method. GAC was added to this solution for 1h and then dried. Followed by calcination at 500°C.	GAC (8 g/L, 1 g/L for TiO_2 control)	Anatase TiO_2	Arsenite (As(III)) (3 mg/L)	0.2 L quartz tubes with 125 W UV Hg lamp (λ max 365 nm) containing 0.1 L of	Adsorbent, TiO_2 control.	Significant loss of BET surface area in IPCA. Very little difference with TiO_2	(Yao *et al.*, 2012)

				solution.		control. Dark adsorption not shown. Improved IPCA performance is likely adsorption. Appears to photodegrade but no evidence of synergy.	
TiO_2 prepared by hydrothermal or reflux sol gel method. AC was added to sol gel solution and dried to create IPCA.	laboratory prepared PAC (0.5g/L)	Anatase TiO_2	Rhodamine B (50 mg/L)	0.05L suspension irradiated in a solarbox with Xe lamp (690W/m^2).	Photolysis, adsorbent, TiO_2	1:10 IPCA is best performing. IPCAs show very little adsorption. Only the IPCA prepared by the reflux method shows promise and the difference between the IPCA and AC is likely just photolysis.	(Asiltürk and Şener, 2012)
AC and P25 in a given ratio were added to 1.5M HNO_3 solution in a Teflon reactor and heated to 150°C. The resulting IPCA was then washed and dried.	GAC (0.4-1.2 g/L)	P25	Reactive black-5 (20-130 mg/L)	0.5 L cylindrical photoreactor (25 cm × 8 cm) with 125 W low pressure Hg lamp (340–400 nm) containing 0.25 L solution.	TiO_2, P25	No photolysis or dark adsorbent controls. Dark adsorption time shown. Results expressed as percentage removal. Performance not much higher than AC	(Mahadwad *et al.*, 2011)
Sol gel method used to prepare Er^{3+}:$YFeO_3$-doped TiO_2. GAC was added to the solution during ultrasonication and then dried and calcined between 400-800°C	GAC (20 g/L) (spherical activated carbon)	Mixed phase Er^{3+}:$YFeO_3$-doped TiO_2	Methyl orange (500 mg/L)	0.05 L solution with 18W-LED lamp (455 nm and 553 nm).	Dark IPCA, Dark adsorbent, Dark control for regeneration.	Dark adsorption not shown but would appear minimal. IPCA appears to show synergy but there is no photolysis control and the solution volume is very small. Not much difference in the removal rate between the light and dark IPCA by the third regeneration cycle: shows minor regeneration potential.	(Hou *et al.*, 2012)
Titanium trichloride was added to a strong ion exchange resin. The dried product was then carbonized at 700°C in a tube furnace and then activated with steam at 900°C.	GAC (5-40 g/L) (spherical activated carbon)	Mixed phase TiO_2, P25 as reference	Methyl orange (50 mg/L)	2 L fluidized bed photoreactor using either UV-C, (λmax 254 nm) or UVA (λmax 365 nm) with aeration (1 L/min).	UVA and UVC light.	No control for regeneration study. Dark adsorption not shown but claimed to have reached equilibrium. No controls, no proof.	(Yoon et al., 2012)

Appendix B, IPCAs Prepared by Dry Method

Preparation method	Adsorbent	Photocatalyst	Substrate	Irradiation source	Controls	Notes	Ref
AP-MOCVD (atmospheric pressure-metal organic chemical vapour deposition) used to prepare the IPCA.	PAC (2 g/L)	Anatase TiO_2	Methyl orange (100 mg/L)	1.5 L cylindrical glass photoreactor, with a central UV lamp (356 nm, 1.2 mW cm^{-2}).	None, IPCA compared to mixture for recycle (10 cycles).	Results expressed as C/C_0. No TiO_2 and photolysis controls. No adsorbent control in the recycle of the IPCA. Mixture was not calcined at 400°C which might invalidate it as a control. Recycle is convincing everything else is not.	(Zhang *et al.*, 2005b)
MOCVD (metal organic chemical vapour deposition) was used to apply TiO_2 to a commercial AC to create an IPCA.	PAC (2 g/L)	Anatase TiO_2	Methyl orange (100 mg/L)	1.5 L cylindrical glass photoreactor, with a UV lamp (356 nm, 1.2 $mWcm^{-2}$) in the centre.	Photolysis, light adsorbent, mixture.	Results expressed as C/C_0. No TiO_2 control. 2h dark adsorption time not shown. IPCA performance could be due to adsorption. Lots of characterisation. TiO_2 concentration. is lower in the mixture.	(Zhang *et al.*, 2006)
As above.	PAC (2 g/L)	Anatase TiO_2	Methyl orange (100 mg/L)	1 L cylindrical glass photoreactor with a 300 W high-pressure Hg lamp (356 nm). Aeration at 1.2 m^3h^{-1})	None	Looks at the effect of different surface treatments.	(Zhang *et al.*, 2005c)
MOCVD – using tetrabutyl orthotitanate and N_2 - was used to apply TiO_2 onto pre-treated PAC.	PAC (2 g/L)	Anatase TiO_2	Methyl orange (100 mg/L)	1.5 L photoreactor with UV lamp (365nm, 1.2 W/cm^{-2})	None	No raw data, all kinetics.	(Zhang and Lei, 2007)
$TiCl_4$ was deposited onto ACFs using Molecular Adsorption–Deposition (MAD), a form of CVD to create an IPCA.	ACF (weight not stated)	Anatase/rutile TiO_2	Methylene blue (2.498 mmol/L)	Pyrex reaction cell (80 mm diameter × 95 mm height) with 24 W low pressure Hg lamp (254 nm)	Photolysis, light adsorbent, None for recycle.	Results expressed as C/C_0 and without error bars. Results seem convincing but it is unclear if the IPCA had the same starting point or how much is degraded.	(Fu *et al.*, 2004a)
As above.	ACF (weight not stated)	Anatase TiO_2	Methylene blue (10 - 16 x 10^{-4} mol/L)	Two pieces of the IPCA, were placed on a reaction cell and aerated at 90 ml min^{-1})	Light and dark IPCA	No photolysis or TiO_2 control. Only 20min dark adsorption (no shown). Slightly convincing.	(Fu *et al.*, 2004b)
TiO_2 was applied to AC using Chemical Vapour Deposition (CVD). Ag was applied to the TiO_2-AC composite using the same method.	PAC (2 g/L)	Anatase TiO_2 doped with Ag.	Methyl orange (200 mg/L)	1 L cylindrical photoreactor with UV lamp (356 nm, 1.2 $mWcm^{-2}$)	Mixture, P25, TiO_2 IPCA. None for recycle.	No photolysis or Ag-TiO_2 control. Results expressed as C/C_0. 2h dark adsorption not shown. Unclear if IPCA is effective at photodegradation but doping appears to improve performance.	(Zhang *et al.*, 2005a)

TiO_2 was applied to AC using MOCVD. A sol gel method was also used to prepare a TiO_2 and AC was added using stirring. IPCA was then calcined at 873K.	PAC (2 g/L)	Anatase TiO_2	Methyl orange (100 mg/L)	1 L cylindrical glass reactor, with a 300 W high pressure Hg lamp and aeration (1.2 m^3 h^{-1})	None, None for recycle.	Results expressed as C/C_0. Good comparison of Sol-gel and MOCVD methods. No photodegradation controls. Includes interesting schematic of MOCVD IPCA. MOCVD seems to be an improvement for both substrate reduction and mineralisation.	(Zhang and Lei, 2008)
CVD was used to apply TiO_2 precursors to the support materials using various conditions for each adsorbent.	EAC, Silica gel, g-Al_2O_3 (Not stated)	Anatase TiO_2	Phenol (400 mg/L)	Photoreactor with 8 W UV fluorescent tube (λmax 356 nm). Oxygen was bubbled through the system.	None	Results expressed as C/C_0. Experiments seem to have been done only once and the results are erratic.	(Ding *et al.*, 2001b)
Different preparation methods used Chemical Vapour Deposition (CVD), Direct Air-Hydrolysis (DAH) and High Temperature Impregnation (HTI).	GAC (0.625 mg/L)	Anatase TiO_2	Methylene blue (10-250 mg/L)	None	None	Study only looks at MB adsorption. Uses Hg and N_2 porosimetry.	(El-Sheikh *et al.*, 2004)
Chemical Vapour Deposition (CVD) was used to prepare the IPCAs. The composites were dried and then calcined at 150°C.	4 types of PAC: unoxidised, oxidised by HNO_3, H_2SO_4 or H_2SO_4 and H_2O_2 (1-10 g/L).	Anatase TiO_2	3-chlorophenol (40 mg/L)	0.25 L photoreactor with 100W Hg lamp (λ max 365 nm, 7 $mWcm^{-2}$ of 365 nm) and 50 ml min^{-1} aeration.	TiO_2	Measures Cl^- production but the lack of a photolysis control for this and TOC means it could be this effect.	(El-Sheikh *et al.*, 2007)
APCVD was then used to apply TiO_2 precursor to the ACF which was followed by calcination.	ACF (0.1 g/L)	Anatase TiO_2	Phenol (50 mg/L)	Cylindrical shallow vessel photoreactor irradiated with a 20 W low pressure Hg lamp (254nm).	None	Results expressed as C/C_0. 30 min dark adsorption shown. It is likely that the photodegradation is largely residual adsorption.	(Yang *et al.*, 2008)

Appendix C Emission Spectra of UV lamps

The emission spectra of the UV lamps used in this study was provided by Ana Carolina de Almeida. The method used to determine these results is documented below.

The emission spectra of the UV (low- and medium-pressure mercury) lamps were obtained by using a spectrometer system from Ocean Optics (Dunedin, Florida, USA). The system was equipped with an USB2000 spectrometer, a LS-I-CAL calibrated light source (for applications with an integrated sphere), a FOS 1 Integrated sphere, an UV-NIR fiber optics cable (600 µm), and a Spectra Suit software. The first step for the acquisition of emission spectrum was to calibrate the spectrometer (Spectroscopy TV 2012). The fibre optic sensor was positioned on a retort stand clamp facing the mercury lamps. A dark control was acquired and the emission spectra of the low-pressure (Appendix C-0-1) and the medium-pressure mercury lamp were recorded (Appendix C-0-2).

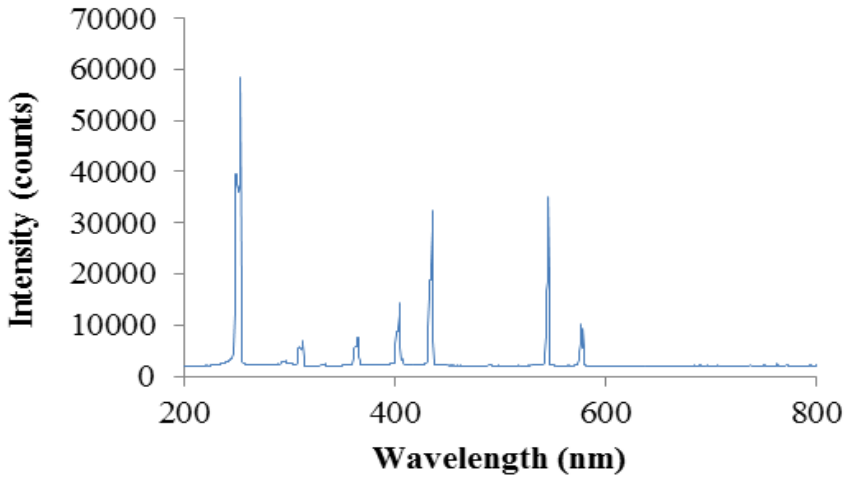

Appendix C-0-1 Emission Spectra of UV-C (15 W) lamp

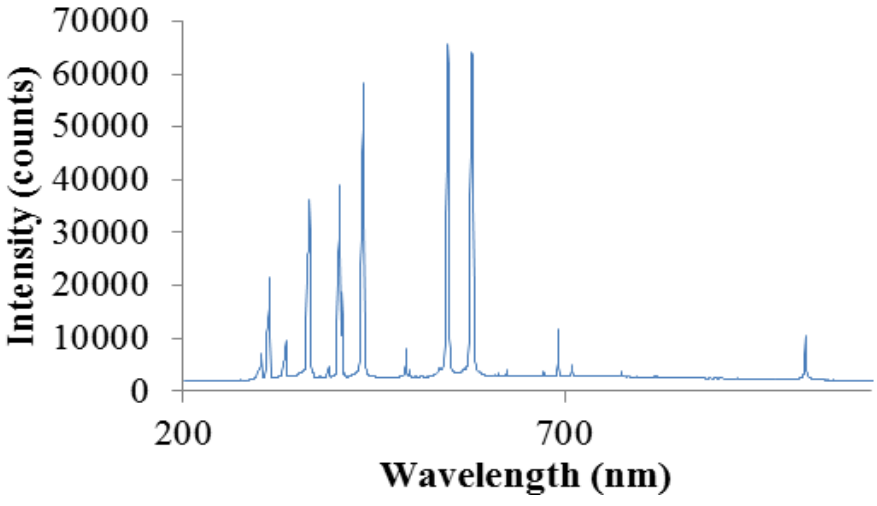

Appendix C-0-2 Emission Spectra of UV-A/B (400 W) lamp

These results are similar to those provided by the lamp manufactures see Appendix C-0-3 and other manufactures see Appendix C-0-4, Appendix C-0-5 and Appendix C-0-6. A comparison with a Xe lamp is provided in Appendix C-0-7.

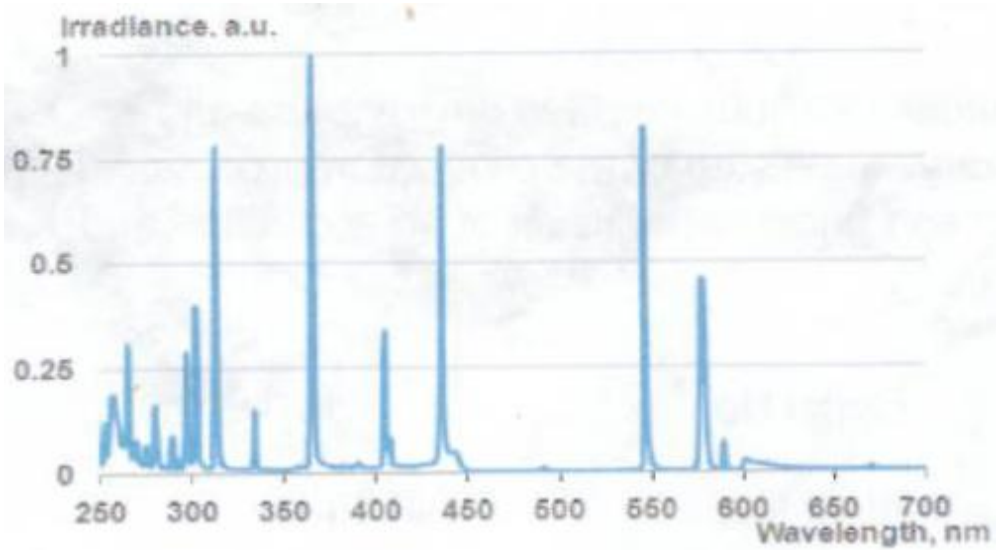

Appendix C-0-3 Test certificate provided by the manufacture for the medium pressure Hg lamp (TQ-150) used for all studies.

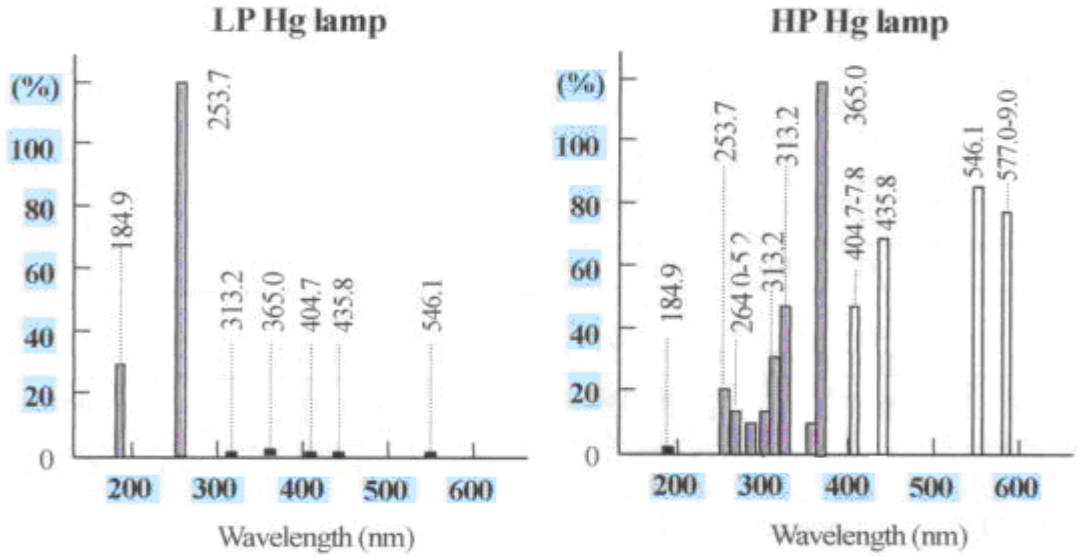

Appendix C-0-4 Relative spectral energy distribution of Hg lamps.

Source: (SEN Lights Corporation 2012)

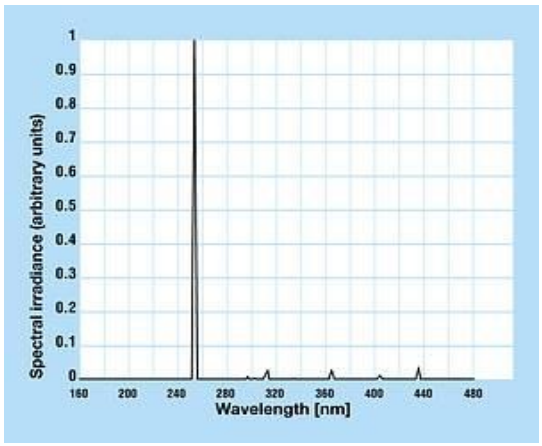

Appendix C-0-5 Low pressure Hg.

Source: (Ardee Environment 2012)

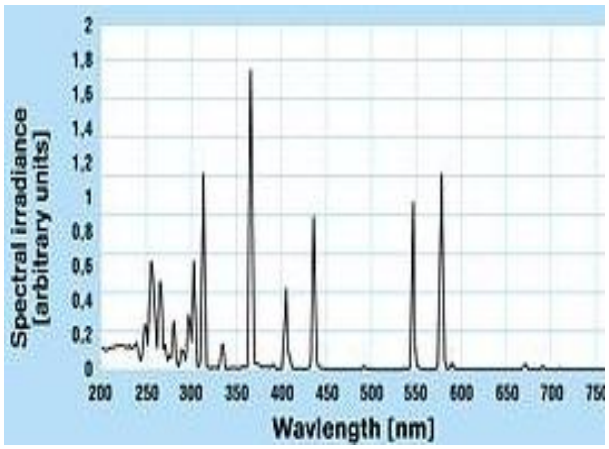

Appendix C-0-6 Medium pressure Hg.

Source: (Ardee Environment 2012)

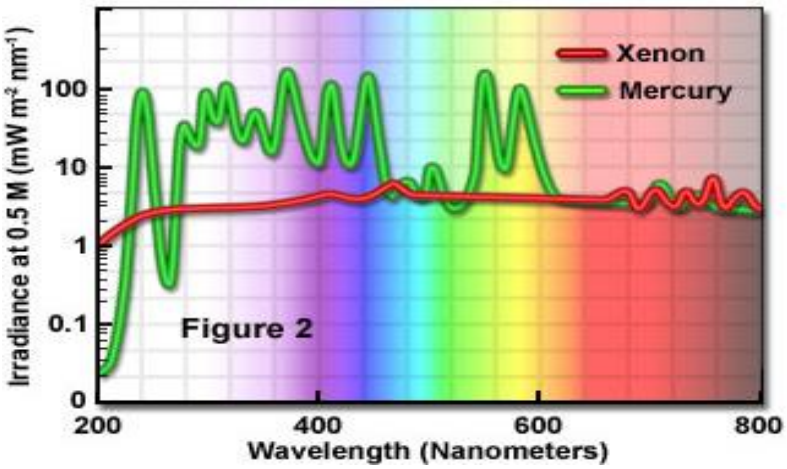

Appendix C-0-7 Spectral Irradiance of Arc-Discharge Lamps using 100 W Hg and 75 W Xe lamp

Source: (Olympus Microscopy Resource Center 2012)